รายงานวิจัยฉบับสมบูรณ์

โครงการ การออกแบบระดับโมเลกุลและฟังก์ชันของสารประกอบเชิงซ้อนเบต้าไดคีโตเนทที่มีไดอิมีนลิแกนด์เป็นองค์ประกอบ

Molecular and functional design of metal β-diketonate complexes incorporating diimine ligands

โดย ผู้ช่วยศาตราจารย์ ดร. พิมผกา ฮาร์ดิง และคณะ

สัญญาเลขที่ RSA5080007

รายงานวิจัยฉบับสมบูรณ์

โครงการ Molecular and functional design of metal β-diketonate complexes incorporating diimine ligands

คณะผู้วิจัย	สังกัด
1. ผศ. ดร. พิมผกา ฮาร์ดิง	มหาวิทยาลัยวลัยลักษณ์
2. รศ. ดร. เดวิด เจมส์ ฮาร์ดิง	มหาวิทยาลัยวลัยลักษณ์

สนับสนุนโดยมหาวิทยาลัยวลัยลักษณ์และสำนักงานกองทุนสนับสนุนการวิจัย

Abstract

The following report details the synthesis and characterization of two types of organic ligands namely, (4-X-phenyl)-pyridin-2-ylmethylene-amine (ppa^X) {X = H, Me, OMe, Et, F, Cl, Br and I} and the briding ligands: bispyridylmethylene-1,3-benzeneamine (1,3-bpmba), bispyridylmethylene-1,4-benzeneamine (1,4-bpmba), bispyridylmethylene-1,5-naphthaleneamine (1,5-bpmna) and bis(pyridyl)methylene-hydrazone (bpmhd).

The reaction between ppa^X ligand and desired metal β-diketonate complexes yield monomeric complexes, [M(β-diketonate)$_2$(ppa^X)] (M = Ni and Co; β-diketonate = dbm, tmhd and hfac). The electron transfer studies show that these complexes are redox active. The oxidation potential is found to be dependent on the type β-diketonate ligand but essentially independent of the substituent, X, on the ppa^X ligand which has been confirmed by DFT calculation of [M(β-diketonate)$_2$(ppa^X)] complexes. Interestingly, the Co complexes exhibit the redox coupled spin-crossover behavior. Further investigation has been explored by isolation the redox paired of [M(β-diketonate)$_2$(ppa^X)] and [M(β-diketonate)$_2$(N-N)] (β-diketonate = dbm and tmhd; N-N = phen, bipy and dmae). Sharp signals in ^{1}H NMR indicate that cationic complexes are Co(III) d^6.

The reaction of bridging ligands and metal β-diketonate complexes yield dimermeric complexes, [(β-diketonate)$_2$M(μ-L)M(β-diketonate)$_2$] (M = Ni and Co; β-diketonate = dbm and tmhd; L = bispyridylmethylene-1,3-benzeneamine (1,3-bpmba), bispyridylmethylene-1,4-benzeneamine (1,4-bpmba), bispyridylmethylene-1,5-naphthaleneamine (1,5-bpmna) and bis(pyridyl)methylene-hydrazone (bpmhd). The cyclic voltammetry studies show that all Ni and Co complexes are redox active. The shorter bridging ligand give more communication between two metals. Furthermore, in case of Co complexes still exhibit redox coupled spin-crossover behavior.

บทคัดย่อ

ในรายงานฉบับสมบูรณ์นี้จะกล่าวถึงการสังเคราะห์และพิสูจน์เอกลักษณ์ของลิแกนด์อินทรีย์ชนิดใหม่ (4-X-phenyl)-pyridin-2-ylmethylene-amine (ppa^X) {X = H, Me, OMe, Et, F, Cl, Br and I} และลิแกนด์ที่ทำหน้าที่เป็นสะพาน bispyridylmethylene-1,3-benzeneamine (1,3-bpmba), bispyridylmethylene-1,4-benzeneamine (1,4-bpmba), bispyridylmethylene-1,5-naphthaleneamine (1,5-bpmna) and bis(pyridyl)methylene-hydrazone (bpmhd).

ปฏิกิริยาระหว่างลิแกนด์ ppa^X ligand และสารประกอบโลหะเบต้าไดคีโตเนทจะได้สารประกอบเชิงซ้อนแบบโมโนเมอร์ [M(β-diketonate)$_2$(ppa^X)] (M = Ni and Co; β-diketonate = dbm, tmhd and hfac) การศึกษาการถ่ายโอนอิเล็กตรอนของสารประกอบเชิงซ้อนแสดงให้เห็นว่าสารประกอบเหล่านี้มีสมบัติแบบรีดอกซ์แอคทีฟ โดยค่าศักย์ไฟฟ้าออกซิเดชันจะขึ้นอยู่กับชนิดของเบต้าไดคีโตเนทแต่จะไม่ขึ้นกับชนิดของหมู่แทนที่ X ในลิแกนด์ ppa^X มากนัก ซึ่งได้รับการยืนยันด้วยการคำนวณ DFT และสิ่งที่น่าสนใจอีกอย่างหนึ่งสำหรับสารประกอบเชิงซ้อนกลุ่มนี้คือ เมื่อโลหะเป็นโคบอลต์จะแสดงสมบัติรีดอกซ์คัพเพิลสปินครอสโอเวอร์ การศึกษาเพิ่มเติมทำโดยการแยกสารประกอบคู่รีดอกซ์ของ [M(β-diketonate)$_2$(ppa^X)] และ [M(β-diketonate)$_2$(N-N)] (β-diketonate = dbm and tmhd; N-N = phen, bipy and dmae) พบว่าสัญญาณใน ^{1}H NMR นั้นชัดเจน ซึ่งแสดงให้เห็นว่าสารประกอบไอออนบวกนี้เป็น Co(III) d^6

ปฏิกิริยาระหว่างลิแกนด์ที่เป็นสะพานกับโลหะเบต้าไดคีโตเนทจะได้สารประกอบไดเมอร์ [(β-diketonate)$_2$M(μ-L)M(β-diketonate)$_2$] (M = Ni and Co; β-diketonate = dbm and tmhd; L = bispyridylmethylene-1,3-benzeneamine (1,3-bpmba), bispyridylmethylene-1,4-benzeneamine (1,4-bpmba), bispyridylmethylene-1,5-naphthaleneamine (1,5-bpmna) และ bis(pyridyl)methylene-hydrazone (bpmhd) การศึกษาโดยไซคลิกโวเทมเมทตรีพบว่าทั้งสารประกอบนิกเกิลและโคบอลต์มีสมบัติแบบรีดอกซ์แอคทีฟ และลิแกนด์ที่มีขนาดสั้นก็จะสามารถทำให้เกิดการสื่อสารระหว่างโลหะทั้งสองได้ดีกว่า นอกจากนี้ยังพบว่าสารประกอบโคบอลต์ก็ยังแสดงสมบัติรีดอกซ์คัพเพิลสปินครอสโอเวอร์

Acknowledgements

I would like to acknowledge at this point the various people who have helped during this project. A number of students have worked on this project during the last three years and their help and determination is gratefully acknowledged.

A large number of crystal structures have also been determined in the course of this project by our research collaborator Harry Adams at the University of Sheffield. I also wish to acknowledge Professor Mike Shaw at Southern Illinois University Edwardsville, USA who has undertaken IR spectroelectrochemistry and UV-Vis spectroelectrochemistry on [Co(β-diketonate)$_2$(N-N)] compounds presented in this report.

A further thank you must also go to Associate Professor Dr Supa Hannongbua at Kasatsart University and Assistant Professor Dr Yuthana Tantirungrotechai, NANOTEC who have undertaken computational studies on [Ni(β-diketonate)$_2$(ppa^X)] and [Co(β-diketonate)$_2$(N-N)] respectively.

Finally, I wish to acknowledge the help and support of Associate Professor Dr David J. Harding for useful discussions and advice during the course of this project. There is no doubt that this project could not have completed without his assistance.

Table of Contents

Executive Summary 1

Objectives 3

Introduction 4

Results and Discussion 10

Synthesis of metal β-diketonate starting materials [M(β-diketonate)$_2$(H$_2$O)$_2$] 10

Synthesis and Characterization of (4-X-phenyl)-pyridin-2-ylmethylene amine ligands (ppa^X) 12

Synthesis and characterization of [Ni(β-diketonate)$_2$(ppa^X)] complexes 15

Experimental 17

X-ray structural studies of [Ni(β-diketonate)$_2$(ppa^X)] complexes 20

Electron transfer studies of [Ni(β-diketonate)$_2$(ppa^X)] complexes 23

Synthesis and characterization of [Co(β-diketonate)$_2$(ppa^X)] complexes 26

Experimental 28

X-ray structural studies of [Ni(β-diketonate)$_2$(ppa^X)] complexes 32

Electron transfer studies of [Co(β-diketonate)$_2$(ppa^X)] 35

Synthesis and characterization of [Co(β-diketonate)$_2$(ppa^X)]OTf complexes 38

Experimental 40

Electron transfer studies of [Co(β-diketonate)$_2$(ppa^X)]OTf complexes 44

Synthesis and characterization of [Co(β-diketonate)$_2$(N-N)][BF$_4$] complexes 45

Experimental 47

Electron transfer studies of [Co(β-diketonate)$_2$(N-N)][BF$_4$] complexes 48

Synthesis and characterization of bridging ligands 51

Experimental 52

Synthesis and characterization of [(β-diketonate)$_2$M(μ-L)M(β-diketonate)$_2$] complexes 52

Experimental 54

X-ray structural studies of [(β-diketonate)$_2$M(μ-L)M(β-diketonate)$_2$] complexes 57

Electron transfer studies of [(β-diketonate)$_2$M(μ-L)M(β-diketonate)$_2$] complexes 60

Computational calculations of [Co(β-diketonate)$_2$(N-N)] complexes 63

References 70

Project Outcomes 73

Publications 73

Presentations 74

Presentations 74

Training new generation of Thai researchers in Inorganic Chemistry 75

1. Executive Summary

Novel organic ligands namely (4-X'-phenyl)-pyridin-2-ylmethylene-amine (ppa^X) when X = H, Me, OMe, Et, F, Cl, Br and I have been prepared by condensation reaction between pyridine-2-carboxaldehyde and *p*-aniline in ether at room temperature yields the ppa^X ligand in moderate yield.

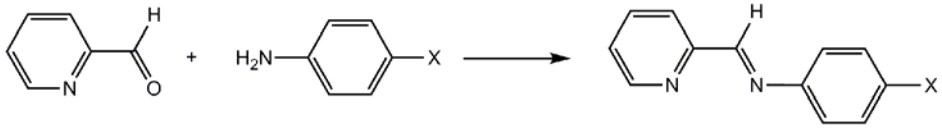

The reaction between the ppa^X ligand and [M(β-diketonate)$_2$] yields novel [M(β-diketonate)$_2$(ppa^X)] complexes (M = Ni and Co, β-diketonate = dbm, tmhd and hfac, X = H, Me, Et, OMe, F, Cl, Br and I).

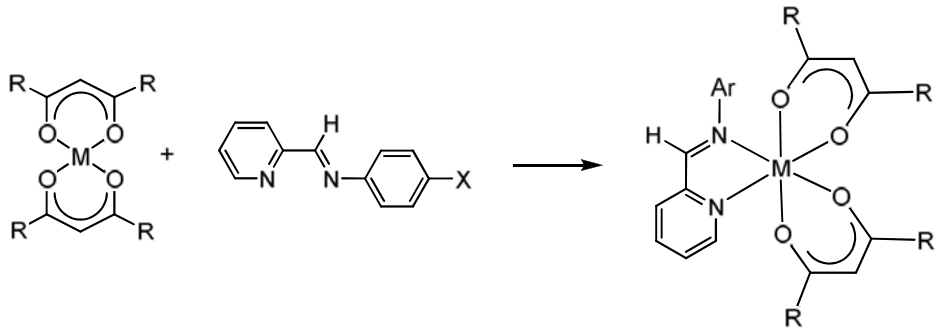

The crystal structures reveal octahedrally coordinated metal centres with the β-diketonate ligands exhibiting both 'bent' and 'planar' bidentate coordination modes with the coordination mode dependent upon the type of ppa^X ligand present. The aryl rings of the ppa^X ligands are found to be non co-planar with the pyridylimine unit with the degree of twisting dependent on the substituent, X.

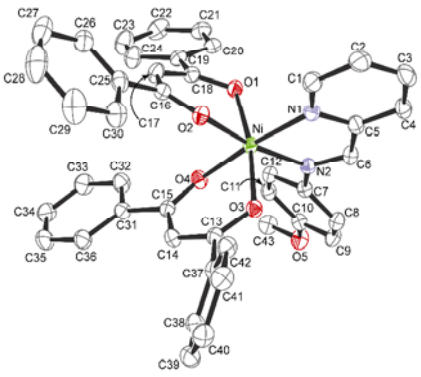

The electrochemical behavior of the complexes reveals reversible or irreversible one-electron oxidation to Ni(III) in the case of the [Ni(tmhd)$_2$(ppa^X)] and [Ni(dbm)$_2$(ppa^X)] complexes, respectively. The oxidation potential is found to be dependent on the type β-diketonate ligand but essentially independent of the substituent, X, on the ppa^X ligand. The [Ni(β-diketonate)$_2$(ppa^X)] complexes (X = F, Cl, Br and I) also undergo a ligand based reduction. [Ni(hfac)$_2$(ppa^X)] show no oxidation processes but undergoes irreversible reduction.

When the metal is changed from Ni(II) to Co(II) the oxidation potential moves to a more negative potential by *ca*. 0.4 V as expected. However, the voltammograms also reveal the electron spin change upon oxidation of $[Co(dbm)_2(ppa^X)]$ and $[Co(tmhd)_2(ppa^X)]$ complexes from high spin d^7 to low spin d^6.

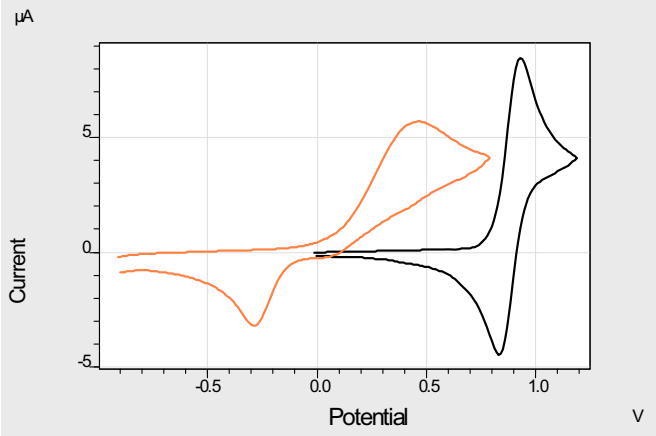

Cyclic voltammograms of $[Ni(tmhd)_2(ppa^F)_2]$ (---) and $[Co(tmhd)_2(ppa^F)]$ (---).

Further studies of the cobalt β-diketonate complexes which show interesting redox behavior by isolation of their cations have been investigated. The one pot reaction of [Co(β-diketonate)$_2$] and the diimine ligands followed by an addition of Ag^+ yields the Co(III) cationic complexes, $[Co(\beta\text{-diketonate})_2(ppa^X)][CF_3SO_3]$ (β-diketonate = dbm and tmhd, X = H, Me, Et, OMe, F, Cl, Br and I) and $[Co(\beta\text{-diketonate})_2(L)][BF_4]$ (β-diketonate = dbm and tmhd, L = phen, 2,2′-bpy and dmae). All complexes show sharp and strong signals in ^1H NMR which confirm the d^6 low spin Co(III) formation. The cyclic voltammetric studies of these complexes show identical oxidation and reduction peaks as in the neutral species. Intensive electrochemical studies by fast scan CV and spectroelectrochemistry of $[Co(\beta\text{-diketonate})_2(L)][BF_4]$ suggest that there is an equilibrium between the high spin d^7 and low spin d^7 and d^6 species.

The DFT calculations of $[Co(\beta\text{-diketonate})_2(N\text{-}N)]$ (N-N = ppa^X, phen, bipy and dmae) complexes have suggested that SOMO of molecules are constituted of Co (*ca.* 40%), β-diketonate (*ca.* 55%) and ppa^X (*ca.* 5%) hence the oxidation potential will depend mostly on the properties of substituents on the β-diketonate.

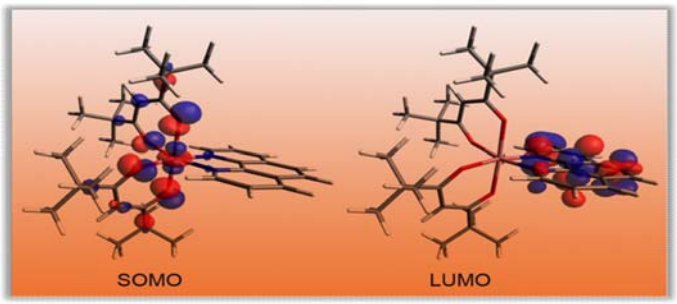

SOMO and LUMO of $[Co(tmhd)_2(phen)]$

Furthermore, we have synthesized and characterized the dimeric metal β-diketonate complexes, [(β-diketonate)$_2$M(μ-L)M(β-diketonate)$_2$] when M = Ni or Co, β-diketonate = dbm and tmhd, and L = 1,3-bpmba, 1,4-bpmba, 1,5-bpmna and bpmhd. The electron transfer of the complexes shows that the right combination of β-diketonate ligand, metal and bridging ligand will result in communication between the two metal centres *e.g.* [(tmhd)$_2$Ni(μ-1,4-bpmba)Ni(tmhd)$_2$] and [(tmhd)$_2$Co(μ-1,3-bpmba)Co(tmhd)$_2$].

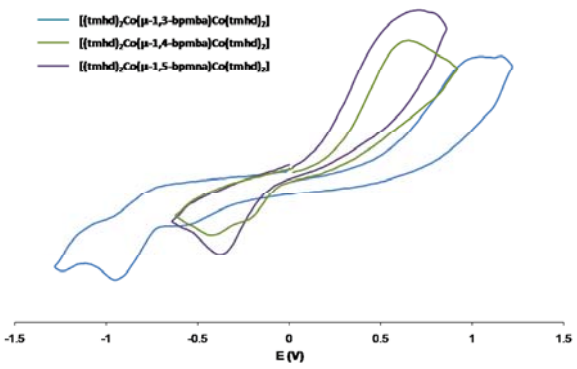

CVs of [(tmhd)$_2$Co(μ-L)Co(tmhd)$_2$]

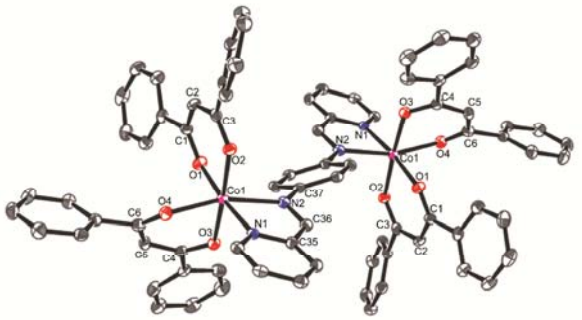

X-ray structure of [(dbm)$_2$Co(μ-1,4-bpmba)Co(dbm)$_2$].

2. Objectives

2.1. Proposed Objectives for the Project

2.1.1. To synthesize organic ligands namely (4-X′-phenyl)-pyridin-2-ylmethylene-amine (ppa^X).

2.1.2. To synthesize new organic ligands namely 4,5-di(2-pyridyl)(R′)imidazole (dpi^X).

2.1.3. To synthesize new organic ligands namely hexaazatriphenylene (HAT)

2.1.4. To synthesize novel mononuclear metal complexes [M(β-dkt^R)$_2$(dpi^X)], [M(β-dkt^R)$_2$(ppa^X)] and [M(β-dkt^R)$_2$(HAT)]

2.1.5. To synthesize novel binuclear metal complexes [(β-dkt^R)$_2$M(μ-dpi$^{R'}$)M(β-dkt^R)$_2$] and [(β-dkt^R)$_2$M(μ-HAT)M(β-dkt^R)$_2$]

2.1.6. To investigate the effect of number and type of metal on magnetic and electron transfer of metal β-diketonate complexes.

2.1.7. To study the effect of substituent groups on ligand on magnetic and electron transfer of metal β-diketonate complexes.

2.1.8. To study inter- and intra molecular forces in metal complexes.

2.1.9. To train a new generation of Thai researchers in inorganic chemistry.

2.1.10. To publish at least 2 international research papers based upon this research.

2.2. Achieved Objectives

2.2.1. To synthesize organic ligands namely (4-X-phenyl)-pyridin-2-ylmethylene-amine (ppa^X).

2.2.2. To synthesize novel mononuclear metal complexes $[M(\beta\text{-}dkt^R)_2(ppa^X)]$.

2.2.3. To synthesize novel mononuclear cation of Co complexes $[Co(\beta\text{-}dkt^R)_2(ppa^X)]^+$ and $[Co(\beta\text{-}dkt^R)_2(N\text{-}N)]^+$.

2.2.4. To synthesized bridging ligands: bispyridylmethylene-1,3-benzeneamine (1,3-bpmba), bispyridylmethylene-1,4-benzeneamine (1,4-bpmba), bispyridylmethylene-1,5-naphthaleneamine (1,5-bpmna) and bis(pyridyl)methylene-hydrazone (bpmhd).

2.2.5. To synthesize novel binuclear metal complexes $[(\beta\text{-}dkt^R)_2M(\mu\text{-}L)M(\beta\text{-}dkt^R)_2]$.

2.2.6. To investigate the effect of number and type of metal on magnetic and electron transfer of metal β-diketonate complexes.

2.2.7. To study the effect of substituent groups on ligand on magnetic and electron transfer of metal β-diketonate complexes.

2.2.8. To study electronic properties of $[M([(\beta\text{-}dkt^R)_2(ppa^X)$ (M = Ni and Co) and Co cations by using DFT calculations.

2.2.9. To study inter- and intra molecular forces in metal complexes.

2.2.10. To train a new generation of Thai researchers in inorganic chemistry.

2.2.11. To publish at least 2 international research papers based upon this research.

3. Introduction

The vastness of transition metal β-diketonate chemistry makes a complete review impractical and therefore in the interests of brevity only the most relevant literature is reviewed. The review begins with an introduction to metal β-diketonate chemistry before moving onto basic coordination chemistry. This is followed by current trends in metal β-diketonate research organized by the potential application and then by a final discussion of the electrochemistry of metal β-diketonate complexes.

Metal β-diketonates

Metal β-diketonate complexes, $[M(\beta\text{-}dkt)_2]$ (M = Mn, Fe, Co, Ni and Cu; β-dkt = substituted β-diketonates) have been known for many years. They are easily prepared, readily soluble in organic solvents and are air stable.[1]

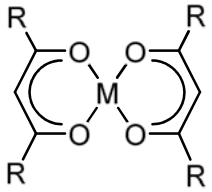

M = Mn, Fe, Co, Ni, Cu
R = Me, CF_3, Ph, *t*-Bu

In addition to their ease of synthesis metal β-diketonates also permit substantial variation in the steric and electronic properties of the compound through changes in the substituent groups. For instance, when R = *t*-Bu the complex is electron rich but sterically demanding, while when R = Ph the substituent is of intermediate steric bulk and electron withdrawing creating an electron poor compound.[2] The fact that the substituent groups may be different allows further flexibility and control over the system.

The metal β-diketonate complexes readily coordinate additional ligands to give octahedral compounds with either *trans* or *cis* configurations.[3] The use of a chelating ligand such as ethylenediamine enforces a *cis* configuration eliminating the formation of different isomers.

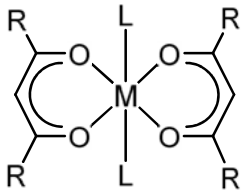

trans

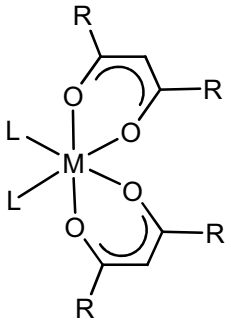

cis

An additional ligand or ligands can significantly alter the physical properties of the complex and may be used to introduce extra functionality into the system. The nature of the ligand(s) is crucial in determining the potential application of the resulting complex. Thus, phosphines favor catalytic applications[4] while diamines are useful in the preparation of metal-oxide thin films.[5] Further applications are in the areas of magnetic materials, optical devices and sensors.

Coordination Complexes

Most metal β-diketonate complexes generally utilize simple monodentate ligands (*e.g.* H_2O, NR_3, py). Chelating ligands such as bipy, en and diphosphines have also been reported.[1] Mixed ligand species were first prepared by Favero *et al* by reacting [Ni(β-dkt)$_2$] with a diphosphine or diamine in the presence of $NaBPh_4$ forming $[Ni(\beta\text{-dkt})(P\text{-}P)]^+$ (P-P = dppe, dppp and dppb) and $[Ni(\beta\text{-dkt})(N\text{-}N)_2]^+$ (N-N = en, bipy), respectively.[6] More recently this methodology has been extended to the more sterically demanding diamine *N*-methyl-1,4-diazacycloheptane forming a four coordinate complex, $[Ni(\beta\text{-dkt})(N\text{-}N)]^+$.[7]

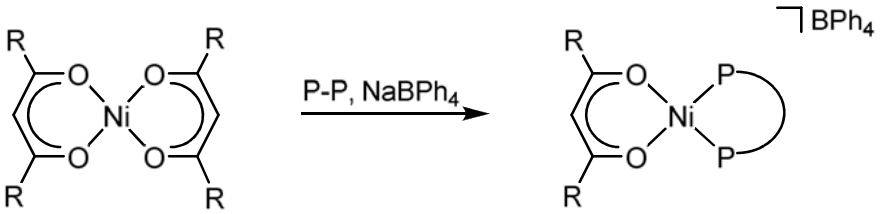

Bidentate linkers (*e.g.* pyrazine and 4,4′-bipy) polymeric 1D chains have been synthesized with a view to creating nanowires.[8] In the case $[Ni(dbm)_2(4,4'\text{-bipy})]_n$ the large supramolecular network formed also permits the inclusive of guest molecules with possible applications as a sensing, deodorizing or storage agent.[9] Further supramolecular architectures have been prepared by Aäkeroy with ligands that utilize H-bonding to form extensive, designed polymeric networks.[10]

Lately, substituted tetrathiafulvalene (TTF) ligands have begun to appear in the literature. This typically involves the synthesis of a pyridine substituted TTF unit which is subsequently coordinated to the metal centre. In the case of $[Cu(hfac)_2(TTF\text{-}py)_2]$ (TTF-py = 4-(2-tetrathiafulvalenyl-ethenyl)pyridine) the complex can be oxidized to $[Cu(hfac)_2(TTF\text{-}py)_2]PF_6$ which reveals stacking of the TTF-py units in the crystal and magnetic exchange between the radical TTF-py units.[11]

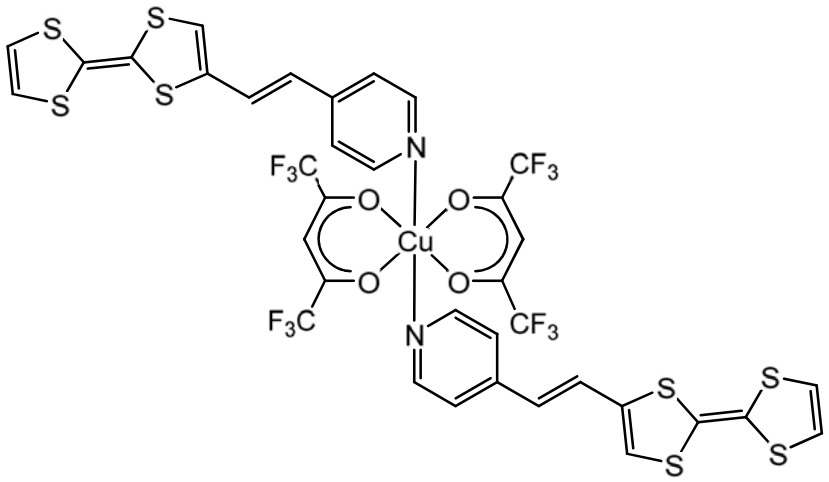

The TTF unit can also be introduced onto the β-diketonate ligand itself as has been demonstrated by Lorcy *et al* in the synthesis of $[M(TTFacac)_2(H_2O)_2]$ (M = Ni, Cu, Zn; TTFacac = 1-(trimethyltetrathiafulvalene)-butane-1,3-dionate).[12]

Bipyrimidine bridged metal β-diketonates have been prepared by Sinn and Brewer. Their studies clearly demonstrated the formation of the bridged complexes and gives rise to antiferromagnetically coupled metal centres.[13]

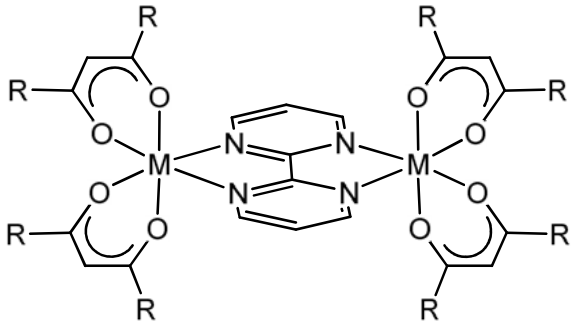

Catalysts

In the area of catalysis most of the research has concentrated on oxygen transfer chemistry notably conversion of aldehydes into carboxylic acids, alkene oxygenation to form alcohols and formation of alkyl peroxo species and epoxides.[4] Work in our own group has shown that $[Co(dbm)_2]$ may also promote the oxygenation of diphosphines giving the polymeric complex $[Co(dbm)_2(dppe\text{-}O_2)]_n$.[14]

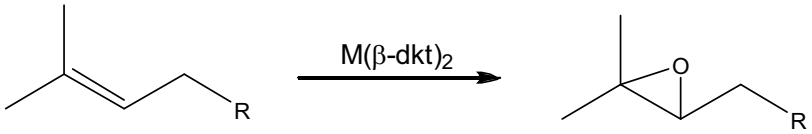

The key to the reactivity of these complexes is the coordinative unsaturation at the metal centre allowing the binding of the substrate prior to reaction. In the majority of cases these catalysts are simple β-diketonate complexes with little work done on $[M(\beta\text{-dkt})_2L]$ (L = phosphine, amine *etc*) systems where the additional ligand may be used to improve or fine tune the catalyst. Such systems have already proved to be moderate alkene polymerization/oligomerization catalysts. More recently, Bouwman *et* al have shown that $[Mn(acac)_2(bipy)]$ may act as an ethyl linoleate oxidation catalyst necessary for the drying of alkyd paints.[15] Indeed, in this instance a patent has also been filed. Furthermore, Buchwald and co-workers have shown that [Cu(β-dkt)] (β-dkt = tetramethylheptane-3,5-dione, 2-acetylcyclohexanone) is an excellent catalyst for C-N coupling reactions.[16]

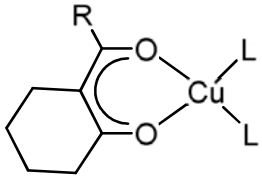

R = Me, Et, *i*-Pr

Finally, $[Ni(\beta\text{-dkt})_2]$ has been shown to be an effective and selective catalyst for the cross coupling of aryl Grignard reagent with aryl halides.[17]

Magnetic Systems

Magnetic systems have been prepared by the reaction of nitrones or nitroxides which are relatively stable organic radicals (see scheme below), with [M(β-dkt)$_2$] to form [M(β-dkt)$_2$L$_2$] where L is a nitrone or nitroxide.

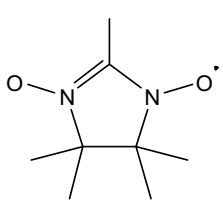

nitronylnitroxide

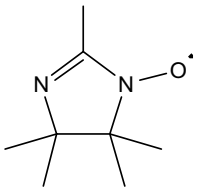

iminoylnitroxide

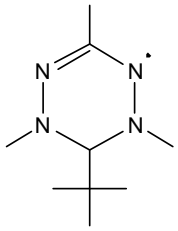

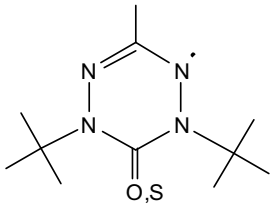

verdazyl

In certain cases if the nitrone is chelating and then the complex has the formula [M(β-dkt)$_2$L]. In most cases the metal and the organic ligand are antiferromagnetically coupled with no evidence of molecular magnetic behavior. However, judicious choice of the organic radical can lead to ferromagnetically coupled systems for example, [Ni(hfac)$_2$(pyDTDA)] (pyDTDA = 4-(2'-pyridyl)1,2,3,5-dithiadiazolyl)[18] and [Ni(acac)$_2$(IMpy)] (IMpy = 2-(2'-pyridyl)-4,4,5,5-tetramethyl-4,5-dihydro-1H-imidazoin-1-oxyl)[19] (see below).

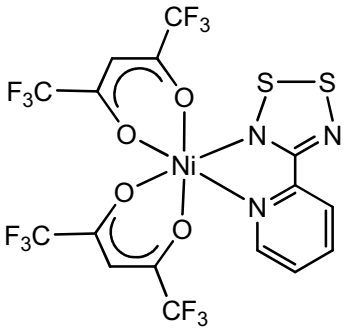

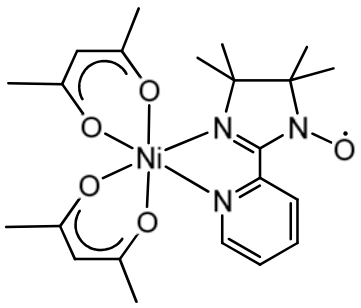

The organic radical can also act as a bridging ligand producing ferrimagnetically coupled systems. The presence of the organic radical is crucial for magnetism as it couples *antiferromagnetically* with both metal centres resulting in the remaining unpaired electrons being aligned with one another.[20]

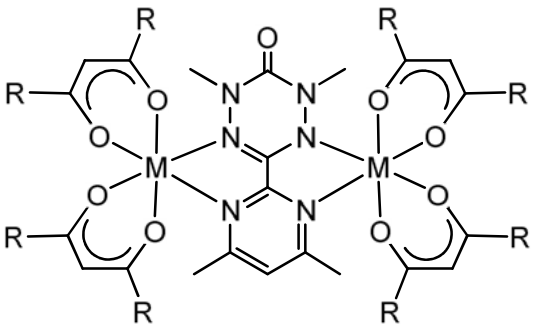

More recently, cyclic dimers have started to appear with most examples utilizing pyrimidine substituted nitroxide or nitronylnitroxide ligands. In contrast, to the above bridged species here the metal centres are well separated from each other by the coordinative requirements of the ligand.[21]

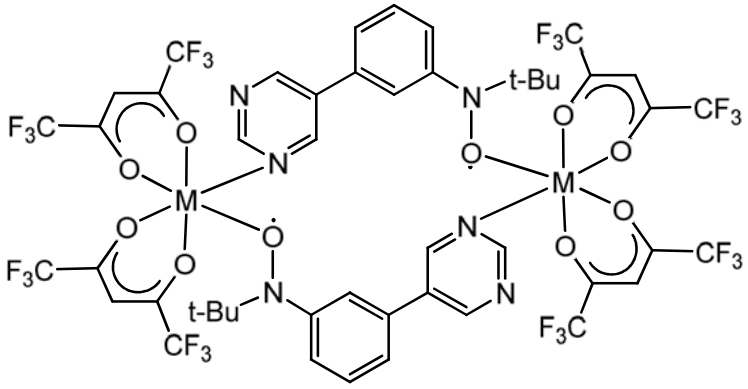

In these instances, in addition to the antiferromagnetic or ferromagnetic coupling between the metal and the organic radical there are interactions between the cyclic dimers which further complicate the magnetic exchange but show the importance of supramolecular interactions in determining the properties of such compounds.

Polymeric metal β-diketonate complexes represent the last class and perhaps the most promising type of compound which incorporate organic radicals. The first single chain magnet, $[Co(hfac)_2(AnNN)]_n$ (AnNN = 2-(4'-methoxyphenyl)-4,4,5,5-tetramethylimidazoin-1-oxyl-3-oxide), was prepared by Gatteschi and co-workers.[22] A related complex, $[Co(hfac)_2(BPNN)]_n$ (BPNN = *p*-butoxylphenyl-NN), has also been synthesized by Ishida *et al* which shows the largest coercivity of any known coordination compound.[23] Similarly hard magnets have been reported by Inoue *et al* in a series of compounds which use a chiral bis(nitroxide) radical namely, 1,3-bis(*N*-*tert*-butyl-*N*-oxylamino)-5-{1'-methyl-1'-[2''-(S)-methylbutoxy]ethyl}benzene is used. Ferromagnetically coupled chains may also be formed using other radicals for example $[Cu(hfac)_2(TTTA)]_n$ (TTTA = 1,3,5-trithia-2,4,6-triazapentalenyl).[24]

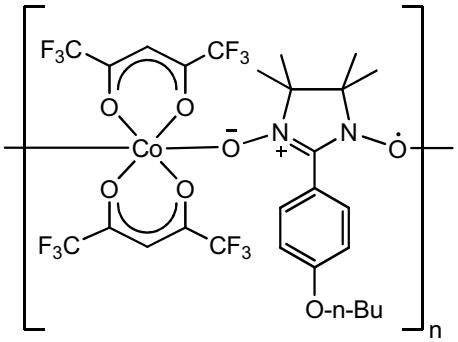

Metal Oxide Thin Films

Simple adducts of cobalt and nickel β-diketonates have also been used as precursors in the preparation of metal-oxide thin films by MOCVD for uses as magnetic detectors, oxygen optical sensors, solar-selective absorbers and protective layers.[5] Most of these studies utilize acac or thmd (R = *t*-Bu) as these are the most volatile and widely available. For instance, $[Co(acac)_2(tmeda)]$ is an

excellent precursor in the formation of cobalt oxides thin films notably that of the magnetic mixed valence Co_3O_4 oxide.

Electrochemistry of Metal β-Diketonates

Despite the wealth of coordination and materials chemistry presented above very few electrochemical studies have been reported.[25] The few studies that there are are mostly limited to the metal β-diketonate complexes. However, recent work in our group has shown that both the nickel and cobalt β-diketonate complexes, [M(β-dkt)$_2$(N-N)] (M = Co, Ni; N- N = bipy, phen and dimethylaminoethylamine) are in fact redox-active. The nickel complexes oxidize, albeit irreversibly to give rare examples of Ni^{III} species.[2,26]

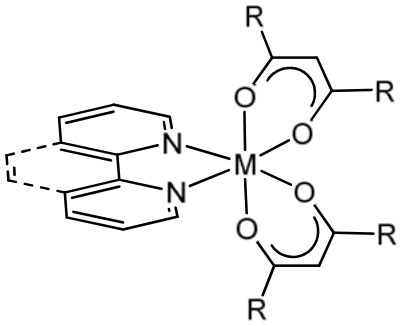

[Mn(acac)$_2$(bipy)] has also been studied by cyclic voltammetry and shows irreversible oxidation to [Mn(acac)$_2$(bipy)]$^+$ which quickly decomposes to [Mn(acac)$_3$].[15] One of the only other reports is for the [M(hfac)$_2$(2-PyBN)] (2-PyBN = *N-tert*-butyl-α-(2-pyridyl)nitrone) series which show irreversible oxidation.[27]

4. Results and Discussion

4.1. Synthesis of metal β-diketonate starting materials [M(β-diketonate)$_2$(H$_2$O)$_2$]

A NaOH solution was added to a solution of the desired β-diketone (dbm = dibenzoylmethane, tmhd = 2,2,6,6-tetramethyl-3,5-heptadione or hfac = hexafluoroacetylacetonato) under reflux and the acetate salt of Ni(II) or Co(II) in ethanol. The metal β-diketonate complexes precipitated almost immediately. The solid was filtered and washed with cool ethanol (Scheme 1). All metal β-diketonate complexes were dried in a dessicator overnight before use.

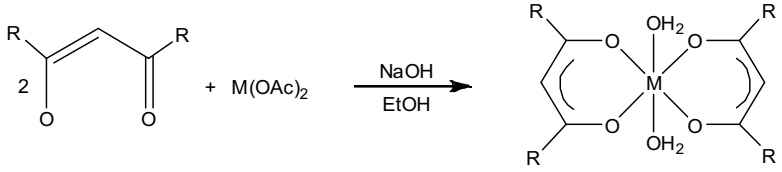

Scheme 1 Synthesis of [M(β-diketone)$_2$(H$_2$O)$_2$].

Experimental

Synthesis of $[Ni(dbm)_2(H_2O)_2]$

A suspension of dbm (2.24 g, 10 mmol) and $Ni(OAc)_2{\cdot}4H_2O$ (1.24 g, 5 mmol) in ethanol (30 ml) was stirred for 25 min. The mixture was refluxed in an oil bath at 100 °C stirred for 10 min and more ethanol (10 ml) added. NaOH (0.40 g, 10 mmol) was added to the solution and stirred for 15 min. The mixture was left at room temperature for 25 min. The green suspension was filtered through a Büchner funnel and washed with acetone (6 ml), diethylether (2 x 2 ml) and more acetone (4 x 3 ml) then dried in the air for 2 days, yield 2.54 g (94%).

Synthesis of $[Ni(tmhd)_2(H_2O)_2]$

A mixture of tmhd (2.05 g, 10 mmol) and $Ni(OAc)_2{\cdot}4H_2O$ (1.24 g, 5 mmol) in ethanol (30 ml) was refluxed and stirred in an oil bath at 100 °C stirred for 15 min; NaOH (0.40 g, 10 mmol) was added to the solution and stirred for 1 hr. The green suspension was filtered using a Büchner funnel washed with acetone (5 ml) and diethylether (5 x 2 ml) and then dried in air. The complex was placed in a dessicator overnight then kept in an oven at 70 °C for 2.50 hr to give a light green solid, yield 1.69 g (73%).

Synthesis of $[Ni(hfac)_2(H_2O)_2]$

Dissolved nickel acetate tetrahydrate (1.2443 g, 5 mmol) in water (20 ml) was dropped a solution of hexafluoroacetylacetonate (1.39 ml, 10 mmol) . The mixture was stirred 15 min. The precipitated was filtered through paper to give a green solid 2.60 g (100%).

Synthesis of $[Co(tmhd)_2(H_2O)_2]$

To a hot solution of cobalt acetate tetrahydrate (1.2454 g, 5 mmol) in 90% ethanol (25 ml) was dropped a hot solution of tetramethyheptane-3,5-dione (2.0600 ml,10 mmol) add NaOH (0.3999 g, 10 mmol) in water (4 ml). The mixture was stirred until all dissolved. The suspension was filtered through paper to give a purple solid 1.7780 g (77%).

Synthesis of $[Co(hfac)_2(H_2O)_2]$

To a solution of cobalt acetate tetrahydrate (1.2454 g, 5 mmol) in water (20 ml) was dropped tetramethyheptane-3,5-dione (1.39 ml,10 mmol). The mixture was stirred until precipitation occurred. The suspension was filtered through paper to give an orange solid 2.0600 g (81%).

4.2. Synthesis and Characterization of (4-X-phenyl)-pyridin-2-ylmethylene amine ligands (ppa^X)

The reaction between pyridine-2-carboxaldehyde and *p*-aniline in ether at room temperature yields the (4-X-phenyl)-pyridin-2-ylmethylene amine ligand in moderate yield (Scheme 2).

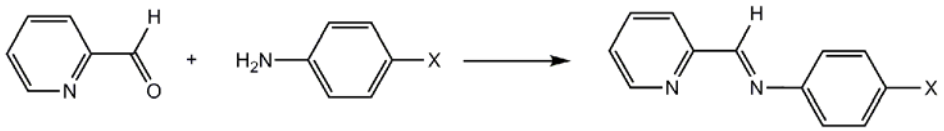

Scheme 2 Synthesis of (4-X-phenyl)-pyridin-2-ylmethylene amine ligands (ppa^X).

However, in most cases there is difficulty in obtaining the pure compound. The ^1H NMR spectrum shows that there are small amounts of starting materials and H_2O which is a by-product of the reaction. This indicates that there might be an equilibrium between the starting materials and products. A new method using molecular sieves to adsorb H_2O produced during the reaction increases the % yield and purity of the ligands (Table 1).

Table 1 Physical, IR and UV-Vis spectroscopic data for ppa^X ligands.

Compound	X	% Yield	Colour	$\nu(C=N)^a/cm^{-1}$	$\lambda/nm(\log \varepsilon/mol^{-1}\ dm^3\ cm^{-1})^b$
1	H	50	Bright yellow	1630[b]	236 (4.07), 278 (3.82), 318 (3.50)
2	Me	62	Yellow	1625	234 (4.23), 280 (4.12), 324 (4.00 sh)
3	Et	59	Brown liquid	1630[b]	234 (4.10), 280 (4.03), 324 (3.93 sh)
4	OMe	67	Light orange	1626	238 (4.11), 286 (4.01), 340 (4.08)
5	F	82	Bright yellow	1627	236 (3.91), 282 (3.91), 318 (3.75 sh)
6	Cl	70	Pale yellow	1624	238 (4.12), 280 (4.09), 320 (3.95 sh)
7	Br	76	Brown	1623	232 (4.12), 280 (4.12), 324 (3.97 sh)
8	I	69	Pale green	1625	242 (4.21), 282 (4.07), 320 (4.00 sh)

[a] As KBr disc. [b] In CH_2Cl_2

Table 2 ^{1}H NMR spectroscopic data for ppa^{X} ligands.

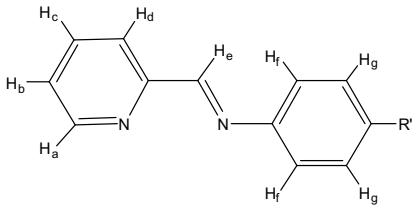

Compound	X	^{1}H NMR[a]
1	H	8.70 (d, 1H, $^{1}J_{HH}$ 4.8, H_a), 8.58 (s, 1H, H_e), 8.19 (d, 1H, $^{1}J_{HH}$ 7.8, H_d), 7.79 (m, 1H, $^{1}J_{HH}$ 7.5, H_c), 7.35 (m, 3H, H_f, H_b), 7.20 (d, 3H, H_g, H)
2	Me	8.71 (d, 1H, $^{1}J_{HH}$ 6.3, H_a), 8.62 (s, 1H, H_e), 8.19 (d, 1H, $^{1}J_{HH}$ 7.8, H_d), 7.80 (m, 1H, $^{1}J_{HH}$ 7.8, H_c), 7.35 (m, 1H, $^{1}J_{HH}$ 6.3, H_b), 7.24 (d, 4H, $^{1}J_{HH}$ 14.7, H_f, H_g), 2.36 (s, 3H, C*H*$_3$)
3	Et	8.73 (d, 1H, $^{1}J_{HH}$ 4.8, H_a), 8.68 (s, 1H, H_e), 8.24 (d, 1H, $^{1}J_{HH}$ 7.8, H_d), 7.85 (m, 1H, $^{1}J_{HH}$ 7.5, H_c), 7.23 (m, 5H, H_b, H_f, H_g), 2.69 (q, 2H, CH_2), 1.23 (t, 3H, CH_3)
4	OMe	8.70 (d, 1H, $^{1}J_{HH}$ 7.2, H_a), 8.65 (s, 1H, H_e), 8.20 (d, 1H, $^{1}J_{HH}$ 7.80, H_d), 7.81 (m, 1H, $^{1}J_{HH}$ 7.65, H_c), 7.36 (m, 1H, H_b, H_g), 6.94 (s, 2H,$^{1}J_{HH}$, H_f), 3.83 (s, 3H, CH_3)
5	F	8.80 (d, 1H, $^{1}J_{HH}$ 4.8, H_a), 8.60 (s, 1H, H_e), 8.20 (d, 1H, $^{1}J_{HH}$ 7.8, H_d), 7.90-7.79 (m, 1H, $^{1}J_{HH}$ 7.8, H_c), 7.40-7.37 (m, 1H, $^{1}J_{HH}$7.5, H_b), 7.31 (s, 2H, $^{1}J_{HH}$ 7.8, H_f), 7.09 (t, 2H, $^{1}J_{HH}$ 8.0, H_g)
6	Cl	8.80 (d, 1H, $^{1}J_{HH}$ 5.1, H_a), 8.66 (t, 1H, H_e), 8.30(d, 1H, $^{1}J_{HH}$ 8.1, H_d), 7.99-7.88 (m, 2H, $^{1}J_{HH}$ 8.1, H_c), 7.47-7.37 (m, 3H, $^{1}J_{HH}$ 9.0, H_c), 7.30 (m, 1H, $^{1}J_{HH}$ 6.9, H_f), 7.01 (t, 1H, $^{1}J_{HH}$ 8.7, H_g)
7	Br	8.79 (d, 1H, $^{1}J_{HH}$ 4.2, H_a), 8.70 (d, 2H, H_e), 8.23(d, 1H, $^{1}J_{HH}$ 7.8, H_d), 7.96-7.50 (m, 1H, $^{1}J_{HH}$ 6.9, H_c), 7.49-7.46 (m, 2H, $^{1}J_{HH}$ 6.9, H_b), 7.21 (m, 5H, $^{1}J_{HH}$ 9.6, H_f), 7.19 (t, 3H, $^{1}J_{HH}$ 4.2, H_g)
8	I	8.74 (d, 1H, $^{1}J_{HH}$ 4.8, H_a), 8.61 (s, 1H, H_e), 8.20 (d, 1H, $^{1}J_{HH}$ 7.8, H_d), 7.90-7.79 (m, 2H, $^{1}J_{HH}$ 7.8, H_c), 7.40-7.37 (m, 2H, $^{1}J_{HH}$ 7.5, H_b), 7.31 (m, 1H, H_f), 7.09 (m, 2H, $^{1}J_{HH}$ 8.0, H_g)

[a] in $CDCl_3$, chemical shift is in ppm.

IR spectroscopy of the ligands (Table 1) reveals a medium intensity imine stretch between 1623 and 1626 cm^{-1} in line with those for previously reported ppa^{X} compounds. The ^{1}H NMR spectra were recorded in $CDCl_3$ showing a singlet between 8.58-8.70 ppm for the imino proton confirming the formation of the desired ppa^{X} ligands. The peaks for the pyridyl and phenylene groups are assigned on the basis of their splitting patterns, coupling constants and intergration values and are typical of such iminopyridine ligands. The UV-Vis spectra show strong absorption in UV region which due to π-π* transitions of the ppa^{X} ligands.

Experimental

Synthesis of (Phenyl)-pyridin-2-ylmethylen-amine (ppa^{H}) 1

To a solution of aniline (273.6 µL, 3 mmol) in diethylether (10 cm^3) over molecular sieves was added pyridine-2-carboxaldehyde (265.6 µL, 3 mmol). The yellow solution was stirred over night. The solution was filter and washed with CH_2Cl_2 (5 cm^3). The solvent was removed *in vacuo* to dryness, yield bright yellow oil 0.273 g (50%).

Synthesis of (4-Methylphenyl)-pyridin-2-ylmethylen-amine (ppa^{Me}) 2

To a solution of *p*-toluidine (0.3237 g, 3 mmol) in diethylether (10 cm^3) over molecular sieves was added pyridine-2-carboxaldehyde (267.4 µL, 3 mmol). The yellow solution was stirred over night. The solution was filter and washed with CH_2Cl_2 (5 cm^3). The solvent was removed *in vacuo* to dryness, yield yellow crystallized solid 0.3604 g (62%).

Synthesis of (4-Ethylphenyl)-pyridin-2-ylmethylen-amine (ppa^{Et}) 3

To a solution of 4-ethylaniline (375.5 µL, 3 mmol) in diethylether (10 cm^3) over molecular sieves was added pyridine-2-carboxaldehyde (265.6 µL, 3 mmol). The orange solution was stirred over night. The solution was filter and washed with CH_2Cl_2 (5 cm^3). The solvent was removed *in vacuo* to dryness, yield orange brown oil 0.3752 g (59%).

Synthesis of (4-Methoxyphenyl)-pyridin-2-ylmethylen-amine (ppa^{OMe}) 4

To a solution of *p*-anisidine (0.3738 g, 3 mmol) in diethylether (10 cm^3) over molecular sieves was added pyridine-2-carboxaldehyde (265.6 µL, 3 mmol). The brown orange solution was stirred over night. The solution was filter and washed with CH_2Cl_2 (5 cm^3). The solvent was removed *in vacuo* to dryness, yield brown orange oil. The product was stored at -20 ^{o}C to yield light orange solid 0.4285 g (67%).

Synthesis of (4-Fluorophenyl)-pyridin-2-ylmethylen-amine (ppa^{F}) 5

To a solution of *p*-fluoroaniline (288.9 µL, 3 mmol) in diethylether (10 cm^3) over molecular sieves was added pyridine-2-carboxaldehyde (286.6 µL, 3 mmol). The yellow solution was stirred over night. The solution was filter and washed with CH_2Cl_2 (5 cm^3). The solvent was removed *in vacuo* to dryness, yield bright yellow crystallized solid 0.4908 g (82%).

Synthesis of (4-chlorophenyl)-pyridin-2-ylmethylen-amine (ppa^{Cl}) 6

To a solution of *p*-chloroaniline (0.3848 g, 3 mmol) in diethylether (10 cm^3) over molecular sieves was added pyridine-2-carboxaldehyde (270 µL, 3 mmol). The yellow solution was stirred over night. The solution was filter and washed with CH_2Cl_2 (5 cm^3). The solvent was removed *in vacuo* to dryness, yield pale yellow crystallized solid 0.4524 g (70%).

Synthesis of (4-Bromophenyl)-pyridin-2-ylmethylen-amine (ppa^{Br}) 7

To a stirred solution of 4-bromoaniline (0.5160 g, 3 mmol) in diethylether (10 cm^3) over molecular sieves was added a solution of pyridine-2-carboxaldehyde (288.6 µL, 3 mmol) in diethylether (10 cm^3). The brown solution was stirred for 4 hours. The solution was filter and washed with CH_2Cl_2 (5 cm^3). The solvent was removed *in vacuo* to small volume then *n*-hexane (15 cm^3). The brown solid was filtered and dried in air, yield 0.5964 g (76%).

Synthesis of (4-Iodophenyl)-pyridin-2-ylmethylen-amine (ppa^{I}) 8

To a solution of 4-iodoaniline (0.6579 g, 3 mmol) in diisopropyl ether (10 cm^3) over molecular sieves was added pyridine-2-carboxadehyde (0.2656 cm^3, 3 mmol). The light green solution was stirred 1 hour then was filtered through paper and washed with CH_2Cl_2 (10 cm^3). Solvent was removed to small volume *in vacuo* then *n*-hexane (15 cm^3) was added. The pale green solid was filtered and dried in air, yield 0.6052 g (65%).

4.3. Synthesis and characterization of [Ni(β-diketonate)$_2$(ppa^X)] complexes

The reaction between the ppa^X ligand and [Ni(β-diketonate)$_2$(H_2O)$_2$] in acetone or CH_2Cl_2 yields metal complexes namely, [Ni(β-diketonate)$_2$(ppa^X)] {β-diketonate = dbm, X = H **9**, Me **10**, Et **11**, OMe **12**, F **13**, Cl **14**, Br **15** and I **16**; β-diketonate = tmhd, X = H **17**, Me **18**, Et **19**, OMe **20**, F **21**, Cl **22**, Br **23** and I **24**; β-diketonate = hfac, X = H **25**, Me **26**, Et **27**, OMe **28**, F **29**, Cl **30**, Br **31** and I **32**}, in good yields (Scheme 3).

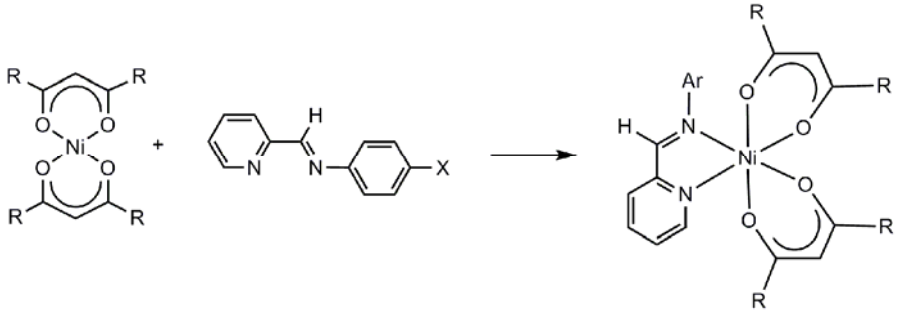

Scheme 3 Synthesis of [Ni(β-diketonate)$_2$(ppa^X)] complexes.

All complexes have been characterized by IR and UV-Vis spectroscopy, CHN analysis and mass spectrometry. CHN analysis and mass spectra confirm the purity of the complexes. IR spectroscopy of complexes **9**-**24** shows a C=O stretch from 1588-1595 cm^{-1} which indicates that the β-diketonate ligands adopt a chelating coordination mode. The position of the bands are similar to those reported for [Ni(β-diketonate)$_2$(L)] (L = phen, 2,2′-bpy, dmae). The C=O stretch for the hfac compounds, **25**-**32**, is on average 60 cm^{-1} higher than **9**-**24** consistent with the strong electron withdrawing effect of the CF_3 groups. The imine stretches of coordinated ppa^X ligands which are

expected to be between 1580 and 1590 cm^{-1} are not observed as they masked by the strong C=O stretch of the β-diketonate ligand.

The red, brown and yellow colours of these compounds are in marked contrast with the related [Ni(β-diketonate)$_2$(L)] (L = bpy, phen) complexes which are green. It is clear that the strong colour of the ppa^X ligands masks the fainter colour caused by metal 'd-d' transitions. The absorptions in the UV region are very strong and shift to higher wavelengths compared with the free ppa^X ligands.

Table 3 Physical and IR spectroscopic data of [Ni(β-diketonate)$_2$(ppa^X)] complexes.

Complex	X	% Yield	Colour	$\nu_{C=O}$[a]/cm^{-1}	λ_{max}/nm (log ε/$mol^{-1}.dm^3.cm^{-1}$)[b]
β-diketonate = dbm					
9	H	61	Yellow	1595	259 (4.84), 277 (4.81), 352 (4.60)
10	Me	55	Brown	1595	248 (4.63), 358 (4.51)
11	Et	64	Brown yellow	1595	246 (4.45), 284 (4.23 sh), 356 (4.48)
12	OMe	68	Brown	1595	250 (4.60), 282 (4.21 sh), 358 (4.54)
13	F	59	Brown yellow	1595	246 (4.66), 284 (4.33 sh), 356 (4.53)
14	Cl	63	Yellow	1594	246 (4.61), 358 (4.50)
15	Br	82	Yellow	1593	247 (4.66), 354.8 (4.47)
16	I	44	Red brown	1594	248 (4.66), 286 (4.28 sh), 354 (4.50)
β-diketonate = tmhd					
17	H	41	Brown	1591	240 (4.36), 294.2 (4.28)
18	Me	52	Red brown	1586	240 (4.46), 272 (4.26 sh), 308 (4.42)
19	Et	40	Brown oil	1591	240 (4.40), 308 (4.35)
20	OMe	37	Red brown	1592	242 (4.51), 316 (4.42) 354 (4.31 sh).
21	F	32	Brown green	1591	238 (4.46), 272 (4.27), 308 (4.45)
22	Cl	42	Red brown	1588	240 (4.27), 303 (4.24)
23	Br	29	Red brown	1592	244 (4.39)
24	I	49	Brown	1592	252 (4.50), 276 (4.38)
β-diketonate = hfac					
25	H	46	Brown yellow	1652	243.5 (4.26), 285 (4.36), 314.8 (4.35)
26	Me	98	Green	1653	242 (4.20), 318 (4.40)
27	Et	31	Yellow green	1654	247 (4.23), 320 (4.31)
28	OMe	54	Brown yellow	1647	255 (4.27), 325 (4.26)
29	F	78	Brown	1651	238 (4.26), 318 (4.45)
30	Cl	58	Green yellow	1651	240 (4.25), 319.4 (4.38)
31	Br	52	Yellow green	1651	241.5 (4.34), 318.5 (4.46)
32	I	54	Green	1654	244 (4.40), 320 (4.41)

[a] As KBr disc. [b] In CH_2Cl_2

Experimental

Synthesis of [Ni(dbm)$_2$(ppa^H)] 9

To a lime green suspension of [Ni(dbm)$_2$(H$_2$O)$_2$] (0.1353 g, 0.25 mmol) in acetone (10 cm^3) was added a solution of ppa^H (0.0456 g, 0.25 mmol) in acetone (3 cm^3). The brown orange solution was stirred over night then concentrated *in vacuo*. *n*-Hexane (10 cm^3) was added to precipitate a brown solid which was washed with *n*-hexane (2 x 5 cm^3) and dried *in vacuo*, yield brown solid 0.1057 g (61%).

Synthesis of [Ni(dbm)$_2$(ppa^{Me})] 10

To a stirred lime green suspension of [Ni(dbm)$_2$(H$_2$O)$_2$] (0.270 g, 0.5 mmol) in acetone (20 cm^3) the light yellow solution of ppa^{Me} (0.1026 g, 0.52 mmol) in acetone (5 cm^3) was added dropwise. The dark red solution was stirred for 2 hours then evaporated to dryness *in vacuo* to give brown green solid. The solid was purified using CH_2Cl_2-*n*-hexane to give green brown micro crystals yield 0.2067 g (55%).

Synthesis of [Ni(dbm)$_2$(ppa^{Et})] 11

To a stirred lime green suspension of [Ni(dbm)$_2$(H$_2$O)$_2$] (0.1359 g, 0.25 mmol) in acetone (10 cm^3) the light yellow solution of ppa^{Et} (0.0547 g, 0.52 mmol) in acetone (2 cm^3) was added dropwise. The brown solution was stirred over night then concentrated *in vacuo*. *n*-Hexane (10 cm^3) was added to precipitate a brown yellow solid which was washed with *n*-hexane (2 x 5 cm^3) and dried *in vacuo*, yield brown yellow solid 0.1152 g (64%)

Synthesis of [Ni(dbm)$_2$(ppa^{OMe})] 12

To a stirred lime green suspension of [Ni(dbm)$_2$(H$_2$O)$_2$] (0.1340 g, 0.25 mmol) in acetone (10 cm^3) the light yellow solution of ppa^{OMe} (0.0527 g, 0.25 mmol) in acetone (3 cm^3) was added dropwise. The red orange solution was stirred over night. The solvent was removed to small volume *in vacuo* then *n*-hexane (15 cm^3) was added. The yellow brown solid was filtered and dried in air, yield 0.1223 g (68%).

Synthesis of [Ni(dbm)$_2$(ppa^F)] 13

To a stirred lime green suspension of [Ni(dbm)$_2$(H$_2$O)$_2$] (0.2706 g, 0.5 mmol) in acetone (20 cm^3) the light yellow solution of ppa^F (0.1051 g, 0.52 mmol) in acetone (5 cm^3) was added dropwise. The red-brown solution was stirred for 2 hours. Solvent was removed to small volume *in vacuo* then *n*-Hexane (5 cm^3) was added. The brown solid was filtered and was purified using CH_2Cl_2-*n*-hexane to give brown-yellow micro crystals yield 0.2222 g (59%).

Synthesis of [Ni(dbm)$_2$(ppa^{Cl})] 14

To a lime green suspension of [Ni(dbm)$_2$(H$_2$O)$_2$] (0.1348 g, 0.25 mmol) in acetone (10 cm^3) was added a solution of ppa^{Cl} (0.0546 g, 0.25 mmol) in acetone (3 cm^3). The orange-yellow solution

was stirred over night then concentrated *in vacuo*. *n*-Hexane (10 cm^3) was added to precipitate a yellow solid which was washed with *n*-hexane (2 x 5 cm^3) and dried *in vacuo*, yield 0.1135 g (63%).

Synthesis of [Ni(dbm)$_2$(ppa^{Br})] 15

To a lime green suspension of [Ni(dbm)$_2$(H_2O)$_2$] (0.1353 g, 0.25 mmol) in acetone (10 cm^3) was added a solution of ppa^{Br} (0.0653 g, 0.25 mmol) in acetone (3 cm^3). The yellow suspension was stirred 1 hour then concentrated *in vacuo*. *n*-Hexane (15 cm^3) was added to precipitate a yellow solid which was washed with *n*-hexane (2 x 5 cm^3) and dried *in vacuo*, yield 0.1577 g (82%).

Synthesis of [Ni(dbm)$_2$(ppa^{I})] 16

To a lime green solution of [Ni(dbm)$_2$(H_2O)$_2$] (0.1353 g, 0.25 mmol) in THF (10 cm^3) was added a solution of ppa^{I} (0.0768 g, 0.25 mmol) in THF (3 cm^3). The dark brown solution was stirred 1 hour then concentrated *in vacuo*. *n*-Hexane (20 cm^3) was added to precipitate a brown solid which was washed with *n*-hexane (2 x 5 cm^3) and dried *in vacuo*, yield 0.0908 g (44%).

Synthesis of [Ni(tmhd)$_2$(ppa^{H})] 17

To a lime green solution of [Ni(tmhd)$_2$(H_2O)$_2$] (0.1153 g, 0.25 mmol) in THF (10 cm^3) was added a yellow solution of ppa^{H} (0.0459 g, 0.25 mmol) in THF (3 cm^3). The brown solution was stirred 2 hours then concentrated *in vacuo*. *n*-Hexane (10 cm^3) was added to precipitate a brown solid which was washed with *n*-hexane (5 cm^3) and dried *in vacuo*, yield 0.0625 g (41%).

Synthesis of [Ni(tmhd)$_2$(ppa^{Me})] 18

To a stirred purple solution of [Ni(tmhd)$_2$(H_2O)$_2$] (0.1172 g, 0.25 mmol) in CH_2Cl_2 (10 cm^3) was added a yellow solution of ppa^{Me} (0.0495 g, 0.25 mmol) in CH_2Cl_2 (5 cm^3). The orange solution was stirred 2 hours then the solution was filtered through celite. The brown needle micro crystals were grown by allowing a solution of the complex to evaporate slowly to dryness, yield 0.0803 g (52%).

Synthesis of [Ni(tmhd)$_2$(ppa^{Et})] 19

To a stirred purple solution of [Ni(tmhd)$_2$(H_2O)$_2$] (0.1181 g, 0.26 mmol) in CH_2Cl_2 (5 cm^3) was added a yellow solution of ppa^{Et} (0.0558 g, 0.28 mmol) in CH_2Cl_2 (2 cm^3). The orange solution was stirred 3 hours then the solution was filtered through celite. The volume was reduced *in vacuo* to give brown oil, yield 0.0661 g (40%).

Synthesis of [Ni(tmhd)$_2$(ppa^{OMe})] 20

To a stirred green solution of [Ni(tmhd)$_2$(H_2O)$_2$] (0.1529 g, 0.33 mmol) in THF (5 cm^3) was added a yellow solution of ppa^{OMe} (0.0705 g, 0.33 mmol) in THF (2 cm^3). The brown solution was stirred 30 minutes then the solution was filtered through celite. The volume was reduced to *ca.* 1 cm^3 *in vacuo* then *n*-hexane (5 cm^3) was added to precipitate a red brown solid which was washed with *n*-hexane (5 cm^3) and dried *in vacuo*, yield 0.0790 g (37%).

Synthesis of [Ni(tmhd)$_2$(ppa^F)] 21

To a stirred purple solution of [Ni(tmhd)$_2$(H$_2$O)$_2$] (0.1115 g, 0.24 mmol) in CH_2Cl_2 (10 cm^3) was added a yellow solution of ppa^F (0.0473 g, 0.25 mmol) in CH_2Cl_2 (5 cm^3). The orange solution was stirred 2 hours then the solution was filtered through celite. The brown needle micro crystals were grown by allowing a solution of the complex to evaporate slowly to dryness, yield 0.048 g (32%).

Synthesis of [Ni(tmhd)$_2$(ppa^{Cl})] 22

To a stirred green solution of [Ni(tmhd)$_2$(H$_2$O)$_2$] (0.1143 g, 0.25 mmol) in THF(5 cm^3) was added a yellow solution of ppa^{Cl} (0.0545 g, 0.25 mmol) in THF (3 cm^3). The brown solution was stirred 30 minutes then the solution was filtered through celite. The volume was reduced *in vacuo* then *n*-hexane (5 cm^3) was added to precipitate a red brown solid which was washed with *n*-hexane (5 cm^3) and dried *in vacuo*, yield 0.0677 g (42%).

Synthesis of [Ni(tmhd)$_2$(ppa^{Br})] 23

To a stirred green solution of [Ni(tmhd)$_2$(H$_2$O)$_2$] (0.1153 g, 0.25 mmol) in THF (10 cm^3) was added a yellow solution of ppa^I (0.0653 g, 0.25 mmol) in THF (3 cm^3). The brown solution was stirred 2 hours then concentrated *in vacuo*. *n*-Hexane (10 cm^3) was added to precipitate a brown solid which was washed with *n*-hexane (5 cm^3) and dried *in vacuo*, yield 0.0511 g (29%).

Synthesis of [Ni(tmhd)$_2$(ppa^I)] 24

To a stirred purple solution of [Ni(tmhd)$_2$(H$_2$O)$_2$] (0.1153 g, 0.25 mmol) in THF (10 cm^3) was added a yellow solution of ppa^I (0.0768 g, 0.25 mmol) in THF (3 cm^3). The brown solution was stirred 2 hours then concentrated *in vacuo*. *n*-Hexane (10 cm^3) was added to precipitate a brown solid which was washed with *n*-hexane (5 cm^3) and dried *in vacuo*, yield 0.0912 g (49%).

Synthesis of [Ni(hfac)$_2$(ppa^H)] 25

To a stirred green solution of [Ni(hfac)$_2$(H$_2$O)$_2$] (0.1272 g, 0.25 mmol) in THF (10 cm^3) was added a yellow solution of ppa^H (0.0528 g, 0.25 mmol) in THF (3 cm^3). The yellow solution was stirred 1 hour then concentrated *in vacuo*. *n*-Hexane (15 cm^3) was added to precipitate a yellow solid which was washed with *n*-hexane (5 cm^3) and dried *in vacuo*, yield 0.0755 g (46%).

Synthesis of [Ni(hfac)$_2$(ppa^{Me})] 26

To a stirred green solution of [Ni(hfac)$_2$(THF)$_2$] (0.156 g, 0.25 mmol) in CH_2Cl_2 (5 cm^3) was added a yellow solution of ppa^{Me} (0.050 g, 0.25 mmol) in CH_2Cl_2 (1 cm^3). The orange solution was stirred over night then concentrated *in vacuo*. *n*-Hexane (10 cm^3) was added to precipitate a green brown solid which was washed with *n*-hexane (5 cm^3) and dried *in vacuo*, yield 0.181 g (98%).

Synthesis of [Ni(hfac)$_2$(ppa^{Et})] 27

To a stirred green solution of [Ni(hfac)$_2$(H$_2$O)$_2$] (0.1272 g, 0.25 mmol) in THF (10 cm^3) was added a yellow solution of ppa^{Et} (0.0528 g, 0.25 mmol) in THF (3 cm^3). The brown solution was

stirred 1 hour then concentrated *in vacuo*. *n*-Hexane (15 cm^3) was added to precipitate a brown solid which was washed with *n*-hexane (5 cm^3) and dried *in vacuo*, yield 0.0545 g (31%).

Synthesis of [Ni(hfac)$_2$(ppa^{OMe})] 28

To a stirred green solution of [Ni(hfac)$_2$(H$_2$O)$_2$] (0.1272 g, 0.25 mmol) in THF (10 cm^3) was added a yellow solution of ppa^{OMe} (0.0528 g, 0.25 mmol) in THF (3 cm^3). The deep yellow solution was stirred 1 hour then concentrated *in vacuo*. *n*-Hexane (15 cm^3) was added to precipitate a deep yellow solid which was washed with *n*-hexane (5 cm^3) and dried *in vacuo*, yield 0.0980 g (54%).

Synthesis of [Ni(hfac)$_2$(ppa^{F})] 29

To a stirred green solution of [Ni(hfac)$_2$(THF)$_2$] (0.1532 g, 0.25 mmol) in CH_2Cl_2 (5 cm^3) was added a yellow solution of ppa^{F} (0.050 g, 0.25 mmol) in CH_2Cl_2 (1 cm^3). The green-yellow solution was stirred over night then concentrated *in vacuo*. *n*-Hexane (10 cm^3) was added to precipitate a brown solid which was washed with *n*-hexane (5 cm^3) and dried *in vacuo*, yield 0.131 g (78%).

Synthesis of [Ni(hfac)$_2$(ppa^{Cl})] 30

To a green solution of [Ni(hfac)$_2$(H$_2$O)$_2$] (0.1272 g, 0.25 mmol) in CH_2Cl_2 (5 cm^3) was added a solution of ppa^{Cl} (0.0542 g, 0.25 mmol) in CH_2Cl_2 (3 cm^3). The golden brown solution was stirred 1 hour then concentrated *in vacuo*. *n*-Hexane (15 cm^3) was added to precipitate a golden brown solid which was washed with *n*-hexane (2 x 5 cm^3) and dried *in vacuo*, yield 0.1008 g (58%).

Synthesis of [Ni(hfac)$_2$(ppa^{Br})] 31

To a green solution of [Ni(hfac)$_2$(H$_2$O)$_2$] (0.1272 g, 0.25 mmol) in CH_2Cl_2 (5 cm^3) was added a solution of ppa^{Br} (0.0653 g, 0.25 mmol) in CH_2Cl_2 (3 cm^3). The deep yellow solution was stirred 1 hour then concentrated *in vacuo*. *n*-Hexane (15 cm^3) was added to precipitate a deep yellow solid which was washed with *n*-hexane (2 x 5 cm^3) and dried *in vacuo*, yield 0.0964 g (52%).

Synthesis of [Ni(hfac)$_2$(ppa^{I})] 32

To a stirred green solution of [Ni(hfac)$_2$(H$_2$O)$_2$] (0.1272 g, 0.25 mmol) in THF (10 cm^3) was added a yellow solution of ppa^{I} (0.0768 g, 0.25 mmol) in THF (3 cm^3). The yellow solution was stirred 1 hour then concentrated *in vacuo*. *n*-Hexane (15 cm^3) was added to precipitate a yellow solid which was washed with *n*-hexane (5 cm^3) and dried *in vacuo*, yield 0.1072 g (54%).

X-ray structural studies of [Ni(β-diketonate)$_2$(ppa^{X})] complexes

Crystals of [Ni(dbm)$_2$(ppa^{Me})] **10**, [Ni(dbm)$_2$(ppa^{OMe})] **12**, [Ni(dbm)$_2$(ppa^{Cl})] **14** and [Ni(hfac)$_2$(ppa^{Br})] **31** were obtained by slow diffusion of *n*-hexane into a concentrated solution of the complex in CH_2Cl_2. The structures and crystallographic data are presented in Figures 1 and 2 for complexes **10** and **12** respectively.

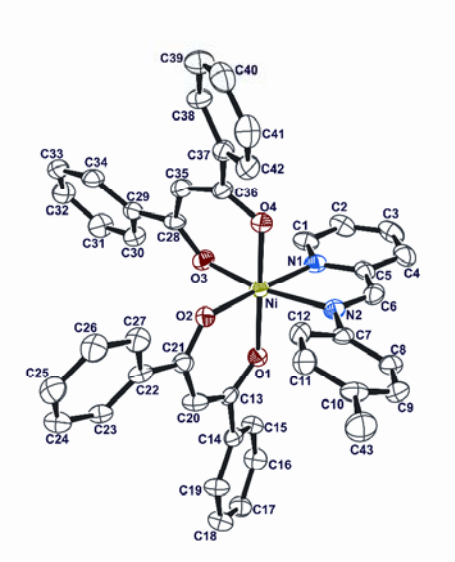

Figure 1 ORTEP diagram of [Ni(dbm)$_2$(ppa^{Me})] **10**. The thermal ellipsoids are drawn to 50% probability level. Hydrogen atoms are omitted for clarity.

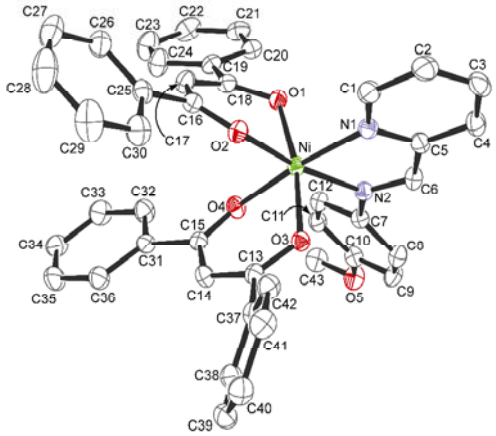

Figure 2 ORTEP diagram of [Ni(dbm)$_2$(ppa^{OMe})] **12**. The thermal ellipsoids are drawn to 50% probability level. Hydrogen atoms are omitted for clarity.

Complexes **10**, **12**, **14** and **31** assume slightly distorted octahedral coordination geometries. The β-diketonate ligands exhibit a *cis* arrangement enforced by the chelating ppa^X ligand. The Ni-O bond lengths vary between 2.005-2.066 Å for the four complexes and are similar to other previously reported nickel β-diketonate adducts, [Ni(dbm)$_2$(en)] {2.009(6), 2.060(7) Å} and [Ni(dbm)$_2$(phen)] {2.035(1), 2.041(1) Å}.

The nickel bond to the pyridine of the ppa^X ligand of complexes **10** and **14** is considerably shorter than the bond to the imine nitrogen differing by *ca*. 0.1 Å. In contrast, the Ni-N bonds lengths for **12** and **31** are different by only 0.03 and 0.05 Å, respectively. It is also interesting to note that in [Cu(ppa^{2Me,3Me})$_2$]ClO$_4$ and [Ru(bipy)$_2$(ppa^H)][PF$_6$]$_2$ the imine nitrogen metal bond is shorter than the pyridine nitrogen metal bond. The reason for this difference remains unclear. The phenyl ring in all the complexes is twisted with respect to the pyridylimine unit. Interestingly, the angle for

12 is 39.5° while those of **10**, **14** and **31** are 22.9°, 24.0° and 30.0°, respectively. By comparison $[Cu(ppa^{2Me,3Me})_2]ClO_4$ and $[Ru(bipy)_2(ppa^{H})][PF_6]_2$ exhibit angles of 69° and 45°, respectively. The phenyl ring is positioned above the pyridyl ring of a neighbouring ppa^{X} ligand but is neither co-planar with, nor perpendicular to, that pyridyl ring.

Table 4 Selected bond lengths (Å) and angles (°) of **10**, **12**, **14** and **31.**

	10	**12**	**14**	**31**
Ni-O(1)	2.013(3)	2.0349(12)	2.0091(16)	2.066(3)
Ni-O(2)	2.005(3)	2.0135(12)	2.0205(17)	2.045(3)
Ni-O(3)	2.027(3)	2.0479(12)	2.0165(16)	2.020(3)
Ni-O(4)	2.010(4)	2.0163(12)	2.0128(16)	2.044(3)
Ni-N(1)	2.090(4)	2.0812(14)	2.091(2)	2.113(4)
Ni-N(2)	2.180(4)	2.1096(14)	2.189(2)	2.063(3)
O(1)-Ni-O(2)	89.05(14)	88.93(5)	90.66(6)	87.99(12)
O(3)-Ni-O(4)	90.58(14)	88.18(5)	89.29(6)	87.79(12)
N(1)-Ni-N(2)	76.81(16)	78.60(6)	77.31(8)	79.35(14)
β^{a}	2.98	31.94	16.57	11.00
	17.06	24.72	1.51	26.80
γ^{b}	22.87	39.50	23.99	30.00
Intermolecular distances[c]				
O(1)-H(8)	2.439			
O(3)-H(8)		2.615	2.396	
O(3)-H(6)		2.578		
O(1)-H(12)				2.532(4)
O(4)-H(11)				2.610(3)

[a] β is the angle between the plane defined by the carbon and oxygen atoms of the β-diketonate ligand and the plane defined by the nickel and two oxygen atoms. [b] γ is the angle between the plane of the pyridylimine unit and the plane of the substituted phenyl ring. [c] Non-bonded metrics and those involving centroids were not included in the structure refinement, and thus do not have an e.s.d.

The β-diketonate ligand is essentially planar and symmetric suggesting that the negative charge is delocalized over the β-diketonate framework. As noted in other nickel β-diketonate adducts the nickel centre lies above the plane of the dbm ligand in a 'bent' coordination mode. The extent of this displacement has been determined by calculating the angle between the plane of the β-diketonate framework and the plane defined by the nickel and two oxygen atoms (see Figure 3). For complex **12** both dbm ligands exhibit a 'bent' coordination mode while for **10**, **14** and **31** only

one of the dbm or hfac ligands is 'bent' with the other assuming a 'planar' coordination mode. This is probably the result of the different substituents on the ppa^X ligands.

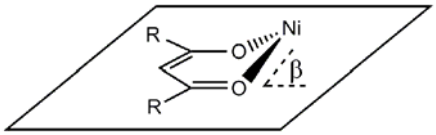

Figure 3 Schematic diagram showing the angle β between the β-diketonate and NiO_2 planes.

The complexes are packed into chiral columns with each column exhibiting the same helicity and adjacent columns of alternate helicity as shown in Figures 4 and 5. The molecules are arranged so that the ppa^X ligands are positioned above one another with the substituent alternately pointing 'in' and 'out'. The interaction principally involved here is between a C-H group from the phenyl ring of the ppa^X ligand and a coordinated oxygen atom from the dbm ligand. The structure of **12** is slightly different revealing a further interaction from the imino C-H to the same oxygen atom. As a result of the stacking of the ppa^X ligands the dbm ligands are also stacked in columns. As might be expected this leads to π-π interactions between two adjacent dbm phenyl rings (centroid-centroid 3.653 and 3.651 Å for **10** and **14**, respectively). The absence of this interaction in the structure of **12** once again seems to stem from the extra space needed to accommodate the ppa^{OMe} ligand and the subsequent 'bent' coordination mode of *both* dbm ligands which preclude this interaction. Surprisingly, the π-π interaction is not replaced by any face to edge CH…π interactions.

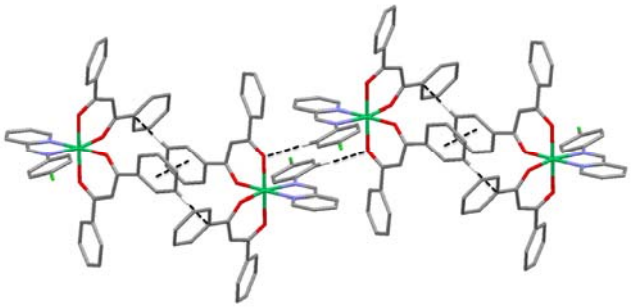

Figure 4 Mercury plot showing the CH...O and π-π interactions in $[Ni(dbm)_2(ppa^{Cl})]$ **14**. For clarity only hydrogen atoms involved in interactions are shown.

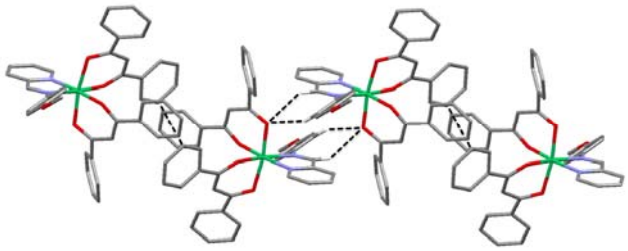

Figure 5 Mercury plot showing the CH...O interactions in $[Ni(dbm)_2(ppa^{OMe})]$ **12**. For clarity only hydrogen atoms involved in interactions are shown.

Electron transfer studies of [Ni(β-diketonate)$_2$(ppa^X)] complexes

Electrochemical studies of metal complexes **9**-**32** were conducted in CH_2Cl_2 between ±1.8 V *versus* Ag-AgCl electrode at room temperature using a three-electrode configuration. The [Ni(dbm)$_2$(ppa^X)] complexes, **9**-**16**, show a one-electron irreversible oxidation process while the [Ni(tmhd)$_2$(ppa^X)] complexes, **17**-**24**, reveal a quasi-reversible one-electron oxidation. As expected, when the β-diketonate is the most electron withdrawing, [Ni(hfac)$_2$(ppa^X)] complexes, **25**-**32**, the oxidation potential cannot be observed which might be due to the higher potential and thus outside the solvent window. In contrast, all the *hfac* complexes undergo irreversible reduction processes (Figure 6 and Table 5).

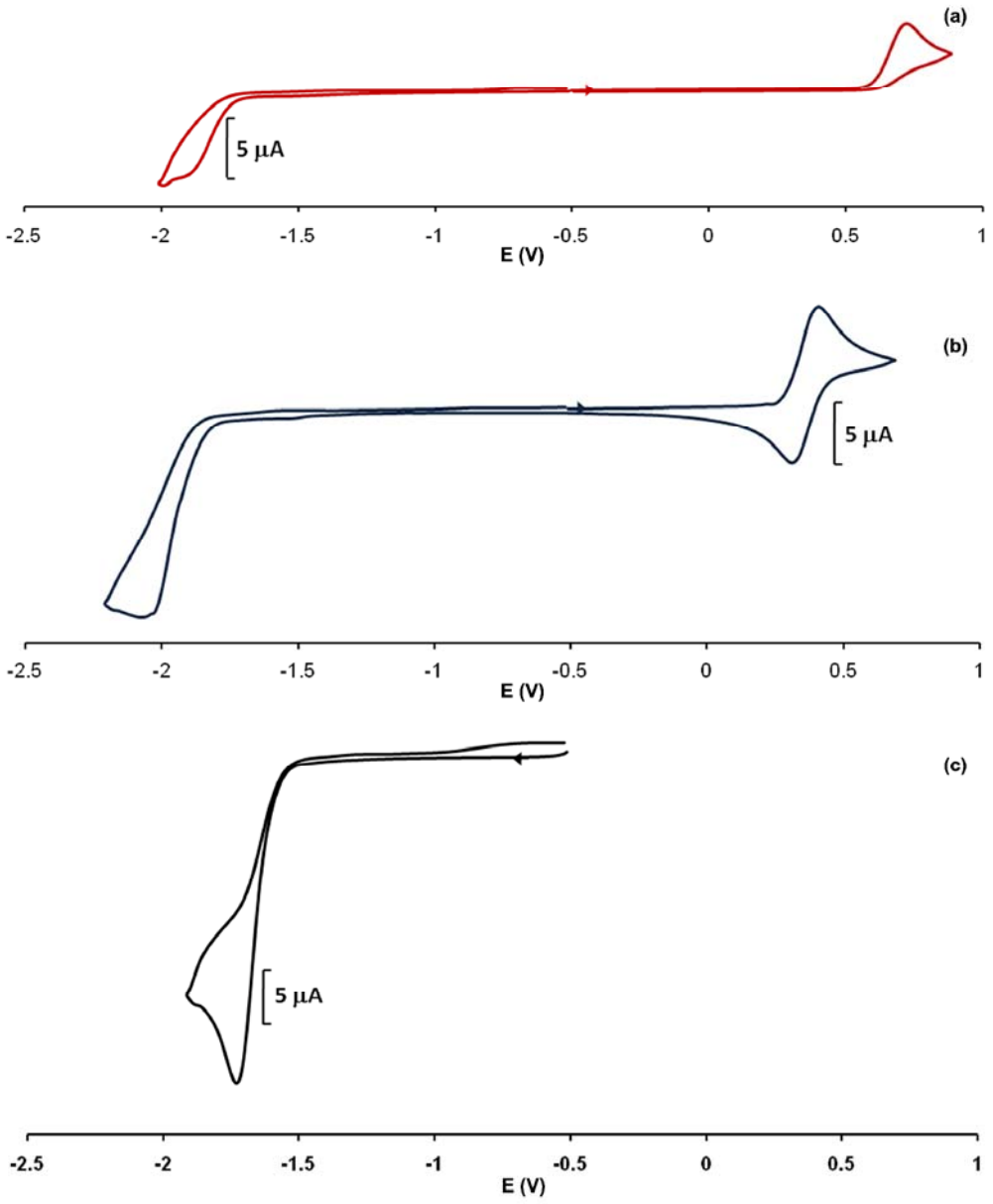

Figure 6 Cyclic voltammograms of (a) [Ni(dbm)$_2$(ppa^F)] **13**, (b) [Ni(tmhd)$_2$(ppa^F)] **21**, (c) [Ni(hfac)$_2$(ppa^F)] **29**.

Table 5 Electrochemical data for [Ni(β-diketonate)$_2$(ppa^X)].[a]

		E_{ox} (V)[b]	E_p^{red} (V)
9	[Ni(dbm)$_2$(ppa^H)]	1.19 (I)	-
10	[Ni(dbm)$_2$(ppa^{Me})]	1.18 (I)	-
11	[Ni(dbm)$_2$(ppa^{Et})]	1.18 (I)	-
12	[Ni(dbm)$_2$(ppa^{OMe})]	1.18 (I)	-
13	[Ni(dbm)$_2$(ppa^F)]	1.20 (I)	-1.42 (I)
14	[Ni(dbm)$_2$(ppa^{Cl})]	1.24 (I)	-1.32 (I)
15	[Ni(dbm)$_2$(ppa^{Br})]	1.20 (I)	-1.33 (I)
16	[Ni(dbm)$_2$(ppa^I)]	1.22 (I)	-1.31 (I)
17	[Ni(tmhd)$_2$(ppa^H)]	0.85	-
18	[Ni(tmhd)$_2$(ppa^{Me})]	0.84	-
19	[Ni(tmhd)$_2$(ppa^{Et})]	0.83	
20	[Ni(tmhd)$_2$(ppa^{OMe})]	0.84, 1.49 (I)	-
21	[Ni(tmhd)$_2$(ppa^F)]	0.87	-1.57 (I)
22	[Ni(tmhd)$_2$(ppa^{Cl})]	0.87	-1.49 (I)
23	[Ni(tmhd)$_2$(ppa^{Br})]	0.88	-1.46 (I)
24	[Ni(tmhd)$_2$(ppa^I)]	0.89	-1.48 (I)
25	[Ni(hfac)$_2$(ppa^H)]	-	-1.24 (I)
26	[Ni(hfac)$_2$(ppa^{Me})]	-	-1.27 (I)[c]
27	[Ni(hfac)$_2$(ppa^{Et})]	-	-1.17 (I)
28	[Ni(hfac)$_2$(ppa^{OMe})]	-	-1.22 (I)
29	[Ni(hfac)$_2$(ppa^F)]	-	-1.21 (I)[c]
30	[Ni(hfac)$_2$(ppa^{Cl})]	-	-1.05 (I)
31	[Ni(hfac)$_2$(ppa^{Br})]	-	-1.09 (I)
32	[Ni(hfac)$_2$(ppa^I)]	1.10 (I)	-1.09 (I)

[a] All measurements were performed at 298 K, in dried and degassed CH_2Cl_2 0.1 M [NBu^n_4][PF_6] solution; scan rate 100 mVs^{-1}; calibrated with [Fe(η-C_5H_5)$_2$], $E^{o\prime}$ = 0.52 V. [b] E_{ox} represents $E^{o\prime}$ if the oxidation is reversible and the peak potential, E_p^{ox} if the oxidation is irreversible. [c] Uncalibrated as the compound reacts with [Fe(η-C_5H_5)$_2$].

In all cases when the substituent on the ppa^X ligands is halide there is an irreversible reduction wave which might due to the reduction of the ppa^X ligands. Interestingly, the oxidation potential of complexes **9**-**24** indicate that the substituent on the ppa^X ligands does not play an important role in the electron transfer behavior of the metal complexes but the substituents on the

β-diketonate are more effective. As predicted, tmhd, the most electron donating substituents on the β-diketonate, has the lowest oxidation potential while hfac, the most electron withdrawing, the oxidation potential is very high beyond the limit of the solvent window. Comparison of oxidation potential of complexes **9**-**24** with those of [Ni(β-diketonate)$_2$(L)] (β-diketonate = dbm or tmhd, L = phen, 2,2′-bpy and dmae) found that the potentials are very similar which confirm that the substituents on β-diketonate ligands are involved in affecting the electron density on the metal more than the N-N ligand.

Attempts to oxidize the *tmhd* compounds did not produce expected cations showing that these compounds are only reversible on the CV time scale. However, preliminary DFT calculations suggest that oxidation occurred at metal centre giving low spin d^7 Ni(III). Further work is underway with Prof. Eric McInnes at University of Manchester, UK to use variable temperature EPR-electrochemistry to confirm these findings.

4.4. Synthesis and characterization of [Co(β-diketonate)$_2$(ppa^X)] complexes

The reaction between the ppa^X ligand and [Co(β-diketonate)$_2$(H_2O)$_2$] in THF yields metal complexes namely, [Co(β-diketonate)$_2$(ppa^X)] {β-diketonate = dbm, X = H **33**, Me **34**, Et **35**, OMe **36**, F **37**, Cl **38**, Br **39** and I **40**; β-diketonate = tmhd, X = H **41**, Me **42**, Et **43**, OMe **44**, F **45**, Cl **46**, Br **47** and I **48**; β-diketonate = hfac, X = H **49**, Me **50**, Et **51**, OMe **52**, F **53**, Cl **54**, Br **55** and I **56**}, in good yield (Scheme 4).

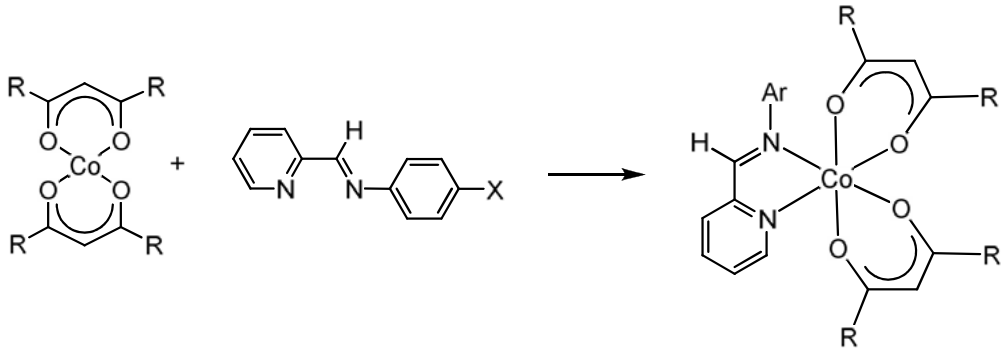

Scheme 4 Synthesis of [Co(β-diketonate)$_2$(ppa^X)] complexes

Table 6 Physical and IR spectroscopic data of [Co(β-diketonate)$_2$(ppa^X)] complexes.

Complex	X	% Yield	Colour	$\nu_{C=O}$[a]/cm^{-1}	λ_{max}/nm (log ε/mol^{-1}.dm^3.cm^{-1})[b]
β-diketonate = dbm					
33	H	76	Red	1594	274 (5.06), 345 (4.56)
34	Me	75	Rusted red	1593	246 (4.62), 342 (4.62)
35	Et	70	Deep red	1594	246 (4.63), 344 (4.63)
36	OMe	49	Orange	1596	250 (4.63), 350 (4.66)
37	F	41	Red	1595	246 (4.62), 346 (4.60)
38	Cl	67	Deep red	1593	246 (4.63), 342 (4.62)
39	Br	72	Red	1592	248 (4.96), 333 (4.47)
40	I	54	Rusted red	1593	250 (4.63), 340 (4.60)
β-diketonate = tmhd					
41	H	80	Red	1586	287 (4.32)
42	Me	52	Red	1590	234 (4.40), 288 (4.38), 336 (4.09 sh)
43	Et	63	Deep red	1588	282 (4.36)
44	OMe	54	Brick red	1589	248 (4.29), 284 (4.30), 348 (4.05 sh)
45	F	31	Red	1588	236 (4.26), 288 (4.30)
46	Cl	69	Bunt red	1590	242 (4.26), 288 (4.30)
47	Br	82	Red	1587	285(4.59)
48	I	52	Red	1588	254 (4.43), 284 (4.40), 336 (4.07 sh)
β-diketonate = hfac					
49	H	88	Orange	1647	242 (4.08), 306 (4.34)
50	Me	87	Orange	1649	244 (4.27), 308 (4.46)
51	Et	51	Orange	1649	245 (4.24), 308 (4.34)
52	OMe	78	Yellow brown	1649	252 (4.20), 307 (4.27)
53	F	91	Orange	1646	242 (4.15), 306 (4.39)
54	Cl	71	Orange	1646	243 (4.19), 309 (4.39)
55	Br	77	Orange	1647	243 (4.24), 309 (4.42)
56	I	52	Golden brown	1648	244 (4.29), 310 (4.34)

[a] As KBr disc. [b] In CH_2Cl_2

All complexes have been characterized by IR and UV-Vis spectroscopy, CHN analysis and mass spectrometry. CHN analysis and mass spectra confirm the purity of the complexes. IR spectroscopy of complexes **33**-**48** shows C=O stretch from 1586-1596 cm^{-1} indicating that the β-

diketonate ligands adopt a chelating coordination mode. The position of the bands are similar to those reported for [Co(β-diketonate)$_2$(L)] (L = phen, 2,2′-bpy, dmae) and the Ni analogues, [Ni(β-diketonate)$_2$(ppa^X)] **9-24**. The C=O stretch for the hfac compounds, **49**-**56**, is on average 60 cm^{-1} higher than **33**-**48** consistent with the strong electron withdrawing effect of the CF_3 groups. The imine stretches of coordinated ppa^X ligands which are expected to be between 1580 and 1590 cm^{-1} are not observed as they masked by the strong C=O stretch of the β-diketonate ligand.

Again the strong colour of the ppa^X ligands masks the fainter colour caused by metal 'd-d' transitions. The absorptions in UV region are very strong and shift to higher wavelength compared with the free ppa^X ligands.

Experimental

Synthesis of [Co(dbm)$_2$(ppa^H)] 33

To a yellow suspension of [Co(dbm)$_2$(H_2O)$_2$] (0.1353 g, 0.25 mmol) in acetone (10 cm^3) was added a solution of ppa^H (0.0456 g, 0.25 mmol) in acetone (3 cm^3). The brown orange solution was stirred over night then concentrated *in vacuo*. *n*-Hexane (10 cm^3) was added to precipitate a brown solid which was washed with *n*-hexane (2 x 5 cm^3) and dried *in vacuo*, yield red solid 0.1320 g (76%).

Synthesis of [Co(dbm)$_2$(ppa^{Me})] 34

To an orange solution of [Co(dbm)$_2$(H_2O)$_2$] (0.1357 g, 0.25 mmol) in THF (20 cm^3) was added a solution of ppa^{Me} (0.0518 g, 0.25 mmol) in THF (2 cm^3). The mixture was stirred for 2 hours to give a red solution then concentrated *in vacuo*. *n*-Hexane (10 cm^3) was added to precipitate a red brown solid. The complex was recrystallized by allowing a concentrated CH_2Cl_2 solution to diffuse slowly into *n*-hexane to give red microcrystals, yield 0.1322 g (75%).

Synthesis of [Co(dbm)$_2$(ppa^{Et})] 35

To a stirred orange solution of [Co(tmhd)$_2$(H_2O)$_2$] (0.1360 g, 0.25 mmol) in THF (10 cm^3) was added a yellow solution of ppa^{Et} (0.0550 g, 0.25 mmol) in THF (3 cm^3). The red solution was stirred over night then concentrated *in vacuo*. *n*-Hexane (10 cm^3) was added to precipitate a deep red solid which was washed with *n*-hexane (5 cm^3) and dried *in vacuo*, yield 0.1251 g (70%).

Synthesis of [Co(dbm)$_2$(ppa^{OMe})] 36

To a stirred orange solution of [Co(tmhd)$_2$(H_2O)$_2$] (0.1346 g, 0.25 mmol) in THF (10 cm^3) was added a yellow solution of ppa^{OMe} (0.0529 g, 0.25 mmol) in THF (3 cm^3). The deep red solution was stirred over night then concentrated *in vacuo*. *n*-Hexane (10 cm^3) was added to precipitate a orange solid which was washed with *n*-hexane (5 cm^3) and dried *in vacuo*, yield 0.0872 g (49%).

Synthesis of [Co(dbm)$_2$(ppa^F)] 37

To a stirred orange solution of [Co(dbm)$_2$(H$_2$O)$_2$] (0.1350 g, 0.25 mmol) in THF (20 cm^3) was added ppa^F (0.050 g, 0.25 mmol). The mixture was stirred for 2 hours, to give a red-brown solution, then the solvent was removed to give a dark red solid. The dark red solid was washed with *n*-hexane and dried in air to give a brown solid 0.1676 g (90%). The complex was recrystallized by allowing a concentrated CH_2Cl_2 solution to diffuse to slowly into *n*-hexane to give red crystals, 0.0772 g (41%).

Synthesis of [Co(dbm)$_2$(ppa^{Cl})] 38

To a orange solution of [Co(dbm)$_2$(H$_2$O)$_2$] (0.1351 g, 0.25 mmol) in THF (10 cm^3) was added a solution of ppa^{Cl} (0.0551 g, 0.25 mmol) in THF (3 cm^3). The deep red solution was stirred over night then concentrated *in vacuo*. *n*-Hexane (15 cm^3) was added to precipitate a deep red solid which was washed with *n*-hexane (2 x 5 cm^3) and dried *in vacuo*, yield 0.1218 g (67%).

Synthesis of [Co(dbm)$_2$(ppa^{Br})] 39

To a yellow suspension of [Co(dbm)$_2$(H$_2$O)$_2$] (0.1353 g, 0.25 mmol) in acetone (10 cm^3) was added a solution of ppa^{Br} (0.0653 g, 0.25 mmol) in acetone (3 cm^3). The deep brown solution was stirred 1 hour then concentrated *in vacuo*. *n*-Hexane (15 cm^3) was added to precipitate a red solid which was washed with *n*-hexane (2 x 5 cm^3) and dried *in vacuo*, yield 0.1385 g (72%).

Synthesis of [Co(dbm)$_2$(ppa^I)] 40

To a orange solution of [Co(dbm)$_2$(H$_2$O)$_2$] (0.1353 g, 0.25 mmol) in THF (10 cm^3) was added a solution of ppa^I (0.0768 g, 0.25 mmol) in THF (3 cm^3). The dark brown solution was stirred 1 hour then concentrated *in vacuo*. *n*-Hexane (20 cm^3) was added to precipitate a deep purple solid which was washed with *n*-hexane (2 x 5 cm^3) and dried *in vacuo*, yield 0.1113 g (54%).

Synthesis of [Co(tmhd)$_2$(ppa^H)] 41

To a stirred purple solution of [Co(tmhd)$_2$(H$_2$O)$_2$] (0.1153 g, 0.25 mmol) in THF (10 cm^3) was added a yellow solution of ppa^H (0.0459 g, 0.25 mmol) in THF (3 cm^3). The deep purple solution was stirred 2 hours then concentrated *in vacuo*. *n*-Hexane (10 cm^3) was added to precipitate a purple solid which was washed with *n*-hexane (5 cm^3) and dried *in vacuo*, yield 0.1219 g (80%).

Synthesis of [Co(tmhd)$_2$(ppa^{Me})] 42

To a purple solution of [Co(tmhd)$_2$(H$_2$O)$_2$] (0.0971 mg, 0.25 mmol) in THF (20 cm^3) was added a solution of ppa^{Me} (0.0531 mg, 0.25 mmol) in THF (2 cm^3). The mixture was stirred for 2 hours then the solvent was removed to dryness. The red solid was dissolved in CH_2Cl_2 and filtered through celite to give an orange solution. Diffusion of *n*-hexane into the CH_2Cl_2 solution gave red microcrystals, yield 0.0709 mg (52%).

Synthesis of [Co(tmhd)$_2$(ppa^{Et})] 43

To a stirred purple solution of [Co(tmhd)$_2$(H$_2$O)$_2$] (0.1153 g, 0.25 mmol) in THF (10 cm^3) was added a yellow solution of ppa^{Et} (0.0528 g, 0.25 mmol) in THF (3 cm^3). The deep brown solution was stirred 1 hour then concentrated *in vacuo*. *n*-Hexane (15 cm^3) was added to precipitate a dark brown solid which was washed with *n*-hexane (5 cm^3) and dried *in vacuo*, yield 0.1011 g (63%).

Synthesis of [Co(tmhd)$_2$(ppa^{OMe})] 44

To a stirred purple solution of [Co(tmhd)$_2$(H$_2$O)$_2$] (0.094 g, 0.25 mmol) in THF (10 cm^3) was added a yellow solution of ppa^{OMe} (0.0535 g, 0.25 mmol) in THF (2 cm^3). The deep red solution was stirred over night then concentrated *in vacuo*. *n*-Hexane (15 cm^3) was added to precipitate a brick red solid which was washed with *n*-hexane (5 cm^3) and dried *in vacuo*, yield 0.0859 g (54%).

Synthesis of [Co(tmhd)$_2$(ppa^{F})] 45

To a stirred purple solution of [Co(tmhd)$_2$(H$_2$O)$_2$] (0.0969 g, 0.25 mmol) in THF (20 cm^3) was added ppa^{F} (0.050 g, 0.25 mmol). The mixture was stirred for 2 hours, to give a red solution, then the solvent was removed to give a red solid 0.1172 g (80%). The complex was recrystallised by allowing a concentrated CH_2Cl_2 solution to diffuse to slowly into *n*-hexane to give red solution. The solid was filtered to give red micro crystals, 0.0322 g (31%).

Synthesis of [Co(tmhd)$_2$(ppa^{Cl})] 46

To a stirred purple solution of [Co(tmhd)$_2$(H$_2$O)$_2$] (0.0981 g, 0.25 mmol) in THF (10 cm^3) was added a yellow solution of ppa^{Cl} (0.0560 g, 0.25 mmol) in THF (2 cm^3). The deep red solution was stirred over night then concentrated *in vacuo*. *n*-Hexane (15 cm^3) was added to precipitate a bunt red solid which was washed with *n*-hexane (5 cm^3) and dried *in vacuo*, yield 0.1112 g (69%).

Synthesis of [Co(tmhd)$_2$(ppa^{Br})] 47

To a stirred purple solution of [Co(tmhd)$_2$(H$_2$O)$_2$] (0.1153 g, 0.25 mmol) in THF (10 cm^3) was added a yellow solution of ppa^{I} (0.0653 g, 0.25 mmol) in THF (3 cm^3). The deep brown solution was stirred 2 hours then concentrated *in vacuo*. *n*-Hexane (10 cm^3) was added to precipitate a purple solid which was washed with *n*-hexane (5 cm^3) and dried *in vacuo*, yield 0.1512 g (88%).

Synthesis of [Co(tmhd)$_2$(ppa^{I})] 48

To a stirred purple solution of [Co(tmhd)$_2$(H$_2$O)$_2$] (0.1153 g, 0.25 mmol) in THF (10 cm^3) was added a yellow solution of ppa^{I} (0.0768 g, 0.25 mmol) in THF (3 cm^3). The red solution was stirred 2 hours then concentrated *in vacuo*. *n*-Hexane (10 cm^3) was added to precipitate a orange solid which was washed with *n*-hexane (5 cm^3) and dried *in vacuo*, yield 0.1025 g (52%).

Synthesis of [Co(hfac)$_2$(ppa^{H})] 49

To a stirred red solution of [Co(hfac)$_2$(H$_2$O)$_2$] (0.149 g, 0.29 mmol) in CH_2Cl_2 (10 cm^3) was added a yellow solution of ppa^{H} (0.0530 g, 0.29 mmol) in CH_2Cl_2 (3 cm^3). The orange solution was stirred 3 hour then concentrated *in vacuo*. *n*-Hexane (15 cm^3) was added to precipitate a brown solid which was washed with *n*-hexane (2 x 5 cm^3) and dried *in vacuo*, yield 0.1057 g (57%).

Synthesis of [Co(hfac)$_2$(ppa^{Me})] 50

To a stirred orange red solution of [Co(hfac)$_2$(THF)$_2$] (0.1553 g, 0.25 mmol) in CH_2Cl_2 (5 cm^3) was added ppa^{Me} (0.0495 g, 0.25 mmol). The deep red solution was stirred over night then concentrated *in vacuo*. *n*-Hexane (10 cm^3) was added to precipitate a orange solid which was washed with *n*-hexane (5 cm^3) and dried *in vacuo*, yield 0.1455 g (87%).

Synthesis of [Co(hfac)$_2$(ppa^{Et})] 51

To a stirred red solution of [Co(hfac)$_2$(H$_2$O)$_2$] (0.1272 g, 0.25 mmol) in THF (10 cm^3) was added a yellow solution of ppa^{Et} (0.0528 g, 0.25 mmol) in THF (3 cm^3). The orange solution was stirred 1 hour then concentrated *in vacuo*. *n*-Hexane (15 cm^3) was added to precipitate a orange solid which was washed with *n*-hexane (5 cm^3) and dried *in vacuo*, yield 0.0887 g (51%).

Synthesis of [Co(hfac)$_2$(ppa^{OMe})] 52

To a stirred red solution of [Co(hfac)$_2$(H$_2$O)$_2$] (0.1272 g, 0.25 mmol) in THF (10 cm^3) was added a orange solution of ppa^{OMe} (0.0528 g, 0.25 mmol) in THF (3 cm^3). The deep yellow solution was stirred 1 hour then concentrated *in vacuo*. *n*-Hexane (15 cm^3) was added to precipitate a orange solid which was washed with *n*-hexane (5 cm^3) and dried *in vacuo*, yield 0.1410 g (78%).

Synthesis of [Co(hfac)$_2$(ppa^{F})] 53

To a stirred orange red solution of [Co(hfac)$_2$(THF)$_2$] (0.1567 g, 0.25 mmol) in CH_2Cl_2 (5 cm^3) was added ppa^{F} (0.0502 g, 0.25 mmol). The deep red solution was stirred over night then concentrated *in vacuo*. *n*-Hexane (10 cm^3) was added to precipitate a orange solid which was washed with *n*-hexane (5 cm^3) and dried *in vacuo*, yield 0.1534 g (91%).

Synthesis of [Co(hfac)$_2$(ppa^{Cl})] 54

To an orange red solution of [Co(hfac)$_2$(H$_2$O)$_2$] (0.1272 g, 0.25 mmol) in CH_2Cl_2 (5 cm^3) was added a solution of ppa^{Cl} (0.0542 g, 0.25 mmol) in CH_2Cl_2 (3 cm^3). The deep orange solution was stirred 1 hour then concentrated *in vacuo*. *n*-Hexane (15 cm^3) was added to precipitate a deep orange solid which was washed with *n*-hexane (2 x 5 cm^3) and dried *in vacuo*, yield 0.1239 g (71%).

Synthesis of [Co(hfac)$_2$(ppa^{Br})] 55

To an orange red solution of [Co(hfac)$_2$(H$_2$O)$_2$] (0.1272 g, 0.25 mmol) in CH_2Cl_2 (5 cm^3) was added a solution of ppa^{Br} (0.0653 g, 0.25 mmol) in CH_2Cl_2 (3 cm^3). The deep orange solution was stirred 1 hour then concentrated *in vacuo*. *n*-Hexane (15 cm^3) was added to precipitate a orange solid which was washed with *n*-hexane (2 x 5 cm^3) and dried *in vacuo*, yield 0.1416 g (77%).

Synthesis of [Co(hfac)$_2$(ppa^{I})] 56

To a stirred red solution of [Co(hfac)$_2$(H$_2$O)$_2$] (0.1273 g, 0.25 mmol) in THF (10 cm^3) was added a yellow solution of ppa^{I} (0.0768 g, 0.25 mmol) in THF (3 cm^3). The orange solution was stirred 1 hour then concentrated *in vacuo*. *n*-Hexane (15 cm^3) was added to precipitate a orange solid which was washed with *n*-hexane (5 cm^3) and dried *in vacuo*, yield 0.1025 g (52%).

X-ray structural studies of [Co(β-diketonate)$_2$(ppa^X)] complexes

Crystals of [Co(dbm)$_2$(ppa^{OMe})] **36**, [Co(dbm)$_2$(ppa^{Cl})] **38** and [Co(hfac)$_2$(ppa^{Br})] **55** were obtained by slow diffusion of *n*-hexane into a concentrated solution of the complex in CH_2Cl_2. The structures and crystallographic data are presented in Figures 7, 8 and 9 for complexes **36**, **38** and **55** respectively.

The Co analogues, complexes **36** and **38**, also assume slightly distorted octahedral coordination geometries with the β-diketonate ligands exhibiting a *cis* arrangement as in the Ni complexes (Figures 6 and 7). The Co-O bond lengths vary between 2.025-2.099 Å for the two complexes and are slightly longer than those found in [Ni(dbm)$_2$(ppa^X)]. Interestingly, [Co(dbm)$_2$(ppa^{OMe})] **36** is recrystallised with two different molecules in the unit cell.

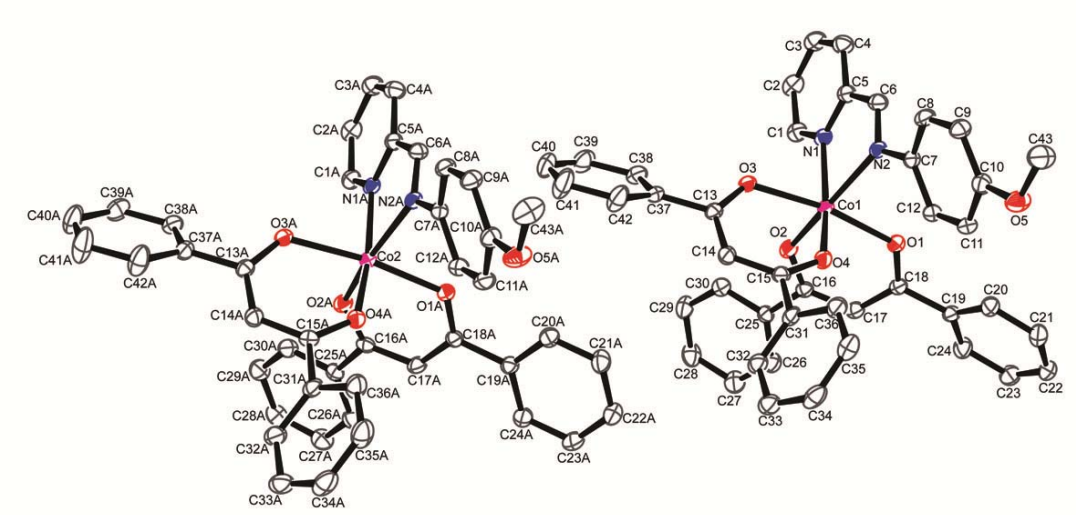

Figure 7 ORTEP diagram of [Co(dbm)$_2$(ppa^{OMe})] **36**. The thermal ellipsoids are drawn to 50% probability level. Hydrogen atoms are omitted for clarity.

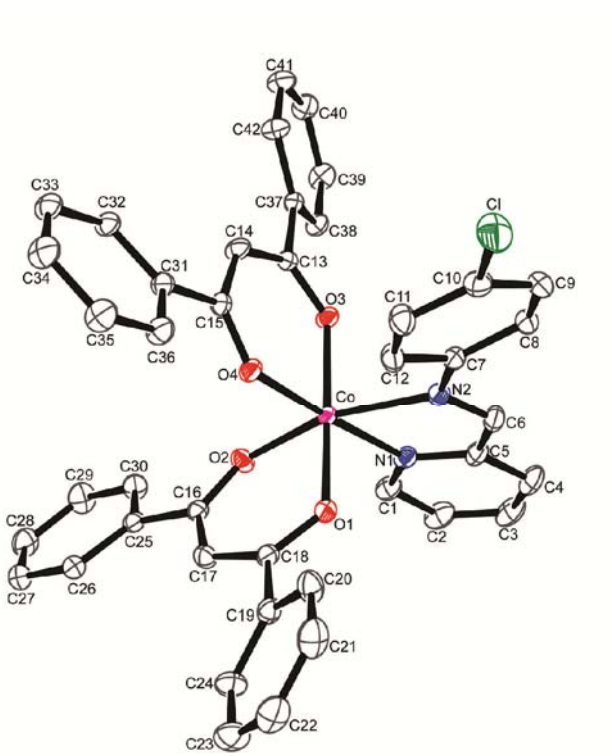

Figure 8 ORTEP diagram of [Co(dbm)$_2$(ppa^{Cl})] **38**. The thermal ellipsoids are drawn to 50% probability level. Hydrogen atoms are omitted for clarity.

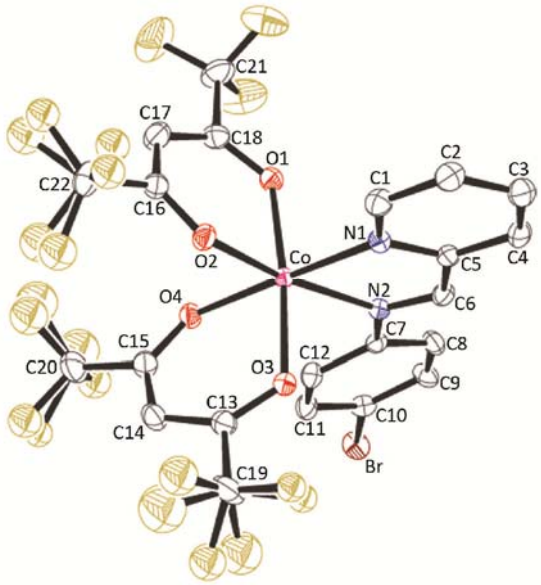

Figure 9 ORTEP diagram of [Co(hfac)$_2$(ppa^{Br})] **55**. The thermal ellipsoids are drawn to 50% probability level. Hydrogen atoms are omitted for clarity.

The cobalt bond to the pyridine of the ppa^{X} ligand of complexes **38** is considerably shorter than the bond to the imine nitrogen differing by *ca*. 0.1 Å while the Co-N bonds lengths for **36** are different by

only 0.05 Å. These are the same trends as observed for the Ni analogues. The phenyl ring in both complexes is twisted with respect to the pyridylimine unit. Interestingly, the angle for **36** is similar to that of **38** which is different from the Ni complexes. This might due to the closer packing of **36** in the unit cell compared with that of [Ni(dbm)$_2$(ppa^{OMe})] **12**. The packing in the structure of **55** involves a weak π-π interactions between the pyridyl and phenyl rings of neighbouring ppa^{Br} ligands. A further weak interaction occurs between the Br on the ppa^{Br} ligand and the β-diketonate ligand creating discrete dimers within the structure.

Table 6 Selected bond lengths (Å) and angles (°) of **36**, **38** and **55**.

	36	**36A**[d]	**38**	**55**
Co-O(1)	2.0769(12)	2.0611(12)	2.0269(8)	2.047(3)
Co-O(2)	2.0260(12)	2.0390(12)	2.0439(9)	2.063(3)
Co-O(3)	2.0988(11)	2.0887(11)	2.0249(8)	2.064(3)
Co-O(4)	2.0450(12)	2.0379(12)	2.0573(8)	2.078(3)
Co-N(1)	2.1408(14)	2.1319(14)	2.1314(10)	2.097(4)
Co-N(2)	2.1951(14)	2.1991(14)	2.2247(10)	2.212(4)
O(1)-Co-O(2)	86.84(5)	86.61(5)	88.41(3)	87.91(12)
O(3)-Co-O(4)	85.97(4)	86.74(5)	87.42(3)	86.42(12)
N(1)-Co-N(2)	76.04(5)	76.22(5)	75.63(4)	77.04(14)
β[a]	21.53	24.05	19.85	
	19.38	18.14	2.47	
γ[b]	24.71	25.17	23.73	
Intermolecular distances[c]				
O(3)-H(8)	2.615	2.615	2.396	
O(3)-H(6)	2.578	2.578		

[a] β is the angle between the plane defined by the carbon and oxygen atoms of the β-diketonate ligand and the plane defined by the nickel and two oxygen atoms. [b] γ is the angle between the plane of the pyridylimine unit and the plane of the substituted phenyl ring. [c] Non-bonded metrics and those involving centroids were not included in the structure refinement, and thus do not have an e.s.d. [d] The second molecule of complex **36** in a unit cell.

Electron transfer studies of [Co(β-diketonate)$_2$(ppa^X)]

The [Co(β-diketonate)$_2$(ppa^X)] complexes (β-diketonate = dbm or tmhd), **33-48**, show one oxidation peak followed by a return peak with a separation larger than for a normal reversible process (Table 7, Figure 10). Complexes **37**-**40** which have a halide substituent on the ppa^X ligand show an irreversible reduction. However, the reduction of complexes **45**-**48** cannot be observed due to the limit of the solvent window.

Table 7 Electrochemical data for [Co(β-diketonate)$_2$(ppa^X)].[a]

		Oxidation			Reduction
		Ep_{ox}/V	Ep_{red}/V	ΔE/mV	Ep/V
33	[Co(dbm)$_2$(ppa^H)]	0.77	-0.06	830	-
34	[Co(dbm)$_2$(ppa^{Me})]	0.85	-0.11	960	-1.31 (I)
35	[Co(dbm)$_2$(ppa^{Et})]	0.83	-0.08	910	-
36	[Co(dbm)$_2$(ppa^{OMe})]	0.68	-0.07	750	-
37	[Co(dbm)$_2$(ppa^F)]	0.83	-0.03	860	-1.31 (I)
38	[Co(dbm)$_2$(ppa^{Cl})]	0.68	-0.01	690	-1.26 (I)
39	[Co(dbm)$_2$(ppa^{Br})]	0.56	0.07	490	-1.23 (I)
40	[Co(dbm)$_2$(ppa^I)]	0.63	0.07	560	-1.24 (I)
41	[Co(tmhd)$_2$(ppa^H)]	0.90	-0.47	1370	-
42	[Co(tmhd)$_2$(ppa^{Me})]	0.59	-0.38	970	-
43	[Co(tmhd)$_2$(ppa^{Et})]	0.71	-0.42	1120	-
44	[Co(tmhd)$_2$(ppa^{OMe})]	0.66	-0.41	1070	-
45	[Co(tmhd)$_2$(ppa^F)]	0.46	-0.26	720	-
46	[Co(tmhd)$_2$(ppa^{Cl})]	0.64	-0.30	940	-
47	[Co(tmhd)$_2$(ppa^{Br})]	0.50	-0.30	800	-
48	[Co(tmhd)$_2$(ppa^I)]	0.54	-0.30	840	-

[a] All measurements were performed at 298 K, in dried and degassed CH_2Cl_2 0.1 M [NBu^n_4][PF_6] solution; scan rate 100 mVs^{-1}; complexes **33**-**40** not calibrated, complexes **41**-**48** calibrated with [Fe(η-C_5Me_5)$_2$], $E^{o\prime}$ = -0.012 V.

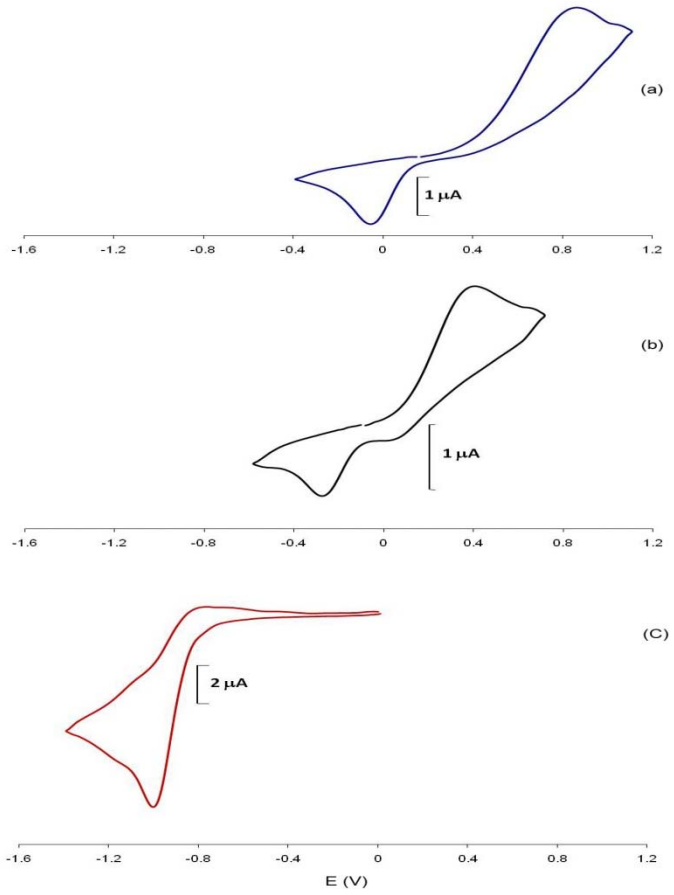

Figure 10 Cyclic voltammogram of (a) $[Co(dbm)_2(ppa^{Cl})]$ **38**, (b) $[Co(tmhd)_2(ppa^{Cl})]$ **46** and (c) $[Co(hfac)_2(ppa^{Cl})]$ **54**.

Comparison of the voltammograms of complexes **33-48** with those of our preliminary work on [Co(β-diketonate)$_2$(N-N)] complexes (β-diketonate = dbm, N-N = phen **57**, 2,2′-bpy **58**, dmae **59**, β-diketonate = tmhd, N-N = phen **60**, 2,2′-bpy **61**, dmae **62**) which have been proved to exhibit *redox coupled spin crossover* we found that they show similar redox behavior (Figure 11). However, voltammogram of **60** shows an extra return peak that is thought to be due to the intermediate high spin d^6 which in cases of **33-48** are not observed.

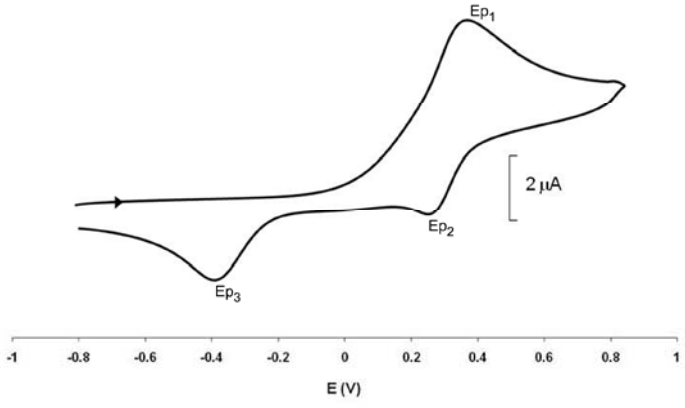

Figure 11 Cyclic voltammogram of $[Co(tmhd)_2(phen)]$ **60**.

The redox behavior of these complexes is an example of *redox coupled-spin crossover*. This behavior is best described by the square scheme shown in Scheme 5. The two processes *1* and *3* represent the oxidation and reduction reactions of the individual spin state isomers while processes *2* and *4* represent the spin exchange reactions in the individual oxidation states.. Redox coupled-spin crossover has also been observed and extensively studied by Schultz *et al*. in a series of $[M(tacn)_2]^{2+/3+}$ (M = Fe, Co; tacn = 1,4,7-triazacyclononane) complexes although in this system the redox processes are fully reversible. Similar redox behavior to **33**-**48** has recently been reported in the dimeric complex $[(bpbp)Co_2(O_2P(OPh)_2)_2]^+$ ($bpbp^-$ = 2,6-bis(N,N′-bis-(2-picolyl)amino)methyl)-4-tertbutylphenolato) which also shows wide separation of the oxidation and reduction peaks. A similar result is also found in the case of $[(Tp^R)_2Co]^{0/+}$ (Tp^R = Tp, pzTp and Tp*) where increasing steric bulk results in a corresponding increase in irreversibility. Comparisons between $[Co(tacn)_2]^{2+}$ and complexes **33**-**48** show that the former is oxidized *ca*. 1.2 V more easily than the latter consistent with the greater stability of the Co^{II} oxidation state for the $[Co(\beta\text{-diketonate})_2(ppa^X)]$ complexes. In addition, the complexes **33-40** and **41-48** are more difficult to oxidize than **57-59** and **60-62**, respectively.

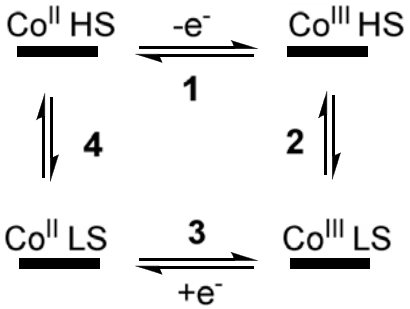

Scheme 5 Square scheme of the redox coupled-spin crossover process showing individual spin crossover and electron transfer processes.

As with the $[Ni(hfac)_2(ppa^X)]$ complexes, the oxidation potential was not observed for the $[Co(hfac)_2(ppa^X)]$ complexes, **49**-**56**. However, there are two reduction waves close together, Ep_1 and Ep_2 at *ca.* -0.95 to -1.05 V and -1.12 to -1.22 V respectively, followed by a small peak of the return wave (Ep_3) between -0.63 to -0.71 V (Figure 12). The first reduction peak (Ep_1) might due to a metal based reduction and the second reduction peak (Ep_2) might due to reduction of the ppa^X ligand.

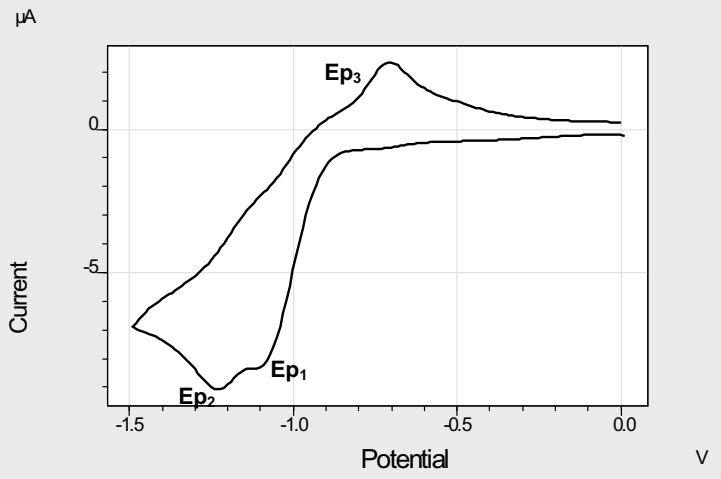

Figure 12 Cyclic voltammogram of $[Co(hfac)_2(ppa^{OMe})]$ **52**.

Table 8 Reduction potentials of $[Co(hfac)_2(ppa^{X})]$.

		Reduction/V[a]		
		Ep_1[b]	Ep_2[b]	Ep_3[c]
49	$[Co(hfac)_2(ppa^{H})]$	-1.02 (I)	-1.13 (I)	-0.71 (I)
50	$[Co(hfac)_2(ppa^{Me})]$	-1.05 (I)	-1.21 (I)	-0.70 (I)
51	$[Co(hfac)_2(ppa^{Et})]$	-1.05 (I)	-1.22 (I)	-0.69 (I)
52	$[Co(hfac)_2(ppa^{OMe})]$	-1.05 (I)	-1.21 (I)	-0.71 (I)
53	$[Co(hfac)_2(ppa^{F})]$	-0.95 (I)	-1.12 (I)	-0.61 (I)
54	$[Co(hfac)_2(ppa^{Cl})]$	-1.00 (I)	-1.19 (I)	-0.73 (I)
55	$[Co(hfac)_2(ppa^{Br})]$	-1.00 (I)	-1.19 (I)	-0.78 (I)
56	$[Co(hfac)_2(ppa^{I})]$	-0.99 (I)	-1.16 (I)	-0.63 (I)

[a] All measurements were performed at 298 K, in dried and degassed CH_2Cl_2 0.1 M $[NBu^n_4][PF_6]$ solution; scan rate 100 mVs^{-1}; calibrated with $[Fe(\eta\text{-}C_5H_5)_2]$, $E^{o\prime}$ = 0.52 V. [b] Ep_1 and Ep_2 were measured by DPV. [c] Ep_3 was measured by CV.

4.5. Synthesis and characterization of $[Co(\beta\text{-diketonate})_2(ppa^{X})]OTf$ complexes

The one pot reaction of $[Co(\beta\text{-diketonate})_2(H_2O)_2]$ (β-diketonate = dbm and tmhd), ppa^X (X = H, Me, Et, OMe, F, Cl, Br and I) and $Ag[CF_3SO_3]$ in CH_2Cl_2 yields a dark green solution after stirring for 2-3 hours. The solution was filtered through celite then reduced to a small volume and *n*-hexane was added to precipitate olive oil green solids of $[Co(\beta\text{-diketonate})_2(ppa^{X})]OTf$ (β-diketonate = dbm, X = H **33**$^+$, Me **34**$^+$, Et **35**$^+$, OMe **36**$^+$, F **37**$^+$, Cl **38**$^+$, Br **39**$^+$ and I **40**$^+$, β-diketonate = tmhd X = H **41**$^+$, Me **42**$^+$, Et **43**$^+$, OMe **44**$^+$, F **45**$^+$, Cl **46**$^+$, Br **47**$^+$ and I **48**$^+$), in moderate yield (Scheme 6).

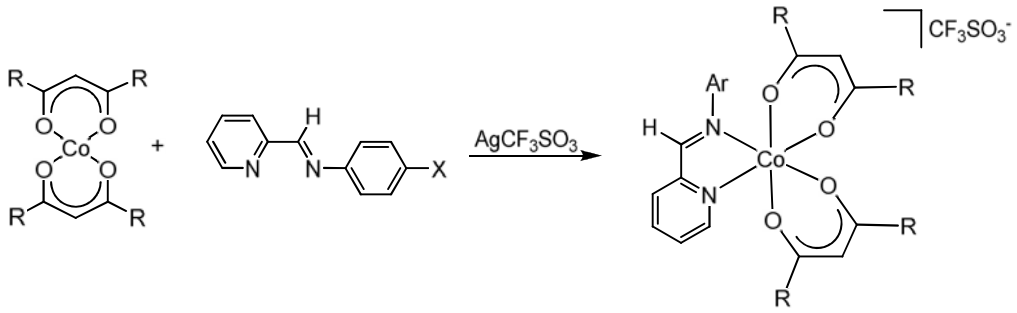

Scheme 6 Synthesis of [Co(β-diketonate)$_2$(ppa^X)]OTf complexes.

All Co^{3+} complexes have been characterized by CHN analysis, mass spectrometry, IR, ^{1}H NMR and UV-Vis spectroscopy (Table 9). The IR spectroscopic studies show that the $\nu_{C=O}$ bands of [Co(β-diketonate)$_2$(ppa^X)]OTf **33$^+$-48$^+$** move to lower wavenumbers compared with their neutral complexes which indicate a change in oxidation state from 2 to 3 of the cobalt centre. The shift of the $\nu_{C=O}$ stretch in the tmhd complexes is more significant than those of the dbm complexes possibly due to greater donation of electron density to the metal centre by the tmhd ligands. The ^{1}H NMR spectra show sharp signals indicative of low spin Co^{3+} complexes (Figure 13). The protons signals of the β-diketonate and ppa^X ligands move to higher chemical shifts compared with the free ligands also confirming coordination of the ligands to the metal centre.

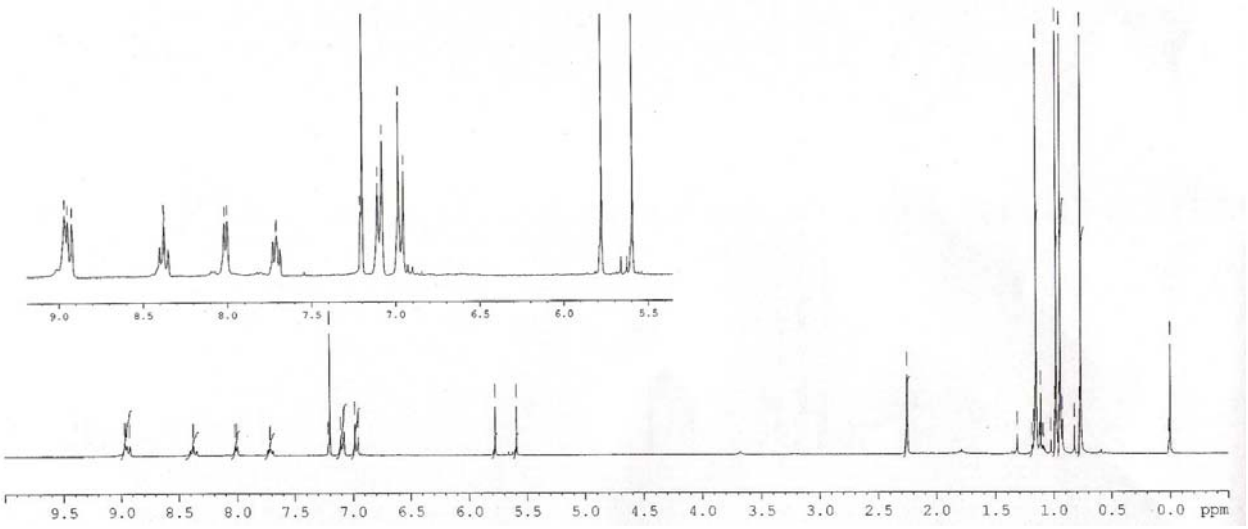

Figure 13 ^{1}H NMR of [Co(tmhd)$_2$(ppa^{OMe})]OTf in $CDCl_3$.

Table 9 Physical properties of [Co(β-diketonate)$_2$(ppa^X)]OTf complexes.

Complex	% Yield	Colour	$\nu_{C=O}$/cm^{-1}
[Co(dbm)$_2$(ppa^H)]OTf **33**$^+$	89	Olive green	1589
[Co(dbm)$_2$(ppa^{Me})]OTf **34**$^+$	43	Olive green	1589
[Co(dbm)$_2$(ppa^{Et})]OTf **35**$^+$	58	Olive green	1589
[Co(dbm)$_2$(ppa^{OMe})]OTf **36**$^+$	73	Olive green	1589
[Co(dbm)$_2$(ppa^F)]OTf **37**$^+$	57	Olive green	1589
[Co(dbm)$_2$(ppa^{Cl})]OTf **38**$^+$	68	Olive green	1589
[Co(dbm)$_2$(ppa^{Br})]OTf **39**$^+$	47	Olive green	1589
[Co(dbm)$_2$(ppa^I)]OTf **40**$^+$	58	Olive green	1589
[Co(tmhd)$_2$(ppa^H)]OTf **41**$^+$	51	Olive green	1560
[Co(tmhd)$_2$(ppa^{Me})]OTf **42**$^+$	55	Olive green	1560
[Co(tmhd)$_2$(ppa^{Et})]OTf **43**$^+$	65	Olive green	1560
[Co(tmhd)$_2$(ppa^{OMe})]OTf **44**$^+$	52	Olive green	1561
[Co(tmhd)$_2$(ppa^F)]OTf **45**$^+$	51	Olive green	1560
[Co(tmhd)$_2$(ppa^{Cl})]OTf **46**$^+$	74	Olive green	1561
[Co(tmhd)$_2$(ppa^{Br})]OTf **47**$^+$	66	Olive green	1560
[Co(tmhd)$_2$(ppa^I)]OTf **48**$^+$	67	Olive green	1561

Experimental

Synthesis of [Co(dbm)$_2$(ppa^H)]OTf 33$^+$

[Co(dbm)$_2$(H$_2$O)$_2$] (0.3405 g, 0.63 mmol) was dissolved in CH_2Cl_2 (10 cm^3) yield an orange suspension. One equivalent of ppa^H ligand (0.1145 g, 0.63 mmol) was added, the deep red solution was stirred for 1 hr. Ag[CF_3SO_3] (0.1621 g, 0.63 mmol) was added, the dark green solution was stirred overnight. The dark green solution was filtered through celite. The solvent was removed to small volume, *n*-hexane was added to induce precipitation. The olive green solid was filtered and dried in air yield 0.4711 g (89%).

Synthesis of [Co(dbm)$_2$(ppa^{Me})]OTf 34$^+$

[Co(dbm)$_2$(H$_2$O)$_2$] (0.1358 g, 0.25 mmol) was dissolved in CH_2Cl_2 (10 cm^3) yield an orange suspension. One equivalent of ppa^{Me} ligand (0.0540 g, 0.25 mmol) was added, the deep red solution was stirred for 1 hr. Ag[CF_3SO_3] (0.0684 g, 0.27 mmol) was added, the dark green solution was stirred overnight. The dark green solution was filtered through celite. The solvent was removed to small volume, *n*-hexane was added to induce precipitation. The olive green solid was filtered and dried in air yield 0.0925 g (43%).

Synthesis of $[Co(dbm)_2(ppa^{Et})]OTf$ 35$^+$

$[Co(dbm)_2(H_2O)_2]$ (0.1452 g, 0.27 mmol) was dissolved in CH_2Cl_2 (10 cm^3) yield an orange suspension. One equivalent of ppa^{Et} ligand (0.0580 g, 0.27 mmol) was added, the deep red solution was stirred for 1 hr. $Ag[CF_3SO_3]$ (0.0720 g, 0.28 mmol) was added, the dark green solution was stirred overnight. The dark green solution was filtered through celite. The solvent was removed to small volume, *n*-hexane was added to induce precipitation. The olive green solid was filtered and dried in air yield 0.1345 g (58%).

Synthesis of $[Co(dbm)_2(ppa^{OMe})]OTf$ 36$^+$

$[Co(dbm)_2(H_2O)_2]$ (0.1358 g, 0.25 mmol) was dissolved in CH_2Cl_2 (10 cm^3) yield an orange suspension. One equivalent of ppa^{OMe} ligand (0.0550 g, 0.26 mmol) was added, the deep red solution was stirred for 1 hr. $Ag[CF_3SO_3]$ (0.0700 g, 0.27 mmol) was added, the dark green solution was stirred overnight. The dark green solution was filtered through celite. The solvent was removed to small volume, *n*-hexane was added to induce precipitation. The olive green solid was filtered and dried in air yield 0.1556 g (73%).

Synthesis of $[Co(dbm)_2(ppa^{F})]OTf$ 37$^+$

$[Co(dbm)_2(H_2O)_2]$ (0.1380 g, 0.26 mmol) was dissolved in CH_2Cl_2 (10 cm^3) yield an orange suspension. One equivalent of ppa^{F} ligand (0.0519 g, 0.26 mmol) was added, the deep red solution was stirred for 1 hr. $Ag[CF_3SO_3]$ (0.0680 g, 0.26 mmol) was added, the dark green solution was stirred overnight. The dark green solution was filtered through celite. The solvent was removed to small volume, *n*-hexane was added to induce precipitation. The olive green solid was filtered and dried in air yield 0.1240 g (57%).

Synthesis of $[Co(dbm)_2(ppa^{Cl})]OTf$ 38$^+$

$[Co(dbm)_2(H_2O)_2]$ (0.1373 g, 0.25 mmol) was dissolved in CH_2Cl_2 (10 cm^3) yield an orange suspension. One equivalent of ppa^{Cl} ligand (0.0550 g, 0.25 mmol) was added, the deep red solution was stirred for 1 hr. $Ag[CF_3SO_3]$ (0.0690 g, 0.27 mmol) was added, the dark green solution was stirred overnight. The dark green solution was filtered through celite. The solvent was removed to small volume, *n*-hexane was added to induce precipitation. The olive green solid was filtered and dried in air yield 0.1503 g (68%).

Synthesis of $[Co(dbm)_2(ppa^{Br})]OTf$ 39$^+$

$[Co(dbm)_2(H_2O)_2]$ (0.1378 g, 0.25 mmol) was dissolved in CH_2Cl_2 (10 cm^3) yield an orange suspension. One equivalent of ppa^{Br} ligand (0.0670 g, 0.26 mmol) was added, the deep red solution was stirred for 1 hr. $Ag[CF_3SO_3]$ (0.0664 g, 0.26 mmol) was added, the dark green solution was stirred overnight. The dark green solution was filtered through celite. The solvent was removed to small

volume, *n*-hexane was added to induce precipitation. The olive green solid was filtered and dried in air yield 0.1100 g (47%).

Synthesis of $[Co(dbm)_2(ppa^I)]OTf$ 40^+

$[Co(dbm)_2(H_2O)_2]$ (0.1343 g, 0.25 mmol) was dissolved in CH_2Cl_2 (10 cm^3) yield an orange suspension. One equivalent of ppa^I ligand (0.0764 g, 0.25 mmol) was added, the deep red solution was stirred for 1 hr. $Ag[CF_3SO_3]$ (0.0664 g, 0.25 mmol) was added, the dark green solution was stirred overnight. The dark green solution was filtered through celite. The solvent was removed to small volume, *n*-hexane was added to induce precipitation. The olive green solid was filtered and dried in air yield 0.1385 g (58%).

Synthesis of $[Co(tmhd)_2(ppa^H)]OTf$ 41^+

$[Co(tmhd)_2(H_2O)_2]$ (0.1068 g, 0.24 mmol) was dissolved in CH_2Cl_2 (10 cm^3) yielding a purple solution. One equivalent of ppa^H ligand (0.0421 g, 0.23 mmol) was added, the deep red solution was stirred for 1 hr. $Ag[CF_3SO_3]$ (0.0583 g, 0.23 mmol) was added, the brown green solution was stirred overnight. The dark green solution was filtered through celite. The solvent was removed to small volume, *n*-hexane was added to induce precipitation. The olive green solid was filtered and dried in air yield 0.0923 g (51%).

Synthesis of $[Co(tmhd)_2(ppa^{Me})]OTf$ 42^+

$[Co(tmhd)_2(H_2O)_2]$ (0.0907 g, 0.20 mmol) was dissolved in CH_2Cl_2 (5 cm^3) yield a purple solution. One equivalent of ppa^{Me} ligand (0.0386 g, 0.20 mmol) was added, the deep red solution was stirred for 1 hr. $Ag[CF_3SO_3]$ (0.0516 g, 0.20 mmol) was added, the brown green solution was stirred overnight. The dark green solution was filtered through celite. The solvent was removed to small volume, *n*-hexane was added to induce precipitation. The olive green solid was filtered and dried in air yield 0.0833 g (55%).

Synthesis of $[Co(tmhd)_2(ppa^{Et})]OTf$ 43^+

$[Co(tmhd)_2(H_2O)_2]$ (0.1061 g, 0.23 mmol) was dissolved in CH_2Cl_2 (5 cm^3) yield a purple solution. One equivalent of ppa^{Et} ligand (0.0493 g, 0.23 mmol) was added, the deep red solution was stirred for 1 hr. $Ag[CF_3SO_3]$ (0.0593 g, 0.23 mmol) was added, the brown green solution was stirred overnight. The dark green solution was filtered through celite. The solvent was removed to small volume, *n*-hexane was added to induce precipitation. The olive green solid was filtered and dried in air yield 0.1180 g (65%).

Synthesis of $[Co(tmhd)_2(ppa^{OMe})]OTf$ 44^+

$[Co(tmhd)_2(H_2O)_2]$ (0.1151 g, 0.25 mmol) was dissolved in CH_2Cl_2 (5 cm^3) yield a purple solution. One equivalent of ppa^{OMe} ligand (0.0534 g, 0.25 mmol) was added, the deep red solution was stirred for 1 hr. $Ag[CF_3SO_3]$ (0.0660 g, 0.26 mmol) was added, the brown green solution was

stirred overnight. The dark green solution was filtered through celite. The solvent was removed to small volume, *n*-hexane was added to induce precipitation. The olive green solid was filtered and dried in air yield 0.1024 g (52%).

Synthesis of $[Co(tmhd)_2(ppa^F)]OTf$ 45$^+$

$[Co(tmhd)_2(H_2O)_2]$ (0.0922 g, 0.20 mmol) was dissolved in CH_2Cl_2 (5 cm^3) yield a purple solution. One equivalent of ppa^F ligand (0.0410 g, 0.20 mmol) was added, the deep red solution was stirred for 1 hr. $Ag[CF_3SO_3]$ (0.0516 g, 0.20 mmol) was added, the brown green solution was stirred overnight. The dark green solution was filtered through celite. The solvent was removed to small volume, *n*-hexane was added to induce precipitation. The olive green solid was filtered and dried in air yield 0.0787 g (51%).

Synthesis of $[Co(tmhd)_2(ppa^{Cl})]OTf$ 46$^+$

$[Co(tmhd)_2(H_2O)_2]$ (0.1163 g, 0.25 mmol) was dissolved in CH_2Cl_2 (5 cm^3) yield a purple solution. One equivalent of ppa^{Cl} ligand (0.0546 g, 0.25 mmol) was added, the deep red solution was stirred for 1 hr. $Ag[CF_3SO_3]$ (0.0657 g, 0.26 mmol) was added, the brown green solution was stirred overnight. The dark green solution was filtered through celite. The solvent was removed to small volume, *n*-hexane was added to induce precipitation. The olive green solid was filtered and dried in air yield 0.1466 g (74%).

Synthesis of $[Co(tmhd)_2(ppa^{Br})]OTf$ 47$^+$

$[Co(tmhd)_2(H_2O)_2]$ (0.1163 g, 0.25 mmol) was dissolved in CH_2Cl_2 (5 cm^3) yield a purple solution. One equivalent of ppa^{Br} ligand (0.0546 g, 0.25 mmol) was added, the deep red solution was stirred for 1 hr. $Ag[CF_3SO_3]$ (0.0657 g, 0.26 mmol) was added, the brown green solution was stirred overnight. The dark green solution was filtered through celite. The solvent was removed to small volume, *n*-hexane was added to induce precipitation. The olive green solid was filtered and dried in air yield 0.1466 g (74%).

Synthesis of $[Co(tmhd)_2(ppa^{I})]OTf$ 48$^+$

$[Co(tmhd)_2(H_2O)_2]$ (0.1200 g, 0.26 mmol) was dissolved in CH_2Cl_2 (5 cm^3) yield a purple solution. One equivalent of ppa^{I} ligand (0.0811 g, 0.26 mmol) was added, the deep red solution was stirred for 1 hr. $Ag[CF_3SO_3]$ (0.0686 g, 0.27 mmol) was added, the brown green solution was stirred overnight. The dark green solution was filtered through celite. The solvent was removed to small volume, *n*-hexane was added to induce precipitation. The olive green solid was filtered and dried in air yield 0.1546 g (67%).

Electron transfer studies of [Co(β-diketonate)$_2$(ppa^X)]OTf complexes

The cyclic voltammograms of [Co(β-diketonate)$_2$(ppa^X)]OTf are almost identical to those found in the neutral analogues although there are slight deviations (Table 10). However, in all the cations we observed that the current of the $Co^{3+/2+}$ process is higher than that of the neutral complexes (Figure 14) at the same concentration. This phenomenon suggests that the diffusion coefficient of the cationic species is greater than that of neutral species which has been confirmed by chronoamperometry. The explanation of this discovery might due to the intermolecular interactions between the neutral complexes which lead to the formation of dimers and thus lower diffusion coefficients.

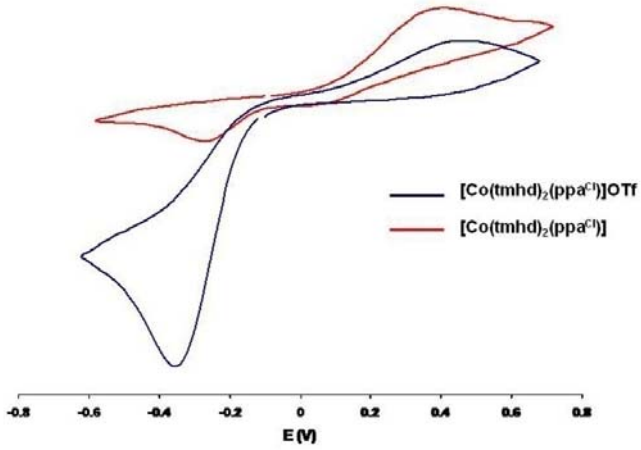

Figure 14 CV of [Co(tmhd)$_2$(ppa^{Cl})] **46** and [Co(tmhd)$_2$(ppa^{Cl}]OTf **46**$^+$.

Table 10 Cyclic voltammetry data of [Co(β-diketonate)$_2$(ppa^X)]OTf complexes.

Complex	Peak potential (V)		
	Ep_1	Ep_2	Ep_3
[Co(dbm)$_2$(ppa^H)]OTf **33**$^+$	0.57	0.38	-0.12
[Co(dbm)$_2$(ppa^{Et})]OTf **35**$^+$	0.73	-	-0.16
[Co(dbm)$_2$(ppa^{Cl})]OTf **38**$^+$	0.65	0.47	-0.03
[Co(tmhd)$_2$(ppa^H)]OTf **41**$^+$	0.45	0.32	-0.44
[Co(tmhd)$_2$(ppa^{Me})]OTf **42**$^+$	0.46	0.19	-0.44
[Co(tmhd)$_2$(ppa^{Et})]OTf **43**$^+$	0.44	0.30	-0.46
[Co(tmhd)$_2$(ppa^{OMe})]OTf **44**$^+$	0.44	0.26	-0.46
[Co(tmhd)$_2$(ppa^F)]OTf **45**$^+$	0.46	0.05	-0.44
[Co(tmhd)$_2$(ppa^{Cl})]OTf **46**$^+$	0.46	-	-0.36
[Co(tmhd)$_2$(ppa^I)]OTf **48**$^+$	0.25	-	-0.27

The UV-Vis spectroelectrochemical studies of [Co(β-diketonate)$_2$(ppa^X)] and their cations show a simultaneous change in the absorptivity of the complex when a constant potential is applied to the electrochemical cell (Figure 15).

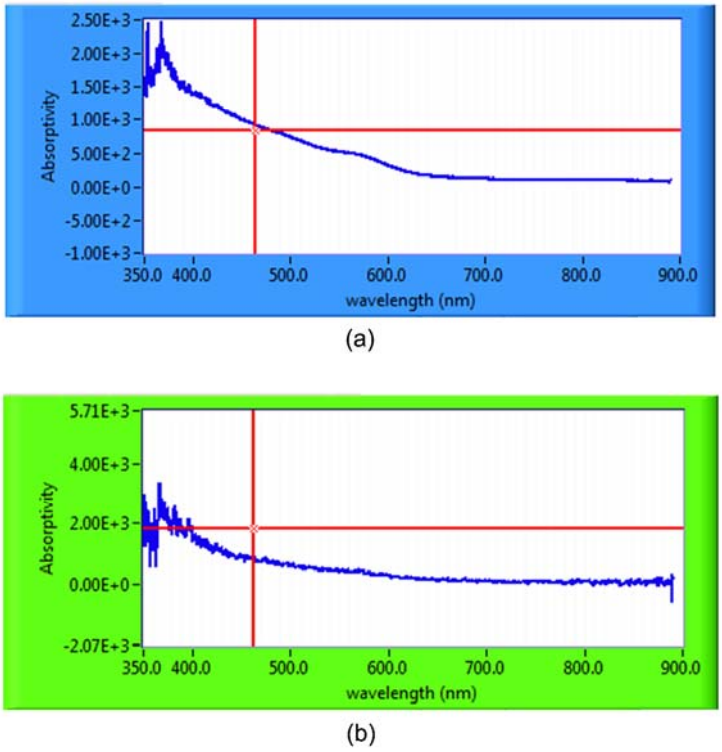

Figure 15 UV-Vis-spectroelectrochemical spectra of [Co(tmhd)$_2$(ppa^{Me})] **34** (a) UV-Vis spectrum of **34** before the voltage was applied (b) UV-Vis spectrum of product after the voltage was applied.

4.6. Synthesis and characterization of [Co(β-diketonate)$_2$(N-N)]BF$_4$ complexes

From our preliminary work on the $Co^{2+/3+}$ redox pair complexes we managed to isolate [Co(β-diketonate)$_2$(N-N)] complexes (β-diketonate = dbm, N-N = phen **57**, 2,2′-bpy **58**, dmae **59**, β-diketonate = tmhd, N-N = phen **60**, 2,2′-bpy **61**, dmae **62**). However, the cations of these complexes had not been isolated. To extend the understanding of this system we synthesized the Co^{3+} redox pairs, [Co(β-diketonate)$_2$(N-N)][BF$_4$] (β-diketonate = dbm, N-N = phen **57**$^+$, 2,2′-bpy **58**$^+$, dmae **59**$^+$, β-diketonate = tmhd, N-N = phen **60**$^+$, 2,2′-bpy **61**$^+$, dmae **62**$^+$). The complexes have been characterized by IR, UV-Vis, NMR spectroscopies, CHN analysis and mass spectrometry (Tables 11 and 12).

Table 11 IR and UV-Vis spectroscopic data for [Co(β-diketonate)$_2$(N-N)]BF_4 complexes.

Complex	% Yield	Colour	IR/cm^{-1}		UV-Vis
			$\nu_{C=O}$	ν_{N-H}	
[Co(dbm)$_2$(phen)]$^+$ **57**$^+$	56	Olive green	1524	-	230 (4.69), 274 (4.88), 296 (4.83 sh), 386 (4.20)
[Co(dbm)$_2$(2,2′-bpy)]$^+$ **58**$^+$	51	Brown green	1524	-	230 (4.70), 292 (4.83), 388 (4.23)
[Co(dbm)$_2$(dmae)]$^+$ **59**$^+$	49	Olive green	1525	3320, 3264	230 (4.48), 282 (4.61), 388 (4.11)
[Co(tmhd)$_2$(phen)]$^+$ **60**$^+$	61	Dark red	1543	-	234 (4.74), 268 (4.60), 300 (4.29 sh)
[Co(tmhd)$_2$(2,2′-bpy)]$^+$ **61**$^+$	64	Maroon	1545	-	236 (4.73), 298 (4.38), 342 (3.81)
[Co(tmhd)$_2$(dmae)]$^+$ **62**$^+$	61	Pastel purple	1560	3310, 3264	238 (4.65), 266 (4.41 sh), 334 (3.81 sh)

The ^{1}H NMR spectra of **57**$^+$-**62**$^+$ show sharp, readily identifiable peaks consistent with a low spin d^6 electron configuration (Table 12). The ^{1}H NMR spectra of **57**$^+$, **58**$^+$, **60**$^+$ and **61**$^+$ show signals in the aromatic region consistent with the presence of coordinated phen and bipy ligands and are assigned on the basis of coupling constants, integration values and comparison with the related [Co(acac)$_2$(N-N)]$^+$ (N-N = bipy and phen) complexes. As expected we observe a single resonance for the central β-diketonate proton indicating that the β-diketonate ligands are magnetically equivalent. In the case of **60**$^+$ and **61**$^+$ there are two singlets between 1.32-0.80 ppm for the *t*-butyl groups. The phenyl protons for the dbm ligands in **57**$^+$ and **58**$^+$ are observed between 6.97-8.04 ppm as a series of multiplets. The dmae complexes show more complex spectra as a result of the asymmetry of the dmae ligand. This is most clearly evidenced by the presence of two singlets for the β-diketonate hydrogen confirming the magnetic inequivalence of the β-diketonate ligands. Moreover, in the case of **62**$^+$ there are three resonances for the *t*-butyl groups integrating in a ratio of 2:1:1 indicating that two of the signals are coincident. As with **57**$^+$ and **58**$^+$, the phenyl protons for the dbm ligands of **59**$^+$ are split into a number of doublets and multiplets between 7.37 and 8.10 ppm. The dmae ligands show two sharp singlets for the methyl groups but four broad resonances for the individual protons on the ligand's backbone. The amino protons are not observed in both cases possibly due to H-bonding.

Table 12 ^{1}H NMR of [Co(β-diketonate)$_2$(N-N)]BF_4 complexes.

Complex	δ (ppm)
57$^+$	9.01 (2H, dd, J_{HH} 8.1 Hz, 0.9 Hz, C*H*^{Phen}), 8.70 (2H, d, J_{HH} 5.1 Hz, C*H*^{Phen}), 8.40 (2H, s, C*H*^{Phen}), 8.12 (2H, dd, J_{HH} 8.1 Hz, 5.1 Hz, C*H*^{Phen}), 8.04 (4H, m, *H*^{Ph}), 7.60-7.55 (6H, m, *H*^{Ph}), 7.50-7.40 (6H, m, *H*^{Ph}), 7.32-7.28 (4H, m, *H*^{Ph}), 7.01 (2H, s, C*H*^{central})
58$^+$	9.03 (2H, d, J_{HH} 7.50 Hz, *H*$^{6, bpy}$), 8.47 (4H, m, *H*$^{6, bpy}$, *H*$^{3, bpy}$), 7.98 (4H, d, J_{HH} 7.20 Hz, *H*^{Ph}), 7.70 (2H, t, J_{HH} 6.90 Hz, *H*$^{4, bpy}$), 7.64 (4H, d, J_{HH} 7.20 Hz, *H*^{Ph}), 7.55-7.34 (12H, m, *H*^{Ph}), 6.97 (2H, s, C*H*^{central})
59$^+$	8.10 (2H, d, J_{HH} 6.90 Hz, *H*^{Ph}), 7.97 (3H, m, *H*^{Ph}), 7.91 (2H, d, J_{HH} 7.2 Hz, *H*^{Ph}), 7.71 (2H, d, J_{HH} 7.50 Hz, *H*^{Ph}), 7.59-7.50 (9H, m, *H*^{Ph}), 7.42-7.37 (4H, m, *H*^{Ph}), 6.97 (1H, s, C*H*^{central}), 6.81 (1H, s, C*H*^{central}), 4.70 (1H, broad, s, N-C*H*$_2$), 4.50 (1H, broad, s, N-C*H*$_2$), 3.2 (1H, broad, s, N-C*H*$_2$), 2.8 (1H, broad, s, N-C*H*$_2$), 2.56 (3H, s, N-C*H*$_3$), 2.01 (3H, s, N-C*H*$_3$)
60$^+$	8.98 (2H, dd, J_{HH} 0.6 Hz, 8.1 Hz, C*H*^{Phen}), 8.38 (2H, d, J_{HH} 5.4 Hz, C*H*^{Phen}), 8.34 (2H, s, C*H*^{Phen}), 8.15 (2H, dd, J_{HH} 8.1 Hz, 5.4 Hz, C*H*^{Phen}), 5.91 (2H, s, C*H*^{central}), 1.31 (18H, s, *t*-Bu), 0.80 (18H, s, *t*-Bu)
61$^+$	8.90 (2H, d, J_{HH} 7.8 Hz, *H*$^{6, bpy}$), 8.42 (2H, t, J_{HH} 7.8 Hz, 6.3 Hz, *H*$^{5, bpy}$), 8.12 (2H, d, J_{HH} 5.1 Hz, *H*$^{3, bpy}$), 7.70 (2H, t, J_{HH} 6.3 Hz, 5.1 Hz, *H*$^{4, bpy}$), 5.86 (2H, s, C*H*^{central}), 1.32 (18H, s, *t*-Bu), 0.87 (18H, s, *t*-Bu)
62$^+$	5.87 (1H, s, C*H*^{central}), 5.80 (1H, s, C*H*^{central}), 4.00 (2H, s, N-C*H*$_2$), 2.80 (2H, s, N-C*H*$_2$), 2.39 (3H, s, N-C*H*$_3$), 1.80 (3H, s, N-C*H*$_3$), 1.21 (18H, s, *t*-Bu), 1.12 (9H, s, *t*-Bu), 1.05 (9H, s, *t*-Bu)

Experimental

Synthesis of [Co(dbm)$_2$(phen)]BF_4 57$^+$

To a stirred orange suspension of [Co(dbm)$_2$(H_2O)$_2$] (0.1678 g, 0.3 mmol) in CH_2Cl_2 (20 cm^3), phen (0.0620 g, 0.3 mmol) was added. The orange solution was stirred for 1 hour then $AgBF_4$ (0.0700 g, 0.36 mmol) added. The olive green solution was stirred over night. The dark green solution was filtered through celite then washed with CH_2Cl_2 (3 x 5 cm^3). The solvent was removed to dryness. The solid was purified using CH_2Cl_2-*n*-hexane to give olive green micro crystals yield 0.1295 g (56%).

Synthesis of [Co(dbm)$_2$(2,2′-bpy)]BF_4 58$^+$

To a stirred orange suspension of [Co(dbm)$_2$(H_2O)$_2$] (0.1586 g, 0.3 mmol) in CH_2Cl_2 (20 cm^3), 2,2′-bpy (0.0470 g, 0.3 mmol) was added. The orange solution was stirred for 1 hour then $AgBF_4$ (0.0646 g, 0.33 mmol) added. The olive green solution was stirred over night. The dark green solution was filtered through celite then washed with CH_2Cl_2 (3 x 5 cm^3). The solvent was removed to dryness. The solid was purified using CH_2Cl_2-*n*-hexane to give green brown micro crystals yield 0.1097 g (51%).

Synthesis of $[Co(dbm)_2(dmae)]BF_4$ 59^+

To a stirred orange suspension of $[Co(dbm)_2(H_2O)_2]$ (0.1718 g, 0.3 mmol) in CH_2Cl_2 (20 cm^3), dmae (34.7 μL, 0.3 mmol) was added. The orange solution was stirred for 1 hour then $AgBF_4$ (0.0710 g, 0.36 mmol) added. The olive green solution was stirred over night. The dark green solution was filtered through celite then washed with CH_2Cl_2 (3 x 5 cm^3). The solvent was removed to dryness. The solid was purified using CH_2Cl_2-*n*-hexane to give olive green micro crystals yield 0.1072 g (49%).

Synthesis of $[Co(tmhd)_2(phen)]BF_4$ 60^+

To a stirred purple solution of $[Co(tmhd)_2(H_2O)_2]$ (0.2303 g, 0.5 mmol) in CH_2Cl_2 (20 cm^3), phen (0.0992 g, 0.5 mmol) was added. The orange solution was stirred for 1 hour then $AgBF_4$ (0.110 g, 0.56 mmol) added. The brown-orange solution was stirred over night. The dark green solution was filtered through celite then washed with CH_2Cl_2 (3 x 5 cm^3). The solvent was removed to dryness. The solid was purified using CH_2Cl_2-diethyl ether to give dark red block crystals yield 0.2120 g (61%).

Synthesis of $[Co(tmhd)_2(2,2'\text{-bpy})]BF_4$ 61^+

To a stirred purple solution of $[Co(tmhd)_2(H_2O)_2]$ (0.2330 g, 0.5 mmol) in CH_2Cl_2 (20 cm^3), 2,2′-bpy (0.0785 g, 0.5 mmol) was added. The orange solution was stirred for 1 hour then $AgBF_4$ (0.110 g, 0.56 mmol) added. The brown-orange solution was stirred over night. The dark green solution was filtered through celite then washed with CH_2Cl_2 (3 x 5 cm^3). The solvent was removed to dryness. The solid was purified using CH_2Cl_2-diethyl ether to give maroon micro crystals yield 0.2138 g (64%).

Synthesis of $[Co(tmhd)_2(dmae)]BF_4$ 62^+

To a stirred purple solution of $[Co(tmhd)_2(H_2O)_2]$ (0.2298 g, 0.5 mmol) in CH_2Cl_2 (20 cm^3), dmae (54.4 μL, 0.5 mmol) was added. The orange solution was stirred for 1 hour then $AgBF_4$ (0.110 g, 0.56 mmol) added. The dark green solution was stirred over night. The deep purple solution was filtered through celite then washed with CH_2Cl_2 (3 x 5 cm^3). The solvent was removed to dryness. The solid was purified using CH_2Cl_2-diethyl ether to give pastel purple micro crystals yield 0.1841 g (61%).

Electron transfer studies of $[Co(\beta\text{-diketonate})_2(N\text{-}N)]BF_4$ complexes

The cations **57^+**-**62^+** were also studied by cyclic voltammetry and show a large reduction peak coupled to a smaller redox couple at a higher potential (Table 13, Figure 16). The peak potentials observed in cyclic voltammograms are almost identical to those found in the neutral analogues although there are slight deviations. Similar results are noted in the complex $[(bpbp)Co_2(O_2P(OPh)_2)_2]^{3+}$ where shifts of up to 180 mV are observed. As with **57**-**62** the peaks for the high spin Co^{III} intermediate are clearly discernable but no peak is apparent for the possible low

spin Co^{II} intermediate implying that the electron transfer reaction may proceed through the high spin intermediate.

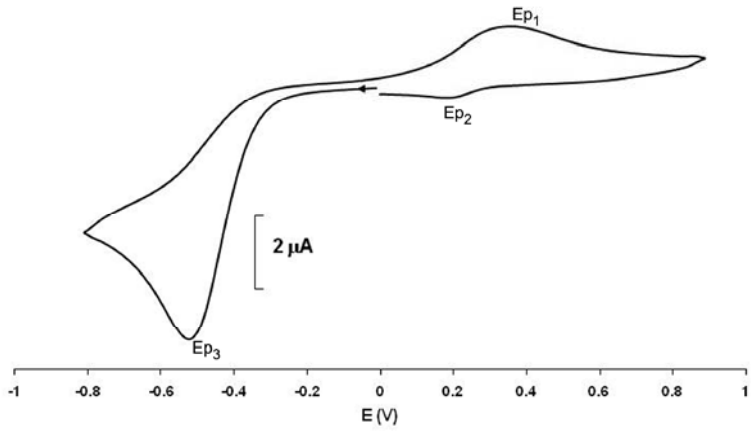

Figure 16 Cyclic voltammograms of $[Co(tmhd)_2(phen)]BF_4$ **60**$^+BF_4^-$.

Table 13 Cyclic voltammetric data of [Co(β-diketonate)$_2$(N-N)] complexes.

Complex	**Peak potential (V)**		
	Ep_1	Ep_2	Ep_3
$[Co(dbm)_2(phen)]BF_4$ **57**$^+$	0.52	0.30	-0.12
$[Co(dbm)_2(2,2'\text{-bpy})]BF_4$ **58**$^+$	0.46	-	-0.15
$[Co(dbm)_2(dmae)]BF_4$ **59**$^+$	0.35	-	-0.20
$[Co(tmhd)_2(phen)]BF_4$ **60**$^+$	0.35	0.18	-0.52
$[Co(tmhd)_2(2,2'\text{-bpy})]BF_4$ **61**$^+$	0.28	0.14	-0.51
$[Co(tmhd)_2(dmae)]BF_4$ **62**$^+$	0.44	0.21	-0.70

To confirm that the products isolated from the chemical oxidation of **57**-**62** were the same as those observed in the cyclic voltammograms we undertook IR spectroelectrochemical studies. The results are detailed in Table 14 with a representative spectrum shown in Figure 17. The oxidation of **57**-**62** are all accompanied by the loss of the β-diketonate ν_{CO} bands at *ca*. 1590, 1570, 1520 and 1500 cm^{-1} and a corresponding increase in bands at between *ca*. 1550 and 1520 cm^{-1} with the anticipated lower bands lost due to interference from the electrolyte. Subsequent reduction restores the original spectrum showing as expected that the chemical oxidation or reduction is reversible. The shift in the bands to lower wavenumbers mirrors exactly what is observed in the isolated complexes. Moreover, the positions of the bands are almost identical between the isolated redox pairs and the results from spectroelectrochemistry confirming that the isolated complexes are the species formed at the electrode. Similar studies on the cationic species **57**$^+$-**62**$^+$ show an exact

opposite trend with bands moving to higher wavenumbers as one would expect. Sadly, we were unable to assign any bands definitively to the high spin Co^{III} intermediate observed in the cyclic voltammograms.

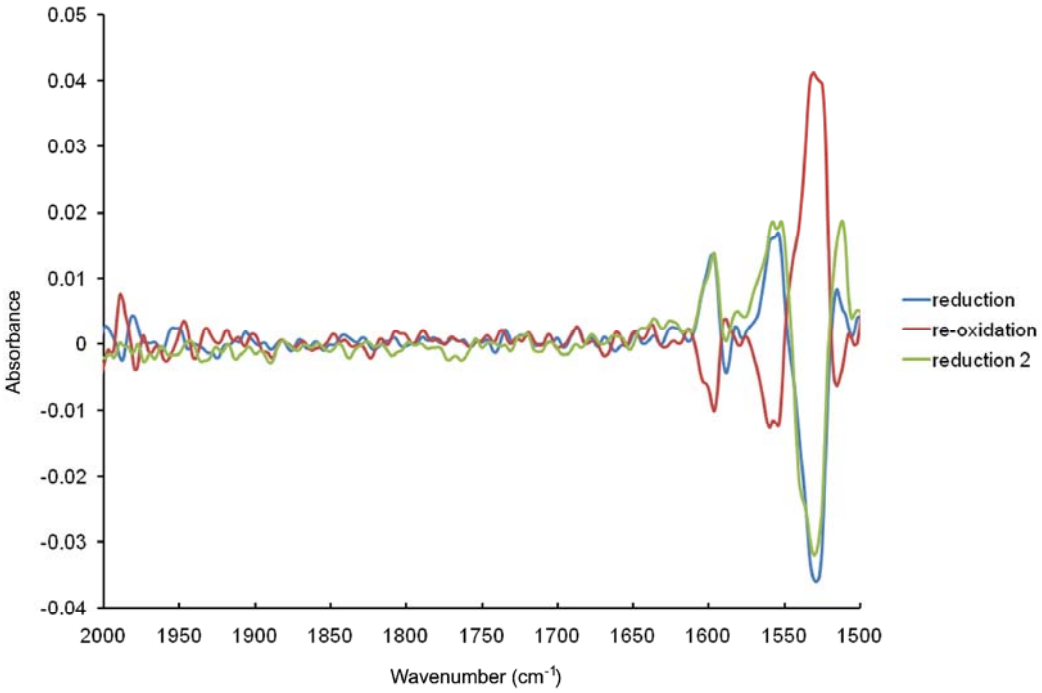

Figure 17 IR-spectroelectrochemical spectrum for $[Co(dbm)_2(phen)]BF_4$ **57**$^+$.

Table 14 IR-spectroelectrochemical data for $[Co(\beta\text{-diketonate})_2(N\text{-}N)]^{0/+}$ complexes.

Complex	Positive Absorbance Bands (cm^{-1})	Negative Absorbance Bands (cm^{-1})
$[Co(dbm)_2(phen)]$ **57**	1587, 1528	1596, 1564, 1554, 1514
$[Co(dbm)_2(2,2'\text{-bpy})]$ **58**	1530	1597, 1563, 1549
$[Co(dbm)_2(dmae)]$ **58**	1526	1563, 1553
$[Co(tmhd)_2(phen)]$ **60**	1552, 1543, 1523	1587, 1572, 1533, 1516, 1505
$[Co(tmhd)_2(2,2'\text{-bpy})]$ **61**	1545, 1527	1588, 1581, 1570, 1518, 1504
$[Co(tmhd)_2(dmae)]$ **62**	1557, 1547, 1533	1592, 1582, 1570
$[Co(dbm)_2(phen)]BF_4$ **57**$^+$	1596, 1557, 1552, 1512	1538 (sh), 1529
$[Co(dbm)_2(2,2'\text{-bpy})]BF_4$ **58**$^+$	1597, 1579, 1554, 1513	1530, 1588
$[Co(dbm)_2(dmae)]BF_4$ **59**$^+$	1596, 1557, 1516	1588, 1540, 1528
$[Co(tmhd)_2(phen)]BF_4$ **60**$^+$	1589, 1573, 1506	1558, 1548, 1525
$[Co(tmhd)_2(2,2'\text{-bpy})]BF_4$ **61**$^+$	1587, 1572, 1506	1552 (sh), 1544, 1531, 1496
$[Co(tmhd)_2(dmae)]BF_4$ **62**$^+$	1596, 1581, 1569	1546, 1534

4.7. Synthesis and characterization of the bridging ligands

The reaction between pyridine-2-carboxaldehyde and the desired diamine *e*.g. 1,3-diaminobenzene, 1,4-diaminobenzene, 1,5-diaminonaphthalene and hydrazine in isopropyl ether or acetylacetate at room temperature yields bispyridylmethylene-1,3-benzeneamine (1,3-bpmba) **63**, bispyridylmethylene-1,4-benzeneamine (1,4-bpmba) **64**, bispyridylmethylene-1,5-naphthaleneamine (1,5-bpmna) **65** and bis(pyridyl)methylene-hydrazone (bpmhd) **66** respectively (Scheme 7).

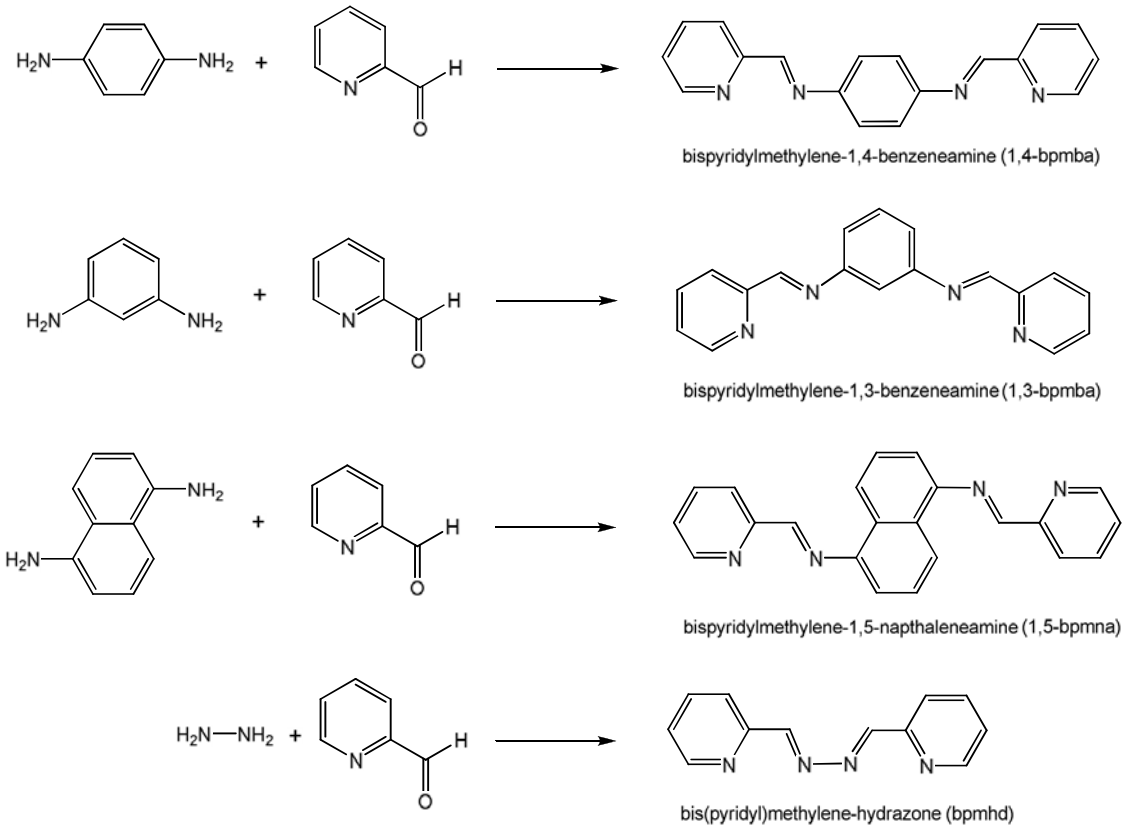

Scheme 7 Synthesis of the bridging ligands.

Table 15 IR and UV-Vis spectroscopic data for the bridging ligands.

Compound	% Yield	Colour	$\nu_{C=N}$	UV-Vis
1,3-bpmba **63**	57	Yellow	1628	254 (22,240), 280 (22,600)
1,4-bpmba **64**	83	Yellow	1619	232 (25,080), 284 (11,960)
1,5-bpmna **65**	67	Yellow	1622	246 (36,221), 370 (14,081)
bpmhd **66**	68	Bright yellow	1630	250 (28,729), 285 (25,653)

IR spectroscopy reveals a strong absorption at between 1619 and 1628 cm^{-1} typical of an imine stretch. The ^{1}H NMR spectra are sharp and agree well with the values previously reported for these ligands. In particular, a singlet is observed low field consistent with the presence of an imine

hydrogen. It is also of note that trace amounts of the starting materials are found in the ^{1}H NMR spectra and indicative of the reversibility of such reactions.

Experimental

Synthesis of bispyridylmethylene-1,3-benzeneamine 63

1,3-diaminobenzene (0.3244 g, 3 mmol) was dissolved in dried isopropyl ether over molecular sieves (20 cm^3). Pyridine-2-carboxaldehyde (0.573 mL, 6 mmol) was added to the light brown solution. The yellow solution was stirred overnight then filtered through paper. The solvent was removed give an oily yellow compound 0.4923 g (57%).

Synthesis of bispyridylmethylene-1,4-benzeneamine 64

1,4-diaminobenzene (0.2762 g, 2.6 mmol) was dissolved in dried isopropyl ether over molecular sieves (20 cm^3). Pyridine-2-carboxaldehyde (0.478 mL, 5 mmol) was added to the light yellow solution. The yellow solution was stirred overnight then filtered through paper. The solvent was removed give yellow crystallize solid. The crystals were washed with *n*-hexane (10 cm^3) yield 0.5938 g (83%).

Synthesis of bispyridylmethylene-1,5-naphthaleneamine 65

1,5-diaminonaphthalene (0.4749 g, 3 mmol) was dissolved in dried isopropyl ether over molecular sieves (20 cm^3). Pyridine-2-carboxaldehyde (0.531 mL, 6 mmol) was added to the light yellow solution. The yellow suspension was stirred overnight then filtered through paper to remove molecular sieves. The yellow solid was dissolved in CH_2Cl_2 (10 cm^3). The solvent was removed to give a yellow solid 0.6757 g (67%).

Synthesis of bis(pyridyl)methylene-hydrazone 66

Hydrazine (0.64 cm^3, 10 mmol) was dissolved in dried ethyl acetate over molecular sieves (10 cm^3). Pyridine-2-carboxaldehyde (1.91 cm^3, 20 mmol) was added to the light yellow solution. The yellow solution was stirred for one hour then the bright yellow crystals started to precipitate. The mixture was stirred another hour then filtered through paper. The bright yellow crystals were separated from molecular sieves yields 1.44 g (68%).

4.8. Synthesis and characterization of [(β-diketonate)$_2$M(μ-L)M(β-diketonate)$_2$] complexes

The reaction between one equivalent of the bridging ligands **63**-**66** with two equivalents of [M(β-diketonate)$_2$(H_2O)$_2$] in CH_2Cl_2 or THF gives the dimeric complexes, [(β-diketonate)$_2$M(μ-L)M(β-diketonate)$_2$] in which M = Ni, β-diketonate = dbm, L = 1,3-bpmba **67**, 1,4-bpmba **68**, 1,5-bpmna **69**, bpmhd **70**; β-diketonate = tmhd, L = 1,3-bpmba **71**, 1,4-bpmba **72**, 1,5-bpmna **73**, bpmhd **74**, M = Co,

β-diketonate = dbm, L = 1,3-bpmba **75**, 1,4-bpmba **76**, 1,5-bpmna **77**, bpmhd **78**; β-diketonate = tmhd, L = 1,3-bpmba **79**, 1,4-bpmba **80**, 1,5-bpmna **81**, bpmhd **82** (Scheme 8).

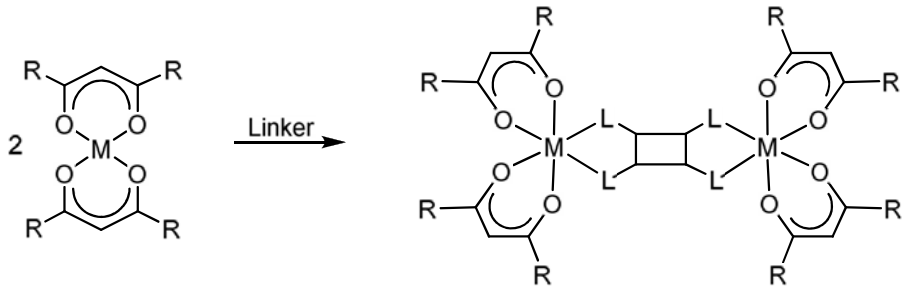

Scheme 8 Synthesis of [(β-diketonate)$_2$M(μ-L)M(β-diketonate)$_2$] complexes.

All complexes have been characterized by IR and UV-Vis spectroscopy, CHN analysis and mass spectrometry. CHN analysis and mass spectra confirm the purity of the complexes (Table 16).

Table 16 Physical and IR spectroscopic data for [(β-diketonate)$_2$M(μ-L)M(β-diketonate)$_2$].

Complex	% Yield	Colour	$\nu_{C=O}$/cm^{-1}
[(dbm)$_2$Ni(μ-1,3-bpmba)Ni(dbm)$_2$] **67**	31	Yellow brown	1594
[(dbm)$_2$Ni(μ-1,4-bpmba)Ni(dbm)$_2$] **68**	89	Red	1595
[(dbm)$_2$Ni(μ-1,5-bpmna)Ni(dbm)$_2$] **69**	75	Golden brown	1592
[(dbm)$_2$Ni(μ-bpmhd)Ni(dbm)$_2$] **70**	45	Yellow brown	1594
[(tmhd)$_2$Ni(μ-1,3-bpmba)Ni(tmhd)$_2$] **71**	48	Yellow orange	1584
[(tmhd)$_2$Ni(μ-1,4-bpmba)Ni(tmhd)$_2$] **72**	55	Red	1584
[(tmhd)$_2$Ni(μ-1,5-bpmna)Ni(tmhd)$_2$] **73**	51	Red brown	1583
[(tmhd)$_2$Ni(μ-bpmhd)Ni(tmhd)$_2$] **74**	22	Salmon pink	1586
[(dbm)$_2$Co(μ-1,3-bpmba)Co(dbm)$_2$] **75**	32	Light brown	1594
[(dbm)$_2$Co(μ-1,4-bpmba)Co(dbm)$_2$] **76**	58	Red	1593
[(dbm)$_2$Co(μ-1,5-bpmna)Co(dbm)$_2$] **77**	74	Orange	1593
[(dbm)$_2$Co(μ-bpmhd)Co(dbm)$_2$] **78**	36	Brown	1593
[(tmhd)$_2$Co(μ-1,3-bpmba)Co(tmhd)$_2$] **79**	64	Dark brown	1590
[(tmhd)$_2$Co(μ-1,4-bpmba)Co(tmhd)$_2$] **80**	79	Dark brown	1590
[(tmhd)$_2$Co(μ-1,5-bpmna)Co(tmhd)$_2$] **81**	76	Red brown	1571
[(tmhd)$_2$Co(μ-bpmhd)Co(tmhd)$_2$] **82**	80	Purple brown	1588

IR spectroscopy of the *dbm* complexes **67**-**70** and **75**-**78** shows a C=O stretch from 1592-1594 cm^{-1} indicating that the β-diketonate ligands adopt a chelating coordination mode. The position of the bands are similar to those reported for [Ni(β-diketonate)$_2$(ppa^X)] and the Co analogues. The C=O

stretch for the *tmhd* compounds, **71**-**74** and **79**-**82** is *ca.* 5-10 cm^{-1} lower than that of *dbm* analogues consistent with the strong electron donating effect of the *t*-butyl groups. The imine stretches of coordinated bridging ligands which are expected to be between 1600 and 1630 cm^{-1} are not observed as they masked by the strong C=O stretch of the β-diketonate ligand.

Experimental

Synthesis of $[(dbm)_2Ni(\mu\text{-}1,3\text{-}bpmba)Ni(dbm)_2]$ 67

To a stirred light green suspension of $[Ni(dbm)_2(H_2O)_2]$ (0.1082 g , 0.2 mmol) in CH_2Cl_2 (10 cm^3) was added 1,3-bpmba (0.0286 g, 0.1 mmol) to give a light yellow brown solution. The light yellow brown solution was stirred overnight. The mixture was filter through filter paper to give a light yellow brown solution and then the solution was evaporated on to rotary evaporator and remove volume to small amount. The residue was washed diethyl ether to give a light yellow brown precipitate, yield 0.0394 g (31 %).

Synthesis of $[(dbm)_2Ni(\mu\text{-}1,4\text{-}bpmba)Ni(dbm)_2]$ 68

To a stirred light green suspension of $[Ni(dbm)_2(H_2O)_2]$ (0.2167 g , 0.4 mmol) in CH_2Cl_2 (10 cm^3) was added 1,4-bpmba (0.0570 g, 0.2 mmol) to give a light yellow brown solution. The yellow brown solution was stirred overnight. The solution was filter through celite to give a light yellow brown solution and then the solution was evaporated on to rotary evaporator and remove volume to small amount. *n*-Hexane (10 cm^3) was added a red crystals precipitated, yield 0.2300 g (89%).

Synthesis of $[(dbm)_2Ni(\mu\text{-}1,5\text{-}bpmna)Ni(dbm)_2]$ 69

To a stirred light green suspension of $[Ni(dbm)_2(H_2O)_2]$ (0.1085 g, 0.2 mmol) in CH_2Cl_2 (10 cm^3) was added 1,5-bpmna (0.0339 g, 0.1 mmol). The solution was then stirred at room temperature. After four hours, the brown solution was filtered and left to evaporate slowly at room temperature to give red- brown crystals, yield 0.1017 g (75%).

Synthesis of $[(dbm)_2Ni(\mu\text{-}bpmhd)Ni(dbm)_2]$ 70

To a stirred lime green solution of $[Ni(dbm)_2(H_2O)_2]$ (0.1509 g, 0.2 mmol) in THF (10 cm^3), bpmhd (0.0213 g, 0.1 mmol) was added. The red-brown solution was stirred for 2 hours then the solvent was removed to small volume. *n*-Hexane (5 cm^3) was added to induce precipitation. The yellow brown micro crystals was filtered and washed with *n*-hexane (2 x 5 cm^3) yields 0.0555 g (45%).

Synthesis of $[(tmhd)_2Ni(\mu\text{-}1,3\text{-}bpmba)Ni(tmhd)_2]$ 71

To a stirred green suspension of $[Ni(tmhd)_2(H_2O)_2]$ (0.0461 g, 0.1 mmol) in THF (5 cm^3) was added 1,3-bpmba (0.0143 g, 0.05 mmol) to give a light yellow brown solution. The light yellow brown solution was stirred overnight. The mixture was filtrated through celite to give a light yellow

brown solution and then the solution was evaporated on to rotary evaporator and remove volume to small amount. The residue was washed diethyl ether to give light yellow orange precipitates, yield 0.0273 g (48%).

Synthesis of [(tmhd)$_2$Ni(μ-1,4-bpmba)Ni(tmhd)$_2$] 72

To a stirred purple solution of [Ni(tmhd)$_2$(H$_2$O)$_2$] (0.0461 g, 0.1 mmol) in CH_2Cl_2 (15 cm^3) was added 1,4-bpmba (0.0567 g, 0.2 mmol) to give a deep orange solution. The solution was stirred overnight. The mixture was filtrated through celite to give a deep orange solution and then the solution was evaporated on to rotary evaporator and remove volume to small amount. The residue was washed diethyl ether to give red precipitates, yield 0.1250 g (55 %).

Synthesis of [(tmhd)$_2$Ni(μ-1,5-bpmna)Ni(tmhd)$_2$] 73

To a stirred purple solution of [Ni(tmhd)$_2$(H$_2$O)$_2$] (0.0923 g, 0.2 mmol) in CH_2Cl_2 (10 cm^3) was added 1,5-bpmna (0.0338 g, 0.1 mmol). After stirring for 24 hours, the dark brown solution was filtered through filtered paper. The solution was then evaporated slowly at room temperature to low volume. Then hexane was added on top of the solution and the solution was left to crystallize to give red-brown crystals yield 0.0611 g (51%).

Synthesis of [(tmhd)$_2$Ni(μ-bpmhd)Ni(tmhd)$_2$] 74

To a stirred green solution of [Ni(tmhd)$_2$(H$_2$O)$_2$] (0.0922 g, 0.2 mmol) in THF (10 cm^3), bpmhd (0.0228 g, 0.1 mmol) was added. The red-orange solution was stirred for 2 hours then the solvent was removed to small volume. *n*-Hexane (5 cm^3) was added to induce precipitation but no precipitation occurred. The solvent was removed to dryness. The salmon pink solid was filtered and dried in air yields 0.0306 g (22%).

Synthesis of [(dbm)$_2$Co(μ-1,3-bpmba)Co(dbm)$_2$] 75

To a stirred light orange yellow suspension of [Co(dbm)$_2$(H$_2$O)$_2$] (0.0542 g, 0.1 mmol) in CH_2Cl_2 (5 cm^3) was added 1,3-bpmba (0.0143 g, 0.05 mmol) to give a dark red suspension. The dark red suspension was stirred overnight. The mixture was filter through filter paper to give a light red brown solution and then the solution was evaporated on to rotary evaporator and remove volume to small amount. The residue was washed diethyl ether to give a light brown precipitate, yield 0.0206 g (32%)

Synthesis of [(dbm)$_2$Co(μ-1,4-bpmba)Co(dbm)$_2$] 76

To a stirred yellow orange suspension of [Co(dbm)$_2$(H$_2$O)$_2$] (0.0541 g, 0.1 mmol) in CH_2Cl_2 (5 cm^3) was added 1,4-bpmba (0.0143 g, 0.05 mmol) to give a red orange suspension. The red orange suspension was stirred overnight. The mixture was filter through filter paper to give a dark red brown solution and then the solution was left to slowly evaporate at room temperature. Then hexane was added on top of the solution to give red crystals, yield 0.0378 g (58%).

Synthesis of [(dbm)$_2$Co(μ-1,5-bpmna)Co(dbm)$_2$] 77 To a stirred purple solution of [Co(dbm)$_2$(H$_2$O)$_2$] (0.1083 g, 0.2 mmol) in THF (7 cm^3) was added 1,5-bpmna (0.0340 g, 0.1 mmol). After 4 hours, the red-brown solution was filtered through celite and left to evaporate slowly at room temperature to give red-brown crystals, yield 0.0744 g (74%).

Synthesis of [(dbm)$_2$Co(μ-bpmhd)Co(dbm)$_2$] 78

To a stirred bright orange solution of [Co(dbm)$_2$(H$_2$O)$_2$] (0.1086 g, 0.2 mmol) in THF (10 cm^3), bpmhd (0.0219 g, 0.1 mmol) was added. The red-brown solution was stirred for 2 hours then the solvent was removed to small volume. *n*-Hexane (5 cm^3) was added to induce precipitation. The brown micro crystals was filtered and washed with *n*-hexane (2 x 5 cm^3) yields 0.044 g (36%).

Synthesis of [(tmhd)$_2$Co(μ-1,3-bpmba)Co(tmhd)$_2$] 79

To a stirred light purple solution of [Co(tmhd)$_2$(H$_2$O)$_2$] (0.0462 g , 0.1 mmol) in THF (5 cm^3) was added 1,3-bpmba (0.0143 g, 0.05 mmol) to give a dark purple brown solution. The dark purple brown solution was stirred 4 hrs. The mixture was filtrated through celite to give a light purple brown solution and then the solution was evaporated on to rotary evaporator and remove volume to small amount. The residue was washed diethyl ether to give a dark brown precipitate, yield 0.0362 g (64%).

Synthesis of [(tmhd)$_2$Co(μ-1,4-bpmba)Co(tmhd)$_2$] 80 To a stirred light purple solution of [Co(tmhd)$_2$(H$_2$O)$_2$] (0.0462 g, 0.1 mmol) in THF (4 cm^3) was added 1,4-bpmba (0.0143 g, 0.05 mmol) to give a dark red brown solution. The dark red brown solution was stirred 3 hours. The mixture was filtrated through celite to give a dark purple brown solution and then the solvent was removed on to rotary evaporator to small amount. Then diethyl ether (10 cm^3) was added to give a dark brown precipitate, yield 0.0448 g (79%).

Synthesis of [(tmhd)$_2$Co(μ-1,5-bpmna)Co(tmhd)$_2$] 81

To a stirred purple solution of [Co(tmhd)$_2$(H$_2$O)$_2$] (0.0924 g, 0.2 mmol) in THF (7 cm^3) was added 1,5-bpmna (0.0339 g, 0.1 mmol). After 4 hours, the brown solution was filtered through celite and left to evaporate slowly at room temperature to give a red-brown crystals, yield 0.0765 g (76%).

Synthesis of [(tmhd)$_2$Co(μ-bpmhd)Co(tmhd)$_2$] 82

To a stirred red solution of [Co(tmhd)$_2$(H$_2$O)$_2$] (0.065 g, 0.14 mmol) in THF (5 cm^3), bpmhd (0.0158 g, 0.075 mmol) was added. The deep purple solution was stirred for 2 hours then the solvent was removed to small volume. *n*-Hexane (5 cm^3) was added to induce precipitation but no precipitation occurred. The solvent was removed to dryness. The purple brown solid was filtered and dried in air yields 0.0635 g (80%).

X-ray structural studies of [(β-diketonate)$_2$M(μ-L)M(β-diketonate)$_2$] complexes

The suitable crystals of [(dbm)$_2$Co(μ-1,4-bpmba)Co(dbm)$_2$] **76** was grown by allowing *n*-hexane to diffuse slowly into a concentrated solution of the complex in CH_2Cl_2 at room temperature. Complex **76** assumes slightly distorted octahedral coordination geometries (Figure 18). The β-diketonate ligands exhibit a *cis* arrangement enforced by the bridging ligand, 1,4-bpmba. The Co-O bond lengths are slightly longer to that of [Co(dbm)$_2$(ppa^{OMe})] **36** and [Co(dbm)$_2$(ppa^{Cl})] **38**. Interestingly, the Co-O4 bond length is considerably longer than the others. The cobalt bond to the pyridine of the bridging ligand of complexes **76** is considerably shorter than the bond to the imine nitrogen differing by *ca*. 0.1 Å.

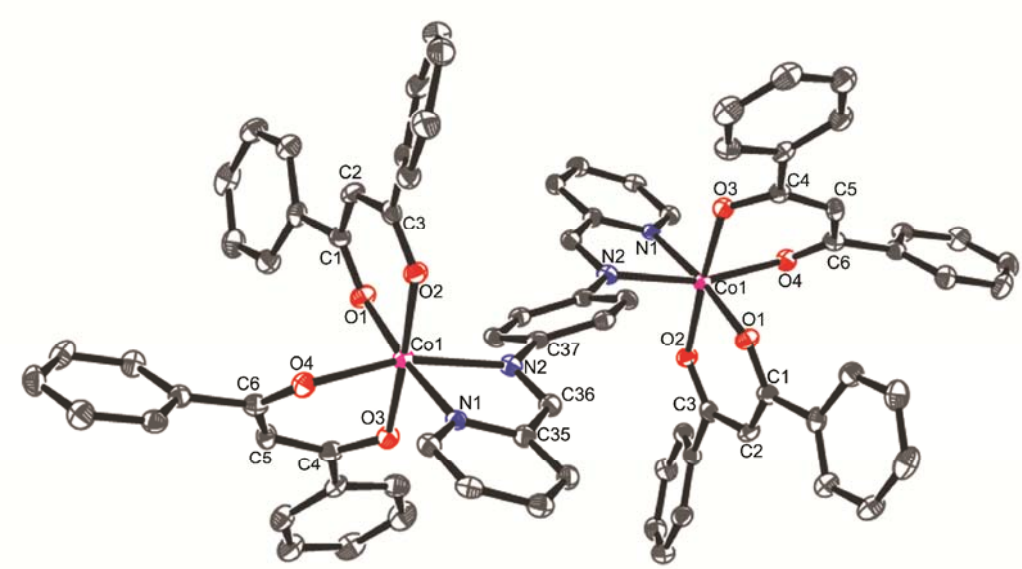

Figure 18 ORTEP diagram of [(dbm)$_2$Co(μ-1,4-bpmba)Co(dbm)$_2$] **76**. The thermal ellipsoids are drawn to 50% probability level. Hydrogen atoms are omitted for clarity.

Table 17 Bond lengths and bond angles of [(dbm)$_2$Co(μ-1,4-bpmba)Co(dbm)$_2$] **76**.

	(Å)		(°)
Co(1)-O(1)	2.045(2)	O(1)-Co(1)-O(2)	87.22(9)
Co(1)-O(2)	2.047(2)	O(1)-Co(1)-O(3)	87.23(9)
Co(1)-O(3)	2.052(2)	O(2)-Co(1)-O(3)	174.45(9)
Co(1)-O(4)	2.095(2)	O(1)-Co(1)-O(4)	91.61(9)
Co(1)-N(1)	2.115(3)	O(2)-Co(1)-O(4)	94.69(9)
Co(1)-N(2)	2.232(2)	O(3)-Co(1)-O(4)	85.37(8)
N(1)-C(31)	1.339(3)	O(1)-Co(1)-N(1)	173.63(9)
N(1)-C(35)	1.357(4)	O(2)-Co(1)-N(1)	88.25(9)
N(2)-C(36)	1.278(4)	O(3)-Co(1)-N(1)	97.29(9)
N(2)-C(37)	1.434(3)	O(4)-Co(1)-N(1)	93.23(9)

O(1)-C(1)	1.267(4)	O(1)-Co(1)-N(2)	99.94(9)
O(2)-C(3)	1.274(4)	O(2)-Co(1)-N(2)	97.87(9)
O(3)-C(4)	1.279(4)	O(3)-Co(1)-N(2)	83.19(9)
O(4)-C(6)	1.272(4)	O(4)-Co(1)-N(2)	163.29(9)
		N(1)-Co(1)-N(2)	76.25(9)

The suitable crystals of $[(dbm)_2M(\mu\text{-bpmhd})M(dbm)_2]$ (M= Ni **70** and Co **78**) were grown by allowing *iso*-propanol to diffuse slowly into a concentrated solution of the complex in CH_2Cl_2 at room temperature. Both structures assume slightly distorted octahedral coordination geometries (Figures 19 and 20). The β-diketonate ligands exhibit a *cis* arrangement enforced by the bridging ligand, bpmhd. The M-O bond in **78** lengths are slightly longer to that of **70** but similar to that of $[(dbm)_2Co(\mu\text{-}1,4\text{-bpmba})Co(dbm)_2]$ **76**. The metal bond to the pyridine of the bridging ligand of complexes **70** and **78** is considerably shorter than the bond to the imine nitrogen differing by *ca*. 0.1 Å.

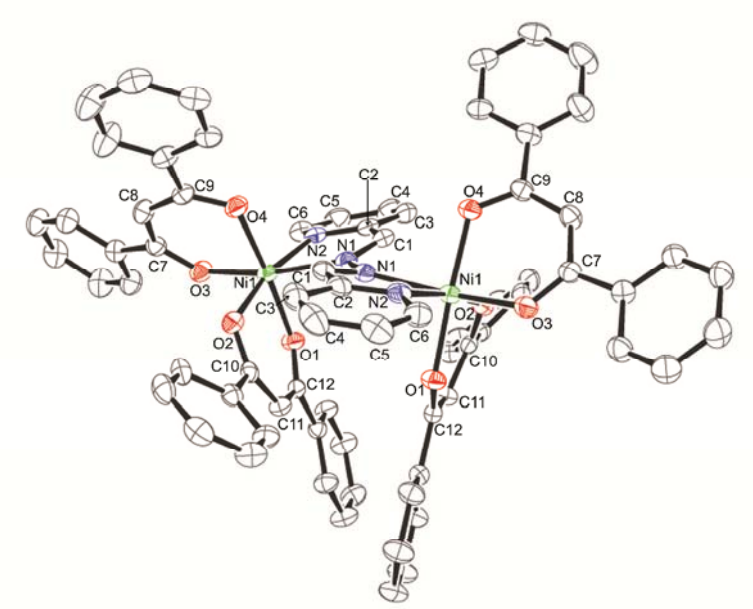

Figure 19 ORTEP diagram of $[(dbm)_2Ni(\mu\text{-bpmhd})Ni(dbm)_2]$ **70**. The thermal ellipsoids are drawn to 50% probability level. Hydrogen atoms are omitted for clarity.

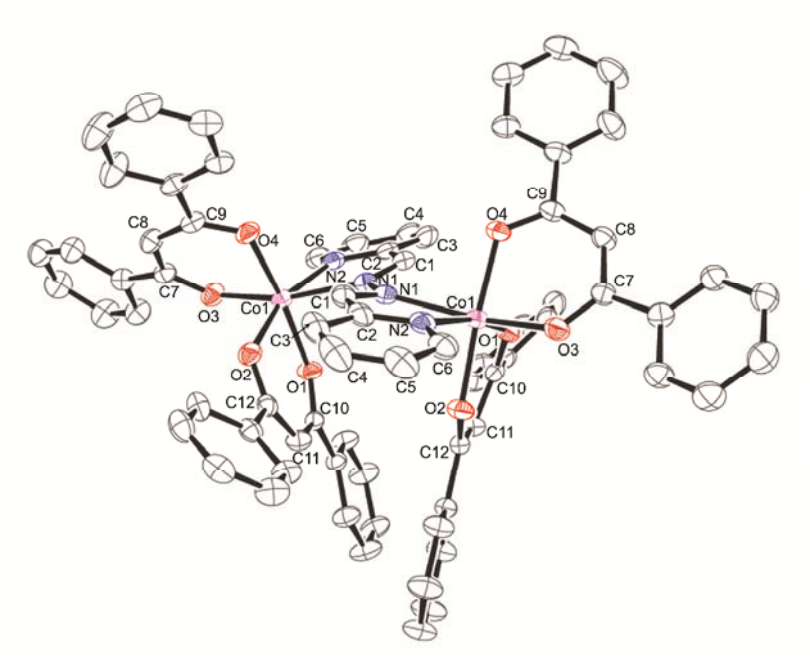

Figure 20 ORTEP diagram of $[(dbm)_2Co(\mu\text{-bpmhd})Co(dbm)_2]$ **78**. The thermal ellipsoids are drawn to 50% probability level. Hydrogen atoms are omitted for clarity.

Table 18 Selected bond lengths (Å) and angles (°) of **70** and **78**

	70	**78**		**70**	**78**
M(1)-O(1)	2.0093(18)	2.0421(13)	O(1)-M(1)-O(2)	88.98(8)	86.12(5)
M(1)-O(2)	1.9949(19)	2.0278(14)	O(1)-M(1)-O(3)	89.84(8)	92.12(6)
M(1)-O(3)	1.996(2)	2.0164(14)	O(1)-M(1)-O(4)	175.21(8)	172.53(6)
M(1)-O(4)	2.0105(18)	2.0261(13)	O(2)-M(1)-O(3)	96.15(8)	98.62(6)
M(1)-N(1)	2.159(2)	2.2122(16)	O(2)-M(1)-O(4)	86.32(8)	86.50(6)
M(1)-N(2)	2.081(2)	2.1173(17)	O(3)-M(1)-O(4)	89.78(8)	87.81(5)
N(1)-C(1)	1.287(4)	1.283(3)	O(1)-M(1)-N(1)	94.18(8)	94.86(6)
N(1)-N(1)’	1.407(5)	1.404(3)	O(2)-M(1)-N(1)	95.06(8)	94.95(6)
N(2)-C(2)	1.347(4)	1.349(3)	O(3)-M(1)-N(1)	168.15(8)	165.12(6)
N(2)-C(6)	1.339(4)	1.333(3)	O(4)-M(1)-N(1)	87.13(8)	86.96(6)
O(1)-C(12)	1.264(3)	1.258(2)	O(1)-M(1)-N(2)	82.87(8)	81.83(6)
O(2)-C(10)	1.269(3)	1.265(2)	O(2)-M(1)-N(2)	167.99(8)	163.68(6)
O(3)-C(7)	1.272(3)	1.271(2)	O(3)-M(1)-N(2)	92.63(9)	92.82(6)
O(4)-C(9)	1.273(3)	1.272(2)	O(4)-M(1)-N(2)	101.92(8)	105.63(6)

Electron transfer studies of [(β-diketonate)$_2$M(μ-L)M(β-diketonate)$_2$] complexes

Electrochemical studies of the dimer complexes **67**-**82** were conducted in CH_2Cl_2 between ±1.8 V *versus* the Ag-AgCl electrode at room temperature using a three-electrode configuration. All of the Ni dimer complexes show two irreversible oxidation peaks with exception of [(tmhd)$_2$Ni(μ-bpmhd)Ni(tmhd)$_2$] **74** that shows two reversible and one irreversible process (Figure 21, Table 19).

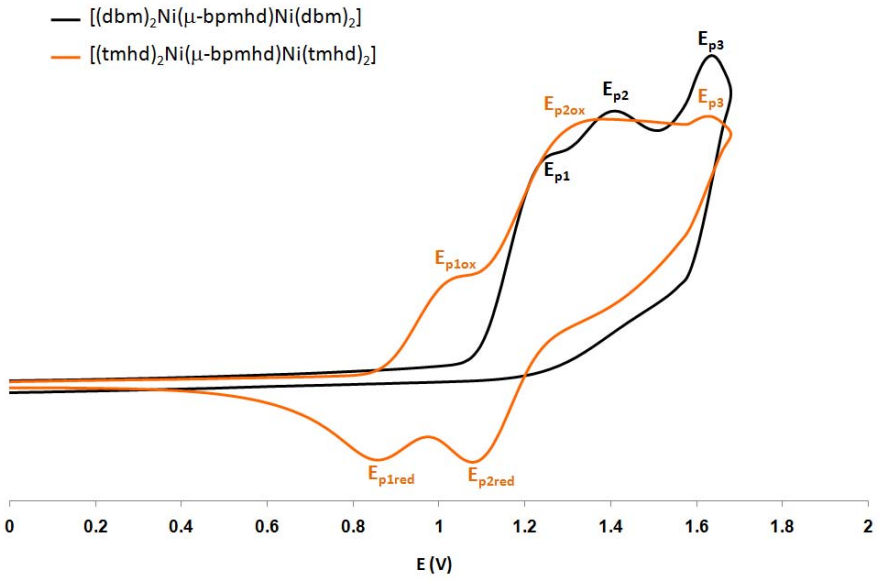

Figure 21 Cyclic voltammograms of [(dbm)$_2$Ni(μ-bpmhd)Ni(dbm)$_2$] **70** and [(tmhd)$_2$Ni(μ-bpmhd)Ni(tmhd)$_2$] **74**.

Table 19 Electrochemical data for [(β-diketonate)$_2$Ni(μ-L)Ni(β-diketonate)$_2$] complexes.

Complex	Peak potential (V)		
	Ep_1	Ep_2	Ep_3
[(dbm)$_2$Ni(μ-1,3-bpmba)Ni(dbm)$_2$] **67**	1.26 (I)	1.54(I)	-
[(dbm)$_2$Ni(μ-1,4-bpmba)Ni(dbm)$_2$]**68**	1.24 (I)	1.61(I)	-
[(dbm)$_2$Ni(μ-1,5-bpmna)Ni(dbm)$_2$] **69**	1.32 (I)	1.68(I)	-
[(dbm)$_2$Ni(μ-bpmhd)Ni(dbm)$_2$] **70**	1.32(I)	1.40(I)	1.64(I)
[(tmhd)$_2$Ni(μ-1,3-bpmba)Ni(tmhd)$_2$] **71**	0.96 (I)	1.54(I)	-
[(tmhd)$_2$Ni(μ-1,4-bpmba)Ni(tmhd)$_2$] **72**	1 03(I)	1.51 (I)	-
[(tmhd)$_2$Ni(μ-1,5-bpmna)Ni(tmhd)$_2$] **73**	0.94 (I)	1.54(I)	-
[(tmhd)$_2$Ni(μ-bpmhd)Ni(tmhd)$_2$] **74**	0.98*	1.23*	1.62(I)

* $E_{1/2}$ for reversible process.

A comparison of the oxidation potential of *dbm* complexes with *tmhd* complexes mirrors the trend observed in the [Ni(β-diketonate)$_2$(ppa^X)] series with the oxidation potential of the *dbm*

complexes higher than that of *tmhd* complexes. The structure of the bridging ligands also plays an important role in controlling the electron transfer properties of the dimer complexes. The difference in the oxidation potential for the different ligands reveals no trend other than that the bpmhd complexes are always the most difficult to oxidize (Figure 22). The presence of two oxidation peaks in the complexes indicates that there is communication between the two metal centres. The shortest bridge *i.e. bpmhd* appears to display a largest difference in oxidation potentials consistent with the strongest communication between the metal centres.

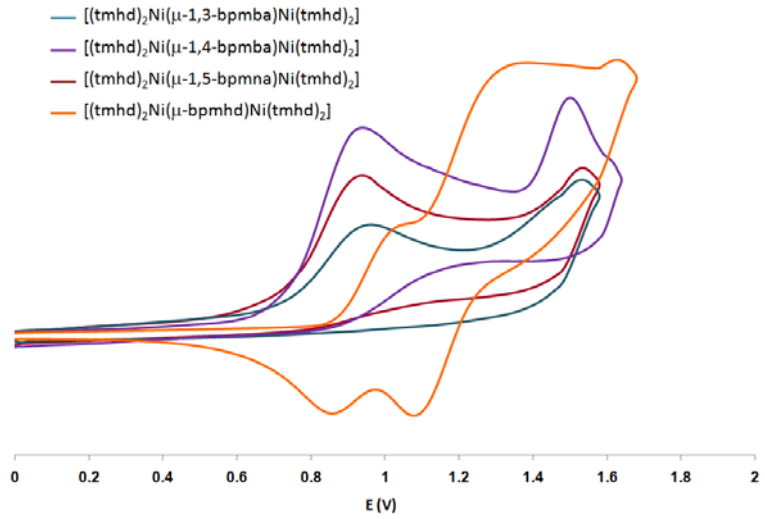

Figure 22 Cyclic voltammograms of $[(tmhd)_2Ni(\mu\text{-}L)Ni(tmhd)_2]$ **71-74**.

In case of the Co dimers **75**-**82** the cyclic voltammograms show oxidation peaks followed by returned peaks which are separated from the oxidation peaks by *ca.* 800-2000 mV indicative of the redox-coupled spin crossover behavior observed in the $[Co(\beta\text{-diketonate})_2(ppa^X)]$ and $[Co(\beta\text{-diketonate})_2(N\text{-}N)]$ complexes (Figures 23 and 24, Table 20).

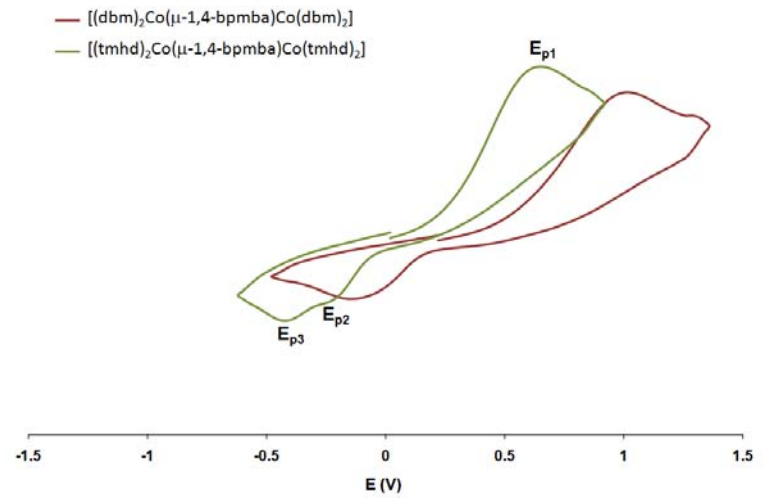

Figure 23 Cyclic voltammetry of $[(dbm)_2Co(\mu\text{-}1,4\text{-bpmba})Co(dbm)_2]$ **76** and $[(tmhd)_2Co(\mu\text{-}1,4\text{-bpmba})Co(tmhd)_2]$ **80**.

Table 20 Electrochemical data for [(β-diketonate)$_2$Co(μ-L)Co(β-diketonate)$_2$] complexes.

Complex	Peak potential (V)		
	Ep_1	Ep_2	Ep_3
[(dbm)$_2$Co(μ-1,3-bpmba)Co(dbm)$_2$] **75**	0.96	-	-0.16
[(dbm)$_2$Co(μ-1,4-bpmba)Co(dbm)$_2$] **76**	1.02	-	-0.14
[(dbm)$_2$Co(μ-1,5-bpmna)Co(dbm)$_2$] **77**	0.88	-	0.04
[(dbm)$_2$Co(μ-bpmhd)Co(dbm)$_2$] **78**	1.16	0.22	-0.12
[(tmhd)$_2$Co(μ-1,3-bpmba)Co(tmhd)$_2$] **79**	1.16	-0.72	-0.96
[(tmhd)$_2$Co(μ-1,4-bpmba)Co(tmhd)$_2$] **80**	0.66	-0.28	-0.42
[(tmhd)$_2$Co(μ-1,5-bpmna)Co(tmhd)$_2$] **81**	0.70	-0.38	-
[(tmhd)$_2$Co(μ-bpmhd)Co(tmhd)$_2$] **82**	1.28	0.14	-0.32

When we compare the oxidation peak potential of the complexes in the *dbm* series we found that the complexes are increasingly easy to oxidize in the order *bpmhd* > *1,4-bpmba* > *1,3-bpmba* > *1,5-bpmba*. While for the *tmhd* series the order is *bpmhd* > *1,3-bpmba* >*1,5-bpmna* > *1,4-bpmba*.

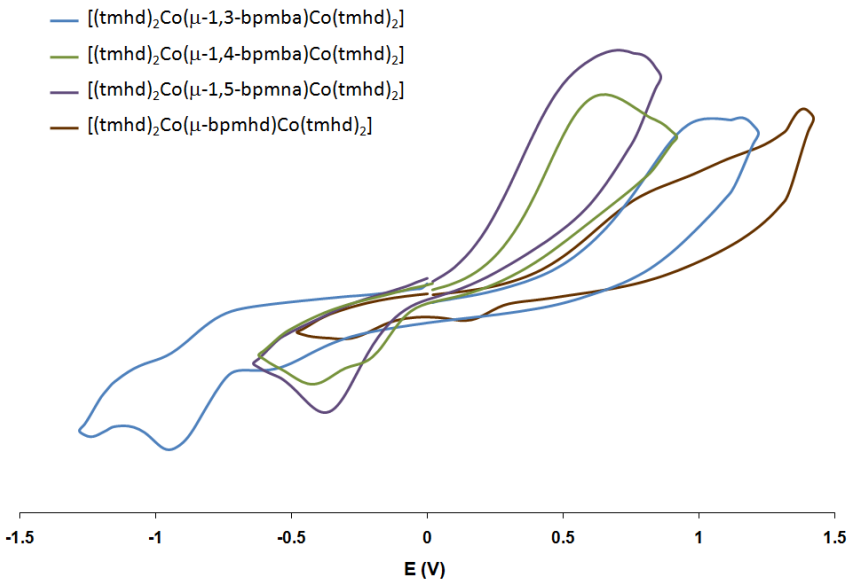

Figure 24 Cyclic voltammograms of [(tmhd)$_2$Co(μ-L)Co(tmhd)$_2$] complexes.

The unusual electron transfer behavior might due to the strong communication between the two metal centres through the bridging ligand. It is also possible that the structural reorganization required upon oxidation is more difficult to achieve as a result of increased steric interactions that would be expected in the 1,3-bpmba ligand complexes. Further studies of these complexes need to be conducted by spectroelectrochemistry and structural studies of redox pairs of the cobalt and if possible the nickel complexes.

4.9. Computational calculations of [Co(β-diketonate)$_2$(N-N)] complexes

In order to better understand the electronic structure of [Co(β-diketonate)$_2$(N-N)]{N-N = ppa^X **33-48**, phen, bpy and dmae **57-62**} and their respective cations, and in particular the role of the electronic structure on the redox coupled-spin crossover process we have undertaken DFT calculations. For a given complex, all possible spin states were considered.

To find the best calculation method for [Co(β-diketonate)$_2$(N-N)] we initially started with complexes **57-62** as there are less compounds in the series. The fact that [Co(dbm)$_2$(phen)] **57** has been structurally characterized by single crystal X-ray crystallography allows a comparison between the computational and experimental geometries (see Figure 24 and Table 21). The computed bond lengths match well with the experimental bond lengths with differences no more than 0.05 Å. The bonds angles show similar agreement between experiment and theory. Good agreements between the X-ray structure and computed geometry of [Co(dbm)$_2$(phen)] in the quartet spin state indicates that these complex exists in a high spin state. It also confirms that the B3LYP/SDD model can be used to describe these types of complexes.

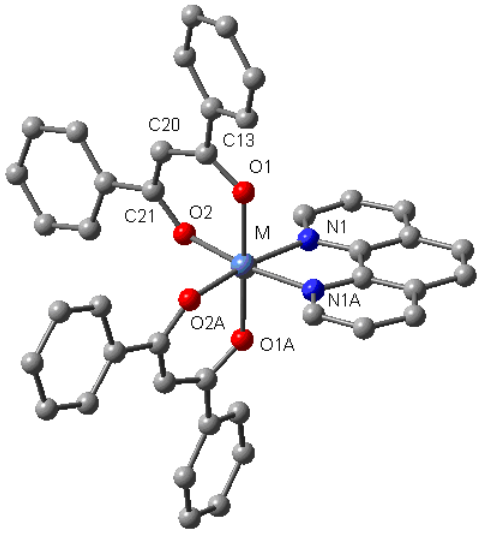

Figure 24 Numbering scheme for [Co(dbm)$_2$(phen)] complex as used for structural comparison with the X-ray structures.

Table 21 Selected computed and X-ray crystallographically determined bond lengths (Å) and bond angles (°) for [Co(dbm)$_2$(phen)] **57**. See Figure 24 for the numbering scheme.

[Co(dbm)$_2$(phen)]	X-ray[1]	Doublet	diff.[2]	Quartet	diff.[2]
Co-O1	2.07	2.15	0.08	2.0627	0.01
Co-O2	2.07	1.94	0.13	2.0544	0.01
Co-N1	2.15	1.96	0.19	2.1493	0.00

C7-O1	1.28	1.29	0.01	1.3022	0.02
C20-O2	1.27	1.31	0.04	1.3052	0.03
C7-C21	1.41	1.43	0.02	1.4019	0.00
C20-C21	1.41	1.41	0.00	1.4163	0.01
O1-Co-O2	86.29	88.63	2.34	85.73	0.56
O2-Co-O2A	102.54	91.92	10.62	98.69	3.85
O1-Co-O2A	83.67	89.01	5.34	91.96	8.29
O1-Co-N1	101.53	92.85	8.68	96.11	5.42
O1-Co-N1A	91.10	89.67	1.43	86.68	4.42
O2-Co-N1	90.49	92.24	1.75	92.43	1.94
O1-Co-O1A	163.92	176.63	12.71	176.42	12.50
N1-Co-N1A	76.87	83.64	6.77	77.58	0.71

[1]From ref. 59.

[2]Difference between X-ray crystallographic and optimized structure

Our B3LYP/SDD calculations confirm the observation that the HS state is the most stable state for the Co^{II} complexes and the LS state is the most stable state for the Co^{III} complexes and as such is consistent with the magnetic susceptibility measurements. In contrast, with the previously studied $[Co(tacn)_2]^{2+/3+}$ redox pair the gas-phase energy difference between the HS and LS states, E(HS)-E(LS), for the neutral Co^{II} complexes is between -12.7 and -15.6 kcal/mol (see Table 22) compared with -0.09 kcal/mol for $[Co(tacn)_2]^{2+}$. However, in the case of the Co^{III} cations the gap is significantly decreased to between 16.1 and 18.1 kcal/mol (*cf*. 45.3 kcal/mol for $[Co(tacn)_2]^{3+}$). Judging from the gas-phase energy, the triplet and quintet states are found to lie close to each other. The differences between E(HS)-E(LS) of **57**$^+$-**62**$^+$ and $[Co(tacn)_2]^{3+}$ are simply explained by the presence of the lower field β-diketonate ligands which are better able to stabilize the HS states. The thmd ligand stabilizes the HS state compared to the LS state to a greater extent than the dbm ligand. Moreover, the phen ligand stabilizes the HS state most in comparison with the other N-N ligands. This might be due to a metal d-π∗ orbital interaction from the low-lying π∗ orbital of the phen ligand. The smaller difference in the LS and HS states in **57**$^+$-**62**$^+$ might also explain why we are able to observe the reduction peak for the HS Co^{III} species in some of the electrochemical studies. These

studies further suggest that the mechanism for the redox coupled-spin crossover involves a HS Co^{III} intermediate as has also been found in the $[Co(tacn)_2]^{2+/3+}$ system.

Table 22 The high-spin and low-spin complex energy difference, E(HS)-E(LS), at B3LYP/SDD level for [Co(β-diketonate)$_2$(N-N)] complexes. For **57$^+$-62$^+$,** the pentet and triplet (in parenthesis) HS states were considered. The E(LUMO)-E(SOMO) gap was estimated from the alpha spin orbital energy of the most stable spin state.

Complex	E(HS)-E(LS)/(kcal.mol^{-1})	E(LUMO)-E(SOMO)/eV
$[Co(dbm)_2(phen)]$ **57**	-13.84	3.13
$[Co(dbm)_2(2,2'\text{-bpy})]$ **58**	-12.80	2.86
$[Co(dbm)_2(dmae)]$ **59**	-13.26	3.75
$[Co(tmhd)_2(phen)]$ **60**	-15.63	2.91
$[Co(tmhd)_2(2,2'\text{-bpy})]$ **61**	-14.55	2.91
$[Co(tmhd)_2(dmae)]$ **62**	-12.67	4.54
$[Co(dbm)_2(phen)]^+$ **57$^+$**	16.93 (17.31)	3.29
$[Co(dbm)_2(2,2'\text{-bpy})]^+$ **58$^+$**	18.01 (18.16)	3.24
$[Co(dbm)_2(dmae)]^+$ **59$^+$**	17.93 (16.61)	3.70
$[Co(tmhd)_2(phen)]^+$ **60$^+$**	16.12 (16.38)	3.48
$[Co(tmhd)_2(2,2'\text{-bpy})]^+$ **61$^+$**	17.15 (17.19)	3.40
$[Co(tmhd)_2(dmae)]^+$ **62$^+$**	17.41 (17.60)	4.27

The molecular orbital analysis reveals that in the case of **59** and **60**-**62** complexes the SOMO is composed of an antibonding interaction between β-diketonate oxygen *p*-orbitals and the cobalt d_{z2} orbital (see Figure 26). The dmae complexes also exhibit an additional antibonding interaction between the metal orbital and a hybrid σ donor orbital on the NMe_2 nitrogen of the dmae ligand. The SOMO of related bipy and phen complexes, **60** and **61** are different from the others with a metal d_{xz} orbital involved in a weaker antibonding interaction with the β-diketonate ligands. The significant electron density on the β-diketonate ligands in **57**-**62** is consistent with the strong influence of the β-

diketonate upon the oxidation potentials of the above complexes. In the case of **57**, **58, 60** and **61**, the LUMO is essentially a low lying phen or bipy π^* orbital while for **59** and **62** the absence of such π^* orbitals results in a LUMO which is dominated by a β-diketonate π^* orbital (Figure 27). Consequently, a much larger SOMO-LUMO gap is observed in the case of the dmae complexes compared with **60**, **61**, **57** and **58** (see Table 22).

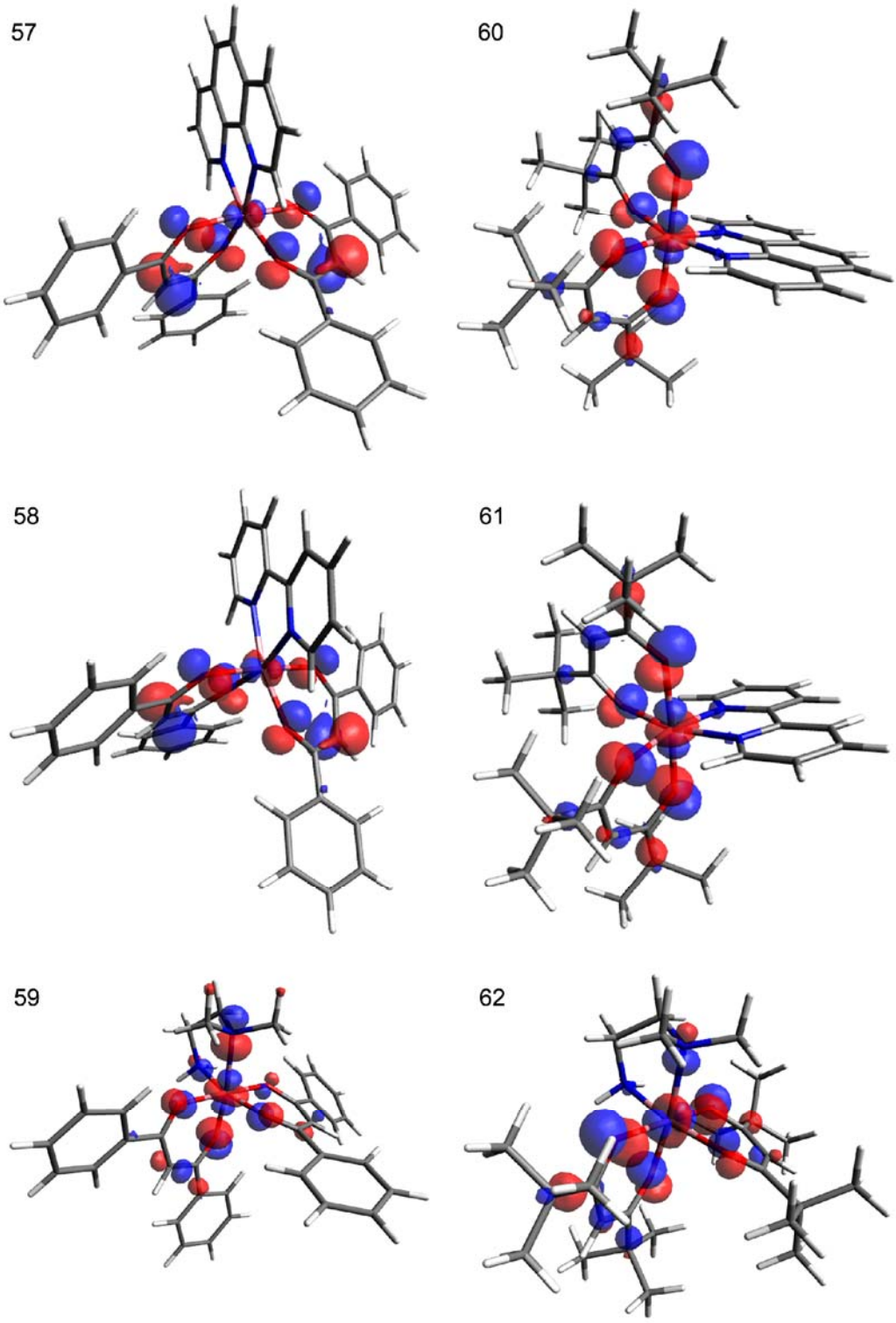

Figure 26 The SOMO orbital of complexes **57-62**.

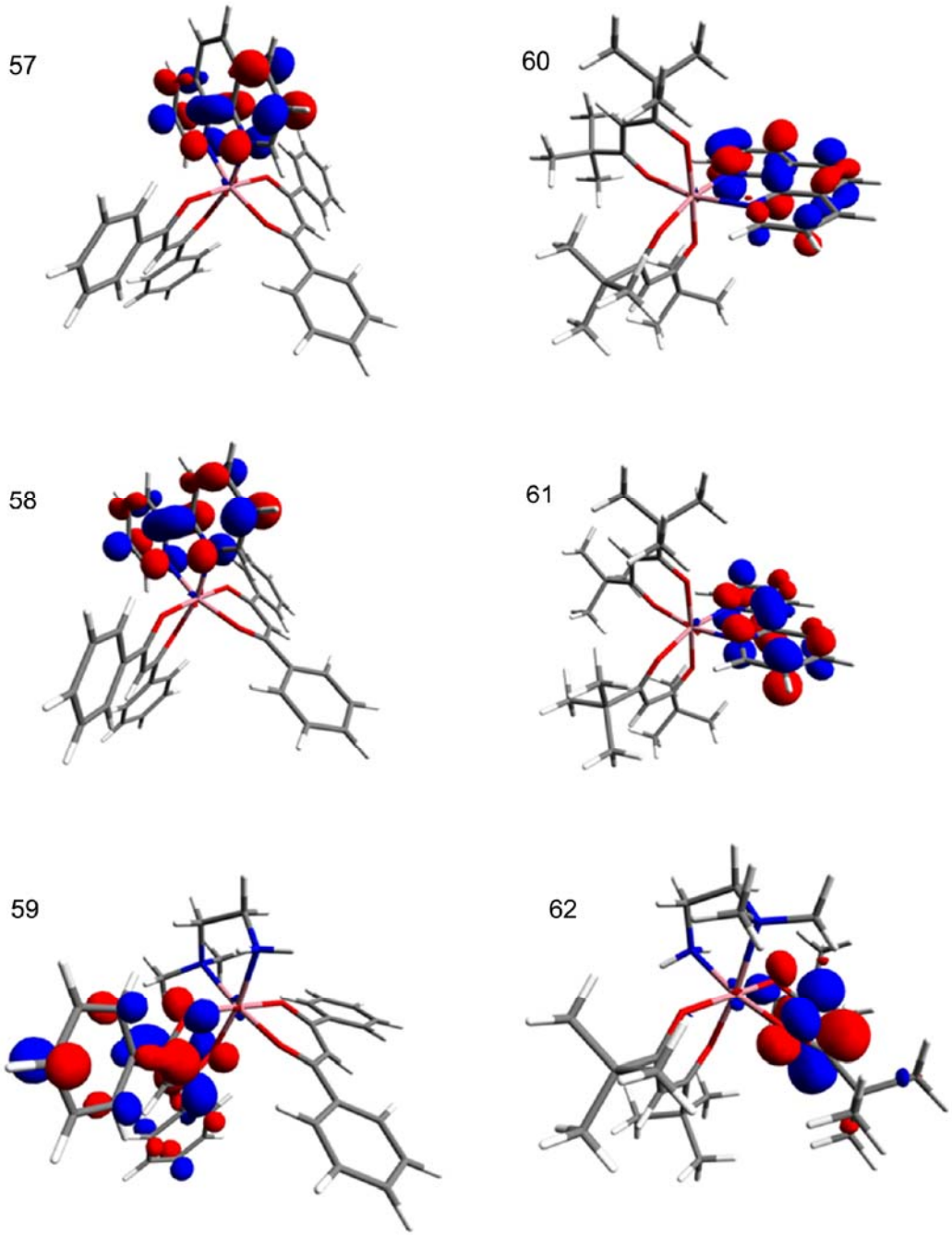

Figure 27 The LUMO orbital of complexes **57-62**.

Further DFT calculations have been undertaken on the [Co(β-diketonate)$_2$(ppa^X)] **33-56** series (Tables 23 and 24) and these confirm the findings from electrochemical studies that the SOMO of the complex is dominated by the Co and β-diketonate orbitals with little contribution from the ppa^X ligand. As with **57**-**62** the LUMO is based strong on the ppa^X ligand suggesting that the strong colours observed for these complexes are the result of MLCT bands from an appropriate metal d-orbital into a low lying π* orbital on the ligand.

Table 23 The high-spin and low-spin complex energy difference, E(HS)-E(LS), at B3LYP/SDD level for [Co(β-diketonate)$_2$(ppa^X)] complexes **33-56**. The E(LUMO)-E(SOMO) gap was estimated from the alpha spin orbital energy of the most stable spin state.

Complex	E(HS)-E(LS)/(kcal.mol^{-1})	E(LUMO)-E(SOMO)/eV
[Co(dbm)$_2$(ppa^H)] **33**	-12.74	2.83
[Co(dbm)$_2$(ppa^{Me})] **34**	-12.74	2.85
[Co(dbm)$_2$(ppa^{Et})] **35**	-12.36	2.84
[Co(dbm)$_2$(ppa^{OMe})] **36**	-12.32	2.86
[Co(dbm)$_2$(ppa^F)] **37**	-12.38	2.76
[Co(dbm)$_2$(ppa^{Cl})] **38**	-12.31	2.73
[Co(dbm)$_2$(ppa^{Br})] **39**	-14.47	2.73
[Co(dbm)$_2$(ppa^I)] **40**	-12.36	2.73
[Co(tmhd)$_2$(ppa^H)] **41**	-13.04	2.62
[Co(tmhd)$_2$(ppa^{Me})] **42**	-13.03	2.66
[Co(tmhd)$_2$(ppa^{Et})] **43**	-12.49	2.67
[Co(tmhd)$_2$(ppa^{OMe})] **44**	-13.16	2.67
[Co(tmhd)$_2$(ppa^F)] **45**	-12.42	2.59
[Co(tmhd)$_2$(ppa^{Cl})] **46**	-12.92	2.56
[Co(tmhd)$_2$(ppa^{Br})] **47**	-13.04	2.56
[Co(tmhd)$_2$(ppa^I)] **48**	-13.10	2.56
[Co(hfac)$_2$(ppa^H)] **49**	-13.34	3.66
[Co(hfac)$_2$(ppa^{Me})] **50**	-13.36	3.52
[Co(hfac)$_2$(ppa^{Et})] **51**	-13.37	3.50
[Co(hfac)$_2$(ppa^{OMe})] **52**	-13.42	3.21
[Co(hfac)$_2$(ppa^F)] **53**	-13.46	3.63
[Co(hfac)$_2$(ppa^{Cl})] **54**	-13.13	3.52
[Co(hfac)$_2$(ppa^{Br})] **55**	-13.14	3.50
[Co(hfac)$_2$(ppa^I)] **56**	-13.39	3.35

Table 24 The high-spin and low-spin complex energy difference, E(HS)-E(LS), at B3LYP/SDD level for $[Co(\beta\text{-diketonate})_2(ppa^X)]^+$ complexes **33^+-56^+**. The E(LUMO)-E(SOMO) gap was estimated from the alpha spin orbital energy of the most stable spin state.

Complex	E(HS)-E(LS)/(kcal.mol^{-1})	E(LUMO)-E(SOMO)/eV
$[Co(dbm)_2(ppa^H)]$OTf **33^+**	15.98	2.85
$[Co(dbm)_2(ppa^{Me})]$OTf **34^+**	15.97	2.90
$[Co(dbm)_2(ppa^{Et})]$OTf **35^+**	16.03	2.90
$[Co(dbm)_2(ppa^{OMe})]$OTf **36^+**	15.93	2.92
$[Co(dbm)_2(ppa^F)]$OTf **37^+**	15.80	2.81
$[Co(dbm)_2(ppa^{Cl})]$OTf **38^+**	15.73	2.80
$[Co(dbm)_2(ppa^{Br})]$OTf **39^+**	15.77	2.80
$[Co(dbm)_2(ppa^I)]$OTf **40^+**	15.74	2.80
$[Co(tmhd)_2(ppa^H)]$OTf **41^+**	15.29	3.02
$[Co(tmhd)_2(ppa^{Me})]$OTf **42^+**	15.46	3.01
$[Co(tmhd)_2(ppa^{Et})]$OTf **43^+**	14.19	3.11
$[Co(tmhd)_2(ppa^{OMe})]$OTf **44^+**	14.64	3.01
$[Co(tmhd)_2(ppa^F)]$OTf **45^+**	15.79	3.05
$[Co(tmhd)_2(ppa^{Cl})]$OTf **46^+**	14.50	3.04
$[Co(tmhd)_2(ppa^{Br})]$OTf **47^+**	15.16	2.98
$[Co(tmhd)_2(ppa^I)]$OTf **48^+**	14.42	3.03
$[Co(hfac)_2(ppa^H)]$OTf **49^+**	18.39	3.35
$[Co(hfac)_2(ppa^{Me})]$OTf **50^+**	18.53	3.03
$[Co(hfac)_2(ppa^{Et})]$OTf **51^+**	18.49	2.99
$[Co(hfac)_2(ppa^{OMe})]$OTf **52^+**	15.97	2.94
$[Co(hfac)_2(ppa^F)]$OTf **53^+**	19.82	3.28
$[Co(hfac)_2(ppa^{Cl})]$OTf **54^+**	24.57	3.00
$[Co(hfac)_2(ppa^{Br})]$OTf **55^+**	18.18	2.80
$[Co(hfac)_2(ppa^I)]$OTf **56^+**	17.86	2.43

The dimers have proved to be much more difficult to model as it is necessary the model the potential communication between the metals. However, preliminary results from these studies indicate that, as expected, the shortest ligand bpmhd, has the strongest degree of communication with the other ligands revealing only weak communication. This is particularly surprising in the case of the 1,5-bpmna ligand as it places the metals very far from each other. Perhaps the large π cloud of

the naphthalene linker aids electronic communication. Further work is still on going to provide more definitive answers into the exact communication process and the orbitals on the metal and ligand that may be used to facilitate it.

5. References

1. Létard, J.-F.; Guionneau, P.; Goux-Capes, L. *Top*. *Curr*. *Chem*. **2004**, *235*, 221.
2. Kahn, O. Martinez, C. J. *Science* **1998**, *279*, 44.
3. Fabbrizzi, L.; Licchelli, M.; Pallavicini, P. *Acc*. *Chem*. *Rev*. **1999**, *32*, 846.
4. Venturi, M.; Credi, A.; Balzani, V. *Coord. Chem. Rev*. **1999**,
5. H. A. Goodwin, *Coord. Chem. Rev.* **1976**, **18**, 293.
6. (a) Real, J. A.; Gaspar, A. B.; Niel, V.; Muñoz, M. C. *Coord. Chem. Rev.* **2003**, *236*, 121. (b) Garcia, Y.; Niel, V.; Muñoz, M. C. and Real, J. A. *Top. Curr. Chem.* **2004**, *233*, 229.
7. Murray, K. S.; Kepert, C. J. *Top. Curr. Chem.* **2004**, *233*, 195.
8. Gaspar, A. B.; Ksenofontov, V.; Real, J. A.; Gütlich, P. *Chem. Phys. Lett.* **2003**, *373*, 385.
9. (a) Spiering, H.; Kohlhaas, T.; Romstedt, H.; Hauser, A.; Bruns-Yilmaz, C.; Gütlich, P. *Coord. Chem. Rev.* **1999**, *190–192*, 629. (b) Gütlich, P.; Hauser, A.; Spiering, H. *Angew. Chem., Int. Ed. Engl.* **1994**, *33*, 2024.
10. (a) Real, J. A. in *Transition Metals in Supramolecular Chemistry*, ed. Sauvage, J. P. John Wiley and Sons, Ltd., Chichester, **1999**, p. 53. (b) Real, J. A.; Gaspar, A. B.; Muñoz, M. C.; Gütlich, P.; Ksenofontov, V.; Spiering, H. *Top. Curr. Chem.* **2004**, *233*, 167.
11. Haasnoot, J. G. *Coord. Chem. Rev.* **2000**, *200*, 131.
12. Breuning, E.; Ruben, M.; Lehn, J. M.; Renz, F.; Garcia, Y.; Ksenofontov, V.; Gütlich, P.; Wegelius, E.; Rissanen, K. *Angew. Chem., Int. Ed.* **2000**, *39*, 2504.
13. Real, J. A.; Andres, E.; Muñoz, M. C.; Julve, M.; Granier, T.; Bousseksou, A.; Varret, F. *Science* **1995**, *268*, 265.
14. Halder, G. J.; Kepert, C. J.; Moubaraki, B.; Murray, K. S.; Cashion, J. D. *Science* **2002**, *298*, 1762.
15. Madeja, K.; König, E. *J. Inorg. Nucl. Chem*. **1963**, *25*, 377.
16. Sieber, R.; Decurtins, S.; Stoeckli, H.; Evans, C.; Wilson, D.; Yufit, J. A. K.; Howard, S. C.; Capelli, A.; Hauser, A. *Chem. Eur. J*. **2000**, *6*, 361.
17. (a) Zerara, M.; Hauser, A. *Chem. Phys. Chem*. **2004**, *5*, 395. (b) Hauser A.; Amstutz, N.; Delahaye, S.; Schenker, S.; Sadki, A.; Sieber, R.; Zerara, M. *Struct. Bond*. **2004**, *106*, 81.
18. (a) Hogg, R.; Wilkins, R. G. *J. Chem. Soc*. **1962**, 341. (b) Judge, J. S.; Baker, W. A. *Inorg. Chim. Acta* **1967**, *1*, 68.

19. Figgis, B. N.; Kucharski, E. S.; White, A.H. *Aust. J. Chem*. **1983**, 36, 1537.
20. Scheidt, W. R.; Reed, C. A. *Chem*. *Rev*. **1981**, *81*, 543.
21. Bertani, I.; Gray, H. B.; Lippard, S. J.; Valentine, J. S. *Bioinorganic Chemistry*, University Science Books, Sausalito, CA, **1994**.
22. Lippard, S. J.; Berg, J. M. *Principles of Bioinorganic Chemistry*, University Science Books, Mill Balley, CA, **1995**.
23. Kaim, W.; Schwederski, B. *Bioinorganic Chemistry: Inorganic Elements in the Chemistry of Life*, Wiley, New York, **1995**.
24. Sligar, S. C. *Biochemistry* **1976**, *15*, 5399.
25. Mueller, E. J.; Lioda, P. J.; Sligar, S. C. in *Cytochrome P450: Structure, Mechanism and Biochemistry*, ed. Ortiz de Montellano, P.R. 2nd ed., Plenum Press, New York, **1995**, Chap. 3.
26. Rees, D. C.; Chan, M. K.; Kim, J. *Adv. Inorg. Chem*. **1993**, *40*, 89.
27. Burgess, B. K.; Lowe, D. J. *Chem. Rev*. **1996**, *96*, 2983.
28. Lopes, H.; Pettigrew, G. W.; Moura, I.; Moura, J. J. G. *J. Biol. Inorg. Chem*. **1998**, *3*, 632.
29. Hendry, P.; Ludi, A. *Adv. Inorg. Chem*. **1990**, *35*, 117.
30. Stynes, H.C.; Ibers, J.A. *Inorg. Chem*. **1971**, *10*, 2304.
31. Buhks, E.; Bixon, M.; Jortner, J.; Navon, G. *Inorg. Chem*. **1979**, *18*, 2014.
32. Geselowitz, D.A., Taube, H. *Adv. Inorg. Bioinorg. Mech*. **1982**, *1*, 391.
33. Larsson, S.; Ståhl, K.; Zerner, M.C. *Inorg. Chem*. **1986**, *25*, 3033.
34. Geselowitz, D.A. *Inorg. Chim. Acta* **1988**, *154*, 225.
35. Newton, M.D. *J. Phys. Chem.* **1991**, *95*, 30.
36. Shalders, R.D.; Swaddle, T.W. *Inorg. Chem*. **1995**, *34*, 4815.
37. Swaddle, T.W. *Can. J. Chem*. **1996**, *74*, 631.
38. Turner, J. W.; Schultz, F. A. *Inorg. Chem*. **1999**, *38*, 358.
39. Turner, J. W.; Schultz, F. A. *J. Phys. Chem. B* **2002**, *106*, 2009.
40. Lord, R. L.; Schultz, F. A., Baik, M.-H. *J. Am. Chem. Soc*. **2009**, *131*, 6189.
41. Nakamoto, K. in *Infrared and Raman Spectra of Inorganic and Coordination Compounds: Part B*, 6th ed., Wiley, New York, **2009**, pp. 96-104.
42. Harding, P.; Harding, D. J.; Phonsri, W.; Saithong, S.; Phetmung, H. *Inorg. Chim. Acta* **2009**, *362*, 78.
43. Cotton, F.A.; Wilkinson, G.; Murillo, C.A.; Bochmann, M. in *Advanced Inorganic Chemistry*, 6th ed.; John Wiley & Sons, New York, **1999**, pp. 817-822.

44. Bandoli, G.; Barreca, D.; Gasparotto, A.; Maccato, C.; Seraglia, R.; Tondello, E.; Devi, A.; Fischer, R. A.; Winter, M. *Inorg. Chem.* **2009**, *48*, 82.
45. Nagashima, N.; Kudoh, S.; Nakata, M. *Chem. Phys. Lett.* **2003**, *374*, 59.
46. Sankhla, D. S.; Mathur, R. C.; Misra, S. N. *J. Inorg. Nuc. Chem.* **1980**, *42*, 489.
47. Chassot, P.; Emmenegger, F. *Inorg. Chem.* **1996**, *35*, 5931.
48. Archer, R. D.; Cotsoradis, B. P. *Inorg. Chem.* **1965**, *4,* 1584.
49. York, R. J.; Bonds, W.D. Jr.; Cotsoradis, B. P.; Archer, R. A. *Inorg. Chem.* **1969**, *8*, 789.
50. Izumi, F.; Kurosawa, R.; Kawamoto, H.; Akaiwa, H. *Bull. Chem. Soc. Jpn.* **1975**, *48*, 3188.
51. Turner, J. W.; Schultz, F. A. *Coord. Chem. Rev.* **2001**, *219-221*, 81.
52. For examples of other Co complexes exhibiting RCSCO see (a) Buhks, E.; Dixon, M.; Jortner, J.; Navon, G. *Inorg. Chem.* **1979**, *18*, 2014. (b) Endicott, J. F.; Brubaker, G. R.; Ramasami, T.; Kumar, K.; Dwarakanath, K.; Cassel, J.; Johnson, D. *Inorg. Chem.* **1983**, *22*, 3754. (c) Hammershøi, A.; Geselowitz, D.; Taube, H. *Inorg. Chem.* **1984**, *32*, 979. (d) Bernhardt, P. V.; Jones, L. A.; Sharpe, P. C. *Inorg. Chem.* **1997**, *36*, 2420.
53. Johansson, F. B.; Bond, A. D.; Nielson, U. G.; Moubaraki, B.; Murray, K. S.; Berry, K. J.; Larrabee, J. A.; McKenzie, C. J. *Inorg. Chem*. **2008,** *47*, 5079.
54. De Alwis, D. C. L.; Schultz, F. A. *Inorg. Chem.* **2003**, *42*, 3616.
55. Wieghardt, K.; Schmidt, W.; Herrmann, W.; Kueppers, H. J. *Inorg. Chem*. **1983**, *22*, 2953.
56. Kueppers, H. J.; Neves, A.; Pomp, C.; Ventur, D.; Wieghardt, K.; Nuber, B.; Weiss, J. *Inorg. Chem*. **1986**, *25*, 2400.
57. Richards, T. C.; Geiger, W.E. *J. Am. Chem. Soc.* **1994**, *116*, 2028.
58. Gaussian 03, Revision D.01, Frisch, M. J.; Trucks, G. W.; Schlegel, H. B.; Scuseria, G. E.; Robb, M. A.; Cheeseman, J. R.; Montgomery, Jr., J. A.; Vreven, T.; Kudin, K. N.; Burant, J. C.; Millam, J. M.; Iyengar, S. S.; Tomasi, J.; Barone, V.; Mennucci, B.; Cossi, M.; Scalmani, G.; Rega, N.; Petersson, G. A.; Nakatsuji, H.; Hada, M.; Ehara, M.; Toyota, K.; Fukuda, R.; Hasegawa, J.; Ishida, M.; Nakajima, T.; Honda, Y.; Kitao, O.; Nakai, H.; Klene, M.; Li, X.; Knox, J. E.; Hratchian, H. P.; Cross, J. B.; Bakken, V.; Adamo, C.; Jaramillo, J.; Gomperts, R.; Stratmann, R. E.; Yazyev, O.; Austin, A. J.; Cammi, R.; Pomelli, C.; Ochterski, J. W.; Ayala, P. Y.; Morokuma, K.; Voth, G. A.; Salvador, P.; Dannenberg, J. J.; Zakrzewski, V. G.; Dapprich, S.; Daniels, A. D.; Strain, M. C.; Farkas, O.; Malick, D. K.; Rabuck, A. D.; Raghavachari, K.; Foresman, J. B.; Ortiz, J. V.; Cui, Q.; Baboul, A. G.; Clifford, S.; Cioslowski, J.; Stefanov, B. B.; Liu, G.; Liashenko, A.; Piskorz, P.; Komaromi, I.; Martin, R. L.; Fox, D. J.; Keith, T.; Al-Laham, M. A.; Peng, C. Y.; Nanayakkara, A.; Challacombe, M.; Gill, P. M. W.; Johnson, B.;

Chen, W.; Wong, M. W.; Gonzalez, C.; and Pople, J. A.; Gaussian, Inc., Wallingford CT, 2004.

59. Meštrović, E; Kaitner, B. *J. Chem. Crystallogr*. **2006**, *36*, 599.
60. Barreca, D.; Massignan, C.; Daolio, S.; Fabrizio, M.; Piccirillo, C.; Armelao, L.; Tondello, E. *Chem. Mater.* **2001**, *13*, 588.
61. Barrios, L. A.; Ribas, J.; Aromí, G.; Ribas-Ariño, J.; Gamez, P.; Roubeau, O.; Teat, S. J. *Inorg. Chem.* **2007**, *46*, 7154.
62. Evans, D. F. *J. Chem. Soc.* **1959**, 2003–2005.
63. Shaw, M. J., Henson, R. L., Houk, S. E., Westhoff, J. W., Richter-Addo, G. B., Jones, M. W. *J. Electroanal. Chem.* **2002**, *534*, 47
64. Becke, A. D. *J. Chem. Phys*. **1993**, *98*, 1372.
65. Stephens, P. J.; Devlin, F. J.; Frisch, M. J.; Chabalowski, C. F. *J. Phys. Chem.* **1994**, *98*, 11623.
66. Dunning Jr., T. H.; Hay, P. J. in *Modern Theoretical Chemistry*, ed. H. F. Schaefer III, Vol. 3 Plenum, New York, **1976**, pp. 1-28.
67. Dolg, M.; Wedig, U.; Stoll, H.; Preuss, H. *J. Chem. Phys.* 86, **1987**, 866.

6. Project Outcomes

6.1. Publications

Two international papers have been published in *Australian Journal of Chemistry* and *Acta Crystallographica Section E*, one has been accepted and a further paper is in the final stages of preparation for submission.

1. P. Harding, D. J. Harding, K. Tinpun, S. Samuadnuan, N. Sophonrat and H. Adams, Synthesis and electrochemical studies of nickel β-diketonate complexes incorporating asymmetric diimine ligands, *Aust. J. Chem*, 2010, **63**, 75.
2. P. Harding, D. J. Harding, N. Sophonrat and H. Adams, Bis(1,1,1,5,5,5-hexafluoropentane-2,4-dionato-κ^2-*O*,*O*')[(4-bromo-phenyl)pyridin-2-ylmethyleneamine-κ^2-*N*,*N*']cobalt(II), *Acta Cryst. Section E*, 2010, E**66**, m1138.
3. P. Harding, D.J. Harding, N. Soponrat and H. Adams, Bis(1,1,1,5,5,5-hexafluoropentane-2,4-dionato-κ^2-*O*,*O*')[(4-bromo-phenyl)pyridin-2-ylmethylene amine–κ^2-*N*,*N*']nickel(II), submitted to *Acta Cryst. Section E.*
4. P. Harding**,** D. J. Harding, R. Daengngern, T. Thurakitsaree, B. M. Schutte, M. J. Shaw and Y. Tantirungrotechai, Redox Coupled-Spin Crossover in Cobalt β-Diketonate Complexes: Observation of the High Spin Co^{III} Intermediate, to be submitted to *Eur. J. Inorg. Chem.*

Two more publications on the nickel dimer complexes [(β-diketonate)$_2$Ni(μ-L)Ni(β-diketonate)$_2$] and the redox coupled spin crossover [Co(β-diketonate)$_2$(ppa^X)] complexes will be prepared shortly. Further DFT calculations of [(β-diketonate)$_2$Co(μ-L)Co(β-diketonate)$_2$] should also provide another publication in a high impact factor journal.

6.2. Presentations

Four oral and three poster presentations have been made upon this work.

1. P. Harding and D.J. Harding, Electronic Communication Between Two Metal β-Diketonate Complexes Bridged by Diimine Linkers, the Pure and Applied Chemistry International Conference 2011 (PACCON 2011), January 2011, Bangkok, Thailand.
2. P. Harding, D.J. Harding, R. Daengngern, T. Thurakitsaree, B.M. Schutte, M.J. Shaw and Y. Tantirungrotechai, Redox Coupled-Spin Crossover in [Co(β-diketonate)$_2$(N-N)]$^{0/+}$ Complexes, the Pure and Applied Chemistry International Conference 2010 (PACCON 2010), February 2010, Ubon Ratchathani, Thailand.
3. P. Harding, D.J. Harding, Y. Tantirungrotechai and A. Sayananon, Redox Coupled-Spin Crossover Cobalt β-Diketonate Complexes: Synthesis, Electron Transfer Studies and DFT Calculations, TRF Annual Meeting, October 2010, Phetchaburi, Thailand.
4. P. Harding, Simultaneous UV-Vis Spectroelectrochemistry, Metrohm Siam Ltd. Seminar, August 2009, Bangkok, Thailand.
5. P. Harding, D.J. Harding, N. Soponrat, K. Tinpun, S. Samuadnuan and H. Adams, Synthesis and Electrochemical Studies of Nickel β-Diketonate Complexes Incorporating Asymmetric Diimine Ligands, The 8th Conference of the Inorganic Chemistry Division, December 2008, Christchurch, New Zealand.
6. P. Harding and D.J. Harding, Electronic Communication in Redox Coupled-Spin Crossover Cobalt Dimers, TRF Annual Meeting, October 2009, Phetchaburi, Thailand.
7. P. Harding, D.J. Harding, N. Soponrat, K. Tinpun, S. Samuadnuan and H. Adams, Electron Transfer Studies of [Ni(β-Diketonate)$_2$(ppa^R)], TRF Annual Meeting, October 2008, Phetchaburi, Thailand.

6.3. Collaborations with International/national Institutes and Awards

As a result of this project we have developed two new collaborations:

1. Professor Mike Shaw at Southern Illinois University Edwardsville, USA is working with us on developing spectroelectrochemistry here in Thailand.

2. Assoc. Prof. Dr. Supa Hannongbau at Kasedsart University, Thailand was supervised undergraduate student from Computational Science program, Walailak University on the DFT calculations of [Ni(β-diketonate)$_2$(ppa^X)] complexes.
3. Assist. Prof. Dr. Yuthana Tantirungrotechai, NANOTEC, Thailand is working with us on the DFT calculations of the Co spin-crossover system.
4. Won the UMAP travelling grant to study the Co spin crossover by using spectroelectrochemistry at Southern Illinois University Edwardsville, USA during May 2009-June 2009.

6.4. Training new generation of Thai researchers in Inorganic Chemistry

There are three schemes for training the young researchers in our laboratory: through "Young researcher training summer project", the undergraduate senior projects and the master thesis project.

Young researcher training summer project	1. Miss Kittiya Tinpun, Thaksin University 2. Miss Sirirat Samuadnuan, Thaksin University 3. Mr. Nitisart Soponrat, Thaksin University 4. Miss Sirikan Thongmeang, Rangsit University 5. Miss Angkana Kongbunkeaw, Thammasat University 6. Miss Tuanjai Somboon, Walailak University
Undergraduate senior projects	1. Miss Tuanjai Somboon, Walailak University 2. Mr. Rathawat Daengngern, Walailak University
Master thesis project	1. Miss Apiraya Sayananon, MSc student, Thammasat University

Appendix One

International Publication

CSIRO PUBLISHING

Full Paper

www.publish.csiro.au/journals/ajc

Aust. J. Chem. **2010**, *63*, 75–82

Synthesis and Electrochemical Studies of Nickel β-Diketonate Complexes Incorporating Asymmetric Diimine Ligands

Phimphaka Harding,[A,D] *David J. Harding*,[A,D] *Nitisastr Soponrat*,[B] *Kittiya Tinpun*,[B] *Sirirat Samuadnuan*,[B] *and Harry Adams*[C]

[A]Molecular Technology Research Unit, School of Science, Walailak University, Thasala, Nakhon Si Thammarat, 80161, Thailand.

[B]Department of Chemistry, Faculty of Science, Taksin University, Songkhla, 90000, Thailand.

[C]Department of Chemistry, University of Sheffield, Brook Hill, Sheffield S3 7HF, UK.

[D]Corresponding authors. Email: kphimpha@wu.ac.th; hdavid@wu.ac.th

The reaction of ppa^X {(4-X-phenyl)-pyridin-2-ylmethylene-amine; X = H, Me, Et, OMe, F, Cl, Br, and I} with [Ni(β-diketonate)$_2$(H$_2$O)$_2$] {β-diketonate = 1,3-diphenylpropanedionate (dbm), 2,2,6,6-tetramethyl-3,5-heptadionate (tmhd), or hexafluoroacetylacetonate (hfac)} yields a series of nickel complexes. X-ray crystallography reveals octahedral coordinated nickel centres with a *cis* arrangement of the β-diketonate ligands. The β-diketonate ligands adopt 'planar' or 'bent' coordination modes, whereas the aryl ring of the ppa^X ligand is twisted with respect to the pyridylimine unit. The electrochemical behaviour of the complexes reveals quasi-reversible or irreversible one-electron oxidation to Ni(III) in the case of the [Ni(tmhd)$_2$(ppa^X)] and [Ni(dbm)$_2$(ppa^X)] complexes, respectively. The peak potential for oxidation is dependent on the type of β-diketonate ligand but essentially independent of the substituent, X, on the ppa^X ligand. The [Ni(β-diketonate)$_2$(ppa^X)] complexes (X = F, Cl, Br, and I) also undergo ligand based reduction.

Manuscript received: 20 April 2009.
Manuscript accepted: 15 July 2009.

Introduction

Metal β-diketonates represent an important class of complexes and have been extensively studied due to their ease of synthesis, ready modification, and multiple applications.[1–3] In the case of divalent metal ions, the [M(β-diketonate)$_2$] complexes are able to coordinate additional ligands forming octahedral metal complexes.[4] The nature of the chelating ligands can have a significant effect on the properties of the complexes and therefore their subsequent application. Thus, chelating alkyl diamines are used to synthesize volatile precursors for the preparation of metal-oxide thin films[5,6] whereas organic radicals may be used to construct single molecule magnets.[7–10] However, in much of the reported literature on such octahedral metal-β-diketonate adducts only acac or hfac ligands (acac = acetylacetonate, hfac = hexafluoroacetyl-acetonate) are used with the larger dbm and tmhd ligands (dbm = 1,3-diphenylpropanedionate, tmhd = 2,2,6,6-tetramethylheptanedionate) remaining poorly represented.

While metal-β-diketonate adducts have found many applications, to date little research has been concerned with the redox chemistry of these systems.[11–13] However, recent studies in our group have shown that the complexes, [Ni(β-diketonate)$_2$(L)] (β-diketonate = dbm, tmhd; L = bipy, phen), which incorporate the less widely used dbm and tmhd ligands and diimines are electrochemically active oxidizing to rare Ni(III) species.[14] In an attempt to develop this area of chemistry we have undertaken a course of research into the chemistry of [M(β-diketonate)$_2$(L)] complexes. The bipyridine and phenanthroline ligands used in this preliminary study, while commercially available, are difficult to derivatize. In contrast, iminopyridines are easy to prepare and readily modified. Moreover, the different substituents on the aryl group might be expected to allow subtle changes in the steric and electronic properties of the ligands, which may in turn, affect the structure and redox chemistry of the complexes. A further point is that unlike bipy and phen, iminopyridines are asymmetric, which may also influence the chemistry of the system. In the following paper we report the synthesis, structural characterization, and redox chemistry of a series of novel [Ni(β-diketonate)$_2$(ppa^X)] complexes.

Results and Discussion

Synthesis and Characterization

The synthesis of the (4-X-phenyl)-pyridin-2-ylmethylene-amine (ppa^X) ligands, where X = H (**1**), Me (**2**), Et (**3**), OMe (**4**), F (**5**), Cl (**6**), Br (**7**), and I (**8**), was achieved by a simple condensation reaction between pyridine-2-carboxaldehyde and the appropriate substituted aniline in diethyl or diisopropyl ether (Scheme 1). While many of these ligands have been reported previously,[15,16] we found that in most cases the reported procedure did not give the expected ppa^X cleanly. Instead considerable quantities of the starting materials remained. Hannon et al. recently reported the use of molecular sieves in an improved preparation of ppa^H, to remove the water produced during the course of the reaction.[17] We therefore added molecular sieves to the reaction mixture and found that this simple addition significantly increased yields, purity, and also reduced reaction times. The molecular sieves are readily removed by filtration once the reaction is complete. The ligands have been characterized by IR, UV-vis, and ^{1}H NMR

 10.1071/CH09232 0004-9425/10/010075

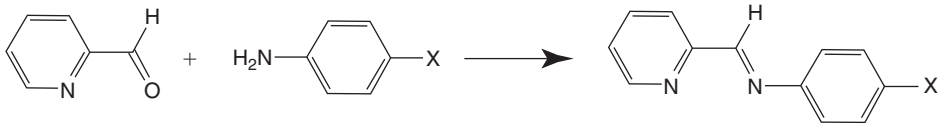

Scheme 1. Synthesis of ppa^X ligands.

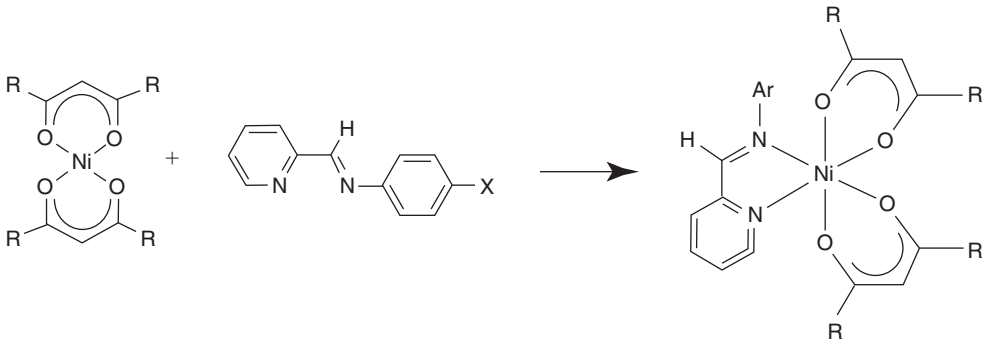

Scheme 2. Synthesis of [Ni(β-diketonate)$_2$(ppa^X)] complexes.

spectroscopy. IR spectroscopy of the ligands revealed a medium intensity imine stretch between 1623 and 1626 cm^{-1} in line with those for previously reported ppa^X compounds.[15–17] The ^1H NMR spectra were recorded in $CDCl_3$ showing a singlet between 8.58 and 8.68 ppm for the imino proton confirming the formation of the desired ppa^X ligands. The peaks for the pyridyl and phenylene groups are assigned on the basis of their splitting patterns, coupling constants, and intergration values and are typical of such iminopyridine ligands.

The reaction of [Ni(dbm)$_2$(H_2O)$_2$], [Ni(tmhd)$_2$(H_2O)$_2$], or [Ni(hfac)$_2$(H_2O)$_2$] with the eight ppa^X ligands, in CH_2Cl_2, THF or acetone affords red, brown, and yellow solids of the octahedral complexes [Ni(dbm)$_2$(ppa^X)] {X = H (**9**), Me (**10**), Et (**11**), OMe (**12**), F (**13**), Cl (**14**), Br (**15**), and I (**16**)}, [Ni(tmhd)$_2$(ppa^X)] {X = H (**17**), Me (**18**), Et (**19**), OMe (**20**), F (**21**), Cl (**22**), Br (**23**), and I (**24**)}, and [Ni(hfac)$_2$(ppa^X)] {X = H (**25**), Me (**26**), Et (**27**), OMe (**28**), F (**29**), Cl (**30**), Br (**31**), and I (**32**)} (Scheme 2). The red, brown, and yellow colours of these compounds are in marked contrast with the related [Ni(β-diketonate)$_2$(L)] (L = bpy, phen) complexes, which are green[14] and indicative of absorption by the ppa^X ligand. The expected *d-d* transitions are unfortunately obscured by these strong UV bands. IR spectroscopy of complexes **9**–**24** shows a C=O stretch from 1588 to 1595 cm^{-1}, similar to that reported for the [Ni(β-diketonate)$_2$(L)] (L = bpy, phen) complexes (1582–1595 cm^{-1}),[14] and indicative of a chelating coordination mode for the β-diketonate ligand.[18] The C=O stretch for the hfac compounds, **25**–**32**, is on average 60 cm^{-1} higher than that observed for complexes **9**–**24**, consistent with the strong electron withdrawing effect of the CF_3 groups. The imine stretches of coordinated ppa^X ligands which are expected to be between 1580 and 1590 cm^{-1} are not observed as they masked by the strong C=O stretch of the β-diketonate ligand.

Crystallographic Studies

The molecular structures of complexes **10**, **12**, and **14** were determined by X-ray crystallography (Table 1). The structures of **10** and **12** are shown in Figs 1 and 2, respectively. Crystals of all complexes were grown by allowing hexane to diffuse slowly into a concentrated solution of the complex in CH_2Cl_2 at room temperature.

Table 1. Selected bond lengths [Å] and angles [°] of 10, 12, and 14

	10	**12**	**14**
Ni–O(1)	2.013(3)	2.0349(12)	2.0091(16)
Ni–O(2)	2.005(3)	2.0135(12)	2.0205(17)
Ni–O(3)	2.027(3)	2.0479(12)	2.0165(16)
Ni–O(4)	2.010(4)	2.0163(12)	2.0128(16)
Ni–N(1)	2.090(4)	2.0812(14)	2.091(2)
Ni–N(2)	2.180(4)	2.1096(14)	2.189(2)
O(1)–Ni–O(2)	89.05(14)	88.93(5)	90.66(6)
O(3)–Ni–O(4)	90.58(14)	88.18(5)	89.29(6)
N(1)–Ni–N(2)	76.81(16)	78.60(6)	77.31(8)
β^A	2.98	31.94	16.57
	17.06	24.72	1.51
γ^B	22.87	39.50	23.99
Intermolecular distances[C]			
O(1)–H(8)	2.439		
O(3)–H(8)		2.615	2.396
O(3)–H(6)		2.578	

[A] β is the angle between the plane defined by the carbon and oxygen atoms of the β-diketonate ligand and the plane defined by the nickel and two oxygen atoms.

[B] γ is the angle between the plane of the pyridylimine unit and the plane of the substituted phenyl ring.

[C] Non-bonded metrics and those involving centroids were not included in the structure refinement, and thus do not have an estimated standard deviation.

Complexes **10**, **12**, and **14** assume slightly distorted octahedral coordination geometries. The β-diketonate ligands exhibit a *cis* arrangement enforced by the chelating ppa^X ligand. The Ni–O bond lengths vary between 2.005 and 2.048 Å for the three complexes and are similar to other previously reported nickel β-diketonate adducts, [Ni(dbm)$_2$(en)] {2.009(6), 2.060(7) Å},[19] and [Ni(dbm)$_2$(phen)] {2.035(1), 2.041(1) Å}.[14]

The nickel bond to the pyridine of the ppa^X ligand of complexes **10** and **14** is considerably shorter than the bond to the imine nitrogen, differing by ~0.1 Å. In contrast, the Ni–N bond lengths for **12** are different by only 0.03 Å. It is also interesting to note that in [Cu($ppa^{2Me,3Me}$)$_2$]ClO_4[16] and [Ru(bipy)$_2$(ppa^H)][PF_6]$_2$,[17] the imine nitrogen metal bond is

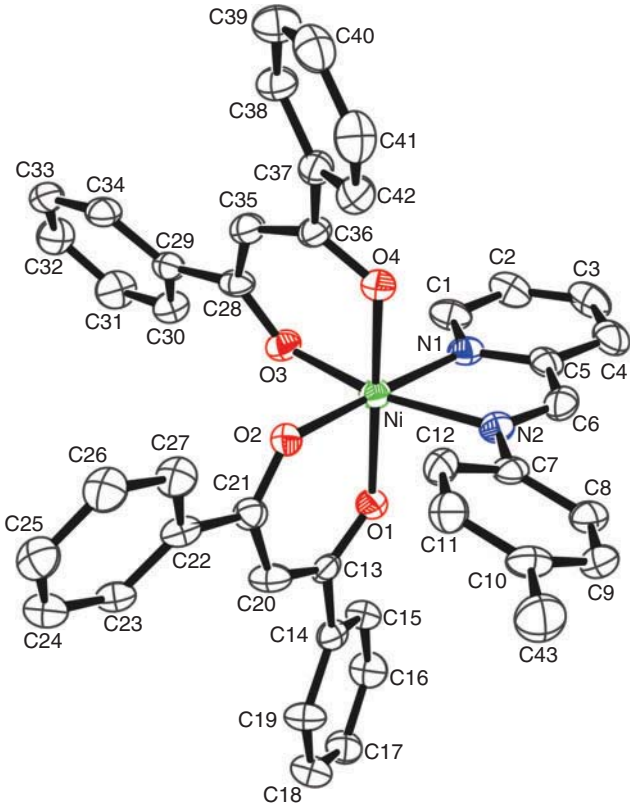

Fig. 1. *ORTEP* diagram of [Ni(dbm)$_2$(ppa^{Me})] **10**. The thermal ellipsoids are drawn to 50% probability level. Hydrogen atoms are omitted for clarity.

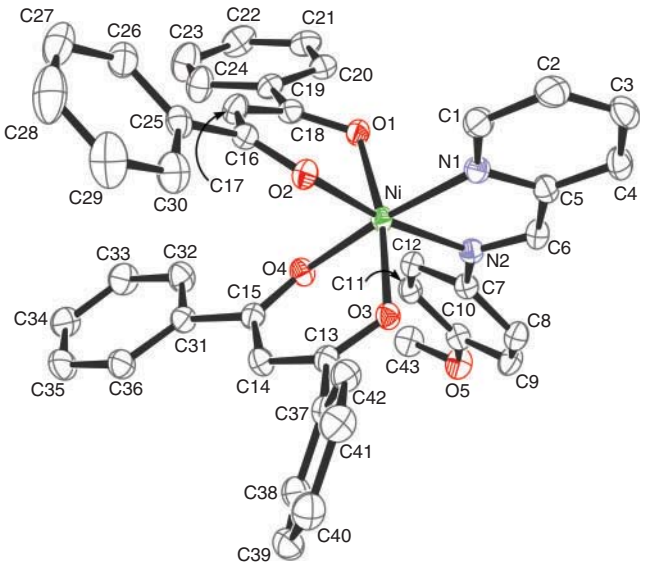

Fig. 2. *ORTEP* diagram of [Ni(dbm)$_2$(ppa^{OMe})] **12**. The thermal ellipsoids are drawn to 50% probability level. Hydrogen atoms are omitted for clarity.

shorter than the pyridine nitrogen metal bond. The reason for this difference remains unclear. The phenyl ring in all the complexes is twisted with respect to the pyridylimine unit. Interestingly, the angle for **12** is 39.5°, whereas those of **10** and **14** are 22.9° and 24.0°, respectively. By comparison [Cu(ppa^{2Me,3Me})$_2$]ClO$_4$ and [Ru(bipy)$_2$(ppa^{H})][PF$_6$]$_2$ exhibit angles of 69° and 45°, respectively.[16,17] The phenyl ring is positioned above the

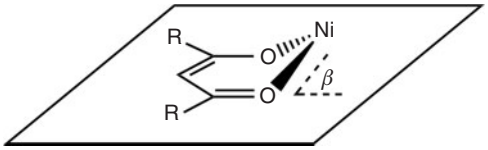

Fig. 3. Schematic diagram showing the angle β between the β-diketonate and NiO_2 planes.

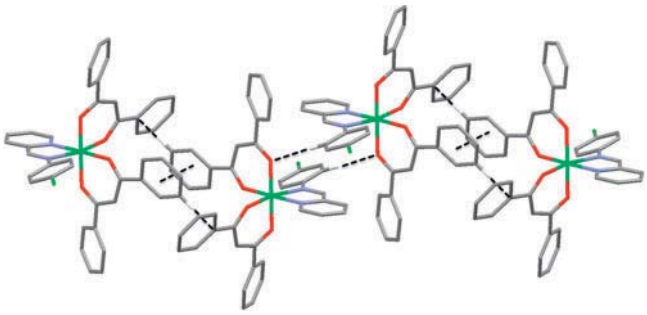

Fig. 4. Mercury plot showing the CH···O and π-π interactions in [Ni(dbm)$_2$(ppa^{Cl})] **14**. For clarity, only hydrogen atoms involved in interactions are shown.

pyridyl ring of a neighbouring ppa^X ligand but is neither co-planar with, nor perpendicular to, that pyridyl ring.

The β-diketonate ligand is essentially planar and symmetric suggesting that the negative charge is delocalized over the β-diketonate framework. As noted in other nickel β-diketonate adducts the nickel centre lies above the plane of the dbm ligand in a 'bent' coordination mode.[14] The extent of this displacement has been determined by calculating the angle between the plane of the β-diketonate framework and the plane defined by the nickel and two oxygen atoms (Fig. 3). For complex **12** both dbm ligands exhibit a 'bent' coordination mode, whereas for **10** and **14** only one of the dbm ligands is 'bent' with the other assuming a 'planar' coordination mode. This is probably the result of the different substituents on the ppa^X ligands.

The complexes are packed into chiral columns with each column exhibiting the same helicity and adjacent columns of alternate helicity as shown in Figs 4 and 5. The molecules are arranged so that the ppa^X ligands are positioned above one another with the substituent alternately pointing 'in' and 'out'. The interaction principally involved here is between a C–H group from the phenyl ring of the ppa^X ligand and a coordinated oxygen atom from the dbm ligand. The structure of **12** is slightly different revealing a further interaction from the imino C–H to the same oxygen atom. As a result of the stacking of the ppa^X ligands, the dbm ligands are also stacked in columns. As might be expected, this leads to π-π interactions between two adjacent dbm phenyl rings (centroid-centroid 3.653 and 3.651 Å for **10** and **14**, respectively). The absence of this interaction in the structure of **12** once again seems to stem from the extra space needed to accommodate the ppa^{OMe} ligand and the subsequent 'bent' coordination mode of *both* dbm ligands which preclude this interaction. Surprisingly, the π-π interaction is not replaced by any face to edge CH-π interactions.

Electrochemical Studies

The redox properties of the complexes **9**–**32** were studied by cyclic voltammetry (CV) in CH_2Cl_2 at 25°C (Table 2). The CVs of **13**, **21**, and **29** are shown in Fig. 6 as representative examples. Complexes **9**–**16** exhibit an irreversible oxidation wave, whereas

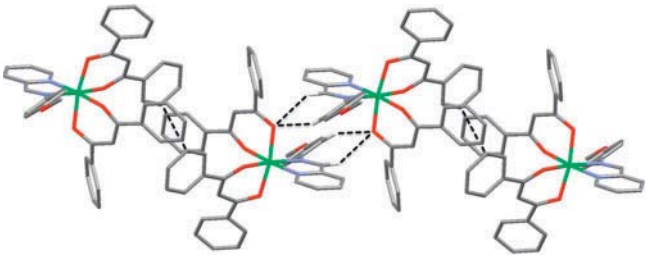

Fig. 5. Mercury plot showing the CH···O interactions in [Ni(dbm)$_2$(ppa^{OMe})] **12**. For clarity, only hydrogen atoms involved in interactions are shown.

Table 2. Electrochemical data of [Ni(β-diketonate)$_2$(ppa^X)] complexes[A]

Complex	Oxidation process $E^{o\prime}/E_p$ [V][B]	Reduction process E_p [V]
9	0.67 (I)	–
10	0.66 (I)	–
11	0.66 (I)	–
12	0.66 (I)	–
13	0.68 (I)	−1.94 (I)
14	0.72 (I)	−1.84 (I)
15	0.68 (I)	−1.85 (I)
16	0.70 (I)	−1.83 (I)
17	0.33	–
18	0.32	–
19	0.31	–
20	0.32, 0.97 (I)	–
21	0.35	−2.09 (I)
22	0.35	−2.01 (I)
23	0.36	−1.98 (I)
24	0.37	−2.00 (I)
25	–	−1.76 (I)
26	–	−1.79 (I)[C]
27	–	−1.69 (I)
28	–	−1.74 (I)
29	–	−1.73 (I)[C]
30	–	−1.57 (I)
31	–	−1.61 (I)
32	0.58 (I)	−1.61 (I)

[A]All measurements were performed at 298 K, in dried and degassed CH_2Cl_2 0.1 M [NBu^n_4][PF_6] solution; scan rate 100 mV s^{-1}; calibrated with [$FeCp_2$], and reported relative to the [$FeCp_2$]$^{0/+}$ couple.
[B]For an irreversible (I) process the oxidation peak potential, $(E_p)_{ox}$, is given.
[C]Uncalibrated as the compound reacts with [$FeCp_2$].

those of **17**–**24** undergo quasi-reversible oxidation, albeit only at scan rates above 200 mV s^{-1}. Comparison with the related cobalt complexes [Co(β-diketonate)$_2$(L)] (β-diketonate = dbm, tmhd, L = bpy, phen), which oxidize between −0.15 and 0.06 V (versus [$FeCp_2$]$^{0/+}$) to give the isolable Co(III) cations, suggest that the oxidation is to Ni(III) and, as such, represent rare examples of Ni(III) species (P. Harding and D. J. Harding, unpubl. data). As expected the [Ni(β-diketonate)$_2$(ppa^X)] complexes are oxidized at potentials very similar to the analogous [Ni(β-diketonate)$_2$(L)] (β-diketonate = dbm, tmhd; L = bpy, phen) complexes.[14] This is unsurprising given the structural similarity between the ligands. Attempts to chemically oxidize the complexes have thus far proved unsuccessful.

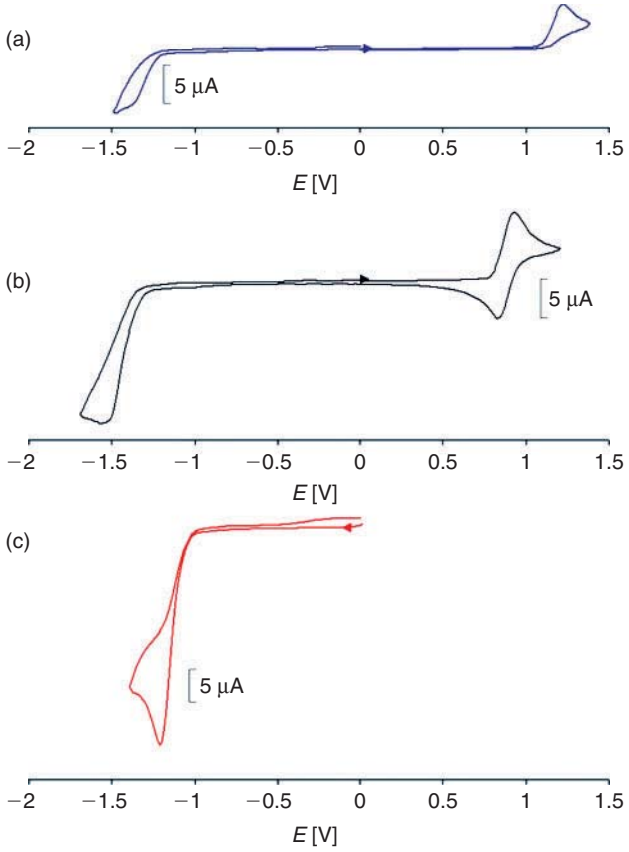

Fig. 6. Cyclic voltammogram of (a) [Ni(dbm)$_2$(ppa^F)] **13**, (b) [Ni(tmhd)$_2$(ppa^F)] **21**, and (c) [Ni(hfac)$_2$(ppa^F)] **29**. All potentials are versus [$FeCp_2$]$^{0/+}$.

The peak potentials for oxidation of **9**–**16** are between 0.32 and 0.37 V more positive than those of **17**–**24**. It is clear that the tmhd ligands are considerably more electron donating than the dbm ligands, presumably as a result of the inductive effect of the *t*-butyl groups on the tmhd ligands. The hfac ligands also have a significant effect on the peak potential for oxidation with no oxidation observed within the solvent window, with the exception of **32**. This is consistent with the findings of Villamena et al., in which the oxidation potential for [Ni(hfac)$_2$(2-pyBN)] (2-pyBN = N-*tert*-butyl-α-(2-pyridyl)nitrone) is observed at 1.80 V (versus Ag/AgCl).[11]

In contrast to the considerable effect that the β-diketonate ligand has on the peak potential for oxidation, the different ppa^X ligands result in only minor changes in the peak potential for oxidation. A similar insensitivity to the substituent has been observed in a series of Cu(I) compounds, [Cu(ppa^X)$_2$]ClO_4 (X = F, Cl, Br, and I).[16] It is possible that the substituent on the ppa^X ligand is simply too remote to significantly affect the peak potential for oxidation. Moreover, the twist between the phenyl ring and the pyridylimine unit seen in the solid state will reduce the degree of conjugation between the rings, thereby limiting the effect of the substituent on the oxidation potential. However, in the case of [Ni(tmhd)$_2$(ppa^{OMe})] a *second* irreversible oxidation is also observed, although whether this is metal-based or ligand-based remains unclear. Further spectroelectrochemical studies are currently underway to determine the nature of this second oxidation and will be reported in a later publication.

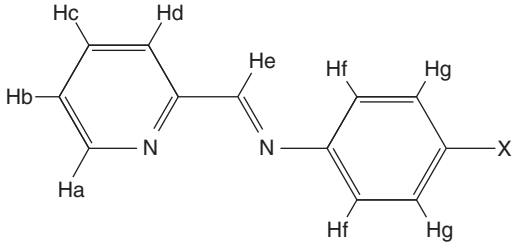

Fig. 7. Hydrogen labels of the ppa^X ligands.

In addition to the metal-based oxidation noted above, the complexes also undergo irreversible reduction. In the case of the complexes with dbm or tmhd ligands, only when X = F, Cl, Br, and I, are reduction peaks observed. Given the absence of any reduction peaks for the other complexes; i.e. where X = H, Me, Et, and OMe; it seems likely that these reductions are ligand based. Despite this, the reductions show considerable variation, with differences between the hfac and dbm complexes being on average 235 mV, whereas those between the dbm and tmhd complexes are 155 mV. The reason for this variation may be the result of the differing degrees of π-backbonding from the metal centre to the ppa^X ligand. Thus, the $[Ni(tmhd)_2(ppa^X)]$ compounds are the most electron rich, resulting in considerable π-backbonding and are therefore, the most difficult to reduce. Conversely, the $[Ni(hfac)_2(ppa^X)]$ complexes are the most electron poor, resulting in minimal π-backbonding, making the ppa^X ligand easier to reduce. It is also noteworthy that when X = F the complexes are more difficult to reduce by ∼0.1 V than for [Ni(β-diketonate)$_2$(ppa^X)] (β-diketonate = dbm, tmhd, hfac; X = Cl, Br, I). A final point of interest is that **25**–**28** also exhibit irreversible reduction waves. Whether this results from the reduction of the hfac or ppa^X ligands remains unclear.

Conclusions

In conclusion, we have prepared a series of [Ni(β-diketonate)$_2$(ppa^X)] complexes and have shown that the ppa^X ligands are convenient alternatives to substituted bipyridine or phenanthroline ligands. The crystal structures reveal octahedral coordinated nickel centres, with the β-diketonate ligands exhibiting both 'bent' and 'planar' bidentate coordination modes dependent upon the type of ppa^X ligand present. The aryl rings of the ppa^X ligands are found to be non-coplanar with the pyridylimine unit, the degree of twisting dependent on the substituent, X. The complexes are irreversibly or quasi-reversibly oxidized to Ni(III) in the case of $[Ni(dbm)_2(ppa^X)]$ and $[Ni(tmhd)_2(ppa^X)]$, respectively. With the exception of $[Ni(hfac)_2(ppa^I)]$ the hfac complexes show no oxidation processes. The $[Ni(tmhd)_2(ppa^X)]$ complexes are more easily oxidized by ∼350 mV than the $[Ni(dbm)_2(ppa^X)]$ complexes indicating that the β-diketonate ligand has a significant effect on the redox potential. In contrast, the ppa^X ligands have only a very minor effect on the redox potential with a difference of ∼50 mV between the various ppa^X ligands.

Experimental

General Remarks

All reactions were conducted in air using HPLC grade solvents. $[Ni(tmhd)_2(H_2O)_2]$, $[Ni(hfac)_2(H_2O)_2]$, and $[Ni(dbm)_2(H_2O)_2]$ were prepared by literature methods.[1,20] Although the ppa^X ligands are known, our synthesis differs from that previously reported and thus, their syntheses are included in the interests of completeness. All other chemicals were purchased from Fluka Chemical Co. and used as received. Infrared spectra were recorded on a Perkin–Elmer Spectrum One infrared spectrophotometer as KBr discs, in the range 400–4000 cm^{-1}. Electronic spectra were recorded in CH_2Cl_2 on a Unicam UV300 UV-Visible spectrometer. Elemental analyses were carried out on a Eurovector EA3000 analyzer. ^{1}H NMR spectra were recorded on a Bruker 300 MHz FT-NMR spectrometer at 298 K in $CDCl_3$ with $SiMe_4$ added as an internal standard. Hydrogen atoms are labelled according to Fig. 7. ESI-MS were carried out on a Bruker Daltonics 7.0T Apex 4 FTICR Mass Spectrometer. Electrochemical studies were carried out using a PalmsensPC Vs 2.11 Potentiosat in conjunction with a three electrode cell. The auxiliary electrode was a platinum rod and the working electrode was a platinum disc (2.0 mm diameter). The reference electrode was a Ag–AgCl electrode (2 M LiCl). Solutions were 5×10^{-4} mol dm^{-3} in the test compound and 0.1 mol dm^{-3} in $[NBu^n_4][PF_6]$ as the supporting electrolyte. Under these conditions, $E^{o\prime}$ for the one-electron oxidation of $[FeCp_2]$ added to the test solutions for internal calibration is 0.52 V.

Synthesis

*Synthesis of (Phenyl)-pyridine-2-ylmethylene-amine (ppa^H) **1***

To a solution of aniline (274 μL, 3 mmol) in diethylether (10 mL) over molecular sieves, was added pyridine-2-carboxaldehyde (266 μL, 3 mmol). The yellow solution was stirred overnight. The solution was filtered and the molecular sieves washed with CH_2Cl_2 (5 mL). The solvent was removed under vacuum, yielding a bright yellow oil (0.273 g, 50%). $\nu_{max}(CH_2Cl_2)/cm^{-1}$ 1630 ($\nu_{C=N}$). $\lambda_{max}(CH_2Cl_2)/nm$ ($\log \varepsilon/M^{-1}\,cm^{-1}$) 236 (4.07), 278 (3.82), 318 (3.50). $\delta_H = 8.70$ (1H, d, $^1J_{HH}$ 4.8, H_a), 8.58 (1H, s, H_e), 8.19 (1H, d, $^1J_{HH}$ 7.8, H_d), 7.79 (1H, m, $^1J_{HH}$ 7.8, H_c), 7.35 (3H, m, H_f, H_b), 7.20 (3H, m, H_g, H_H).

Ligands **2**–**8** were synthesized using the same procedure. Analytical and spectroscopic data are given for each compound.

*Synthesis of (4-Methylphenyl)-pyridine-2-ylmethylene-amine (ppa^{Me}) **2***

Yellow crystalline solid (0.360 g, 62%). ν_{max}(KBr)/cm^{-1} 1625 ($\nu_{C=N}$). $\lambda_{max}(CH_2Cl_2)/nm$ ($\log \varepsilon/M^{-1}\,cm^{-1}$) 234 (4.23), 280 (4.12), 324 (4.00 sh). $\delta_H = 8.71$ (1H, d, $^1J_{HH}$ 6.3, H_a), 8.62 (1H, s, H_e), 8.19 (1H, d, $^1J_{HH}$ 7.8, H_d), 7.80 (1H, m, $^1J_{HH}$ 7.8, H_c), 7.35 (1H, m, $^1J_{HH}$ 6.3, H_b), 7.24 (4H, m, H_f, H_g), 2.36 (3H, s, CH_3).

*Synthesis of (4-Ethylphenyl)-pyridine-2-ylmethylene-amine (ppa^{Et}) **3***

Dull orange oil (0.375 g, 59%). $\nu_{max}(CH_2Cl_2)/cm^{-1}$ 1630 ($\nu_{C=N}$). $\lambda_{max}(CH_2Cl_2)/nm$ ($\log \varepsilon/M^{-1}\,cm^{-1}$) 234 (4.10), 280 (4.03), 324 (3.93 sh). $\delta_H = 8.73$ (1H, d, $^1J_{HH}$ 4.8, H_a), 8.68 (1H, s, H_e), 8.24 (1H, d, $^1J_{HH}$ 7.8, H_d), 7.85 (1H, m, $^1J_{HH}$ 7.5, H_c), 7.23 (5H, m, H_b, H_f, H_g), 2.69 (2H, q, $^1J_{HH}$ 7.2, CH_2), 1.23 (3H, t, $^1J_{HH}$ 7.2, CH_3).

*Synthesis of (4-Methoxyphenyl)-pyridine-2-ylmethylene-amine (ppa^{OMe}) **4***

Light orange solid (0.423 g, 67%). ν_{max}(KBr)/cm^{-1} 1626 ($\nu_{C=N}$). $\lambda_{max}(CH_2Cl_2)/nm$ ($\log \varepsilon/M^{-1}\,cm^{-1}$) 238 (4.11), 286 (4.01), 340 (4.08). $\delta_H = 8.70$ (1H, d, $^1J_{HH}$ 7.2, H_a), 8.65 (1H, s, H_e), 8.20 (1H, d, $^1J_{HH}$ 7.8, H_d), 7.81 (1H, dd, $^1J_{HH}$ 8.1, 7.8,

H_c), 7.36 (3H, m, H_b, H_g), 6.94 (2H, m, $^1J_{HH}$ 8.7, H_f), 3.83 (3H, s, CH_3).

Synthesis of (4-Fluorophenyl)-pyridine-2-ylmethyleneamine (ppa^F) ***5***

Bright yellow crystalline solid (0.491 g, 82%). ν_{max}(KBr)/cm^{-1} 1627 ($\nu_{C=N}$). $\lambda_{max}(CH_2Cl_2)$/nm (log $\varepsilon/M^{-1}\,cm^{-1}$) 236 (3.91), 282 (3.91), 318 (3.75 sh). $\delta_H = 8.80$ (1H, d, $^1J_{HH}$ 4.8, H_a), 8.60 (1H, s, H_e), 8.20 (1H, d, $^1J_{HH}$ 7.8, H_d), 7.85 (1H, dd, $^1J_{HH}$ 7.5, 7.8, H_c), 7.38 (1H, dd, $^1J_{HH}$ 7.5, 4.8, H_b), 7.31 (2H, dd, $^1J_{HH}$ 8.1, 7.9, H_f), 7.09 (2H, dd, $^1J_{HH}$ 7.9, 8.1, H_g).

Synthesis of (4-Chlorophenyl)-pyridine-2-ylmethyleneamine (ppa^{Cl}) ***6***

Pale yellow crystalline solid (0.452 g, 70%). ν_{max}(KBr)/cm^{-1} 1624 ($\nu_{C=N}$). $\lambda_{max}(CH_2Cl_2)$/nm (log $\varepsilon/M^{-1}\,cm^{-1}$) 238 (4.12), 280 (4.09), 320 (3.95 sh). $\delta_H = 8.80$ (1H, d, $^1J_{HH}$ 5.1, H_a), 8.66 (1H, s, H_e), 8.30 (1H, d, $^1J_{HH}$ 8.1, H_d), 7.89 (1H, dd, $^1J_{HH}$ 8.1, 7.8, H_c), 7.44 (1H, dd, $^1J_{HH}$ 5.1, 7.8, H_b), 7.30 (2H, d, $^1J_{HH}$ 8.7, H_f), 7.01 (2H, d, $^1J_{HH}$ 8.7, H_g).

Synthesis of (4-Bromophenyl)-pyridine-2-ylmethyleneamine (ppa^{Br}) ***7***

Brown solid (0.596 g, 76%). ν_{max}(KBr)/cm^{-1} 1623 ($\nu_{C=N}$). $\lambda_{max}(CH_2Cl_2)$/nm (log $\varepsilon/M^{-1}\,cm^{-1}$) 232 (4.12), 280 (4.12), 324 (3.97 sh). $\delta_H = 8.73$ (1H, d, $^1J_{HH}$ 4.8, H_a), 8.62 (1H, s, H_e), 8.21 (1H, d, $^1J_{HH}$ 7.5, H_d), 7.86 (1H, t, $^1J_{HH}$ 7.5, 6.9, H_c), 7.53 (2H, d, $^1J_{HH}$ 7.8, H_f), 7.42 (1H, dd, $^1J_{HH}$ 6.9, 4.8, H_b), 7.18 (2H, d, $^1J_{HH}$ 7.8, H_g).

Synthesis of (4-Iodophenyl)-pyridine-2-ylmethyleneamine (ppa^I) ***8***

Pale green solid (prepared in *i*-Pr_2O) (0.605 g, 65%). ν_{max}(KBr)/cm^{-1} 1625 ($\nu_{C=N}$). $\lambda_{max}(CH_2Cl_2)$/nm (log $\varepsilon/M^{-1}\,cm^{-1}$) 242 (4.21), 282 (4.07), 320 (4.00 sh). $\delta_H = 8.72$ (1H, dd, $^1J_{HH}$ 1.5, 4.8, H_a), 8.58 (1H, s, H_e), 8.15 (1H, d, $^1J_{HH}$ 8.1, H_d), 7.96 (1H, ddd, $^1J_{HH}$ 1.5, 7.8, 8.1, H_c), 7.54 (1H, ddd, $^1J_{HH}$ 0.9, 4.8, 7.8, H_b), 7.31 (2H, d, $^1J_{HH}$ 8.4, H_f), 7.09 (2H, d, $^1J_{HH}$ 8.4, H_g).

Synthesis of [Ni(dbm)$_2$(ppa^H)] ***9***

To a lime green suspension of [Ni(dbm)$_2$(H_2O)$_2$] (0.135 g, 0.25 mmol) in acetone (10 mL), was added a solution of ppa^H (0.046 g, 0.25 mmol) in acetone (3 mL). The brown orange solution was stirred overnight then concentrated under vacuum. *n*-Hexane (10 mL) was added to precipitate a brown solid, which was washed with additional *n*-hexane (2 × 5 mL) and dried under vacuum, yielding a brown solid (0.106 g, 61%) (Found: C 73.4, H 4.6, N 3.9. Calc. for $C_{42}H_{32}N_2NiO_4$: C 73.4, H 4.7, N 4.1%). *m/z* (ESI) 463 (100%, [M-dbm$^-$]$^+$). ν_{max}(KBr)/cm^{-1} 1595 ($\nu_{C=O}$). $\lambda_{max}(CH_2Cl_2)$/nm (log $\varepsilon/M^{-1}\,cm^{-1}$) 259 (4.84), 277 (4.81), 352 (4.60).

Complexes **10**–**32** were synthesized by the same general procedure using acetone, THF, or CH_2Cl_2 in the case of [Ni(dbm)$_2$(H_2O)$_2$], [Ni(tmhd)$_2$(H_2O)$_2$], and [Ni(hfac)$_2$(H_2O)$_2$], respectively. They were crystallized from the solvents indicated.

Synthesis of [Ni(dbm)$_2$(ppa^{Me})] ***10***

Dull green microcrystals (CH_2Cl_2/*n*-hexane) (0.207 g, 55%) (Found: C 73.5, H 4.9, N 4.1. Calc. for $C_{43}H_{34}N_2NiO_4$: C 73.6, H 4.9, N 4.0%). *m/z* (ESI) 477 (100%, [M-dbm$^-$]$^+$). ν_{max}(KBr)/cm^{-1} 1595 ($\nu_{C=O}$). $\lambda_{max}(CH_2Cl_2)$/nm (log $\varepsilon/M^{-1}\,cm^{-1}$) 248 (4.63), 358 (4.51).

Synthesis of [Ni(dbm)$_2$(ppa^{Et})] ***11***

Brown-yellow solid (acetone/*n*-hexane) (0.115 g, 64%) (Found: C 73.5, H 5.1, N 4.0. Calc. for $C_{44}H_{36}N_2NiO_4$: C 73.9, H 5.1, N 3.9%). *m/z* (ESI) 701 (100%, [M-dbm$^-$ + ppa^{Et}]$^+$), 491 (28%, [M-dbm$^-$]$^+$). ν_{max}(KBr)/cm^{-1} 1595 ($\nu_{C=O}$). $\lambda_{max}(CH_2Cl_2)$/nm (log $\varepsilon/M^{-1}\,cm^{-1}$) 246 (4.45), 284 (4.23 sh), 356 (4.48).

Synthesis of [Ni(dbm)$_2$(ppa^{OMe})] ***12***

Brown-yellow solid (acetone/*n*-hexane) (0.122 g, 68%) (Found: C 72.2 H 5.0, N 3.9. Calc. for $C_{43}H_{34}N_2NiO_5$: C 72.0 H 4.8, N 3.9%). *m/z* (ESI) 493 (100%, [M-dbm$^-$]$^+$). ν_{max}(KBr)/cm^{-1} 1595 ($\nu_{C=O}$). $\lambda_{max}(CH_2Cl_2)$/nm (log $\varepsilon/M^{-1}\,cm^{-1}$) 250 (4.60), 282 (4.21 sh), 358 (4.54).

Synthesis of [Ni(dbm)$_2$(ppa^F)] ***13***

Brown-yellow microcrystals (CH_2Cl_2/*n*-hexane) (0.222 g, 59%) (Found: C 71.2, H 4.6, N 4.2. Calc. for $C_{42}H_{31}FN_2NiO_4$: C 71.5, H 4.4, N 4.0%). *m/z* (ESI) 481 (100%, [M-dbm$^-$]$^+$). ν_{max}(KBr)/cm^{-1} 1595 ($\nu_{C=O}$). $\lambda_{max}(CH_2Cl_2)$/nm (log $\varepsilon/M^{-1}\,cm^{-1}$) 246 (4.66), 284 (4.33 sh), 356 (4.53).

Synthesis of [Ni(dbm)$_2$(ppa^{Cl})] ***14***

Yellow solid (acetone/*n*-hexane) (0.114 g, 63%) (Found: C 71.2, H 4.7, N 3.9. Calc. for $C_{42}H_{31}ClN_2NiO_4$: C 69.9, H 4.3, N 3.9%). *m/z* (ESI) 497 (100%, [M-dbm$^-$]$^+$). ν_{max}(KBr)/cm^{-1} 1594 ($\nu_{C=O}$). $\lambda_{max}(CH_2Cl_2)$/nm (log $\varepsilon/M^{-1}\,cm^{-1}$) 246 (4.61), 358 (4.50).

Synthesis of [Ni(dbm)$_2$(ppa^{Br})] ***15***

Yellow solid (acetone/*n*-hexane) (0.158 g, 82%) (Found: C 65.9, H 4.0, N 3.9. Calc. for $C_{42}H_{31}BrN_2NiO_4$: C 65.8, H 4.1, N 3.6%). *m/z* (ESI) 543 (100%, [M-dbm$^-$]$^+$). ν_{max}(KBr)/cm^{-1} 1593 ($\nu_{C=O}$). $\lambda_{max}(CH_2Cl_2)$/nm (log $\varepsilon/M^{-1}\,cm^{-1}$) 247 (4.66), 355 (4.47).

Synthesis of [Ni(dbm)$_2$(ppa^I)] ***16***

Brown solid (THF/*n*-hexane) (0.091 g, 44%) (Found: C 61.9, H 4.2, N 3.2. Calc. for $C_{42}H_{31}IN_2NiO_4$: C 62.0, H 3.8, N 3.4%). *m/z* (ESI) 897 (100%, [M-dbm$^-$ + ppa^I]$^+$), 589 (85%, [M-dbm$^-$]$^+$). ν_{max}(KBr)/cm^{-1} 1594 ($\nu_{C=O}$). $\lambda_{max}(CH_2Cl_2)$/nm (log $\varepsilon/M^{-1}\,cm^{-1}$) 248 (4.66), 286 (4.28 sh), 354 (4.50).

Synthesis of [Ni(tmhd)$_2$(ppa^H)] ***17***

Brown solid (THF/*n*-hexane) (0.063 g, 41%) (Found: C 67.8, H 7.9, N 4.8. Calc. for $C_{34}H_{48}N_2NiO_4$: C 67.2, H 8.0, N 4.6%). *m/z* (ESI) 605 (37%, [M-tmhd$^-$ + ppa^H]$^+$), 423 (100%, [M-tmhd$^-$]$^+$). ν_{max}(KBr)/cm^{-1} 1591 ($\nu_{C=O}$). $\lambda_{max}(CH_2Cl_2)$/nm (log $\varepsilon/M^{-1}\,cm^{-1}$) 240 (4.36), 294 (4.28).

Synthesis of [Ni(tmhd)$_2$(ppa^{Me})] ***18***

Brown needles (slow evaporation of CH_2Cl_2) (0.080 g, 52%) (Found: C 67.0, H 7.9, N 4.4. Calc. for $C_{35}H_{50}N_2NiO_4$: C 67.6, H 8.1, N 4.5%). *m/z* (ESI) 633 (100%, [M-tmhd$^-$ + ppa^{Me}]$^+$), 437 (88%, [M-tmhd$^-$]$^+$). ν_{max}(KBr)/cm^{-1} 1586 ($\nu_{C=O}$). $\lambda_{max}(CH_2Cl_2)$/nm (log $\varepsilon/M^{-1}\,cm^{-1}$) 240 (4.46), 272 (4.26 sh), 308 (4.42).

Synthesis of [Ni(tmhd)$_2$(ppa^{Et})] ***19***

Brown oil (0.066 g, 40%) (Found: C 67.8, H 8.0, N 4.1. Calc. for $C_{36}H_{52}N_2NiO_4$: C 68.0, H 8.2, N 4.4%). *m/z* (ESI) 451 (100%, [M-tmhd$^-$]$^+$). ν_{max}(KBr)/cm^{-1} 1591 ($\nu_{C=O}$). λ_{max}(CH_2Cl_2)/nm (log ε/M^{-1} cm^{-1}) 240 (4.40), 308 (4.35).

Synthesis of [Ni(tmhd)$_2$(ppa^{OMe})] ***20***

Red-brown solid (THF/*n*-hexane) (0.079 g, 37%) (Found: C 65.7, H 7.4, N 4.5. Calc. for $C_{35}H_{50}N_2NiO_5$: C 65.9, H 7.9, N 4.4%). *m/z* (ESI) 665 (100%, [M-tmhd$^-$ + ppa^{OMe}]$^+$), 453 (73%, [M-tmhd$^-$]$^+$). ν_{max}(KBr)/cm^{-1} 1592 ($\nu_{C=O}$). λ_{max}(CH_2Cl_2)/nm (log ε/M^{-1} cm^{-1}) 242 (4.51), 316 (4.42) 354 (4.31 sh).

Synthesis of [Ni(tmhd)$_2$(ppa^{F})] ***21***

Brown needles (slow evaporation of CH_2Cl_2) (0.048 g, 32%) (Found: C 65.3, H 7.5, N 4.8. Calc. for $C_{34}H_{47}FN_2NiO_4$: C 65.3, H 7.6, N 4.5%). *m/z* (ESI) 641 (13%, [M-tmhd$^-$ + ppa^F]$^+$), 441 (100%, [M-tmhd$^-$]$^+$). ν_{max}(KBr)/cm^{-1} 1591 ($\nu_{C=O}$). λ_{max}(CH_2Cl_2)/nm (log ε/M^{-1} cm^{-1}) 238 (4.46), 272 (4.27), 308 (4.45).

Synthesis of [Ni(tmhd)$_2$(ppa^{Cl})] ***22***

Red-brown solid (THF/*n*-hexane) (0.068 g, 42%) (Found: C 63.3, H 7.3, N 4.7. Calc. for $C_{34}H_{47}ClN_2NiO_4$: C 63.6, H 7.4, N 4.4%). *m/z* (ESI) 675 (13%, [M-tmhd$^-$ + ppa^{Cl}]$^+$), 457 (100%, [M-tmhd$^-$]$^+$). ν_{max}(KBr)/cm^{-1} 1588 ($\nu_{C=O}$). λ_{max}(CH_2Cl_2)/nm (log ε/M^{-1} cm^{-1}) 240 (4.27), 303 (4.24).

Synthesis of [Ni(tmhd)$_2$(ppa^{Br})] ***23***

Brown solid (THF/*n*-hexane) (0.051 g, 29%) (Found: C 59.2, H 6.6, N 4.3. Calc. for $C_{34}H_{47}BrN_2NiO_4$: C 59.5, H 6.9, N 4.1%). *m/z* (ESI) 763 (100%, [M-tmhd$^-$ + ppa^{Br}]$^+$), 503 (88%, [M-tmhd$^-$]$^+$). ν_{max}(KBr)/cm^{-1} 1592 ($\nu_{C=O}$). λ_{max}(CH_2Cl_2)/nm (log ε/M^{-1} cm^{-1}) 244 (4.39).

Synthesis of [Ni(tmhd)$_2$(ppa^{I})] ***24***

Brown solid (THF/*n*-hexane) (0.091 g, 49%) (Found: C 55.2, H 6.5, N 3.7. Calc. for $C_{34}H_{47}IN_2NiO_4$: C 55.7, H 6.5, N 3.8%). *m/z* (ESI) 857 (100%, [M-tmhd$^-$ + ppa^I]$^+$), 549 (90%, [M-tmhd$^-$]$^+$). ν_{max}(KBr)/cm^{-1} 1592 ($\nu_{C=O}$). λ_{max}(CH_2Cl_2)/nm (log ε/M^{-1} cm^{-1}) 252 (4.50), 276 (4.38).

Synthesis of [Ni(hfac)$_2$(ppa^{H})]·0.5THF ***25***

Yellow solid (THF/*n*-hexane) (0.076 g, 46%) (Found: C 41.3, H 2.2, N 4.3. Calc. for $C_{24}H_{16}F_{12}N_2NiO_{4.5}$: C 41.7, H 2.3, N 4.0%). *m/z* (ESI) 447 (100%, [M-hfac$^-$]$^+$). ν_{max}(KBr)/cm^{-1} 1652 ($\nu_{C=O}$). λ_{max}(CH_2Cl_2)/nm (log ε/M^{-1} cm^{-1}) 243.5 (4.26), 285 (4.36), 315 (4.35).

Synthesis of [Ni(hfac)$_2$(ppa^{Me})]·0.5CH_2Cl_2 ***26***

Green-brown solid (CH_2Cl_2/*n*-hexane) (0.181 g, 98%) (Found: C 40.3, H 2.6, N 3.6. Calc. for $C_{23.5}H_{15}ClF_{12}N_2NiO_4$: C 40.0, H 2.1, N 3.9%). *m/z* (ESI) 657 (100%, [M-hfac$^-$ + ppa^{Me}]$^+$), 461 (26%, [M-hfac$^-$]$^+$). ν_{max}(KBr)/cm^{-1} 1653 ($\nu_{C=O}$). λ_{max}(CH_2Cl_2)/nm (log ε/M^{-1} cm^{-1}) 242 (4.20), 318 (4.40).

Synthesis of [Ni(hfac)$_2$(ppa^{Et})] ***27***

Brown solid (THF/*n*-hexane) (0.055 g, 31%) (Found: C 42.5, H 2.5, N 4.2. Calc. for $C_{24}H_{16}F_{12}N_2NiO_4$: C 42.2, H 2.4, N 4.1%). *m/z* (ESI) 685 (100%, [M-hfac$^-$ + ppa^{Et}]$^+$), 475 (84%, [M-hfac$^-$]$^+$). ν_{max}(KBr)/cm^{-1} 1654 ($\nu_{C=O}$). λ_{max}(CH_2Cl_2)/nm (log ε/M^{-1} cm^{-1}) 247 (4.23), 320 (4.31).

Synthesis of [Ni(hfac)$_2$(ppa^{OMe})] ***28***

Deep yellow solid (THF/*n*-hexane) (0.098 g, 54%) (Found: C 40.3, H 2.4, N 4.3. Calc. for $C_{23}H_{14}F_{12}N_2NiO_5$: C 40.3, H 2.1, N 4.1%). *m/z* (ESI) 477 (100%, [M-hfac$^-$]$^+$). ν_{max}(KBr)/cm^{-1} 1647 ($\nu_{C=O}$). λ_{max}(CH_2Cl_2)/nm (log ε/M^{-1} cm^{-1}) 255 (4.27), 325 (4.26).

Synthesis of [Ni(hfac)$_2$(ppa^{F})]·0.5C_6H_{14} ***29***

Brown solid (CH_2Cl_2/*n*-hexane) (0.131 g, 78%) (Found: C 41.6, H 2.3, N 3.7. Calc. for $C_{25}H_{18}F_{13}N_2NiO_4$: C 41.9, H 2.5, N 3.9%). *m/z* (ESI) 665 (100%, [M-hfac$^-$ + ppa^F]$^+$), 465 (27%, [M-hfac$^-$]$^+$). ν_{max}(KBr)/cm^{-1} 1651 ($\nu_{C=O}$). λ_{max}(CH_2Cl_2)/nm (log ε/M^{-1} cm^{-1}) 238 (4.26), 318 (4.45).

Synthesis of [Ni(hfac)$_2$(ppa^{Cl})] ***30***

Golden brown solid (CH_2Cl_2/*n*-hexane) (0.101 g, 58%) (Found: C 38.5, H 1.7, N 4.2. Calc. for $C_{22}H_{11}ClF_{12}N_2NiO_4$: C 38.3, H 1.6, N 4.1%). *m/z* (ESI) 481 (100%, [M-hfac$^-$]$^+$). ν_{max}(KBr)/cm^{-1} 1651 ($\nu_{C=O}$). λ_{max}(CH_2Cl_2)/nm (log ε/M^{-1} cm^{-1}) 240 (4.25), 319 (4.38).

Synthesis of [Ni(hfac)$_2$(ppa^{Br})] ***31***

Deep yellow solid (CH_2Cl_2/*n*-hexane) (0.096 g, 52%) (Found: C 36.2, H 1.7, N 3.9. Calc. for $C_{22}H_{11}BrF_{12}N_2NiO_4$: C 36.0, H 1.5, N 3.8%). *m/z* (ESI) 527 (100%, [M-hfac$^-$]$^+$). ν_{max}(KBr)/cm^{-1} 1651 ($\nu_{C=O}$). λ_{max}(CH_2Cl_2)/nm (log ε/M^{-1} cm^{-1}) 319 (4.46), 342 (4.34).

Synthesis of [Ni(hfac)$_2$(ppa^{I})] ***32***

Yellow solid (THF/*n*-hexane) (0.107 g, 54%) (Found: C 33.6, H 1.9, N 3.6. Calc. for $C_{22}H_{11}F_{12}IN_2NiO_4$: C 33.8, H 1.4, N 3.6%). *m/z* (ESI) 881 (100%, [M-hfac$^-$ + ppa^I]$^+$), 573 (82%, [M-hfac$^-$]$^+$). ν_{max}(KBr)/cm^{-1} 1654 ($\nu_{C=O}$). λ_{max}(CH_2Cl_2)/nm (log ε/M^{-1} cm^{-1}) 244 (4.40), 320 (4.41).

Crystal Structure Determinations

Crystal data for the structures of **10**, **12**, and **14** are given in Table 1. X-ray quality crystals of **10**, **12**, and **14** were grown by allowing hexane to diffuse into a concentrated solution of the complex in CH_2Cl_2. Crystals were mounted on a glass fibre using perfluoropolyether oil and cooled rapidly to 150 K for **10** and **12** and 100 K for **14** in a stream of cold nitrogen. All diffraction data were collected on a Bruker Smart CCD area detector with graphite monochromated *Mo Kα* (λ = 0.71073 Å). After data collection, in each case an empirical absorption correction (SADABS) was applied,[21] and the structures were then solved by direct methods and refined on all F^2 data using the *SHELX* suite of programs.[22] In all cases non-hydrogen atoms were refined with anisotropic thermal parameters; hydrogen atoms were included in calculated positions and refined with isotropic thermal parameters, which were ~1.2 × (aromatic CH) or 1.5 × (Me) the equivalent isotropic thermal parameters of their parent carbon atoms.

10: $C_{43}H_{34}N_2NiO_4$, *M* 701.43, yellow needle, triclinic, space group *P-1*, *a* 9.6344(15), *b* 11.9506(18), *c* 16.267(3) Å, *α* 85.726(12), *β* 87.747(11), *γ* 66.802(10)°, *U* 1716.6(5) Å^3, *Z* 2, *D* 1.357 Mg m^{-3}, μ($Mo_{K\alpha}$) 0.612 mm^{-1}, *F(000)* 732, *T* 150 K, 20118 reflections, 6429 unique (R_{int} 0.0806), R_1 0.0655 (6429 reflections, $I > 2.0\sigma(I)$), wR_2 0.1449, R_1 0.1316 (all data), wR_2 0.1796 (all data), *S* 1.008.

12: $C_{43}H_{34}N_2NiO_5$, *M* 717.43, yellow plate, triclinic, space group *P-1*, *a* 9.9252(3), *b* 11.2859(3), *c* 17.4359(4) Å, α 73.2240(10), β 86.0220(10), γ 68.8910(10)°, *U* 1743.17(8) Å^3, *Z* 2, *D* 1.367 Mg m^{-3}, μ($Mo_{K\alpha}$) 0.607 mm^{-1}, *F(000)* 748, *T* 150 K, 23492 reflections, 7901 unique (R_{int} 0.0318), R_1 0.0372 (7901 reflections, $I > 2.0\sigma(I)$), wR_2 0.0922, R_1 0.0480 (all data), wR_2 0.0987 (all data), *S* 1.037.

14: $C_{42}H_{31}ClN_2NiO_4$, *M* 721.85, red needle, triclinic, space group *P-1*, *a* 9.6098(4), *b* 12.0443(5), *c* 16.1292(7) Å, α 85.154(2), β 86.882(2), γ 66.725(2)°, *U* 1708.34(12) Å^3, *Z* 2, *D* 1.403 Mg m^{-3}, μ($Mo_{K\alpha}$) 0.693 mm^{-1}, *F(000)* 748, *T* 100 K, 31160 reflections, 7710 unique (R_{int} 0.0334), R_1 0.0466 (7710 reflections, $I > 2.0\sigma(I)$), wR_2 0.1209, R_1 0.0626 (all data), wR_2 0.1278 (all data), *S* 1.094.

Acknowledgements

We gratefully acknowledge the Thailand Research Fund and Walailak University (Grant No. RSA5080007) for funding this research. We also thank the School of Chemistry, University of Bristol for elemental analysis and MS services.

References

[1] F. A. Cotton, G. Wilkinson, C. A. Murillo, M. Bochmann, in *Advanced Inorganic Chemistry, 6th edn* **1999**, pp. 479–482 (John Wiley Sons: New York, NY).

[2] N. S. Nandurkar, D. S. Patil, B. M. Bhanage, *Inorg. Chem. Commun.* **2008**, *11*, 733. doi:10.1016/J.INOCHE.2008.03.014

[3] (a) R. G. Miller, T. J. Kealy, A. L. Barney, *J. Am. Chem. Soc.* **1967**, *89*, 3756. doi:10.1021/JA00991A013
(b) T. Yamada, O. Rhode, T. Takai, T. Mukaiyama, *Chem. Lett.* **1991**, *20*, 5. doi:10.1246/CL.1991.5
(c) T. Yamada, T. Takai, O. Rhode, T. Mukaiyama, *Bull. Chem. Soc. Jpn.* **1991**, *64*, 2109. doi:10.1246/BCSJ.64.2109
(d) Y. Nishida, T. Fujimoto, N. Tanaka, *Chem. Lett.* **1992**, *21*, 1291. doi:10.1246/CL.1992.1291

[4] (a) P. Chassot, F. Emmenegger, *Inorg. Chem.* **1996**, *35*, 5931. doi:10.1021/IC9605130
(b) F. Emmenegger, C. W. Schlaepfer, H. Stoeckli-Evans, M. Piccand, H. Piekarski, *Inorg. Chem.* **2001**, *40*, 3884. doi:10.1021/IC0014540

[5] (a) S. Pasko, L. G. Hubert-Pfalzgraf, A. Abrutis, J. Vaissermann, *Polyhedron* **2004**, *23*, 735. doi:10.1016/J.POLY.2003.11.044
(b) L. G. Hubert-Pfalzgraf, *Inorg. Chem. Commun.* **2003**, *6*, 102. doi:10.1016/S1387-7003(02)00664-0

[6] D. Barreca, C. Massignan, S. Daolio, M. Fabrizio, C. Piccirillo, L. Armelao, E. Tondello, *Chem. Mater.* **2001**, *13*, 588. doi:10.1021/CM001041X

[7] (a) M. H. Dickman, *Acta Crystallogr. C* **1997**, *53*, 1192. doi:10.1107/S0108270197005945
(b) M. H. Dickman, J. P. Ward, F. A. Villamena, D. R. Crist, *Acta Crystallogr. C* **1998**, *54*, 929. doi:10.1107/S0108270198000730
(c) F. A. Villamena, M. H. Dickman, D. R. Crist, *Inorg. Chem.* **1998**, *37*, 1446. doi:10.1021/IC9709741
(d) F. A. Villamena, M. H. Dickman, D. R. Crist, *Inorg. Chem.* **1998**, *37*, 1454. doi:10.1021/IC971215L

[8] (a) R. G. Hicks, M. T. Lemaire, L. K. Thompson, T. M. Barclay, *J. Am. Chem. Soc.* **2000**, *122*, 8077. doi:10.1021/JA001627K
(b) T. M. Barclay, R. G. Hicks, M. T. Lemaire, L. K. Thompson, *Inorg. Chem.* **2001**, *40*, 5581. doi:10.1021/IC010542X

[9] (a) L. M. Field, P. M. Lahti, *Inorg. Chem.* **2003**, *42*, 7447. doi:10.1021/IC0349050
(b) M. Baskett, P. M. Lahti, A. Paduan-Filho, N. F. Oliveira, Jr, *Inorg. Chem.* **2005**, *44*, 6725. doi:10.1021/IC050435T

[10] (a) A. Caneschi, D. Gatteschi, J. Laugier, P. Rey, R. Sessoli, *Inorg. Chem.* **1988**, *27*, 1553. doi:10.1021/IC00282A009
(b) A. Caneschi, D. Gatteschi, J. P. Renard, P. Rey, R. Sessoli, *Inorg. Chem.* **1989**, *28*, 2940. doi:10.1021/IC00314A013
(c) D. Luneau, G. Risoan, P. Rey, A. Caneschi, D. Gatteschi, J. Laugier, *Inorg. Chem.* **1993**, *32*, 5616. doi:10.1021/IC00076A032

[11] F. A. Villamena, V. Horak, D. R. Crist, *Inorg. Chim. Acta* **2003**, *342*, 125. doi:10.1016/S0020-1693(02)01154-4

[12] S. Kudo, A. Iwase, N. Tanaka, *Inorg. Chem.* **1985**, *24*, 2388. doi:10.1021/IC00209A015

[13] G. M. Denison, A. O. Evans, C. A. Bessel, D. W. Skaf, R. W. Murray, J. M. DeSimone, *J. Electrochem. Soc.* **2005**, *152*, B435. doi:10.1149/1.2047387

[14] P. Harding, D. J. Harding, W. Phonsri, S. Saithong, H. Phetmung, *Inorg. Chim. Acta* **2009**, *362*, 78. doi:10.1016/J.ICA.2008.03.014

[15] S. Dehghanpour, A. Mahmoudi, *Main Group Chemistry* **2007**, *6*, 121. doi:10.1080/10241220801889025

[16] S. Dehghanpour, N. Bouslimani, R. Welter, F. Mojahed, *Polyhedron* **2007**, *26*, 154. doi:10.1016/J.POLY.2006.08.011

[17] A. C. G. Hotze, J. A. Faiz, N. Mourtzis, G. I. Pascu, P. R. A. Webber, G. J. Clarkson, K. Yannakopoulou, Z. Pikramenou, M. J. Hannon, *Dalton Trans.* **2006**, 3025. doi:10.1039/B518027A

[18] K. Nakamoto, in *Infrared and Raman Spectra of Inorganic and Coordination Compounds: Part B, 5th edn* **1997**, pp. 91–99 (Wiley: New York, NY).

[19] A. J. Jircitano, R. F. Henry, R. R. Hammond, *Acta Crystallogr. C* **1990**, *46*, 1799. doi:10.1107/S0108270190000944

[20] D. V. Soldatov, A. T. Henegouwen, G. D. Duright, C. I. Ratcliffe, J. A. Ripmeester, *Inorg. Chem.* **2001**, *40*, 1626. doi:10.1021/IC000981G

[21] SMART Bruker, *XSCANS, SHEXTL and SADABS* **2005** (Bruker AXS Inc.: Madison, WI).

[22] G. M. Sheldrick, *SHELXS97 and SHELXL97* **1997** (University of Göttingen: Germany).

Appendix Two

International Publication

Acta Crystallographica Section E
Structure Reports Online
ISSN 1600-5368
Editors: **W. T. A. Harrison, J. Simpson and M. Weil**

[(4-Bromophenyl)(2-pyridylmethylidene)amine-κ^2N,N']bis-(1,1,1,5,5,5-hexafluoropentane-2,4-dionato-κ^2O,O')cobalt(II)

Phimphaka Harding, David J. Harding, Nitisastr Soponrat and Harry Adams

Acta Cryst. (2010). E**66**, m1138–m1139

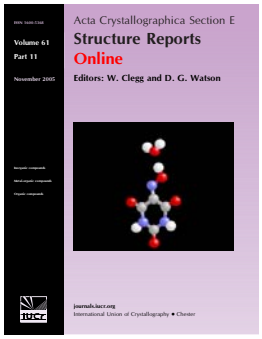

Acta Crystallographica Section E
Structure Reports Online
ISSN 1600-5368

[(4-Bromophenyl)(2-pyridylmethylidene)amine-κ^2N,N']bis(1,1,1,5,5,5-hexafluoropentane-2,4-dionato-κ^2O,O')cobalt(II)

Phimphaka Harding,[a]* David J. Harding,[a] Nitisastr Soponrat[b] and Harry Adams[c]

[a]Molecular Technology Research Unit, Department of Chemistry, Walailak University, Thasala, Nakhon Si Thammarat 80161, Thailand, [b]Department of Chemistry, Faculty of Science, Taksin University, Songkhla 90000, Thailand, and [c]Department of Chemistry, Faculty of Science, University of Sheffield, Brook Hill, Sheffield S3 7HF, England
Correspondence e-mail: kphimpha@wu.ac.th

Received 3 August 2010; accepted 14 August 2010

Key indicators: single-crystal X-ray study; T = 150 K; mean σ(C–C) = 0.005 Å; R factor = 0.035; wR factor = 0.090; data-to-parameter ratio = 13.7.

In the title complex, $[Co(C_5HF_6O_2)_2(C_{12}H_9BrN_2)]$, the Co^{II} atom exhibits a pseudo-octahedral coordination geometry, comprising two *N*-donor atoms from a bidentate chelate (4-bromophenyl)(2-pyridylmethylidene)amine (ppa^{Br}) ligand [Co—N = 2.098 (2) and 2.209 (2) Å] and four *O*-donor atoms from two bidentate chelate 1,1,1,5,5,5-hexafluoropentane-2,4-dionate (hfac) ligands [Co—O range = 2.0452 (19)–2.0796 (19) Å]. The packing of the structure involves weak π–π interactions between the pyridyl and benzene rings of neighbouring ppa^{Br} ligands [centroid–centroid distance = 3.928 (2) Å] and interactions between the Br atom on the ppa^{Br} ligand and the hfac ligand [Br···C = 3.531 (2) Å].

Related literature

For a review of halogen bonding, see: Corradi *et al.* (2000); Walsh *et al.* (2001); Liantonio *et al.* (2003). For an introduction to crystal engineering, see: Braga *et al.* (2002). For related structures, see: Harding, Harding, Sophonrat & Adams (2010); Harding, Harding, Tinpun *et al.* (2010); Aäkeroy *et al.* (2004, 2007). For a description of the Cambridge Structural database, see: Allen *et al.* (2002).

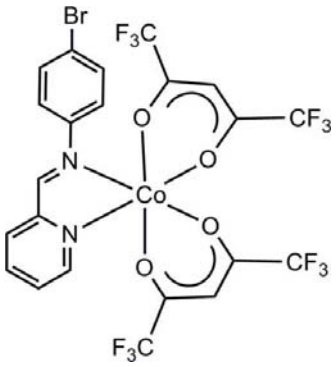

Experimental

Crystal data

$[Co(C_5HF_6O_2)_2(C_{12}H_9BrN_2)]$
M_r = 734.17
Triclinic, $P\overline{1}$
a = 8.3568 (2) Å
b = 10.9420 (2) Å
c = 14.8151 (3) Å
α = 74.042 (1)°
β = 86.510 (1)°
γ = 77.080 (1)°
V = 1269.51 (5) Å^3
Z = 2
Mo $K\alpha$ radiation
μ = 2.37 mm^{-1}
T = 150 K
0.60 × 0.30 × 0.03 mm

Data collection

Bruker SMART CCD area-detector diffractometer
Absorption correction: multi-scan (*SADABS*; Bruker, 1997)
T_{min} = 0.330, T_{max} = 0.932
21525 measured reflections
5176 independent reflections
4508 reflections with $I > 2\sigma(I)$
R_{int} = 0.021

Refinement

$R[F^2 > 2\sigma(F^2)]$ = 0.035
$wR(F^2)$ = 0.090
S = 1.08
5176 reflections
379 parameters
H-atom parameters constrained
$\Delta\rho_{max}$ = 1.23 e Å^{-3}
$\Delta\rho_{min}$ = −0.91 e Å^{-3}

Data collection: *SMART* (Bruker, 1997); cell refinement: *SAINT* (Bruker, 1997); data reduction: *SAINT*; program(s) used to solve structure: *SHELXS97* (Sheldrick, 2008); program(s) used to refine structure: *SHELXL97* (Sheldrick, 2008); molecular graphics: *SHELXTL* (Sheldrick, 2008); software used to prepare material for publication: *SHELXTL*.

We thank the Thailand Research Fund (Grant No.: RSA5080007) for funding this research.

Supplementary data and figures for this paper are available from the IUCr electronic archives (Reference: ZS2056).

References

Aäkeroy, C. B., Desper, J. & V.-Martínez, J., (2004). *CrystEngComm*, **6**, 413–418.
Aäkeroy, C. B., Schultheiss, N., Desper, J. & Moore, C. (2007). *CrystEngComm*, **9**, 421–426.
Allen, F. H. (2002). *Acta Cryst.* B**58**, 380–388.
Braga, D., Desiraju, G. R., Miller, J. S., Orpen, A. G. & Price, S. L. (2002). *CrystEngComm*, **4**, 500–509.
Bruker (1997). *SMART*, *SAINT* and *SADABS*. Bruker AXS Inc., Madison, Wisconsin, USA.
Corradi, E., Meille, M. T., Messina, S. V., Metrangolo, P. & Resnati, R. (2000). *Angew. Chem. Int. Ed.* **39**, 1782–1786.

Harding, P., Harding, D. J., Sophonrat, N. & Adams, H. (2010). Unpublished results.
Harding, P., Harding, D. J., Tinpun, K., Samuadnuan, S., Sophonrat, N. & Adams, H. (2010). *Aust. J. Chem.* **63**, 75–82.
Liantonio, R., Metrangolo, P., Pilati, T., Resnati, G. & Stevenazzi, A. (2003). *Cryst. Growth Des.* **3**, 799–803.
Sheldrick, G. M. (2008). *Acta Cryst.* A**64**, 112–122.
Walsh, R. B., Padgett, C. W., Metrangolo, P., Resnati, G., Hanks, T. W. & Pennington, W. T. (2001). *Cryst. Growth Des.* **1**, 165–175.

supplementary materials

Acta Cryst. (2010). E**66**, m1138-m1139 [**doi:10.1107/S1600536810032757**]

[(4-Bromophenyl)(2-pyridylmethylidene)amine-κ^2N,N']bis(1,1,1,5,5,5-hexafluoropentane-2,4-dionato-κ^2O,O')cobalt(II)

P. Harding, D. J. Harding, N. Soponrat and H. Adams

Comment

The construction of supramolecular networks with designed architectures still remains the goal of crystal engineering and represents a significant challenge (Braga *et al.*, 2002). Although complementary hydrogen-bonding ligands have been successfully used (Aäkeroy *et al.*, 2004) in the construction of a number of networks, halogen-bonding (Walsh *et al.*, 2001; Liantonio *et al.*, 2003) and halogen···halogen interactions remain less well represented despite the fact that these interactions can be as strong as hydrogen-bonding interactions (Corradi *et al.*, 2000). In this paper we report the synthesis and structure of [Co(hfac)$_2$(ppa^{Br})] [hfac = 1,1,1,5,5,5-hexafluoropentane-2,4-dionato; ppa^{Br} = (4-bromo-phenyl)pyridin-2-yl-methyleneamine].

The reaction of [Co(hfac)$_2$(H$_2$O)$_2$] with ppa^{Br} in CH_2Cl_2 yields [Co(hfac)$_2$(ppa^{Br})] (I) (Fig. 1) which crystallizes from CH_2Cl_2/hexane. In (I) the cobalt metal centre is six-coordinate with a distorted octahedral geometry, the hfac ligands adopting a *cis* arrangement enforced by the chelating ppa^{Br} ligand. The CF_3 groups of the hfac ligand in some cases exhibit large thermal ellipsoids due to thermal motion of these groups. The Co—N and Co—O bond lengths are comparable with related cobalt hfac and diimine complexes reported in the CSD (Allen, 2002) (mean Co—O distance = 2.01 Å, Co—N distance = 2.11 Å). The β-diketonate ligands exhibit a *bent* coordination mode in which the angles between the planes defined by the Co and oxygen atoms and the carbon and oxygen atoms of the β-diketonate ligand are 18.9° and 24.7°. In contrast, in *trans*-[*M*(hfac)$_2$(py-CH=CH—C_6F_4Br)$_2$] (*M* = Co, Cu) the β-diketonate ligands exhibit a *planar* coordination mode (Aäkeroy *et al.*, 2007). In addition, the phenyl ring is twisted with respect to the pyridylimine unit by 17.6° and is similar to the angle observed in [Ni(dbm)$_2$(ppa^X)] [*X* = Me, 22.9°; Cl, 24.0° (Harding, Harding, Tinpun *et al.*, 2010)].

The packing in the structure of (I) involves a weak π–π interaction between the pyridyl and phenyl rings of neighbouring ppa^{Br} ligands as shown in Fig. 2 (*Cg*1···*Cg*2 = 3.928 (2) Å where *Cg*1 and *Cg*2 are the centroids of the rings C1—C6 and C8—C12—N2). A further weak interaction occurs between the Br atom on the ppa^{Br} ligand and the β-diketonate ligand creating discrete dimers within the structure [Br···C20, 3.531 (2) Å, see Fig. 3]. These dimers are then connected *via* the π–π interaction mentioned above resulting in one-dimensional chains. A similar interaction is also observed in the structure of *trans*-[*M*(hfac)$_2$(py-CH=CH—C_6F_4Br)$_2$] (Aäkeroy *et al.*, 2007). Interestingly, the corresponding Ni analogue, [Ni(hfac)$_2$(ppa^{Br})] has a completely different set of interactions with Br···CH interactions clearly evident (Harding, Harding, Sophonrat & Adams, 2010), once again highlighting the difficulties involved in attempting to use specific interactions in the design of supramolecular networks.

Experimental

To an orange red solution of $[Co(hfac)_2(H_2O)_2]$ (0.127 g, 0.25 mmol) in CH_2Cl_2 (5 cm^3) was added a solution of ppa^{Br} (0.065 g, 0.25 mmol) in CH_2Cl_2 (3 cm^3). The deep orange solution was stirred for 1 h and then concentrated *in vacuo*. *n*-Hexane (15 cm^3) was added to precipitate an orange solid which was washed with *n*-hexane (2 *x* 5 cm^3) and dried *in vacuo*: yield 0.142 g (77%). IR in KBr disc $\nu_{C=O}$ 1647 cm^{-1}. UV-Vis (in CH_2Cl_2, log ε $mol.dm^{-3}cm^{-1}$) 243 (4.24), 309 (4.42). $C_{22}H_{11}O_4N_2F_{12}BrCo$; calc. C 36.0, H 1.5, N 3.8%; found C 36.5, H 1.5, N 3.8%.

Refinement

Hydrogen atoms were placed geometrically and refined using a riding model with C–H = 0.95 Å and U_{iso} constrained to be 1.2 times U_{eq} of the carrier atom.

Figures

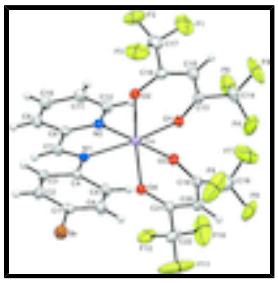

Fig. 1. The molecular structure of (I) showing the atom-labelling scheme. Displacement ellipsoids are drawn at the 50% probability level.

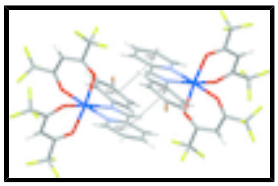

Fig. 2. The molecular packing in (I) showing the π–π interactions between the phenyl and pyridyl rings of the ppa^{Br} ligand. Only selected atoms are labelled for clarity. [Symmetry code: (i) -*x* + 2, -*y*, -*z* + 2].

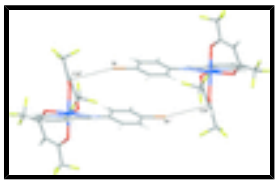

Fig. 3. The molecular packing in (I) showing the Br···β-diketonate interactions of the discrete dimers. Only selected atoms are labelled for clarity. [Symmetry code: (i) -*x* + 1, -*y* + 1, -*z* + 2].

[(4-Bromophenyl)(2-pyridylmethylidene)amine- κ^2N,N']bis(1,1,1,5,5,5-hexafluoropentane-2,4-dionato-κ^2O,O')cobalt(II)

Crystal data

$[Co(C_5HF_6O_2)_2(C_{12}H_9BrN_2)]$	$Z = 2$
$M_r = 734.17$	$F(000) = 718$
Triclinic, $P\overline{1}$	$D_x = 1.921$ Mg m^{-3}

Hall symbol: -P 1	Mo $K\alpha$ radiation, $\lambda = 0.71073$ Å
$a = 8.3568$ (2) Å	Cell parameters from 9953 reflections
$b = 10.9420$ (2) Å	$\theta = 2.9$–$32.8°$
$c = 14.8151$ (3) Å	$\mu = 2.37$ mm^{-1}
$\alpha = 74.042$ (1)°	$T = 150$ K
$\beta = 86.510$ (1)°	Plate, orange
$\gamma = 77.080$ (1)°	0.60 × 0.30 × 0.03 mm
$V = 1269.51$ (5) Å^3	

Data collection

Bruker SMART CCD area-detector diffractometer	5176 independent reflections
Radiation source: fine-focus sealed tube	4508 reflections with $I > 2\sigma(I)$
graphite	$R_{int} = 0.021$
φ and ω scans	$\theta_{max} = 26.4°$, $\theta_{min} = 2.0°$
Absorption correction: multi-scan (*SADABS*; Bruker, 1997)	$h = -10 \rightarrow 10$
$T_{min} = 0.330$, $T_{max} = 0.932$	$k = -13 \rightarrow 13$
21525 measured reflections	$l = -18 \rightarrow 18$

Refinement

Refinement on F^2	Primary atom site location: structure-invariant direct methods
Least-squares matrix: full	Secondary atom site location: difference Fourier map
$R[F^2 > 2\sigma(F^2)] = 0.035$	Hydrogen site location: inferred from neighbouring sites
$wR(F^2) = 0.090$	H-atom parameters constrained
$S = 1.08$	$w = 1/[\sigma^2(F_o^2) + (0.0399P)^2 + 2.417P]$ where $P = (F_o^2 + 2F_c^2)/3$
5176 reflections	$(\Delta/\sigma)_{max} = 0.001$
379 parameters	$\Delta\rho_{max} = 1.23$ e Å^{-3}
0 restraints	$\Delta\rho_{min} = -0.91$ e Å^{-3}

Special details

Geometry. All e.s.d.'s (except the e.s.d. in the dihedral angle between two l.s. planes) are estimated using the full covariance matrix. The cell e.s.d.'s are taken into account individually in the estimation of e.s.d.'s in distances, angles and torsion angles; correlations between e.s.d.'s in cell parameters are only used when they are defined by crystal symmetry. An approximate (isotropic) treatment of cell e.s.d.'s is used for estimating e.s.d.'s involving l.s. planes.

Refinement. Refinement of F^2 against ALL reflections. The weighted *R*-factor *wR* and goodness of fit *S* are based on F^2, conventional *R*-factors *R* are based on *F*, with *F* set to zero for negative F^2. The threshold expression of $F^2 > \sigma(F^2)$ is used only for calculating *R*-factors(gt) *etc*. and is not relevant to the choice of reflections for refinement. *R*-factors based on F^2 are statistically about twice as large as those based on *F*, and *R*- factors based on ALL data will be even larger.

Fractional atomic coordinates and isotropic or equivalent isotropic displacement parameters (Å^2)

	x	*y*	*z*	U_{iso}*/U_{eq}
Br1	0.24966 (4)	0.40512 (3)	1.12788 (2)	0.02627 (10)
C1	0.4059 (3)	0.3017 (3)	1.0652 (2)	0.0190 (6)
C2	0.4540 (4)	0.1698 (3)	1.1069 (2)	0.0234 (6)
H2	0.4096	0.1318	1.1659	0.028*
C3	0.5671 (4)	0.0937 (3)	1.0621 (2)	0.0220 (6)
H3	0.6002	0.0028	1.0903	0.026*
C4	0.6331 (3)	0.1491 (3)	0.97587 (19)	0.0165 (5)
C5	0.5813 (3)	0.2824 (3)	0.93439 (19)	0.0198 (6)
H5	0.6237	0.3208	0.8750	0.024*
C6	0.4680 (4)	0.3591 (3)	0.9796 (2)	0.0218 (6)
H6	0.4337	0.4500	0.9519	0.026*
C7	0.8328 (3)	−0.0354 (3)	0.96759 (19)	0.0182 (5)
H7	0.8186	−0.0694	1.0331	0.022*
C8	0.9486 (3)	−0.1115 (3)	0.91526 (19)	0.0172 (5)
C9	1.0341 (4)	−0.2363 (3)	0.9576 (2)	0.0221 (6)
H9	1.0201	−0.2753	1.0225	0.027*
C10	1.1404 (4)	−0.3031 (3)	0.9032 (2)	0.0240 (6)
H10	1.1991	−0.3896	0.9301	0.029*
C11	1.1601 (4)	−0.2431 (3)	0.8099 (2)	0.0242 (6)
H11	1.2336	−0.2869	0.7718	0.029*
C12	1.0707 (4)	−0.1171 (3)	0.7723 (2)	0.0217 (6)
H12	1.0847	−0.0757	0.7078	0.026*
C13	0.8228 (4)	0.1729 (3)	0.5708 (2)	0.0215 (6)
C14	0.9068 (4)	0.2216 (3)	0.4767 (2)	0.0322 (7)
C15	0.6657 (4)	0.1503 (3)	0.5689 (2)	0.0258 (6)
H15	0.6125	0.1698	0.5102	0.031*
C16	0.5849 (4)	0.0998 (3)	0.6508 (2)	0.0246 (6)
C17	0.4252 (4)	0.0581 (4)	0.6393 (2)	0.0361 (8)
C18	0.7556 (4)	0.4215 (3)	0.6922 (2)	0.0223 (6)
C19	0.6383 (5)	0.5432 (3)	0.6348 (3)	0.0414 (9)
C20	0.9177 (4)	0.4284 (3)	0.7033 (2)	0.0231 (6)
H20	0.9542	0.5051	0.6707	0.028*
C21	1.0267 (4)	0.3261 (3)	0.7608 (2)	0.0203 (6)
C22	1.1961 (4)	0.3521 (3)	0.7732 (3)	0.0330 (8)
Co1	0.82077 (4)	0.13568 (3)	0.77538 (2)	0.01482 (10)
F1	0.3604 (3)	0.1057 (3)	0.55597 (18)	0.0696 (8)
F2	0.4576 (3)	−0.0730 (2)	0.65283 (19)	0.0578 (7)
F3	0.3172 (3)	0.0779 (3)	0.70502 (19)	0.0578 (7)
F4	0.9544 (4)	0.3293 (3)	0.47281 (18)	0.0768 (10)
F5	0.8123 (3)	0.2441 (3)	0.40289 (14)	0.0636 (8)
F6	1.0401 (3)	0.1358 (2)	0.46507 (15)	0.0508 (6)
F7	0.5963 (6)	0.5260 (3)	0.5585 (3)	0.130 (2)
F8	0.5029 (3)	0.5703 (2)	0.6848 (3)	0.0862 (11)
F9	0.6978 (3)	0.64976 (19)	0.61453 (18)	0.0505 (6)
F10	1.2729 (3)	0.3815 (4)	0.6912 (2)	0.0974 (13)

F11	1.1845 (4)	0.4500 (3)	0.8083 (3)	0.1054 (15)
F12	1.2953 (2)	0.25146 (19)	0.82617 (16)	0.0406 (5)
N1	0.7503 (3)	0.0775 (2)	0.92465 (16)	0.0159 (5)
N2	0.9660 (3)	−0.0524 (2)	0.82359 (16)	0.0171 (5)
O1	0.9099 (2)	0.15687 (19)	0.64017 (13)	0.0195 (4)
O2	0.6285 (2)	0.07571 (19)	0.73472 (14)	0.0207 (4)
O3	0.6895 (2)	0.32603 (18)	0.72450 (13)	0.0194 (4)
O4	1.0045 (2)	0.21558 (18)	0.80721 (13)	0.0192 (4)

Atomic displacement parameters (Å^2)

	U^{11}	U^{22}	U^{33}	U^{12}	U^{13}	U^{23}
Br1	0.02487 (16)	0.02549 (16)	0.02822 (17)	−0.00312 (12)	0.00920 (12)	−0.01065 (12)
C1	0.0152 (13)	0.0234 (14)	0.0211 (14)	−0.0036 (11)	0.0022 (11)	−0.0116 (11)
C2	0.0295 (16)	0.0212 (14)	0.0213 (14)	−0.0111 (12)	0.0086 (12)	−0.0061 (12)
C3	0.0280 (15)	0.0158 (13)	0.0219 (14)	−0.0066 (12)	0.0031 (12)	−0.0036 (11)
C4	0.0159 (13)	0.0189 (13)	0.0166 (13)	−0.0056 (11)	−0.0007 (10)	−0.0061 (10)
C5	0.0201 (14)	0.0212 (14)	0.0152 (13)	−0.0026 (11)	0.0008 (11)	−0.0021 (11)
C6	0.0222 (14)	0.0179 (13)	0.0214 (14)	0.0010 (11)	−0.0018 (11)	−0.0026 (11)
C7	0.0207 (14)	0.0194 (13)	0.0140 (13)	−0.0048 (11)	−0.0011 (11)	−0.0032 (10)
C8	0.0172 (13)	0.0169 (13)	0.0179 (13)	−0.0040 (11)	−0.0035 (10)	−0.0044 (10)
C9	0.0240 (15)	0.0202 (14)	0.0192 (14)	−0.0010 (12)	−0.0058 (11)	−0.0026 (11)
C10	0.0232 (15)	0.0190 (13)	0.0269 (15)	0.0036 (12)	−0.0074 (12)	−0.0063 (12)
C11	0.0207 (14)	0.0244 (14)	0.0270 (15)	0.0004 (12)	−0.0010 (12)	−0.0102 (12)
C12	0.0224 (14)	0.0227 (14)	0.0195 (14)	−0.0036 (12)	−0.0001 (11)	−0.0057 (11)
C13	0.0279 (15)	0.0176 (13)	0.0181 (14)	−0.0028 (12)	0.0005 (12)	−0.0050 (11)
C14	0.0380 (19)	0.0381 (18)	0.0193 (15)	−0.0089 (15)	0.0039 (13)	−0.0058 (13)
C15	0.0278 (16)	0.0287 (15)	0.0206 (15)	−0.0050 (13)	−0.0044 (12)	−0.0060 (12)
C16	0.0245 (15)	0.0239 (14)	0.0269 (16)	−0.0075 (12)	−0.0044 (12)	−0.0065 (12)
C17	0.0330 (18)	0.050 (2)	0.0322 (18)	−0.0197 (16)	−0.0029 (15)	−0.0127 (16)
C18	0.0281 (16)	0.0191 (14)	0.0175 (14)	−0.0024 (12)	−0.0025 (12)	−0.0030 (11)
C19	0.041 (2)	0.0228 (16)	0.054 (2)	−0.0067 (15)	−0.0224 (18)	0.0045 (16)
C20	0.0279 (15)	0.0195 (14)	0.0218 (14)	−0.0095 (12)	0.0018 (12)	−0.0025 (11)
C21	0.0216 (14)	0.0208 (14)	0.0206 (14)	−0.0074 (11)	0.0005 (11)	−0.0069 (11)
C22	0.0295 (17)	0.0220 (15)	0.048 (2)	−0.0120 (14)	−0.0081 (15)	−0.0028 (14)
Co1	0.01588 (19)	0.01408 (18)	0.01382 (18)	−0.00367 (14)	−0.00033 (14)	−0.00219 (14)
F1	0.0544 (16)	0.104 (2)	0.0513 (15)	−0.0445 (16)	−0.0281 (12)	0.0049 (14)
F2	0.0614 (16)	0.0504 (14)	0.0774 (18)	−0.0309 (12)	0.0001 (13)	−0.0281 (13)
F3	0.0297 (11)	0.0890 (19)	0.0739 (17)	−0.0283 (12)	0.0120 (11)	−0.0436 (15)
F4	0.141 (3)	0.0613 (16)	0.0414 (14)	−0.0620 (18)	0.0404 (16)	−0.0119 (12)
F5	0.0408 (13)	0.118 (2)	0.0176 (10)	−0.0071 (14)	−0.0015 (9)	−0.0019 (12)
F6	0.0361 (12)	0.0704 (16)	0.0345 (12)	0.0019 (11)	0.0130 (9)	−0.0088 (11)
F7	0.238 (5)	0.0398 (15)	0.102 (3)	0.010 (2)	−0.137 (3)	−0.0037 (16)
F8	0.0272 (13)	0.0385 (14)	0.159 (3)	0.0060 (11)	0.0007 (16)	0.0188 (17)
F9	0.0464 (13)	0.0239 (10)	0.0674 (16)	−0.0076 (9)	−0.0113 (11)	0.0128 (10)
F10	0.0476 (16)	0.158 (3)	0.0688 (19)	−0.062 (2)	−0.0036 (14)	0.031 (2)
F11	0.0547 (17)	0.0586 (17)	0.230 (4)	0.0108 (14)	−0.065 (2)	−0.088 (2)
F12	0.0260 (10)	0.0309 (10)	0.0644 (14)	−0.0070 (8)	−0.0163 (10)	−0.0077 (10)

N1	0.0160 (11)	0.0154 (11)	0.0174 (11)	−0.0043 (9)	−0.0008 (9)	−0.0055 (9)
N2	0.0179 (11)	0.0164 (11)	0.0174 (11)	−0.0047 (9)	−0.0002 (9)	−0.0040 (9)
O1	0.0210 (10)	0.0214 (10)	0.0155 (9)	−0.0057 (8)	0.0001 (8)	−0.0031 (8)
O2	0.0224 (10)	0.0206 (10)	0.0195 (10)	−0.0090 (8)	−0.0007 (8)	−0.0025 (8)
O3	0.0192 (10)	0.0179 (9)	0.0194 (10)	−0.0035 (8)	−0.0010 (8)	−0.0026 (8)
O4	0.0209 (10)	0.0181 (9)	0.0190 (10)	−0.0064 (8)	−0.0022 (8)	−0.0031 (8)

Geometric parameters (Å, °)

Br1—C1	1.902 (3)	C14—F6	1.322 (4)
C1—C6	1.378 (4)	C14—F5	1.322 (4)
C1—C2	1.382 (4)	C15—C16	1.391 (4)
C2—C3	1.379 (4)	C15—H15	0.9500
C2—H2	0.9500	C16—O2	1.256 (4)
C3—C4	1.394 (4)	C16—C17	1.537 (4)
C3—H3	0.9500	C17—F1	1.300 (4)
C4—C5	1.397 (4)	C17—F3	1.316 (4)
C4—N1	1.429 (3)	C17—F2	1.358 (4)
C5—C6	1.388 (4)	C18—O3	1.255 (4)
C5—H5	0.9500	C18—C20	1.396 (4)
C6—H6	0.9500	C18—C19	1.534 (4)
C7—N1	1.284 (4)	C19—F7	1.278 (5)
C7—C8	1.461 (4)	C19—F9	1.321 (4)
C7—H7	0.9500	C19—F8	1.336 (5)
C8—N2	1.349 (4)	C20—C21	1.387 (4)
C8—C9	1.384 (4)	C20—H20	0.9500
C9—C10	1.385 (4)	C21—O4	1.264 (3)
C9—H9	0.9500	C21—C22	1.537 (4)
C10—C11	1.375 (4)	C22—F11	1.296 (4)
C10—H10	0.9500	C22—F12	1.308 (4)
C11—C12	1.392 (4)	C22—F10	1.332 (5)
C11—H11	0.9500	Co1—O2	2.0452 (19)
C12—N2	1.335 (4)	Co1—O4	2.0639 (19)
C12—H12	0.9500	Co1—O1	2.0644 (19)
C13—O1	1.246 (3)	Co1—O3	2.0796 (19)
C13—C15	1.392 (4)	Co1—N2	2.098 (2)
C13—C14	1.537 (4)	Co1—N1	2.209 (2)
C14—F4	1.312 (4)		
C6—C1—C2	121.5 (3)	F1—C17—F2	104.7 (3)
C6—C1—Br1	119.8 (2)	F3—C17—F2	103.7 (3)
C2—C1—Br1	118.7 (2)	F1—C17—C16	114.6 (3)
C3—C2—C1	119.3 (3)	F3—C17—C16	112.2 (3)
C3—C2—H2	120.4	F2—C17—C16	109.1 (3)
C1—C2—H2	120.4	O3—C18—C20	128.0 (3)
C2—C3—C4	120.5 (3)	O3—C18—C19	113.7 (3)
C2—C3—H3	119.7	C20—C18—C19	118.3 (3)
C4—C3—H3	119.7	F7—C19—F9	108.7 (4)
C3—C4—C5	119.2 (3)	F7—C19—F8	108.4 (4)
C3—C4—N1	124.2 (2)	F9—C19—F8	104.6 (3)

C5—C4—N1	116.6 (2)	F7—C19—C18	111.1 (3)
C6—C5—C4	120.3 (3)	F9—C19—C18	114.0 (3)
C6—C5—H5	119.9	F8—C19—C18	109.6 (3)
C4—C5—H5	119.9	C21—C20—C18	121.5 (3)
C1—C6—C5	119.2 (3)	C21—C20—H20	119.3
C1—C6—H6	120.4	C18—C20—H20	119.3
C5—C6—H6	120.4	O4—C21—C20	129.1 (3)
N1—C7—C8	119.7 (2)	O4—C21—C22	115.2 (3)
N1—C7—H7	120.1	C20—C21—C22	115.7 (3)
C8—C7—H7	120.1	F11—C22—F12	108.3 (3)
N2—C8—C9	122.5 (3)	F11—C22—F10	106.4 (4)
N2—C8—C7	115.7 (2)	F12—C22—F10	105.6 (3)
C9—C8—C7	121.7 (3)	F11—C22—C21	111.6 (3)
C10—C9—C8	118.5 (3)	F12—C22—C21	113.1 (3)
C10—C9—H9	120.7	F10—C22—C21	111.3 (3)
C8—C9—H9	120.7	O2—Co1—O4	173.89 (8)
C11—C10—C9	119.3 (3)	O2—Co1—O1	87.88 (8)
C11—C10—H10	120.3	O4—Co1—O1	89.87 (8)
C9—C10—H10	120.3	O2—Co1—O3	87.74 (8)
C10—C11—C12	119.0 (3)	O4—Co1—O3	86.41 (8)
C10—C11—H11	120.5	O1—Co1—O3	85.05 (8)
C12—C11—H11	120.5	O2—Co1—N2	94.96 (8)
N2—C12—C11	122.3 (3)	O4—Co1—N2	90.82 (8)
N2—C12—H12	118.9	O1—Co1—N2	92.91 (8)
C11—C12—H12	118.9	O3—Co1—N2	176.56 (8)
O1—C13—C15	128.6 (3)	O2—Co1—N1	91.80 (8)
O1—C13—C14	113.3 (3)	O4—Co1—N1	91.41 (8)
C15—C13—C14	118.1 (3)	O1—Co1—N1	169.94 (8)
F4—C14—F6	106.5 (3)	O3—Co1—N1	104.98 (8)
F4—C14—F5	107.8 (3)	N2—Co1—N1	77.10 (9)
F6—C14—F5	106.3 (3)	C7—N1—C4	119.2 (2)
F4—C14—C13	111.0 (3)	C7—N1—Co1	111.94 (18)
F6—C14—C13	111.4 (3)	C4—N1—Co1	128.79 (17)
F5—C14—C13	113.5 (3)	C12—N2—C8	118.4 (2)
C16—C15—C13	121.6 (3)	C12—N2—Co1	126.20 (19)
C16—C15—H15	119.2	C8—N2—Co1	115.41 (18)
C13—C15—H15	119.2	C13—O1—Co1	123.71 (19)
O2—C16—C15	129.1 (3)	C16—O2—Co1	123.95 (19)
O2—C16—C17	114.0 (3)	C18—O3—Co1	123.68 (19)
C15—C16—C17	116.7 (3)	C21—O4—Co1	122.51 (18)
F1—C17—F3	111.6 (3)		
C6—C1—C2—C3	0.2 (4)	C5—C4—N1—C7	162.6 (3)
Br1—C1—C2—C3	179.9 (2)	C3—C4—N1—Co1	163.1 (2)
C1—C2—C3—C4	0.4 (4)	C5—C4—N1—Co1	−15.6 (3)
C2—C3—C4—C5	−1.1 (4)	O2—Co1—N1—C7	97.18 (19)
C2—C3—C4—N1	−179.8 (3)	O4—Co1—N1—C7	−88.02 (19)
C3—C4—C5—C6	1.4 (4)	O1—Co1—N1—C7	9.2 (6)
N1—C4—C5—C6	−179.8 (2)	O3—Co1—N1—C7	−174.68 (18)
C2—C1—C6—C5	0.1 (4)	N2—Co1—N1—C7	2.50 (18)

Br1—C1—C6—C5	−179.7 (2)	O2—Co1—N1—C4	−84.5 (2)
C4—C5—C6—C1	−0.9 (4)	O4—Co1—N1—C4	90.3 (2)
N1—C7—C8—N2	3.1 (4)	O1—Co1—N1—C4	−172.5 (4)
N1—C7—C8—C9	−176.7 (3)	O3—Co1—N1—C4	3.6 (2)
N2—C8—C9—C10	−0.5 (4)	N2—Co1—N1—C4	−179.2 (2)
C7—C8—C9—C10	179.2 (3)	C11—C12—N2—C8	0.8 (4)
C8—C9—C10—C11	1.2 (4)	C11—C12—N2—Co1	−178.8 (2)
C9—C10—C11—C12	−0.9 (4)	C9—C8—N2—C12	−0.5 (4)
C10—C11—C12—N2	−0.2 (4)	C7—C8—N2—C12	179.8 (2)
O1—C13—C14—F4	−55.7 (4)	C9—C8—N2—Co1	179.2 (2)
C15—C13—C14—F4	125.5 (3)	C7—C8—N2—Co1	−0.6 (3)
O1—C13—C14—F6	62.7 (4)	O2—Co1—N2—C12	88.0 (2)
C15—C13—C14—F6	−116.0 (3)	O4—Co1—N2—C12	−90.1 (2)
O1—C13—C14—F5	−177.3 (3)	O1—Co1—N2—C12	−0.2 (2)
C15—C13—C14—F5	3.9 (4)	N1—Co1—N2—C12	178.7 (2)
O1—C13—C15—C16	−2.0 (5)	O2—Co1—N2—C8	−91.62 (19)
C14—C13—C15—C16	176.6 (3)	O4—Co1—N2—C8	90.35 (19)
C13—C15—C16—O2	5.1 (5)	O1—Co1—N2—C8	−179.74 (19)
C13—C15—C16—C17	−170.3 (3)	N1—Co1—N2—C8	−0.91 (18)
O2—C16—C17—F1	166.4 (3)	C15—C13—O1—Co1	−16.6 (4)
C15—C16—C17—F1	−17.5 (5)	C14—C13—O1—Co1	164.79 (19)
O2—C16—C17—F3	37.7 (4)	O2—Co1—O1—C13	23.0 (2)
C15—C16—C17—F3	−146.2 (3)	O4—Co1—O1—C13	−151.3 (2)
O2—C16—C17—F2	−76.6 (4)	O3—Co1—O1—C13	−64.9 (2)
C15—C16—C17—F2	99.4 (3)	N2—Co1—O1—C13	117.9 (2)
O3—C18—C19—F7	−67.9 (5)	N1—Co1—O1—C13	111.4 (5)
C20—C18—C19—F7	112.6 (4)	C15—C16—O2—Co1	11.3 (4)
O3—C18—C19—F9	168.8 (3)	C17—C16—O2—Co1	−173.2 (2)
C20—C18—C19—F9	−10.7 (5)	O1—Co1—O2—C16	−20.5 (2)
O3—C18—C19—F8	51.9 (4)	O3—Co1—O2—C16	64.7 (2)
C20—C18—C19—F8	−127.5 (3)	N2—Co1—O2—C16	−113.2 (2)
O3—C18—C20—C21	−5.0 (5)	N1—Co1—O2—C16	169.6 (2)
C19—C18—C20—C21	174.4 (3)	C20—C18—O3—Co1	−16.7 (4)
C18—C20—C21—O4	2.5 (5)	C19—C18—O3—Co1	163.9 (2)
C18—C20—C21—C22	−174.7 (3)	O2—Co1—O3—C18	−150.4 (2)
O4—C21—C22—F11	−118.6 (4)	O4—Co1—O3—C18	27.8 (2)
C20—C21—C22—F11	59.0 (4)	O1—Co1—O3—C18	−62.3 (2)
O4—C21—C22—F12	3.9 (4)	N1—Co1—O3—C18	118.3 (2)
C20—C21—C22—F12	−178.4 (3)	C20—C21—O4—Co1	21.0 (4)
O4—C21—C22—F10	122.6 (3)	C22—C21—O4—Co1	−161.8 (2)
C20—C21—C22—F10	−59.7 (4)	O1—Co1—O4—C21	55.7 (2)
C8—C7—N1—C4	177.8 (2)	O3—Co1—O4—C21	−29.4 (2)
C8—C7—N1—Co1	−3.7 (3)	N2—Co1—O4—C21	148.6 (2)
C3—C4—N1—C7	−18.7 (4)	N1—Co1—O4—C21	−134.3 (2)

Fig. 1

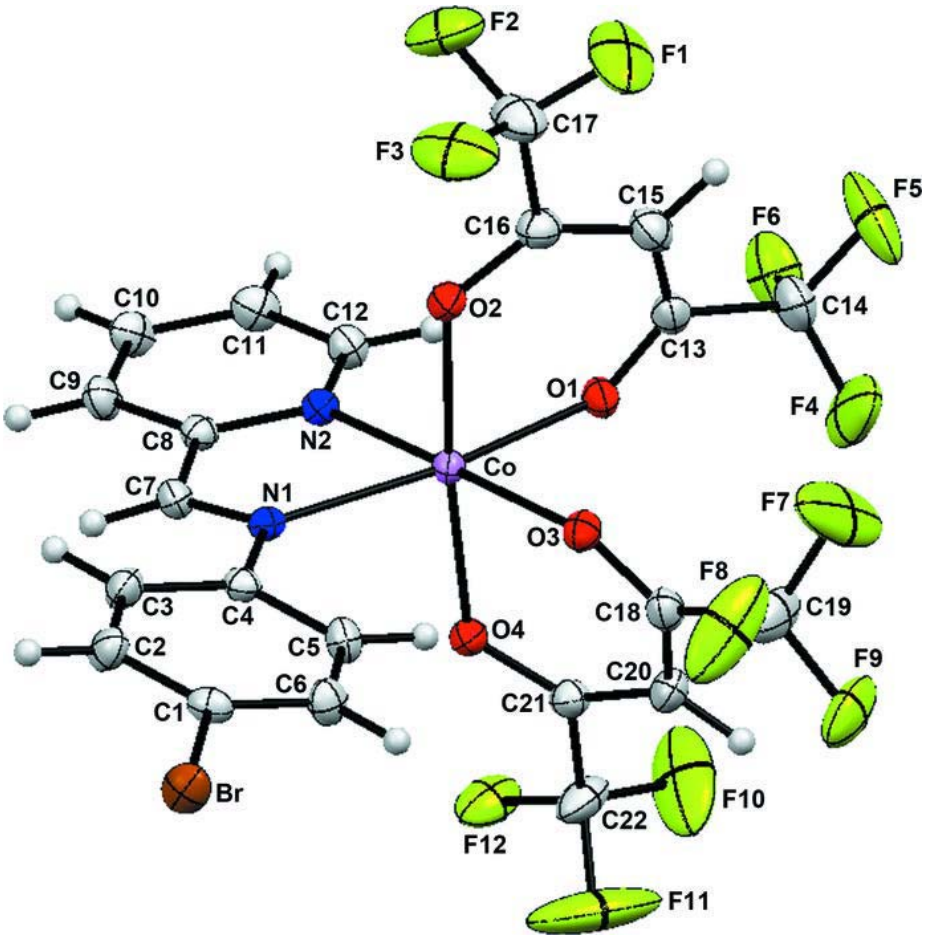

Fig. 2

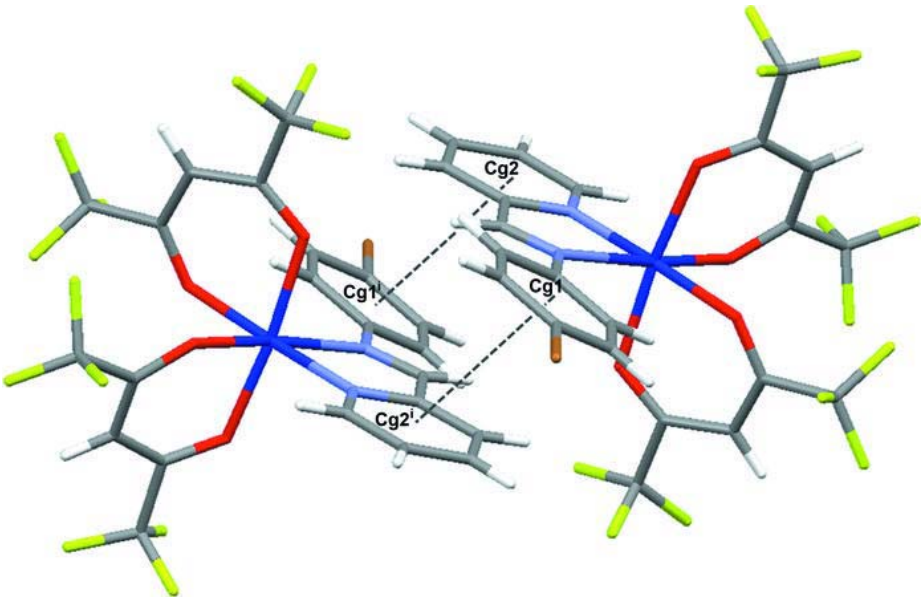

Fig. 3

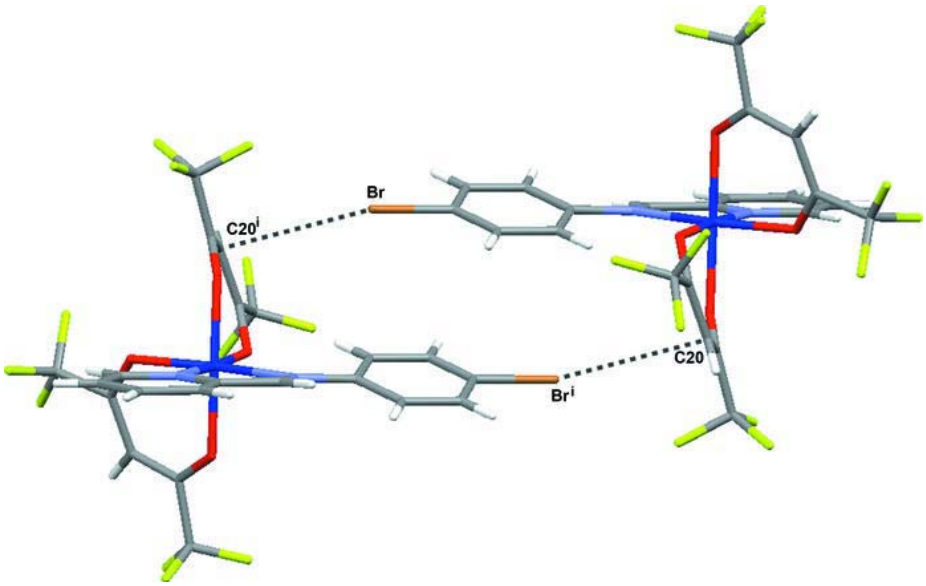

Appendix Three

Manuscript I

Acta Crystallographica Section E
Structure Reports
Online
ISSN 1600-5368
Editors: **W.T. A. Harrison, J. Simpson and M. Weil**

Bis(1,1,1,5,5,5-hexafluoropentane-2,4-dionato-κ^2-*O*,*O*′)[(4-bromophenyl)pyridin-2-ylmethylene amine–κ^2-*N*,*N*′]nickel(II)

Phimphaka Harding, David J. Harding, Nitisastr Soponrat and Harry Adams

Category: *metal-organic compounds*

Co-editor:
David Billing
School of Chemistry, University of the Witwatersrand, Private Bag 3, PO Wits, Johannesburg 2050, South Africa
Telephone: 27(11)717659
Fax: 27(11)7176749
Email: dave.billing@wits.ac.za

Contact author:
Assistant Phimphaka Harding
Thailand
Telephone: ++66-75-672100
Fax: ++66-75-672004
Email: kphimpha@wu.ac.th

checkCIF/PLATON results for paper zb2010

checkCIF/PLATON results
Ellipsoid plot

checkCIF/PLATON results

```
No syntax errors found.      CIF dictionary      Interpreting this report
Bond precision:    C-C = 0.0065 A   Wavelength=0.71073
Cell: a=31.251(8)  b=10.006(3)  c=17.653(5)
      alpha=90  beta=103.952(5)  gamma=90
Temperature: 150 K

                       Calculated                Reported
Volume                 5357(3)                   5358(2)
Space group            C 2/c                     C2/c
Hall group             -C 2yc                    -C2yc
Moiety formula         C22 H11 Br F12 N2 Ni O4   C22 H11 Br F12 N2 Ni O4
Sum formula            C22 H11 Br F12 N2 Ni O4   C22 H11 Br F12 N2 Ni O4
Mr                     733.92                    733.95
Dx,g cm-3              1.820                     1.820
Z                      8                         8
Mu (mm-1)              2.332                     2.332
F000                   2880.0                    2880.0
F000'                  2882.74
h,k,lmax               40,12,22                  40,12,22
Nref                   6149                      5988
Tmin,Tmax              0.722,0.774               0.628,0.784
Tmin'                  0.593

Correction method= MULTI-SCAN
Data completeness= 0.974
Theta(max)= 27.500
R(reflections)= 0.0542(  3422) wR2(reflections)= 0.1322(  5988)
S = 0.909 Npar= 379
```

Alert level C

```
RINTA01_ALERT_3_C  The value of Rint is greater than 0.12
           Rint given   0.145
PLAT213_ALERT_2_C Atom F5              has ADP max/min Ratio .....       3.10 prola
PLAT230_ALERT_2_C Hirshfeld Test Diff for    C5     --  C6      ..       5.48 su
PLAT230_ALERT_2_C Hirshfeld Test Diff for    C7     --  C8      ..       6.28 su
PLAT242_ALERT_2_C Check Low       Ueq as Compared to Neighbors for        C14
PLAT242_ALERT_2_C Check Low       Ueq as Compared to Neighbors for        C17
PLAT242_ALERT_2_C Check Low       Ueq as Compared to Neighbors for        C19
PLAT341_ALERT_3_C Low Bond Precision on  C-C Bonds (x 1000) Ang ..         7
PLAT601_ALERT_2_C Structure Contains Solvent Accessible VOIDS of .      42.00 A   3
PLAT911_ALERT_3_C Missing # FCF Refl Between THmin & STh/L=  0.600        83
PLAT912_ALERT_4_C Missing # of FCF Reflections Above STh/L=  0.600        77
```

```
   0 ALERT level A = In general: serious problem
   0 ALERT level B = Potentially serious problem
  11 ALERT level C = Check and explain
```

```
0 ALERT level G = General alerts; check

0 ALERT type 1 CIF construction/syntax error, inconsistent or missing data
7 ALERT type 2 Indicator that the structure model may be wrong or deficient
3 ALERT type 3 Indicator that the structure quality may be low
1 ALERT type 4 Improvement, methodology, query or suggestion
0 ALERT type 5 Informative message, check
```

---

database duplication summary

- **Chemical name =**
- *R* factor = 0.054
- Space group = C2/c
- Formula = C22 H11 Br F12 N2 Ni O4
- a=31.251 b=10.006 c=17.653
- alpha=90 beta=103.952 gamma=90

No duplication found.

Datablock I - ellipsoid plot

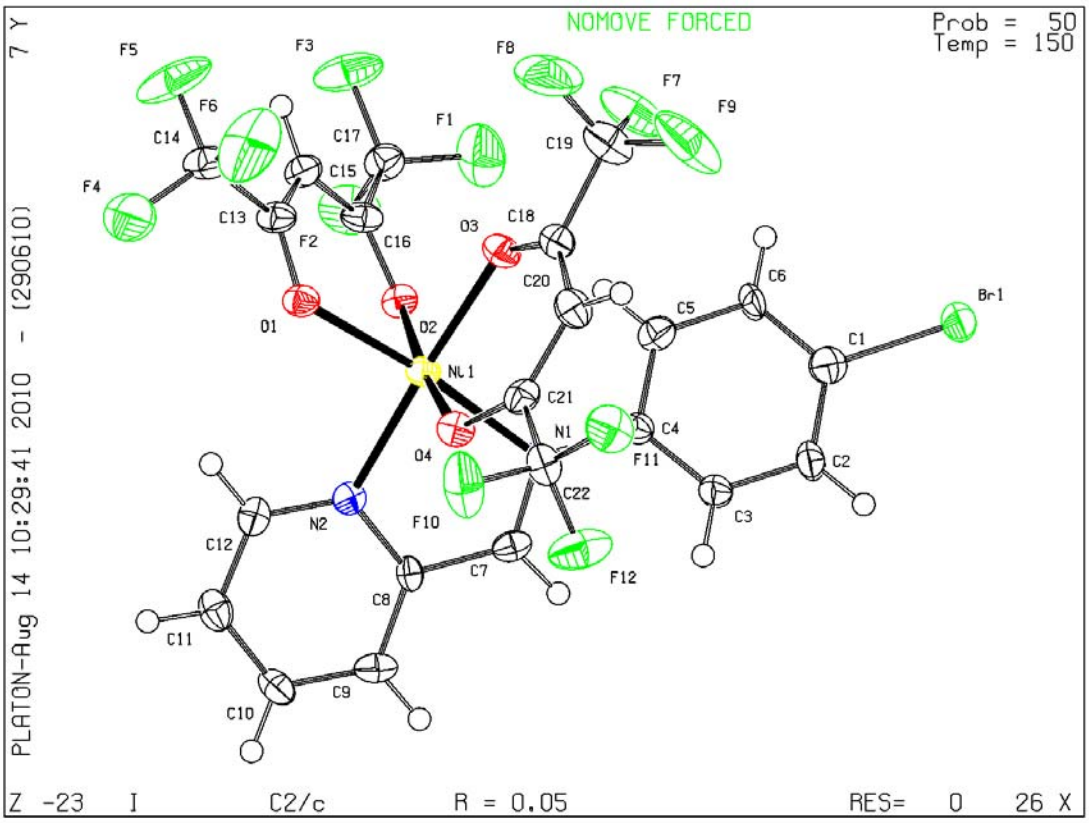

Submitted to *Acta Cryst. E*

Bis(1,1,1,5,5,5-hexafluoropentane-2,4-dionato-κ^2-*O*,*O*′)[(4-bromo-phenyl)pyridin-2-ylmethylene amine–κ^2-*N*,*N*']nickel(II)

Phimphaka Harding*,[a] David J. Harding,[a] Nitisastr Soponrat[b] and Harry Adams[c]

[a]Molecular Technology Research Unit, Department of Chemistry, Walailak University, Thasala, Nakhon Si Thammarat, 80161, THAILAND, [b]Department of Chemistry, Faculty of Science, Taksin University, Songkhla, 90000, THAILAND, and [c]Department of Chemistry, Faculty of Science, University of Sheffield, Brook Hill, Sheffield, S3 7HF, UK

Correspondence email: **kphimpha@wu.ac.th**

Abstract

[Ni(hfac)$_2$(ppa^{Br})] **1** crystallizes in the space group *C*2/c and exhibits a *pseudo*-octahedral coordination geometry. The structure packs through C—H···Br interactions (H6···Br 3.015 Å, H2···Br 3.017 Å) forming a hydrogen bonding ladder and strong hydrogen bonding interactions between two of the oxygen atoms of the β-diketonate ligands and two hydrogen atoms on the pyridyl ring of the ppa^{Br} (O1···H12 2.532 Å, O4···H11 2.610 Å).

Related literature

For related literature see: Harding *et al.* (2010); Aäkeroy *et al*. (2004, 2005, 2007). For a general introduction to crystal engineering see: Braga *et al.*, (2002).

Computing details

Data collection: Bruker *SMART* (Bruker, 1997); cell refinement: Bruker *SMART*; data reduction: Bruker *SAINT* (Bruker, 1997); program(s) used to solve structure: *SHELXS97* (Sheldrick, 2008); program(s) used to refine structure: *SHELXL97* (Sheldrick, 2008); molecular graphics: Bruker *SHELXTL* (Bruker, 1997); software used to prepare material for publication: Bruker *SHELXTL*.

Bis(1,1,1,5,5,5-hexafluoropentane-2,4-dionato-κ^2-*O*,*O*′) [(4-bromo-phenyl)pyridin-2-ylmethylene amine-κ^2-*N*,*N*'] nickel(II)

Crystal data

$C_{22}H_{11}BrF_{12}N_2NiO_4$	V = 5358 (2) Å^3
M_r = 733.95	Z = 8
Monoclinic, *C*2/*c*	Mo *K*α radiation

a = 31.251 (8) Å	μ = 2.33 mm^{-1}
b = 10.006 (3) Å	T = 150 K
c = 17.653 (5) Å	0.22 × 0.12 × 0.11 mm
β = 103.952 (5)°	

Data collection

CCD area detector diffractometer	5988 independent reflections
Absorption correction: multi-scan *SADABS* (Bruker, 1997)	3422 reflections with $I > 2\sigma(I)$
T_{min} = 0.628, T_{max} = 0.784	R_{int} = 0.145
27645 measured reflections	θ_{max} = 27.5°

Refinement

$R[F^2 > 2\sigma(F^2)]$ = 0.054	H-atom parameters constrained
$wR(F^2)$ = 0.132	$\Delta\rho_{max}$ = 1.24 e Å^{-3}
S = 0.91	$\Delta\rho_{min}$ = −1.12 e Å^{-3}
5988 reflections	Absolute structure: ?
379 parameters	Flack parameter: ?
0 restraints	Rogers parameter: ?

Table 1
Selected geometric parameters (Å)

Ni1—O3	2.020 (3)	Ni1—N2	2.063 (3)
Ni1—O4	2.044 (3)	Ni1—O1	2.066 (3)
Ni1—O2	2.045 (3)	Ni1—N1	2.113 (4)

Acknowledgements

We thank the Thailand Research Fund (Grant No.: RSA5080007) for funding this research.

References

Aäkeroy, C. B., Schultheiss, N., Desper, J. & Moore, C. (2007). *CrystEngComm*, **9**, 421–426.
Aäkeroy, C. B., Desper, J. & V.-Martínez, J., (2004). *CrystEngComm*, **6**, 413–418.
Aäkeroy, C. B., Schultheiss, N. & Desper, J. (2005). *Inorg. Chem.* **44**, 4983–4991.
Allen, F. H. (2002). *Acta Crsyt.*, **B58**, 380-388.
Braga, D., Desiraju, G. R., Miller, J. S., Orpen, A. G. & Price, S. L. (2002). *CrystEngComm*, **4**, 500–509.
Bruker (1997). *SMART*, *SAINT, SHELXTL* and *SADABS*. Bruker AXS Inc., Madison, Wisconsin, USA.
Cotton, F. A., Wilkinson, G., Murillo, C. A. & Bochmann, M. (1999). *Advanced Inorganic Chemistry*, 6th ed.; John Wiley&Sons: New York, pp. 479-482.
Chassot, P. & Emmenegger, F. (1996). *Inorg. Chem.* **35**, 5931–5934.
Emmenegger, F., Schlaepfer, C. W., Stoeckli-Evans, H., Piccand, M. & Piekarski, H. (2001). *Inorg. Chem.* **40**, 3884–3888.

Harding, P., Harding, D. J., Tinpun, K., Samuadnuan, S., Sophonrat, N. & Adams, H. (2010). *Aust. J. Chem.* **63**, 75–82.
Harding, P., Harding, D. J., Sophonrat, N. & Adams, H. (2010). Unpublished results.
Sheldrick, G. M. (2008). *Acta Cryst.* A**64**, 112–122.

Scheme 1

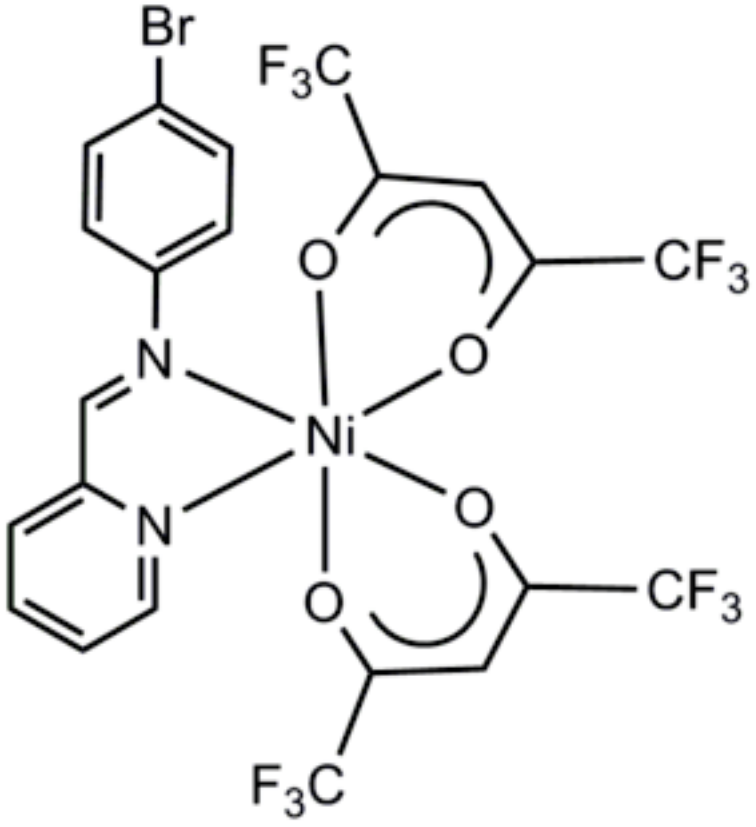

supplementary materials

Bis(1,1,1,5,5,5-hexafluoropentane-2,4-dionato-κ^2-*O*,*O*′)[(4-bromo-phenyl)pyridin-2-ylmethylene amine–κ^2-*N*,*N*']nickel(II)

Phimphaka Harding*,[a] David J. Harding,[a] Nitisastr Soponrat[b] and Harry Adams[c]

Comment

Metal β-diketonates represent an important class of complexes and are much studied owing to their ease of synthesis, ready modification and multiple applications (Cotton *et al.*, 1999). In the case of divalent metal ions, the [*M*(β-diketonate)$_2$] complexes are able to coordinate additional ligands forming either *cis*- or *trans*-octahedral metal complexes (Chassot & Emmenegger, 1996; Emmenegger *et al.*, 2001). Of particular relevence to this paper is the use metal β-diketonates complexes in the preparation of crystal engineered networks (Braga *et al.*, 2002) and while hydrogen bonded *trans*-isomers are well represented few compounds containing *cis*-isomers are described (Aäkeroy *et al.*, 2004, 2005, 2007). In this paper we describe the synthesis and structure of [Ni(hfac)$_2$(ppa^{Br})] (hfac = 1,1,1,5,5,5-hexafluoropentane-2,4-dionato; ppa^{Br} = (4-bromo-phenyl)pyridin-2-ylmethylene amine).

[Ni(hfac)$_2$(H$_2$O)$_2$] reacts readily with ppa^{Br} to give [Ni(hfac)$_2$(ppa^{Br})] **1** which recrystallizes from CH_2Cl_2/*n*-hexane to give yellow crystals in the space group *C*2/c (Figure 1). This contrasts markedly with the analogous cobalt compound which crystallizes in $P\bar{1}$ (Harding, Harding, Soponrat and Adams, 2010). The nickel metal centre is *pseudo*-octahedral with a *cis*-arrangement enforced by the chelating ppa^{Br} ligand. The Ni—O and Ni—N bond lengths are typical of values reported for other nickel hfac and diimine complexes reported in the CSD (mean Ni—O distance = 2.01 Å, Ni—N distance = 2.11 Å, Allen, 2002). The β-diketonate ligands exhibit a *bent* coordination mode in which the angles between the planes defined by the Ni and oxygen atoms and the carbon and oxygen atoms of the β-diketonate ligand are 11.0° and 26.8°. In contrast, in *trans*-[*M*(hfac)$_2$(py-CH=CH—C_6F_4Br)$_2$] (*M* = Co, Cu) the β-diketonate ligands exhibit a *planar* coordination mode (Aäkeroy *et al.*, 2007). In addition, the phenyl ring is twisted with to the pyridylimine unit by 30.0° a little greater than the angle observed in [Ni(dbm)$_2$(ppa^X)] (*X* = Me 22.9°, Cl 24.0°, Harding *et al.*, 2010).

The packing in the structure is composed of two sets of interactions. The first set is involves a series of C—H···Br interactions (H6···Br 3.015 (3) Å, H2···Br 3.017 (3) Å) forming a hydrogen bonding ladder (Figure 2). The second interaction involves a strong hydrogen bonding interactions between two of the oxygen atoms of the β-diketonate ligands and two hydrogen atoms on the pyridyl ring of the ppa^{Br} ligand (O1···H12 2.532 (4) Å, O4···H11 2.610 (3) Å) forming a dimer (Figure 3). In contrast, the cobalt analogue has extensive π···π interactions and interactions between the Br atom on the ppa^{Br} ligand and the β-diketonate ligand (Harding, Harding, Soponrat and Adams, 2010).

Experimental

To a green solution of [Ni(hfac)$_2$(H$_2$O)$_2$] (0.128 g, 0.25 mmol) in CH_2Cl_2 (10 ml) was added a solution of ppa^{Br} (0.065 g, 0.25 mmol) in CH_2Cl_2 (3 ml). The orange solution was stirred overnight then concentrated *in vacuo. n*-Hexane (10 ml) was added to precipitate a yellow brown solid which was washed with *n*-hexane (2 *x* 5 ml) and dried *in vacuo* yielding a deep

yellow solid (0.096 g, 52%). Found: C 36.2, H 1.7, N 3.9. Calc. for $C_{22}H_{11}BrF_{12}N_2NiO_4$: C 36.0, H 1.5, N 3.8%. *m*/*z* (ESI) 527 [*M*-hfac$^-$]$^+$. n_{max}(KBr)/cm^{-1} 1651 ($n_{C=O}$). l_{max}(CH_2Cl_2)/nm (log e/*M*$^{-1}$cm^{-1}) 319 (4.46), 342 (4.34).

Refinement

Hydrogen atoms were placed geometrically and refined with a riding model and with U_{iso} constrained to be 1.2 (aromatic CH) times U_{eq} of the carrier atom.

Figures

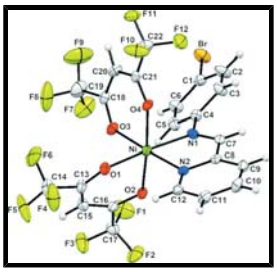

Fig. 1. The molecular structure of (**1**) showing the atom-labelling scheme. Displacement ellipsoids are drawn at the 50% probability level.

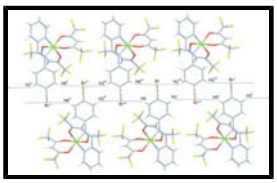

Fig. 2. The molecular packing in (**1**) showing the C—H···Br interactions between neighbouring ppa^{Br} ligands. Only selected atoms are labelled for clairty. [Symmetry codes: (i) *x*, -1 + *y*, *z*; (ii) *x*, 1 + *y*, *z*; (iii) 1/2 - *x*, 1/2 - *y*, -*z*; (iv) 1/2 - *x*, 3/2 - *y*, -*z*; (v) 1/2 - *x*, 5/2 - *y*, -*z*].

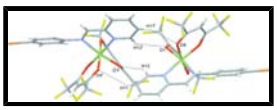

Fig. 3. The molecular packing in (**1**) showing the O···H interactions between the oxygen atoms of the β-diketonate ligands and the two hydrogen of the ppa^{Br} ligand. Only selected atoms are labelled for clairty. [Symmetry codes: (i) -*x*, *y*, 1/2 - *z*].

Bis(1,1,1,5,5,5-hexafluoropentane-2,4-dionato-κ^2-*O*,*O*′) [(4-bromo-phenyl)pyridin-2-ylmethylene amine-κ^2-*N*,*N*′] nickel(II)

Crystal data

$C_{22}H_{11}BrF_{12}N_2NiO_4$	$F(000)$ = 2880
M_r = 733.95	D_x = 1.820 Mg m^{-3}
Monoclinic, *C*2/*c*	Mo *K*α radiation, λ = 0.71073 Å
Hall symbol: -C2yc	Cell parameters from 3767 reflections
a = 31.251 (8) Å	θ = 2.4–24.9°
b = 10.006 (3) Å	μ = 2.33 mm^{-1}
c = 17.653 (5) Å	*T* = 150 K
β = 103.952 (5)°	Block, brown
V = 5358 (2) Å^3	0.22 × 0.12 × 0.11 mm
Z = 8	

Data collection

CCD area detector	5988 independent reflections

diffractometer

Radiation source: fine-focus sealed tube

graphite

Detector resolution: 100 pixels mm^{-1}

phi and ω scans

Absorption correction: multi-scan *SADABS* (Bruker, 1997)

T_{min} = 0.628, T_{max} = 0.784

27645 measured reflections

3422 reflections with $I > 2\sigma(I)$

R_{int} = 0.145

θ_{max} = 27.5°, θ_{min} = 1.3°

h = −39→40

k = −12→12

l = −22→22

Refinement

Refinement on F^2

Least-squares matrix: full

$R[F^2 > 2\sigma(F^2)]$ = 0.054

$wR(F^2)$ = 0.132

S = 0.91

5988 reflections

379 parameters

0 restraints

Primary atom site location: structure-invariant direct methods

Secondary atom site location: difference Fourier map

Hydrogen site location: inferred from neighbouring sites

H-atom parameters constrained

$w = 1/[\sigma^2(F_o^2) + (0.0546P)^2]$ where $P = (F_o^2 + 2F_c^2)/3$

$(\Delta/\sigma)_{max} < 0.001$

$\Delta\rho_{max}$ = 1.24 e $Å^{-3}$

$\Delta\rho_{min}$ = −1.12 e $Å^{-3}$

Special details

Geometry. All e.s.d.'s (except the e.s.d. in the dihedral angle between two l.s. planes) are estimated using the full covariance matrix. The cell e.s.d.'s are taken into account individually in the estimation of e.s.d.'s in distances, angles and torsion angles; correlations between e.s.d.'s in cell parameters are only used when they are defined by crystal symmetry. An approximate (isotropic) treatment of cell e.s.d.'s is used for estimating e.s.d.'s involving l.s. planes.

Refinement. Refinement of F^2 against ALL reflections. The weighted *R*-factor *wR* and goodness of fit *S* are based on F^2, conventional *R*-factors *R* are based on *F*, with *F* set to zero for negative F^2. The threshold expression of $F^2 > \sigma(F^2)$ is used only for calculating *R*-factors(gt) *etc*. and is not relevant to the choice of reflections for refinement. *R*-factors based on F^2 are statistically about twice as large as those based on *F*, and *R*- factors based on ALL data will be even larger.

Fractional atomic coordinates and isotropic or equivalent isotropic displacement parameters ($Å^2$)

	x	*y*	*z*	U_{iso}*/U_{eq}
Ni1	0.089498 (18)	0.60018 (5)	0.17271 (3)	0.01947 (16)
Br1	0.279804 (16)	0.50379 (5)	−0.01356 (3)	0.03493 (16)
N1	0.10544 (11)	0.4874 (3)	0.0821 (2)	0.0180 (8)
N2	0.03045 (12)	0.5037 (3)	0.1283 (2)	0.0193 (8)
O1	0.06741 (10)	0.7013 (3)	0.25796 (16)	0.0227 (7)
O2	0.07571 (10)	0.7678 (3)	0.10485 (16)	0.0206 (7)
O3	0.14882 (9)	0.6873 (3)	0.21444 (17)	0.0253 (7)
O4	0.10989 (9)	0.4413 (3)	0.24516 (16)	0.0215 (7)
C1	0.22491 (15)	0.4979 (4)	0.0144 (3)	0.0268 (11)

C2	0.20348 (15)	0.3757 (5)	0.0139 (3)	0.0318 (12)
H2	0.2157	0.2965	−0.0018	0.038*
C3	0.16424 (15)	0.3716 (4)	0.0365 (3)	0.0269 (11)
H3	0.1497	0.2885	0.0375	0.032*
C4	0.14579 (14)	0.4876 (4)	0.0578 (3)	0.0197 (10)
C5	0.16748 (15)	0.6093 (4)	0.0566 (3)	0.0257 (11)
H5	0.1549	0.6892	0.0707	0.031*
C6	0.20726 (14)	0.6144 (4)	0.0351 (3)	0.0236 (10)
H6	0.2221	0.6971	0.0347	0.028*
C7	0.07464 (14)	0.4036 (4)	0.0519 (3)	0.0222 (10)
H7	0.0788	0.3410	0.0139	0.027*
C8	0.03340 (13)	0.4058 (4)	0.0765 (2)	0.0168 (9)
C9	−0.00087 (15)	0.3178 (4)	0.0481 (3)	0.0255 (11)
H9	0.0019	0.2505	0.0116	0.031*
C10	−0.03943 (15)	0.3295 (4)	0.0736 (3)	0.0261 (11)
H10	−0.0632	0.2691	0.0560	0.031*
C11	−0.04250 (15)	0.4301 (5)	0.1249 (3)	0.0265 (11)
H11	−0.0687	0.4407	0.1426	0.032*
C12	−0.00710 (14)	0.5167 (4)	0.1508 (3)	0.0223 (10)
H12	−0.0098	0.5870	0.1855	0.027*
C13	0.07108 (15)	0.8261 (4)	0.2653 (2)	0.0236 (10)
C14	0.06750 (18)	0.8781 (5)	0.3451 (3)	0.0326 (12)
C15	0.07746 (15)	0.9195 (4)	0.2105 (3)	0.0249 (11)
H15	0.0810	1.0110	0.2250	0.030*
C16	0.07882 (15)	0.8822 (4)	0.1348 (3)	0.0241 (11)
C17	0.08415 (17)	0.9929 (4)	0.0773 (3)	0.0278 (11)
C18	0.18236 (15)	0.6331 (4)	0.2566 (3)	0.0227 (10)
C19	0.22211 (17)	0.7250 (6)	0.2750 (3)	0.0410 (14)
C20	0.18587 (15)	0.5046 (4)	0.2881 (3)	0.0281 (11)
H20	0.2140	0.4740	0.3162	0.034*
C21	0.14966 (15)	0.4192 (4)	0.2797 (3)	0.0232 (10)
C22	0.15671 (15)	0.2806 (5)	0.3172 (3)	0.0286 (11)
F1	0.11909 (12)	0.9686 (3)	0.0484 (2)	0.0590 (10)
F2	0.04965 (11)	0.9967 (3)	0.01655 (16)	0.0474 (9)
F3	0.08890 (12)	1.1150 (3)	0.10758 (16)	0.0516 (9)
F4	0.03084 (12)	0.8339 (3)	0.3627 (2)	0.0651 (10)
F5	0.06729 (15)	1.0080 (3)	0.35147 (18)	0.0703 (12)
F6	0.09967 (13)	0.8311 (4)	0.40128 (18)	0.0775 (13)
F7	0.22453 (10)	0.8019 (3)	0.2159 (2)	0.0584 (10)
F8	0.21997 (13)	0.8058 (4)	0.3339 (2)	0.0789 (13)
F9	0.26008 (10)	0.6604 (4)	0.2971 (3)	0.0827 (14)
F10	0.13059 (10)	0.2608 (3)	0.3655 (2)	0.0540 (9)
F11	0.19792 (9)	0.2582 (3)	0.35786 (17)	0.0395 (8)
F12	0.14753 (11)	0.1857 (3)	0.26264 (18)	0.0522 (9)

Atomic displacement parameters (Å^2)

	U^{11}	U^{22}	U^{33}	U^{12}	U^{13}	U^{23}

Ni1	0.0209 (3)	0.0193 (3)	0.0168 (3)	−0.0020 (2)	0.0019 (2)	−0.0002 (2)
Br1	0.0284 (3)	0.0261 (3)	0.0550 (4)	−0.0007 (2)	0.0192 (3)	−0.0007 (2)
N1	0.0176 (19)	0.0186 (19)	0.020 (2)	0.0011 (15)	0.0087 (16)	0.0019 (15)
N2	0.019 (2)	0.0198 (18)	0.0171 (19)	0.0022 (15)	0.0002 (16)	0.0014 (15)
O1	0.0265 (17)	0.0234 (17)	0.0181 (16)	−0.0041 (13)	0.0051 (14)	−0.0022 (13)
O2	0.0269 (17)	0.0229 (16)	0.0123 (15)	−0.0012 (13)	0.0052 (14)	0.0002 (12)
O3	0.0202 (17)	0.0289 (17)	0.0248 (17)	−0.0049 (14)	0.0014 (15)	−0.0015 (14)
O4	0.0239 (17)	0.0250 (16)	0.0134 (15)	−0.0003 (13)	0.0001 (14)	0.0030 (13)
C1	0.023 (3)	0.026 (2)	0.028 (3)	0.003 (2)	0.000 (2)	0.001 (2)
C2	0.021 (3)	0.025 (3)	0.055 (4)	0.002 (2)	0.019 (2)	0.000 (2)
C3	0.024 (3)	0.018 (2)	0.041 (3)	−0.0019 (18)	0.013 (2)	0.000 (2)
C4	0.020 (2)	0.020 (2)	0.019 (2)	−0.0013 (18)	0.005 (2)	0.0001 (18)
C5	0.031 (3)	0.023 (2)	0.024 (2)	0.000 (2)	0.008 (2)	−0.002 (2)
C6	0.019 (2)	0.025 (2)	0.032 (3)	−0.0018 (19)	0.016 (2)	0.002 (2)
C7	0.028 (3)	0.016 (2)	0.019 (2)	0.0015 (19)	0.000 (2)	0.0013 (18)
C8	0.016 (2)	0.021 (2)	0.014 (2)	0.0027 (18)	0.0062 (18)	0.0056 (18)
C9	0.030 (3)	0.019 (2)	0.023 (2)	−0.0042 (19)	−0.001 (2)	−0.0012 (19)
C10	0.020 (3)	0.035 (3)	0.023 (3)	−0.008 (2)	0.005 (2)	−0.001 (2)
C11	0.023 (3)	0.038 (3)	0.020 (2)	−0.001 (2)	0.007 (2)	0.002 (2)
C12	0.022 (3)	0.027 (2)	0.017 (2)	0.0056 (19)	0.003 (2)	0.0011 (18)
C13	0.029 (3)	0.024 (2)	0.017 (2)	−0.005 (2)	0.003 (2)	−0.0033 (19)
C14	0.049 (3)	0.027 (3)	0.024 (3)	−0.012 (2)	0.012 (3)	−0.005 (2)
C15	0.031 (3)	0.020 (2)	0.025 (3)	−0.0018 (19)	0.009 (2)	−0.0032 (19)
C16	0.025 (3)	0.019 (2)	0.023 (2)	−0.0035 (18)	−0.003 (2)	0.0025 (19)
C17	0.034 (3)	0.024 (2)	0.026 (3)	−0.001 (2)	0.009 (2)	0.001 (2)
C18	0.025 (3)	0.029 (3)	0.015 (2)	−0.005 (2)	0.007 (2)	−0.0012 (19)
C19	0.030 (3)	0.044 (3)	0.046 (4)	−0.011 (3)	0.003 (3)	0.005 (3)
C20	0.020 (2)	0.034 (3)	0.027 (3)	0.001 (2)	0.000 (2)	0.002 (2)
C21	0.026 (3)	0.026 (2)	0.016 (2)	0.002 (2)	0.002 (2)	−0.0045 (19)
C22	0.023 (3)	0.033 (3)	0.030 (3)	0.001 (2)	0.008 (2)	0.003 (2)
F1	0.064 (2)	0.051 (2)	0.075 (3)	0.0070 (17)	0.042 (2)	0.0280 (18)
F2	0.059 (2)	0.0475 (19)	0.0271 (16)	−0.0053 (15)	−0.0060 (16)	0.0152 (14)
F3	0.100 (3)	0.0219 (15)	0.0304 (17)	−0.0123 (16)	0.0116 (18)	0.0018 (13)
F4	0.077 (3)	0.076 (2)	0.058 (2)	−0.030 (2)	0.045 (2)	−0.0352 (19)
F5	0.158 (4)	0.0290 (18)	0.0383 (19)	−0.0167 (19)	0.052 (2)	−0.0129 (14)
F6	0.086 (3)	0.113 (3)	0.0216 (17)	0.031 (2)	−0.0094 (19)	−0.0215 (19)
F7	0.050 (2)	0.066 (2)	0.056 (2)	−0.0321 (17)	0.0068 (18)	0.0199 (18)
F8	0.081 (3)	0.090 (3)	0.069 (3)	−0.051 (2)	0.022 (2)	−0.045 (2)
F9	0.0247 (18)	0.076 (3)	0.136 (4)	−0.0113 (18)	−0.004 (2)	0.041 (3)
F10	0.046 (2)	0.054 (2)	0.072 (2)	0.0198 (15)	0.0331 (19)	0.0345 (17)
F11	0.0330 (16)	0.0378 (16)	0.0419 (18)	0.0070 (13)	−0.0021 (15)	0.0108 (13)
F12	0.068 (2)	0.0274 (16)	0.050 (2)	0.0015 (15)	−0.0074 (18)	−0.0033 (15)

Geometric parameters (Å, °)

Ni1—O3	2.020 (3)	C9—H9	0.9500
Ni1—O4	2.044 (3)	C10—C11	1.372 (6)
Ni1—O2	2.045 (3)	C10—H10	0.9500
Ni1—N2	2.063 (3)	C11—C12	1.393 (6)

Ni1—O1	2.066 (3)	C11—H11	0.9500
Ni1—N1	2.113 (4)	C12—H12	0.9500
Br1—C1	1.897 (5)	C13—C15	1.394 (6)
N1—C7	1.291 (5)	C13—C14	1.531 (7)
N1—C4	1.426 (6)	C14—F5	1.304 (5)
N2—C12	1.332 (6)	C14—F6	1.317 (6)
N2—C8	1.358 (5)	C14—F4	1.332 (6)
O1—C13	1.258 (5)	C15—C16	1.399 (6)
O2—C16	1.255 (5)	C15—H15	0.9500
O3—C18	1.253 (5)	C16—C17	1.538 (6)
O4—C21	1.265 (5)	C17—F2	1.326 (5)
C1—C6	1.376 (6)	C17—F3	1.327 (5)
C1—C2	1.393 (6)	C17—F1	1.334 (6)
C2—C3	1.379 (6)	C18—C20	1.394 (6)
C2—H2	0.9500	C18—C19	1.517 (7)
C3—C4	1.388 (6)	C19—F7	1.313 (6)
C3—H3	0.9500	C19—F9	1.325 (6)
C4—C5	1.396 (6)	C19—F8	1.331 (7)
C5—C6	1.386 (6)	C20—C21	1.397 (6)
C5—H5	0.9500	C20—H20	0.9500
C6—H6	0.9500	C21—C22	1.529 (6)
C7—C8	1.456 (6)	C22—F10	1.330 (6)
C7—H7	0.9500	C22—F12	1.333 (5)
C8—C9	1.384 (6)	C22—F11	1.333 (5)
C9—C10	1.390 (7)		
O3—Ni1—O4	89.27 (12)	C11—C10—C9	118.7 (4)
O3—Ni1—O2	84.55 (12)	C11—C10—H10	120.7
O4—Ni1—O2	173.82 (12)	C9—C10—H10	120.7
O3—Ni1—N2	177.27 (13)	C10—C11—C12	119.8 (5)
O4—Ni1—N2	89.36 (12)	C10—C11—H11	120.1
O2—Ni1—N2	96.80 (12)	C12—C11—H11	120.1
O3—Ni1—O1	87.79 (12)	N2—C12—C11	121.9 (4)
O4—Ni1—O1	91.93 (12)	N2—C12—H12	119.1
O2—Ni1—O1	87.99 (12)	C11—C12—H12	119.1
N2—Ni1—O1	94.62 (13)	O1—C13—C15	128.3 (4)
O3—Ni1—N1	98.24 (13)	O1—C13—C14	114.1 (4)
O4—Ni1—N1	87.91 (12)	C15—C13—C14	117.7 (4)
O2—Ni1—N1	92.82 (12)	F5—C14—F6	108.1 (4)
N2—Ni1—N1	79.35 (14)	F5—C14—F4	106.8 (5)
O1—Ni1—N1	173.97 (13)	F6—C14—F4	104.4 (4)
C7—N1—C4	120.1 (4)	F5—C14—C13	114.9 (4)
C7—N1—Ni1	111.8 (3)	F6—C14—C13	111.0 (4)
C4—N1—Ni1	127.9 (3)	F4—C14—C13	111.0 (4)
C12—N2—C8	118.6 (4)	C13—C15—C16	121.8 (4)
C12—N2—Ni1	127.8 (3)	C13—C15—H15	119.1
C8—N2—Ni1	113.2 (3)	C16—C15—H15	119.1
C13—O1—Ni1	121.6 (3)	O2—C16—C15	129.0 (4)
C16—O2—Ni1	121.2 (3)	O2—C16—C17	112.9 (4)
C18—O3—Ni1	126.3 (3)	C15—C16—C17	118.1 (4)

C21—O4—Ni1	124.0 (3)	F2—C17—F3	106.8 (4)
C6—C1—C2	121.5 (5)	F2—C17—F1	106.0 (4)
C6—C1—Br1	119.2 (3)	F3—C17—F1	107.4 (4)
C2—C1—Br1	119.2 (3)	F2—C17—C16	111.0 (4)
C3—C2—C1	118.9 (4)	F3—C17—C16	114.7 (4)
C3—C2—H2	120.5	F1—C17—C16	110.5 (4)
C1—C2—H2	120.5	O3—C18—C20	127.6 (4)
C2—C3—C4	120.7 (4)	O3—C18—C19	112.9 (4)
C2—C3—H3	119.7	C20—C18—C19	119.5 (4)
C4—C3—H3	119.7	F7—C19—F9	107.5 (5)
C3—C4—C5	119.4 (4)	F7—C19—F8	106.8 (5)
C3—C4—N1	122.4 (4)	F9—C19—F8	106.1 (5)
C5—C4—N1	118.2 (4)	F7—C19—C18	112.7 (4)
C6—C5—C4	120.5 (4)	F9—C19—C18	113.3 (4)
C6—C5—H5	119.8	F8—C19—C18	110.0 (5)
C4—C5—H5	119.8	C18—C20—C21	122.6 (4)
C1—C6—C5	119.0 (4)	C18—C20—H20	118.7
C1—C6—H6	120.5	C21—C20—H20	118.7
C5—C6—H6	120.5	O4—C21—C20	128.4 (4)
N1—C7—C8	119.5 (4)	O4—C21—C22	112.9 (4)
N1—C7—H7	120.3	C20—C21—C22	118.7 (4)
C8—C7—H7	120.3	F10—C22—F12	107.4 (4)
N2—C8—C9	122.1 (4)	F10—C22—F11	107.0 (4)
N2—C8—C7	114.9 (4)	F12—C22—F11	106.3 (4)
C9—C8—C7	123.0 (4)	F10—C22—C21	111.5 (4)
C8—C9—C10	119.0 (4)	F12—C22—C21	110.5 (4)
C8—C9—H9	120.5	F11—C22—C21	113.9 (4)
C10—C9—H9	120.5		

Fig. 1

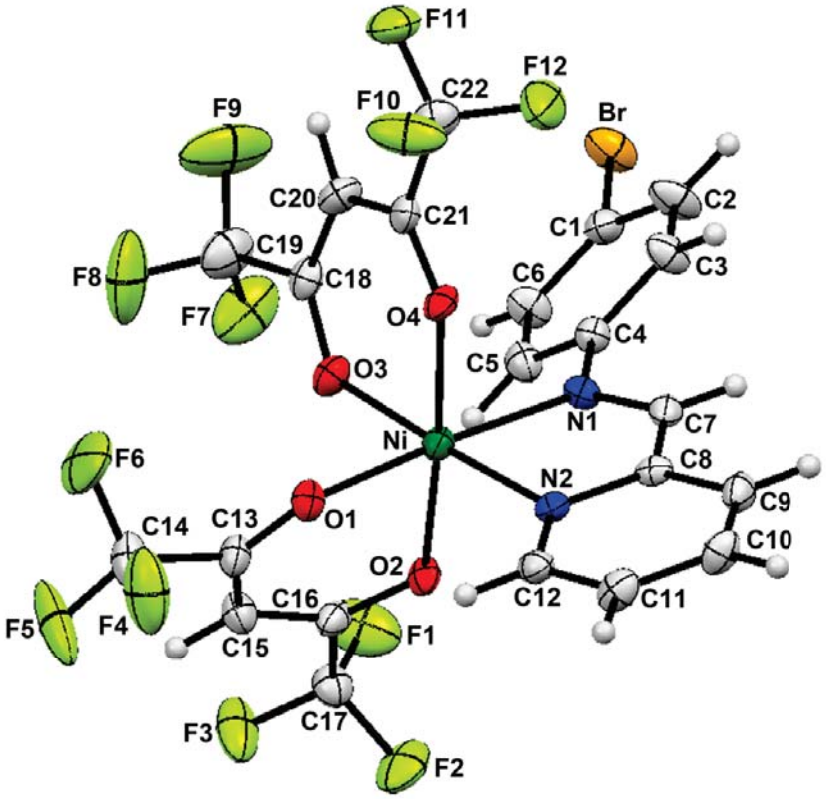
F11
F12
C22
F10
F9
Br
C20
C21
C2
C1
C19
C3
F8
C18
C6
F7
O4
C4
O3
C5
N1
C7
Ni
F6
C8
N2
C9
C14
C13
O1
C10
O2
C12
C11
C16
F5
F4
F1
C15
C17
F3
F2

Fig. 2

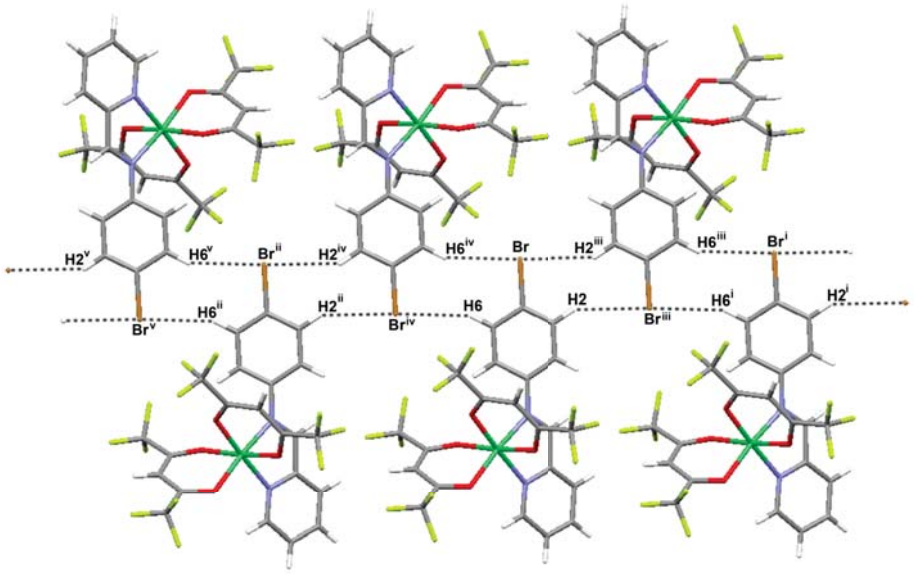
H2v
H6v
Brii
H2iv
H6iv
Br
H2iii
H6iii
Bri
Brv
H6ii
H2ii
Briv
H6
H2
Briii
H6i
H2i

Fig. 3

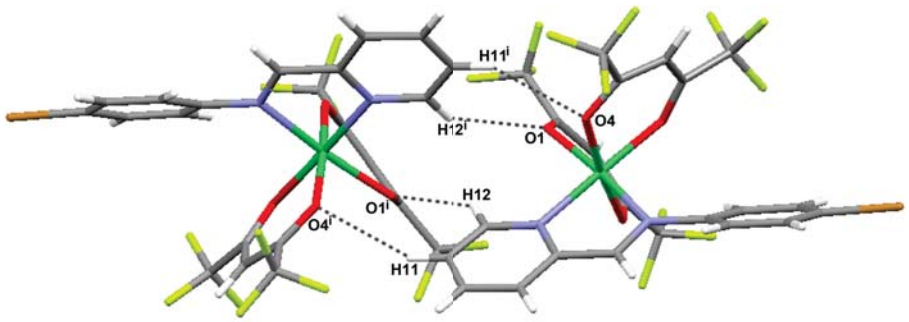

Appendix Four

Manuscript II

Redox Coupled-Spin Crossover in Cobalt β-Diketonate Complexes: Observation of the High Spin Co^{III} Intermediate

*Phimphaka Harding,**[a] *David J. Harding,**[a] *Rattawat Daengngern,*[a] *Theeraphol Thurakitsaree,*[b] *Brian M. Schutte,*[c] *Michael J. Shaw*[c] and *Yuthana Tantirungrotechai*[d]

Molecular Technology Research Unit, School of Science, Walailak University, Thasala, Nakhon Si Thammarat, 80161, Thailand.

E-mail: kphimpha@wu.ac.th or hdavid@wu.ac.th

RECEIVED DATE (to be automatically inserted after your manuscript is accepted if required according to the journal that you are submitting your paper to)

TITLE RUNNING HEAD 'Redox-Coupled Spin Crossover in $[Co(\beta\text{-diketonate})_2(N\text{-}N)]^{0/+}$ Complexes'

[a] Molecular Technology Research Unit, School of Science, Walailak University, Thasala, Nakhon Si Thammarat, 80161, Thailand, [b] Department of Physics, Faculty of Science, Chiang Mai University, Chiang Mai, 50200, Thailand, [c] Box 1652, Department of Chemistry, Southern Illinois University Edwardsville, IL, USA, [d] National Nanotechnology Center, National Science and Development Agency, Pathumthani, 12120, Thailand

ABSTRACT

Electrochemical, spectroelectrochemical, magnetic and spectroscopic properties are reported for the octahedral cobalt β-diketonate complexes, $[Co(\beta\text{-diketonate})_2(N\text{-}N)]$ {β-diketonate = 2,2,6,6-tetramethylheptane-3,5-dionate (tmhd); N-N = 1,10-phenanthroline (phen) **1**, 2,2′-bipyridine (2,2′-bpy) **2** and dimethylaminoethylamine (dmae) **3**; β-diketonate = 1,3-diphenylpropane-1,3-dionate (dbm); N-N =

phen **4**, 2,2′-bpy **5**, dmae **6**}. Cyclic voltammetry of **1**-**6** reveals an irreversible one-electron oxidation to Co^{III} with large peak separations between the oxidation and reduction peaks, indicative of redox coupled-spin crossover (RCSCO); i.e. [Co(β-diketonate)$_2$(N-N)] (S = 3/2) ↔ [Co(β-diketonate)$_2$(N-N)]$^+$ + e^- (S = 0). Notably, the high spin Co^{III} intermediate has been observed electrochemically for the *first time*. Moreover, the complexes represent rare examples of RCSCO species with a CoO_4N_2 coordination sphere. The tmhd complexes are more easily oxidized than the respective dbm analogues with the oxidation peak potentials in the order bipy < phen < dmae. Oxidation of **1**-**6** with $AgBF_4$ yields the corresponding Co^{III} cations, [Co(β-diketonate)$_2$(N-N)]BF_4 **1**$^+$-**6**$^+$ which has been confirmed by ^{1}H NMR spectroscopy. Spectroelectrochemistry of the redox pairs [Co(β-diketonate)$_2$(N-N)]$^{0/+}$ is consistent with the isolated compounds being identical to the species formed at the electrode. Theoretical studies reveal that the SOMO is essentially metal *d*-orbital and β-diketonate based, consistent with the strong effect of the β-diketonate ligand on the oxidation potential. In addition, there are substantial changes in the relative stabilities of the various spin states compared with [Co(tacn)$_2$]$^{2+/3+}$ such that the high spin states become more accessible. The above results are consistent with a square scheme mechanism in which oxidation and reduction proceeds through high spin Co^{III} and low spin Co^{II} intermediates, respectively.

Introduction

Spin crossover is one of the most interesting and widely studied phenomena of transition metal complexes in part due to the possible applications of such complexes in fields such as molecular electronics, memory storage and display devices.[1-4] In principle, a coordination complex with any electron configuration from d^4-d^7 may exhibit spin crossover but the most extensively studied systems are those of d^6 Fe^{II}.[5-14] In addition, in most reported cases the iron center is surrounded by six nitrogen donors as this provides the intermediate ligand field required for spin crossover (e.g. [Fe(phen)$_2$(NCS)$_2$]).[15] Unlike Fe^{II}, spin crossover in cobalt(II) complexes is rather rare with [Co(bipy)$_3$]$^{2+}$ and [Co(terpy)$_2$]$^{2+}$ as perhaps the best known examples.[16-19]

While spin crossover systems have been widely studied, comparatively little attention has been given to reactions in which the spin crossover is coupled to electron transfer. This situation is surprising given that reactions in which electron transfer is accompanied by a change in spin state are widespread in both chemistry and biology.[2-4,20-23] For instance in cytochrome P450, substrate binding produces a change in spin state of the Fe^{III} heme active site thereby shifting the redox potential and triggering an electron transfer which initiates the catalytic cycle of the enzyme.[24,25] Further examples include the iron-molybdenum cofactor of nitrogenase and cytochrome *c* peroxidases.[26-28] In relation to coordination chemistry the oxidation of high spin (HS) Co^{II} to low spin (LS) Co^{III} is a well known example of redox

coupled-spin crossover (RCSCO).[29] As with the spin crossover complexes discussed earlier most complexes exhibiting RCSCO have N_6 coordination environments. Furthermore, although the mechanism of such reactions has been debated for many years it is still unclear whether the reaction proceeds in a concerted fashion or via higher energy spin state intermediates.[30-37] However, recently Schultz and co-workers have shown that the reduction of $[Co(tacn)_2]^{3+}$ (tacn = 1,4,7-triazacyclononane) appears to proceed through a high spin Co^{III} intermediate.[38-40]

In this paper we report the synthesis of a series of octahedral cobalt β-diketonate complexes, [Co(β-diketonate)$_2$(N-N)] {β-diketonate = 2,2,6,6-tetramethylheptane-3,5-dionate (tmhd); N-N = 1,10-phenanthroline (phen) **1**, 2,2′-bipyridine (2,2′-bpy) **2** and dimethylaminoethylamine (dmae) **3**; β-diketonate = 1,3-diphenylpropane-1,3-dionate (dbm); N-N = phen **4**, 2,2′-bpy **5**, dmae **6**} which are shown to undergo redox coupled-spin crossover. Oxidation of these complexes yields the low spin d^6 Co^{III} cations $[Co(\beta\text{-diketonate})_2(N\text{-}N)]^+$. Electrochemical studies show the presence of the HS Co^{III} intermediate, a first for any RCSCO system. Moreover, unusually for redox coupled-spin crossover species the complexes possess a CoN_2O_4 coordination sphere rather than the more common CoN_6 coordination environment. Finally, through computational studies we attempt to rationalize the observed behavior in these complexes.

Results and Discussion

Synthesis of [Co(β-diketonate)$_2$(N-N)]. Reaction of $[Co(tmhd)_2(H_2O)_2]$ or $[Co(dbm)_2(H_2O)_2]$ (tmhd = 2,2,6,6-tetramethylheptane-3,5-dionate, dbm = 1,3-diphenylpropane-1,3-dionate) and N-N donor ligands in THF or CH_2Cl_2 yields the Co^{II} complexes [Co(β-diketonate)$_2$(N-N)] {β-diketonate = tmhd; N-N = 1,10-phenanthroline (phen) **1**, 2,2′-bipyridine (2,2′-bpy) **2** and dimethylaminoethylamine (dmae) **3**; β-diketonate = dbm; N-N = phen **4**, 2,2′-bpy **5**, dmae **6**; Scheme 1}. The complexes are orange and air stable. IR spectroscopy of **1**-**6** shows the ν_{CO} band between 1583 and 1595 cm^{-1} indicating that the β-diketonate ligands adopt a chelating coordination mode (Table 1).[41] Similar bands have been observed in the related Ni analogues which are observed between 1582 and 1595 cm^{-1}.[42] The two dmae complexes, **3** and **6**, also exhibit ν_{NH} bands at 3362 and 3365 cm^{-1}, respectively, and are again almost identical with those of their Ni counterparts. Magnetic susceptibility measurements indicate that the complexes are paramagnetic with μ_{eff} between 4.41 and 5.03 BM consistent with high spin Co^{II}.[43]

UV-Vis spectroscopy of the compounds in CH_2Cl_2 supports an octahedral Co^{II} coordination environment with a low intensity band at *ca*. 570 nm which by comparison with $[Co(hfac)_2(tmeda)]$ (hfac = hexafluoroacetylacetonate) is assigned to an overlap between the $^4T_{1g}$ (F) → $^4T_{2g}$ (P) and $^4T_{1g}$ (F) → $^4A_{2g}$ (F) transitions.[44] Additional, very intense bands are found in the UV region which are

ascribed to ligand centered $\pi \rightarrow \pi^*$ transitions.[45] Similar bands are observed for other [Co(β-diketonate)$_2$(N-N)] (β-diketonate = acac, hfac; N-N = en, 2,2′-bipy, phen) complexes.[46,47]

Synthesis of [Co(β-diketonate)$_2$(N-N)]$^+$. The peak potentials from the electrochemical studies suggested that oxidation of the neutral complexes could be achieved with Ag^+ (*vide infra*). Thus, addition of one equivalent of $AgBF_4$ to the isolated Co^{II} species affords the cationic complexes [Co(tmhd)$_2$(N-N)][BF_4] (N-N = phen **1**$^+$, 2,2′-bpy **2**$^+$ and dmae **3**$^+$) and [Co(dbm)$_2$(N-N)][BF_4] (N-N = phen **4**$^+$, 2,2′-bpy **5**$^+$ and dmae **6**$^+$) as green-brown or purple compounds (Table 3). They may also be prepared in a stepwise, one pot reaction from [Co(β-diketonate)$_2$(H_2O)$_2$] followed by addition of the appropriate ligand and subsequent addition of $AgBF_4$ giving **1**$^+$-**6**$^+$. The ν_{CO} of **1**$^+$-**6**$^+$ shift to lower wavenumbers by *ca.* 40 or 70 cm^{-1} for the tmhd and dbm complexes respectively. Related [Co(acac)$_2$(N-N)]$^+$ (N-N = 2,2′-bpy, en) complexes show ν_{CO} bands at 1524 and 1528 cm^{-1} confirming that the Co^{III} complexes have been formed.[48-50]

The cationic complexes despite their different colors exhibit very similar electronic spectra to **1**-**6** with a band at *ca.* 550 nm which by comparison with [Co(acac)$_2$(N-N)]$^+$ (N-N = en, bipy, phen) is assigned to the $^1A_{1g}$ (F) $\rightarrow$ $^1T_{1g}$ transition.[48-50] As with the neutral complexes additional charge transfer transitions are evident below 350 nm. The band at *ca.* 290 nm for **1**$^+$, **2**$^+$, **4**$^+$ and **5**$^+$, is assigned to an MLCT transition while the other bands are assigned to β-diketonate $\pi \rightarrow \pi^*$ transitions.[48]

NMR Spectroscopy. The ^{1}H NMR spectra of **1**$^+$-**6**$^+$ show sharp, readily identifiable peaks consistent with a low spin d^6 electron configuration (Table 3). The ^{1}H NMR spectra of **1**$^+$, **2**$^+$, **4**$^+$ and **5**$^+$ show signals in the aromatic region consistent with the presence of coordinated phen and bipy ligands and are assigned on the basis of coupling constants, integration values and comparison with the related [Co(acac)$_2$(N-N)]$^+$ (N- N = bipy and phen) complexes.[48, 49] As expected we observe a single resonance for the central β-diketonate proton indicating that the β-diketonate ligands are magnetically equivalent. In the case of **1**$^+$ and **2**$^+$ there are two singlets between 1.32-0.80 ppm for the *t*-butyl groups. The phenyl protons for the dbm ligands in **4**$^+$ and **5**$^+$ are observed between 6.97-8.04 ppm as a series of multiplets.

The dmae complexes show more complex spectra as a result of the asymmetry of the dmae ligand. This is most clearly evidenced by the presence of two singlets for the β-diketonate hydrogen confirming the magnetic inequivalence of the β-diketonate ligands. Moreover, in the case of **3**$^+$ there are three resonances for the *t*-butyl groups integrating in a ratio of 2:1:1 indicating that two of the singlets are coincident. As with **4**$^+$ and **5**$^+$, the phenyl protons for the dbm ligands of **6**$^+$ are split into a number of doublets and multiplets between 7.37 and 8.10 ppm. The dmae ligands show two sharp singlets for the

methyl groups but four broad resonances for the individual protons on the ligand's backbone. The amino protons are not observed in both cases possibly due to H-bonding.[42]

Electrochemistry. The complexes **1**-**6** have been studied by cyclic voltammetry (CV) and square wave voltammetry in dry CH_2Cl_2 under anaerobic conditions and reveal irreversible one-electron oxidation. The CV of $[Co(tmhd)_2(phen)]$ is shown in Figure 1a as a representative example. The cyclic voltammograms (CVs) are broadly similar, exhibiting a single oxidation peak, Epa_1, and in most cases a small reduction peak, Epc_1, followed by a much larger reduction peak, Epc_2, which is widely separated from Epa_1 (Table 2). The irreversibility of the redox processes, which contrast with the Ni analogues which show either quasi-reversible oxidation or completely chemically irreversible oxidations with no corresponding reduction peaks,[42] suggests that the oxidation/reduction is accompanied by a structural and electronic rearrangement. Thus the oxidation of **1-6** to Co^{III} (Epa_1) initially produces a high spin Co^{III} intermediate (Epc_1) which can be re-reduced close to the oxidation peak, Epa_1. Epc_1 is presumably the cathodic partner to the anodic peak represented by Epa_1 and is to the best of our knowledge the *first time the HS Co^{III} intermediate has been observed electrochemically in a redox coupled-spin crossover system*. The high spin Co^{III} species rapidly undergoes spin crossover to the more stable low spin Co^{III} isomer which is reduced at a significantly more negative potential (Epc_2) resulting in a wide separation between the oxidation and reduction peak potentials, Epa_1 and Epc_2. The redox behavior of these complexes is an example of *redox coupled-spin crossover*.[51,52] This behavior is best described by the square scheme shown in Scheme 2. The two processes *1* and *3* represent the oxidation and reduction reactions of the individual spin state isomers while processes *2* and *4* represent the spin exchange reactions in the individual oxidation states.. Redox coupled-spin crossover has also been observed and extensively studied by Schultz *et al*. in a series of $[M(tacn)_2]^{2+/3+}$ (M = Fe, Co; tacn = 1,4,7-triazacyclononane) complexes although in this system the redox processes are fully reversible.[38-40] Similar redox behavior to **1**-**6** has recently been reported in the dimeric complex $[(bpbp)Co_2(O_2P(OPh)_2)_2]^+$ ($bpbp^-$ = 2,6-bis(N,N′-bis-(2-picolyl)amino)methyl)-4-tertbutylphenolato) which also shows wide separation of the oxidation and reduction peaks.[53] A similar result is also found in the case of $[(Tp^R)_2Co]^{0/+}$ (Tp^R = Tp, pzTp and Tp*) where increasing steric bulk results in a corresponding increase in irreversibility.[54] Comparisons between $[Co(tacn)_2]^{2+}$ and complexes **1**-**6** show that the former is oxidized *ca*. 0.9 V more easily than the latter consistent with the greater stability of the Co^{II} oxidation state for the $[Co(\beta\text{-diketonate})_2(N\text{-}N)]$ complexes. In contrast, the $[(bpbp)Co_2(O_2P(OPh)_2)_2]^+$ dimer oxidizes at a higher potential, 0.42 V (vs. $[FeCp_2]^{0/+}$).

The oxidation peak potentials for **1**-**6** are ca. 0.54 V more negative than the related Ni compounds.[42] A similar difference in the redox potentials has also been observed in the two series $[M(tacn)_2]^{2+/3+}$ and $[(Tp^R)_2M]^{0/+}$ (Tp^R = Tp, pzTp and Tp*; M = Co, Ni).[38,54-56] Within the two series of

1-**6** we find that the tmhd complexes are easier to oxidize than the corresponding dbm complexes by *ca*. 0.14 V indicating that the inductive effects of the *t*-butyl groups increase the electron density on the metal thereby making it easier to oxidize. A similar trend is observed for the Ni analogues although the difference is larger by ca. 0.30 V.[42] The Co complexes show oxidation peak potentials in the order bipy < phen < dmae. This order is surprising given that for the [Ni(β-diketonate)$_2$(N-N)] complexes the dmae compounds are the most easily oxidized which is more in line with the typical electron donating properties of diamine and diimine ligands. The difference in the order of the peak potentials may be the result of the spin change which occurs upon oxidation. The difference in the oxidation and reduction peak potentials ($\Delta E = Epa_1$-Epc_2) varies from 0.54-1.06 V with **1**-**3** exhibiting larger ΔE values than **4**-**6**, thereby indicating that the greater steric bulk of the *t*-butyl groups results in a reduction in the rate of electron-transfer. Similar observations in the $[(Tp^R)_2Co]^{0/+}$ series are also attributed to steric effects.[54] In the case of $[(bpbp)Co_2(O_2P(OPh)_2)_2]^+$ ΔE = 1.04 and 0.61 V for the two redox reactions which agrees well with our findings for **1**-**6**.[53]

It is interesting to note that while the $[Co(tacn)_2]^{2+/3+}$ and $[(Tp^R)_2Co]^{0/+}$ redox pairs have a CoN_6 coordination sphere **1**-**6** and $[(bpbp)Co_2(O_2P(OPh)_2)_2]^+$ possess CoN_2O_4 and CoN_3O_3 coordination spheres, respectively. The presence of the weaker field oxygen donors would be expected to favor the high spin isomers and may be responsible for the irreversibility seen in these systems. It may also explain why we are able to observe a reduction peak for the high spin Co^{III} intermediate in some of the complexes.

In an attempt to better understand the redox coupled-spin crossover process in complexes **1**-**6** we undertook cyclic voltammetric studies at high scan rates using a microelectrode. There was little change in the reversibility of the complexes even at moderately fast scan rates (10 Vs^{-1}) consistent with a rapid spin exchange equilibrium and slow electron transfer as is frequently observed in these systems (Figure 2).[29,52] This result seems reasonable since going from the high spin to the low spin state does not require any bonds to be broken but rather optimization of the Co-ligand bond lengths. Similar irreversibility at high scans rates is also observed in the $[(bpbp)Co_2(O_2P(OPh)_2)_2]^+$ dimer. In addition, studies on a wide range of cobalt am(m)ine systems also reveal slow electron transfer.[52]

Despite the fact that redox coupled-spin crossover reactions are well documented the mechanism still remains the subject of considerable debate with a pathway via high energy spin-state intermediates and a concerted pathway both proposed.[30-37] Schultz and co-workers have shown that in the case of the $[Co(tacn)_2]^{2+/3+}$ redox pair the reaction proceeds via a high-spin intermediate.[39,40] As noted earlier the cyclic voltammograms of **1**-**6** clearly show the presence of peaks attributable to a high spin Co^{III} intermediate and suggest that the mechanism for the oxidation of **1**-**6** also proceeds via a high spin intermediate. In contrast, at all applied scan rates (0.02 to 10 Vs^{-1}) we were unable observe a peak for

the low spin Co^{II} intermediate suggesting that the lifetime of this intermediate is very short as a result of an exceedingly rapid spin exchange reaction (equilibrium *4* in Scheme 2).

The square wave voltammograms show peak potentials similar to those found in the CVs. The slight deviations between the two methods might be due to the dependence of the peak potentials on scan rate noted in the CVs. The peaks also exhibit slight asymmetry consistent with the electrochemical irreversibility observed in the CVs.

The cations $\mathbf{1}^{+}$-$\mathbf{6}^{+}$ were also studied by cyclic voltammetry and show a large reduction peak coupled to a smaller redox couple at a higher potential (Figure 1-b). The peak potentials observed in the cyclic voltammograms are almost identical to those found in the neutral analogues although there are slight deviations. Similar results are noted in the complex $[(bpbp)Co_2(O_2P(OPh)_2)_2]^{3+}$ where shifts of up to 0.18 V are observed.[53] As with **1**-**6** the peaks for the high spin Co^{III} intermediate are clearly discernable but no peak is apparent (i.e. "Epa_2") for the low spin Co^{II} intermediate. Such behavior is typical of square scheme systems which involve first order isomerization of an initial electrode product to the final observed form.[57] Furthermore, the apparent reversibility of the CV's do not change with concentration a result which rules out significant contribution of the second-order homogeneous cross reaction (i.e. LS Co^{II} + HS Co^{III} → LS Co^{III} + HS Co^{II}) to the observed current.[57] In such a reaction, the HS Co^{III} produced by equilibrium *2* in Scheme 2 would react with electrogenerated LS Co^{II}. Thus, the reduction of the LS Co^{III} to HS Co^{II} proceeds by the expected LS Co^{II} intermediate. Similar reasoning leads to the conclusion that the oxidation of the HS Co^{II} to LS Co^{III} proceeds by the observed HS Co^{III} intermediate.

To confirm that the products isolated from the chemical oxidation of **1**-**6** were the same as those observed in the cyclic voltammograms we undertook IR spectroelectrochemical studies. The results are detailed in Table 4 with a representative difference spectrum shown in Figure 3. The oxidation of **1**-**6** are all accompanied by the loss (i.e. downward-pointing features) of the β-diketonate ν_{CO} bands at *ca*. 1590, 1570, 1520 and 1500 cm^{-1} due to the Co^{II} starting materials and a corresponding increase in bands at between *ca*. 1550 and 1520 cm^{-1} due to the Co^{III} products. Bands at frequencies lower than 1500 cm^{-1} are lost due to interference from the electrolyte. Subsequent reduction restores the original spectrum showing (as expected) that the chemical oxidation or reduction is reversible. The shift in the bands to lower wavenumbers mirrors exactly what is observed in the isolated complexes and is consistent with the higher Co^{III} oxidation state. Moreover, the positions of the bands are almost identical between the isolated redox pairs and the results from spectroelectrochemistry confirm that the isolated complexes are the species formed at the electrode. Similar studies on the cationic species $\mathbf{1}^{+}$-$\mathbf{6}^{+}$ show an exact opposite trend with bands moving to higher wavenumbers as one would expect. Consistent with the CV results,

no features due to HS Co^{III} were observed, consistent with the presence of a very small equilibrium concentration.

Computational Studies. In order to better understand the electronic structure of **1**-**6**, and their respective cations, and in particular the role of the electronic structure on the redox coupled-spin crossover process we have undertaken DFT calculations.[58] For a given complex, all possible spin states were considered.

The fact that $[Co(dbm)_2(phen)]$ (**4**) has been structurally characterized by single crystal X-ray crystallography allows a comparison between the computational and experimental geometries (see Figure 4 and Table 5).[59] The computed bond lengths match well with the experimental bond lengths with differences no more than 0.05 Å. The bonds angles show similar agreement between experiment and theory. Good agreements between the X-ray structure and computed geometry of $[Co(dbm)_2(phen)]$ in the quartet spin state indicates that these complex exists in a high spin state. It also confirms that the B3LYP/SDD model can be used to describe these types of complexes.

Our B3LYP/SDD calculations confirm the observation that the HS state is the most stable state for the Co^{II} complexes and the LS state is the most stable state for the Co^{III} complexes and as such is consistent the magnetic susceptibility measurements. In contrast, with the previously studied $[Co(tacn)_2]^{2+/3+}$ redox pair the gas-phase energy difference between the HS and LS states, E(HS)-E(LS), for the neutral Co^{II} complexes is between -12.7 and -15.6 kcal/mol (see Table 6) compared with -0.09 kcal/mol for $[Co(tacn)_2]^{2+}$. However, in the case of the Co^{III} cations the gap is significantly decreased to between 16.1 and 18.1 kcal/mol (*cf.* 45.3 kcal/mol for $[Co(tacn)_2]^{3+}$). Judging from the gas-phase energy, the triplet and quintet states are found to lie close to each other. The differences between E(HS)-E(LS) of $\mathbf{1}^+$-$\mathbf{6}^+$ and $[Co(tacn)_2]^{3+}$ are simply explained by the presence of the lower field β-diketonate ligands which are better able to stabilize the HS states. The thmd ligand stabilizes the HS state compared to the LS state to a greater extent than the dbm ligand. Moreover, the phen ligand stabilizes the HS state most in comparison with the other N-N ligands. This might be due to a d-π∗ orbital interaction from the low-lying π∗ orbital of the phen ligand. The smaller difference in the LS and HS states in $\mathbf{1}^+$-$\mathbf{6}^+$ might also explain why we are able to observe the reduction peak for the HS Co^{III} species in some of the electrochemical studies. These studies further suggest that the mechanism for the redox coupled-spin crossover involves a HS Co^{III} intermediate as has also been found in the $[Co(tacn)_2]^{2+/3+}$ system.

The molecular orbital analysis reveals that in the case of **1**-**3** and **6** complexes the SOMO is composed of an antibonding interaction between β-diketonate oxygen *p*-orbitals and the cobalt d_{z2} orbital (see Figure 5). The dmae complexes also exhibit an additional antibonding interaction between

the metal orbital and a hybrid σ donor orbital on the NMe_2 nitrogen of the dmae ligand. The SOMO of related bipy and phen complexes, **4** and **5** are different from the others with a metal d_{xz} orbital involved in a weaker antibonding interaction with the β-diketonate ligands. The significant electron density on the β-diketonate ligands in **1**-**6** is consistent with the strong influence of the β-diketonate upon the oxidation potentials of the above complexes. In the case of **1**, **2**, **4** and **5** the LUMO is essentially a low lying phen or bipy π* orbital while for **3** and **6** the absence of such π* orbitals results in a LUMO which is dominated by a β-diketonate π* orbital (Figure 6). Consequently, a much larger SOMO-LUMO gap is observed in the case of the dmae complexes compared with **1**, **2**, **4** and **5** (see Table 6).

Conclusions. In summary, six redox-active Co β-diketonate complexes have been prepared in two oxidation states which undergo a rare redox coupled-spin crossover from high spin d^7 to low spin d^6 which has been confirmed by cyclic voltammetry and spectroelectrochemical studies. Chemical oxidation of the Co β-diketonate compounds permits isolation of the Co^{III} cations which are indeed low spin as shown by NMR spectroscopy. Electrochemical and computational studies on the redox pairs strongly suggest that the redox coupled-spin crossover in the above complexes proceeds via a square scheme mechanism which does not involve significant amount of homogenous cross-reaction.

Experimental Section

Materials. All reactions were conducted in air using HPLC grade solvents. $[Co(tmhd)_2(H_2O)_2]$, and $[Co(dbm)_2(H_2O)_2]$ were prepared by literature methods.[60,61] All other chemicals were purchased from Fluka Chemical Company and used as received. Elemental analyses and ESI-MS were carried out by the staff of the School of Chemistry, University of Bristol, UK. Elemental analyses were carried out on a Eurovector EA3000 analyser. ESI-MS were carried out on a Bruker Daltonics 7.0T Apex 4 FTICR Mass Spectrometer. Magnetic susceptibilities were determined using the Evan's method at 297 K.[62]

Spectroscopy. Infrared spectra, as KBr discs, were recorded on a Perkin-Elmer Spectrum One infrared spectrophotometer in the range 400-4000 cm^{-1}. Electronic spectra were recorded in CH_2Cl_2 on a Unicam UV300 UV-Visible spectrometer. ^1H NMR spectra were recorded on a Bruker 300 MHz FT-NMR spectrometer at 298 K in $CDCl_3$ with $SiMe_4$ added as an internal standard.

Electrochemistry. Electrochemical studies were carried out using a palmsensPC Vs 2.11 potentiostat in conjunction with a three electrode cell. The auxiliary electrode was a platinum rod and the working electrode was a platinum disc (2.0 mm diameter). The reference electrode was a Ag-AgCl electrode. Solutions were 5 x 10^{-4} M in the test compound and 0.1 M in $[NBu^n_4][PF_6]$ as the supporting electrolyte. Under these conditions, $E^{o\prime}$ for the one-electron oxidation of $[Fe(\eta\text{-}C_5H_5)_2]$ added to the test solutions as

an internal calibrant is 0.52 V. For the electrochemical studies at high scan rates a 50 μm platinum disc microelectrode was used as the working electrode with a silver and platinum wire used as the reference and auxiliary electrode, respectively. Fiber-optic difference IR spectroelectrochemical measurements were obtained as previously described.[63]

Calculations

All calculations were performed by using the Gaussian 03 package.[58] The B3LYP hybrid functional with the Stuttgart/Dresden SDD effective core potential basis set was used in all calculations.[64-67] The geometries of complexes for a given spin state were optimized and verified by performing Hessian calculations. The molecular orbital analyses were then conducted at those geometries.[58] The SOMO and LUMO three-dimensional isosurface plots were generated using the Avogadro program.[68]

[Co(tmhd)$_2$(phen)] 1. To a stirred purple solution of [Co(tmhd)$_2$] (0.0826 g, 0.2 mmol) in CH_2Cl_2 (15 cm^3), phen (0.0396 g, 0.2 mmol) was added. The orange solution was stirred for 1 hour at room temperature then filtered through celite. The solution was left to slowly evaporate at room temperature yields deep red needle crystals 0.0772 g (64%). Magnetic moment (μ_{eff}/μ_B, 297 K): 4.51. $C_{34}H_{46}N_2O_4Co$; calc. C 67.4, H 7.7, N 4.6; found C 67.5, H 7.4, N 5.6. Electrospray ionization (ESI) mass data: *m/z* 605 (100%, $[M]^+$), 422 (24%, $[M - tmhd]^+$).

[Co(tmhd)$_2$(2,2′-bpy)] 2. To a stirred purple solution of [Co(tmhd)$_2$] (0.0638 g, 0.15 mmol) in CH_2Cl_2 (5 cm^3), 2,2′-bpy (0.0240 g, 0.15 mmol) was added. The orange solution was stirred for 1 hour then filtered through celite. The solution was left to slowly evaporate at room temperature yields orange needle crystals 0.0451 g (53%). Magnetic moment (μ_{eff}/μ_B, 297 K): 4.53. $C_{32}H_{46}N_2O_4Co$; calc. C 66.1, H 8.0, N 4.8; found C 66.3, H 7.8, N 5.1. Electrospray ionization (ESI) mass data: *m/z* 581 (100%, $[M]^+$), 398 (20%, $[M - tmhd]^+$).

[Co(tmhd)$_2$(dmae)] 3. To a stirred purple solution of [Co(tmhd)$_2$] (0.0637 g, 0.15 mmol) in CH_2Cl_2 (10 cm^3), dmae (150 μL, 0.15 mmol) was added. The orange solution was stirred for 1 hour at room temperature then filtered through celite. The solution was left to slowly evaporate at room temperature yields deep red needle crystals 0.0313 g (54%). Magnetic moment (μ_{eff}/μ_B, 297 K): 4.53. $C_{26}H_{50}N_2O_4Co$; calc. C 60.8, H 9.8, N 5.4; found C 52.6, H 8.9, N 5.9. Electrospray ionization (ESI) mass data: *m/z* 513 (100%, $[M]^+$), 330 (8%, $[M - tmhd]^+$)..

[Co(dbm)$_2$(phen)] 4. To a stirred red-orange solution of [Co(dbm)$_2$] (0.0816 g, 0.15 mmol) in THF (20 cm^3) at 70 °C, phen (0.0301 g, 0.15 mmol) was added. The deep red solution was stirred for 1 hour at room temperature then filtered through celite. The solution was left to slowly evaporate at room temperature yields deep red needle crystals 0.0914 g (88%). Magnetic moment (μ_{eff}/μ_B, 297 K): 5.03.

$C_{42}H_{34}N_2O_4Co$; calc. C 73.1, H 5.0, N 4.1; found C 73.4, H 4.6, N 4.3. Electrospray ionization (ESI) mass data: *m/z* 689 (100%, $[M]^+$), 462 (18%, $[M - dbm]^+$).

$[Co(dbm)_2(2,2'\text{-bpy})]$ 5. To a stirred red-orange solution of $[Co(dbm)_2]$ (0.0811 g, 0.15 mmol) in THF (20 cm^3) at 70 °C, 2,2′-bpy (0.0234 g, 0.15 mmol) was added. The deep red solution was stirred for 1 hour at room temperature then the solution was left to slowly evaporate at room temperature yields deep red needle crystals 0.1014 g (100%). Magnetic moment (μ_{eff}/μ_B, 297 K): 4.41. $C_{40}H_{30}N_2O_4Co$; calc. C 72.6, H 4.6, N 4.2; found C 72.6, H 5.3, N 4.1. Electrospray ionization (ESI) mass data: *m/z* 661 $[M]^+$, 438 $[M - dbm]^+$. Electrospray ionization (ESI) mass data: *m/z* 661 (4%, $[M]^+$), 438 (100%, $[M - dbm]^+$).

$[Co(dbm)_2(dmae)]$ 6. To a stirred red-orange solution of $[Co(dbm)_2]$ (0.0811 g, 0.15 mmol) in THF (20 cm^3) at 70 °C, dmae (150 μL, 0.15 mmol) was added. The orange solution was stirred for 1 hour at room temperature then filtered through celite. The solution was left to slowly evaporate at room temperature yields deep red needle crystals 0.0646 g (73%). Magnetic moment (μ_{eff}/μ_B, 297 K): 4.98. $C_{34}H_{34}N_2O_4Co$; calc. C 68.8, H 5.7, N 4.7; found C 68.8, H 5.7, N 5.0 Electrospray ionization (ESI) mass data: *m/z* 593 (100%, $[M]^+$), 370 (68%, $[M - dbm]^+$)

$[Co(tmhd)_2(phen)][BF_4]$ 1^+. To a stirred purple solution of $[Co(tmhd)_2(H_2O)_2]$ (0.2303 g, 0.5 mmol) in CH_2Cl_2 (20 cm^3), phen (0.0992 g, 0.5 mmol) was added. The orange solution was stirred for 1 hour then $AgBF_4$ (0.110 g, 0.56 mmol) added. The brown-orange solution was stirred overnight. The dark green solution was filtered through celite then washed with CH_2Cl_2 (3 x 5 cm^3). The solvent was removed to dryness. The solid was purified using CH_2Cl_2-diethyl ether to give dark red block crystals yield 0.2120 g (61%). $C_{34}H_{46}BCoF_4N_2O_4$; calc. C 59.0, H 6.7, N 4.0; found C 58.7, H 6.9, N 4.3. Electrospray ionization (ESI) mass data: *m/z* 605 (100%, $[M - BF_4]^+$), 422 (35%, $[M - BF_4 - tmhd]^+$).

$[Co(tmhd)_2(2,2'\text{-bpy})][BF_4]$ 2^+. To a stirred purple solution of $[Co(tmhd)_2(H_2O)_2]$ (0.2330 g, 0.5 mmol) in CH_2Cl_2 (20 cm^3), 2,2′-bpy (0.0785 g, 0.5 mmol) was added. The orange solution was stirred for 1 hour then $AgBF_4$ (0.110 g, 0.56 mmol) added. The brown-orange solution was stirred overnight. The dark green solution was filtered through celite then washed with CH_2Cl_2 (3 x 5 cm^3). The solvent was removed to dryness. The solid was purified using CH_2Cl_2-diethyl ether to give maroon microcrystals yield 0.2138 g (64%). $C_{32}H_{46}BCoF_4N_2O_4$; calc. C 57.5, H 6.9, N 4.2; found C 57.5, H 6.9, N 4.6. Electrospray ionization (ESI) mass data: *m/z* 581 (100%, $[M - BF_4]^+$), 398 (42%, $[M - BF_4 - tmhd]^+$).

$[Co(tmhd)_2(dmae)][BF_4]$ 3^+. To a stirred purple solution of $[Co(tmhd)_2(H_2O)_2]$ (0.2298 g, 0.5 mmol) in CH_2Cl_2 (20 cm^3), dmae (54.4 μL, 0.5 mmol) was added. The orange solution was stirred for 1 hour then $AgBF_4$ (0.110 g, 0.56 mmol) added. The dark green solution was stirred overnight. The deep purple solution was filtered through celite then washed with CH_2Cl_2 (3 x 5 cm^3). The solvent was removed to dryness. The solid was purified using CH_2Cl_2-diethyl ether to give pastel purple microcrystals yield

0.1841 g (61%). $C_{26}H_{50}BCoF_4N_2O_4$; calc. C 52.0, H 8.4, N 4.7; found C 52.7, H 8.6, N 5.2. Electrospray ionization (ESI) mass data: *m/z* 513 (100%, $[M - BF_4]^+$), 330 (94%, $[M - BF_4 - tmhd]^+$).

$[Co(dbm)_2(phen)][BF_4]$ 4^+. To a stirred orange suspension of $[Co(dbm)_2(H_2O)_2]$ (0.1678 g, 0.3 mmol) in CH_2Cl_2 (20 cm^3), phen (0.0620 g, 0.3 mmol) was added. The orange solution was stirred for 1 hour then $AgBF_4$ (0.0700 g, 0.36 mmol) added. The olive green solution was stirred overnight. The dark green solution was filtered through celite then washed with CH_2Cl_2 (3 x 5 cm^3). The solvent was removed to dryness. The solid was purified using CH_2Cl_2-*n*-hexane to give olive green microcrystals yield 0.1295 g (56%). $C_{42}H_{34}BCoF_4N_2O_4$; calc. C 65.0, H 4.4, N 3.6; found C 66.5, H 4.2, N 3.9. Electrospray ionization (ESI) mass data: *m/z* 689 (84%, $[M - BF_4]^+$), 462 (100%, $[M - BF_4 - dbm]^+$).

$[Co(dbm)_2(2,2'\text{-bpy})][BF_4]$ 5^+. To a stirred orange suspension of $[Co(dbm)_2(H_2O)_2]$ (0.1586 g, 0.3 mmol) in CH_2Cl_2 (20 cm^3), 2,2′-bpy (0.0470 g, 0.3 mmol) was added. The orange solution was stirred for 1 hour then $AgBF_4$ (0.0646 g, 0.33 mmol) added. The olive green solution was stirred overnight. The dark green solution was filtered through celite then washed with CH_2Cl_2 (3 x 5 cm^3). The solvent was removed to dryness. The solid was purified using CH_2Cl_2-*n*-hexane to give green brown microcrystals yield 0.1097 g (51%). $C_{40}H_{30}BCoF_4N_2O_4$; calc. C 64.2, H 4.0, N 3.7; found C 65.2, H 4.3, N 3.9. Electrospray ionization (ESI) mass data: *m/z* 661 (54%, $[M - BF_4]^+$), 438 (100%, $[M - BF_4 - dbm]^+$).

$[Co(dbm)_2(dmae)][BF_4]$ 6^+. To a stirred orange suspension of $[Co(dbm)_2(H_2O)_2]$ (0.1718 g, 0.3 mmol) in CH_2Cl_2 (20 cm^3), dmae (34.7 μL, 0.3 mmol) was added. The orange solution was stirred for 1 hour then $AgBF_4$ (0.0710 g, 0.36 mmol) added. The olive green solution was stirred overnight. The dark green solution was filtered through celite then washed with CH_2Cl_2 (3 x 5 cm^3). The solvent was removed to dryness. The solid was purified using CH_2Cl_2-*n*-hexane to give olive green microcrystals yield 0.1072 g (49%). $C_{34}H_{34}BCoF_4N_2O_4$; calc. C 60.0, H 5.0, N 4.1; found C 62.7, H 5.3, N 3.7. Electrospray ionization (ESI) mass data: *m/z* 593 (84%, $[M - BF_4]^+$), 370 (100%, $[M - BF_4 - dbm]^+$).

ACKNOWLEDGMENTS We thank the Walailak University Research Fund (grant number 5/2549) and the Thailand Research Fund (RSA5080007 and RSA5180010) for partial financial support. Computational resources: National Nanotechnology Center (NANOTEC) Thailand.

FIGURE CAPTIONS

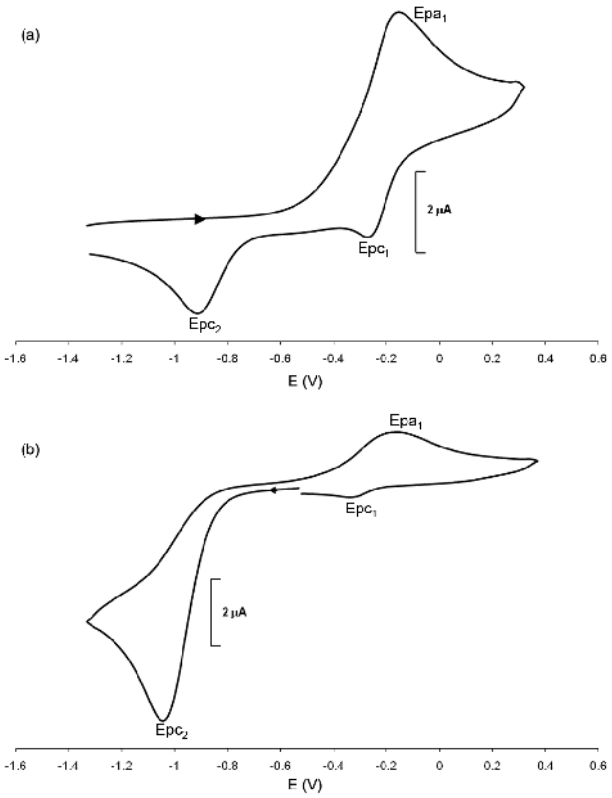

Figure 1. Cyclic voltammograms of (a) [Co(tmhd)$_2$(phen)] **1** (b) [Co(tmhd)$_2$(phen)][BF$_4$] **1**$^+$[BF$_4$].

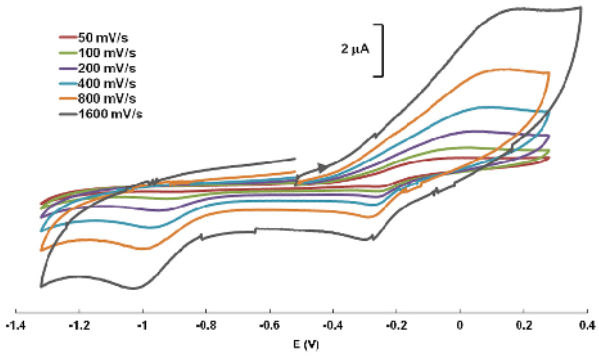

Figure 2. Cyclic voltammograms of [Co(tmhd)$_2$(phen)] at scan rates of 50 to 1600 mV/s.

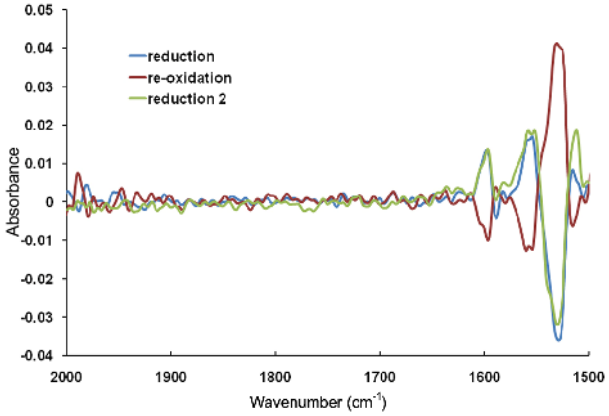

Figure 3. IR spectroelectrochemical difference spectra of $[Co(dbm)_2(phen)][BF_4]$ $\mathbf{4}^{+}[BF_4]$.

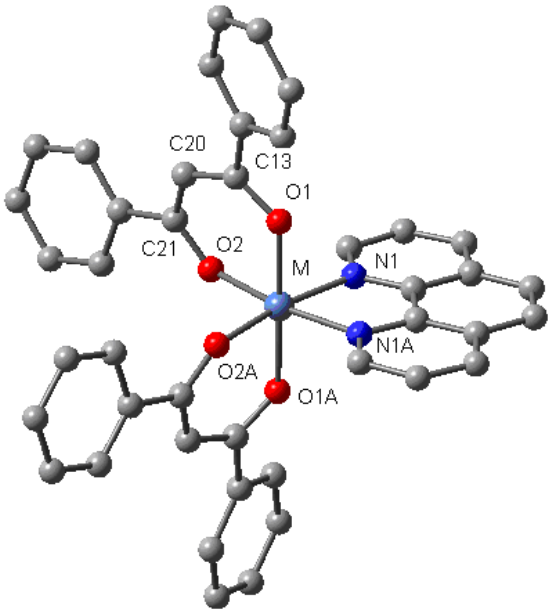

Figure 4. Numbering scheme for $[Co(dbm)_2(phen)]$ complex as used for structural comparison with the X-ray structures.

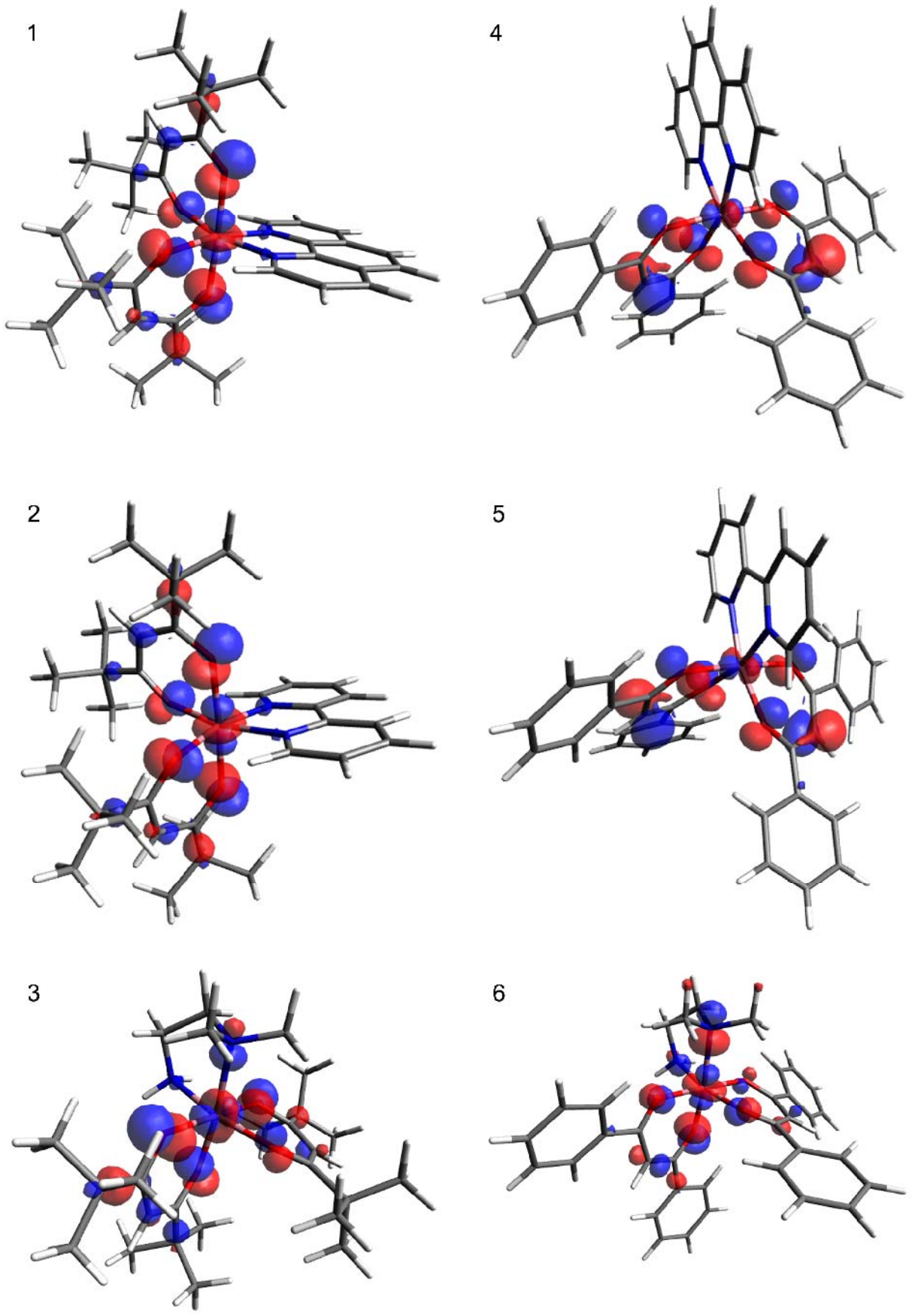

Figure 5. The SOMO orbital of complexes **1-6**

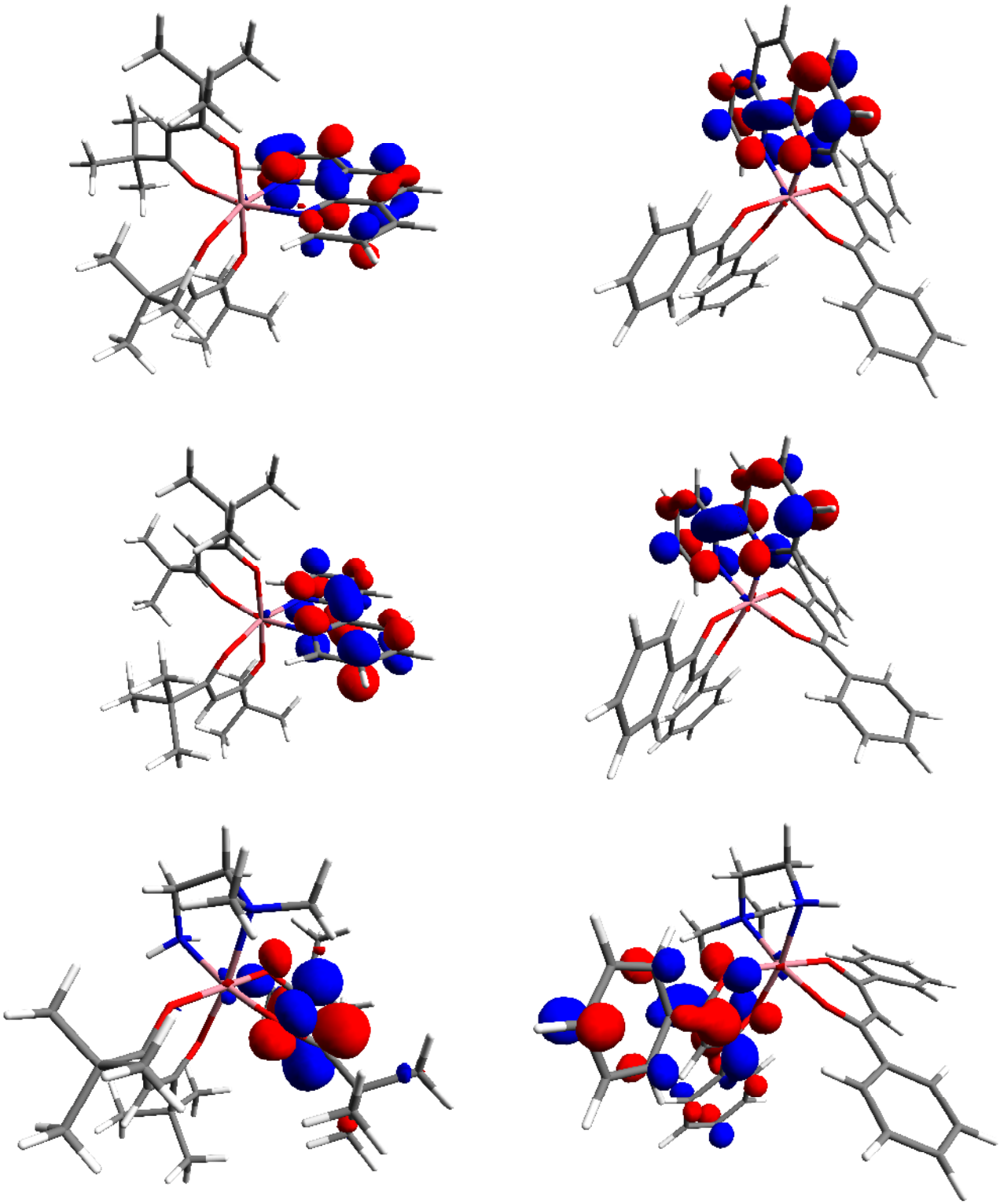

Figure 6. The LUMO orbital of complexes **1-6**

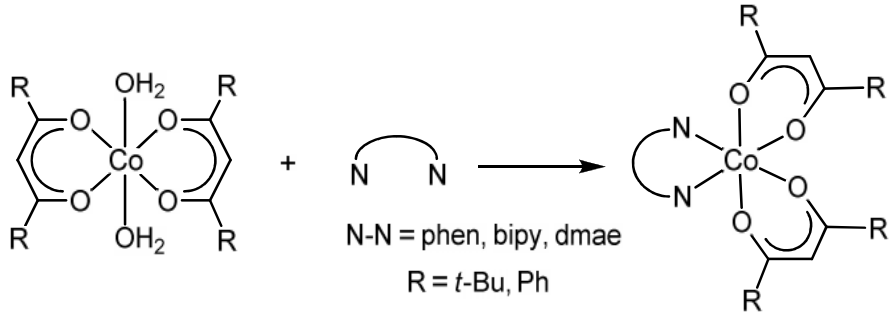

Scheme 1. Synthesis of [Co(β-diketonate)$_2$(N-N)].

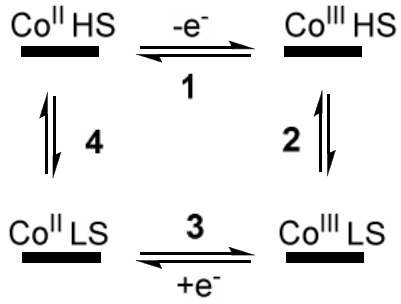

Scheme 2. Square scheme of the redox coupled-spin crossover process showing individual spin crossover and electron transfer processes.

Table 1. IR and UV-Vis spectroscopic data for [Co(β-diketonate)$_2$(N-N)] complexes.

Complex	% Yield	Color	IR		λ/nm(log ε/mol^{-1} dm^3 cm^{-1})
			$\nu_{C=O}$	ν_{N-H}	
[Co(tmhd)$_2$(phen)] **1**	64	Deep red		-	268 (5.00), 289 (4.77, sh), 399 (3.03, sh), 438 (3.09), 532 (2.47, sh)
[Co(tmhd)$_2$(2,2′-bpy)] **2**	53	Orange	1561	-	288 (4.85), 430 (3.02), 541 (3.37)
[Co(tmhd)$_2$(dmae)] **3**	54	Deep red	1583	3365	268 (4.49), 345 (3.72, sh), 554 (2.10)
[Co(dbm)$_2$(phen)] **4**	88	Red	1595	-	268 (5.02), 287 (4.64, sh), 349 (4.81), 368 (4.55, sh), 413 (3.40)
[Co(dbm)$_2$(2,2′-bpy)] **5**	100	Red	1596	-	291 (4.62), 351 (4.75), 370 (4.54, sh), 415 (3.43), 549 (2.09, sh)
[Co(dbm)$_2$(dmae)] **6**	73	Red	1594	-	345 (4.34), 382 (3.85), 548 (1.99)
[Co(tmhd)$_2$(phen)]$^+$ **1**$^+$	61	Dark red	1543	-	268 (4.48), 298 (4.17, sh), 344(3.63, sh), 576 (2.18)
[Co(tmhd)$_2$(2,2′-bpy)]$^+$ **2**$^+$	64	Maroon	1545	-	299 (4.67), 309 (4.65), 341 (4.12), 569 (2.22)
[Co(tmhd)$_2$(dmae)]$^+$ **3**$^+$	61	Pastel purple	1560	3310, 3264	300 (4.32, sh), 337 (4.00), 574 (2.28)
[Co(dbm)$_2$(phen)]$^+$ **4**$^+$	56	Olive green	1524	-	273 (4.54), 292 (4.50, sh), 350 (3.91), 376 (3.92), 578 (2.37)
[Co(dbm)$_2$(2,2′-bpy)]$^+$ **5**$^+$	51	Brown green	1524	-	262 (4.96, sh), 292 (5.15), 382 (4.56), 413 (3.43), 422 (3.40), 574 (2.40)
[Co(dbm)$_2$(dmae)]$^+$ **6**$^+$	49	Olive green	1525	3320, 3264	284 (5.07), 384 (4.50), 415 (3.42), 427 (3.40), 578 (2.33)

Table 2. Cyclic voltammetric data of [Co(β-diketonate)$_2$(N-N)].

Complex	Peak potential (V)		
	Epa_1	Epc_1	Epc_2
[Co(tmhd)$_2$(phen)] **1**	-0.15	-0.27	-1.18
[Co(tmhd)$_2$(2,2′-bpy)] **2**	-0.11	-	-1.08
[Co(tmhd)$_2$(dmae)] **3**	-0.13	-	-1.32
[Co(dbm)$_2$(phen)] **4**	0.03	-0.37	-0.98
[Co(dbm)$_2$(2,2′-bpy)] **5**	-0.07	-0.38	-0.61
[Co(dbm)$_2$(dmae)] **6**	0.06	-0.43	-1.21
[Co(tmhd)$_2$(phen)][BF_4] $\mathbf{1}^+$	-0.17	-0.34	-1.38
[Co(tmhd)$_2$(2,2′-bpy)][BF_4] $\mathbf{2}^+$	-0.24	-0.38	-1.41
[Co(tmhd)$_2$(dmae)][BF_4] $\mathbf{3}^+$	-0.08	-0.31	-1.53
[Co(dbm)$_2$(phen)][BF_4] $\mathbf{4}^+$	0.00	-0.22	-0.86
[Co(dbm)$_2$(2,2′-bpy)][BF_4] $\mathbf{5}^+$	-0.06	-	-0.73
[Co(dbm)$_2$(dmae)][BF_4] $\mathbf{6}^+$	-0.17	-	-0.72

All measurements were performed at 298 K, in dried and degassed CH_2Cl_2 0.1 M [NBu^n_4][PF_6] solution; scan rate 100 mVs^{-1}; calibrated with [$FeCp_2$], and reported relative to the $[FeCp_2]^{0/+}$ couple.

Table 3. ^{1}H NMR spectroscopic data of [Co(β-diketonate)$_2$(N-N)][BF_4] complexes.

Complex	δ (ppm)
[Co(tmhd)$_2$(phen)][BF_4] **1**$^+$	8.98 (2H, dd, J_{HH} 0.6 Hz, 8.1 Hz, C*H*^{Phen}), 8.38 (2H, d, J_{HH} 5.4 Hz, C*H*^{Phen}), 8.34 (2H, s, C*H*^{Phen}), 8.15 (2H, dd, J_{HH} 8.1 Hz, 5.4 Hz, C*H*^{Phen}), 5.91 (2H, s, C*H*^{central}), 1.31 (18H, s, *t*-Bu), 0.80 (18H, s, *t*-Bu)
[Co(tmhd)$_2$(2,2′-bpy)][BF_4] **2**$^+$	8.90 (2H, d, J_{HH} 7.8 Hz, *H*$^{6,\ bpy}$), 8.42 (2H, t, J_{HH} 7.8 Hz, 6.3 Hz, *H*$^{5,\ bpy}$), 8.12 (2H, d, J_{HH} 5.1 Hz, *H*$^{3,\ bpy}$), 7.70 (2H, t, J_{HH} 6.3 Hz, 5.1 Hz, *H*$^{4,\ bpy}$), 5.86 (2H, s, C*H*^{central}), 1.32 (18H, s, *t*-Bu), 0.87 (18H, s, *t*-Bu)
[Co(tmhd)$_2$(dmae)][BF_4] **3**$^+$	5.87 (1H, s, C*H*^{central}), 5.80 (1H, s, C*H*^{central}), 4.00 (2H, s, N-C*H$_2$*), 2.80 (2H, s, N-C*H$_2$*), 2.39 (3H, s, N-C*H$_3$*), 1.80 (3H, s, N-C*H$_3$*), 1.21 (18H, s, *t*-Bu), 1.12 (9H, s, *t*-Bu), 1.05 (9H, s, *t*-Bu)
[Co(dbm)$_2$(phen)][BF_4] **4**$^+$	9.01 (2H, dd, J_{HH} 8.1 Hz, 0.9 Hz, C*H*^{Phen}), 8.70 (2H, d, J_{HH} 5.1 Hz, C*H*^{Phen}), 8.40 (2H, s, C*H*^{Phen}), 8.12 (2H, dd, J_{HH} 8.1 Hz, 5.1 Hz, C*H*^{Phen}), 8.04 (4H, m, *H*^{Ph}), 7.60-7.55 (6H, m, *H*^{Ph}), 7.50-7.40 (6H, m, *H*^{Ph}), 7.32-7.28 (4H, m, *H*^{Ph}), 7.01 (2H, s, C*H*^{central})
[Co(dbm)$_2$(2,2′-bpy)][BF_4] **5**$^+$	9.03 (2H, d, J_{HH} 7.50 Hz, *H*$^{6,\ bpy}$), 8.47 (4H, m, *H*$^{6,\ bpy}$, *H*$^{3,\ bpy}$), 7.98 (4H, d, J_{HH} 7.20 Hz, *H*^{Ph}), 7.70 (2H, t, J_{HH} 6.90 Hz, *H*$^{4,\ bpy}$), 7.64 (4H, d, J_{HH} 7.20 Hz, *H*^{Ph}), 7.55-7.34 (12H, m, *H*^{Ph}), 6.97 (2H, s, C*H*^{central})
[Co(dbm)$_2$(dmae)][BF_4] **6**$^+$	8.10 (2H, d, J_{HH} 6.90 Hz, *H*^{Ph}), 7.97 (3H, m, *H*^{Ph}), 7.91 (2H, d, J_{HH} 7.2 Hz, *H*^{Ph}), 7.71 (2H, d, J_{HH} 7.50 Hz, *H*^{Ph}), 7.59-7.50 (9H, m, *H*^{Ph}), 7.42-7.37 (4H, m, *H*^{Ph}), 6.97 (1H, s, C*H*^{central}), 6.81 (1H, s, C*H*^{central}), 4.70 (1H, broad, s, N-C*H$_2$*), 4.50 (1H, broad, s, N-C*H$_2$*), 3.2 (1H, broad, s, N-C*H$_2$*), 2.8 (1H, broad, s, N-C*H$_2$*), 2.56 (3H, s, N-C*H$_3$*), 2.01 (3H, s, N-C*H$_3$*)

Table 4. IR spectroelectrochemical difference data of [Co(β-diketonate)$_2$(N-N)] complexes.

Complex	Bands of species produced (cm^{-1})	Bands of starting material consumed (cm^{-1})
[Co(tmhd)$_2$(phen)] **1** [a]	1552, 1543, 1523	1587, 1572, 1533, 1516, 1505
[Co(tmhd)$_2$(2,2′-bpy)] **2** [a]	1545, 1527	1588, 1581, 1570, 1518, 1504
[Co(tmhd)$_2$(dmae)] **3** [a]	1557, 1547, 1533	1592, 1582, 1570
[Co(dbm)$_2$(phen)] **4** [a]	1587, 1528	1596, 1564, 1554, 1514
[Co(dbm)$_2$(2,2′-bpy)] **5** [a]	1530	1597, 1563, 1549
[Co(dbm)$_2$(dmae)] **6** [a]	1526	1563, 1553
[Co(tmhd)$_2$(phen)]$^+$ **1**$^+$ [b]	1589, 1573, 1506	1558, 1548, 1525
[Co(tmhd)$_2$(2,2′-bpy)]$^+$ **2**$^+$ [b]	1587, 1572, 1506	1552 (sh), 1544, 1531, 1496
[Co(tmhd)$_2$(dmae)]$^+$ **3**$^+$ [b]	1596, 1581, 1569	1546, 1534
[Co(dbm)$_2$(phen)]$^+$ **4**$^+$ [b]	1596, 1557, 1552, 1512	1538 (sh), 1529
[Co(dbm)$_2$(2,2′-bpy)]$^+$ **5**$^+$ [b]	1597, 1579, 1554, 1513	1530, 1588
[Co(dbm)$_2$(dmae)]$^+$ **6**$^+$ [b]	1596, 1557, 1516	1588, 1540, 1528

[a] Oxidized at ca Epa_1. [b] Reduced at Epc_2

Table 5. Selected computed and X-ray crystallographically determined bond lengths (Å) and bond angles (^{o}) for [Co(dbm)$_2$(phen)]. See Figure 4 for the numbering scheme.

[Co(dbm)$_2$(phen)]	X-ray[1]	Doublet	diff.[2]	Quartet	diff.[2]
Co-O1	2.07	2.15	0.08	2.0627	0.01
Co-O2	2.07	1.94	0.13	2.0544	0.01
Co-N1	2.15	1.96	0.19	2.1493	0.00
C7-O1	1.28	1.29	0.01	1.3022	0.02
C20-O2	1.27	1.31	0.04	1.3052	0.03
C7-C21	1.41	1.43	0.02	1.4019	0.00
C20-C21	1.41	1.41	0.00	1.4163	0.01
O1-Co-O2	86.29	88.63	2.34	85.73	0.56
O2-Co-O2A	102.54	91.92	10.62	98.69	3.85
O1-Co-O2A	83.67	89.01	5.34	91.96	8.29
O1-Co-N1	101.53	92.85	8.68	96.11	5.42
O1-Co-N1A	91.10	89.67	1.43	86.68	4.42
O2-Co-N1	90.49	92.24	1.75	92.43	1.94
O1-Co-O1A	163.92	176.63	12.71	176.42	12.50
N1-Co-N1A	76.87	83.64	6.77	77.58	0.71

[1]From ref. 59.
[2]Difference between X-ray crystallographic and optimized structure.

Table 6. The high-spin and low-spin complex energy difference, E(HS)-E(LS), at B3LYP/SDD level for [Co(β-diketonate)$_2$(N-N)] complexes. For **1**$^+$**-6**$^+$**,** the pentet and triplet (in parenthesis) HS states were considered. The E(LUMO)-E(SOMO) gap was estimated from the alpha spin orbital energy of the most stable spin state.

Complex	E(HS)-E(LS)/(kcal.mol^{-1})	E(LUMO)-E(SOMO)/eV
[Co(tmhd)$_2$(phen)] **1**	-15.63	2.91
[Co(tmhd)$_2$(2,2′-bpy)] **2**	-14.55	2.91
[Co(tmhd)$_2$(dmae)] **3**	-12.67	4.54
[Co(dbm)$_2$(phen)] **4**	-13.84	3.13
[Co(dbm)$_2$(2,2′-bpy)] **5**	-12.80	2.86
[Co(dbm)$_2$(dmae)] **6**	-13.26	3.75
[Co(tmhd)$_2$(phen)]$^+$ **1**$^+$	16.12 (16.38)	3.48
[Co(tmhd)$_2$(2,2′-bpy)]$^+$ **2**$^+$	17.15 (17.19)	3.40
[Co(tmhd)$_2$(dmae)]$^+$ **3**$^+$	17.41 (17.60)	4.27
[Co(dbm)$_2$(phen)]$^+$ **4**$^+$	16.93 (17.31)	3.29
[Co(dbm)$_2$(2,2′-bpy)]$^+$ **5**$^+$	18.01 (18.16)	3.24
[Co(dbm)$_2$(dmae)]$^+$ **6**$^+$	17.93 (16.61)	3.70

REFERENCES

1. Létard, J.-F.; Guionneau, P.; Goux-Capes, L. *Top. Curr. Chem*. **2004**, *235*, 221.
2. Kahn, O. Martinez, C. J. *Science* **1998**, *279*, 44.
3. Fabbrizzi, L.; Licchelli, M.; Pallavicini, P. *Acc. Chem. Rev*. **1999**, *32*, 846.
4. Venturi, M.; Credi, A.; Balzani, V. *Coord. Chem. Rev*. **1999**,
5. H. A. Goodwin, *Coord. Chem. Rev.* **1976**, **18**, 293.
6. (a) Real, J. A.; Gaspar, A. B.; Niel, V.; Muñoz, M. C. *Coord. Chem. Rev.* **2003**, *236*, 121. (b) Garcia, Y.; Niel, V.; Muñoz, M. C. and Real, J. A. *Top. Curr. Chem.* **2004**, *233*, 229.
7. Murray, K. S.; Kepert, C. J. *Top. Curr. Chem.* **2004**, *233*, 195.
8. Gaspar, A. B.; Ksenofontov, V.; Real, J. A.; Gütlich, P. *Chem. Phys. Lett.* **2003**, *373*, 385.
9. (a) Spiering, H.; Kohlhaas, T.; Romstedt, H.; Hauser, A.; Bruns-Yilmaz, C.; Gütlich, P. *Coord. Chem. Rev.* **1999**, *190–192*, 629. (b) Gütlich, P.; Hauser, A.; Spiering, H. *Angew. Chem., Int. Ed. Engl.* **1994**, *33*, 2024.
10. (a) Real, J. A. in *Transition Metals in Supramolecular Chemistry*, ed. Sauvage, J. P. John Wiley and Sons, Ltd., Chichester, **1999**, p. 53. (b) Real, J. A.; Gaspar, A. B.; Muñoz, M. C.; Gütlich, P.; Ksenofontov, V.; Spiering, H. *Top. Curr. Chem.* **2004**, *233*, 167.
11. Haasnoot, J. G. *Coord. Chem. Rev.* **2000**, *200*, 131.
12. Breuning, E.; Ruben, M.; Lehn, J. M.; Renz, F.; Garcia, Y.; Ksenofontov, V.; Gütlich, P.; Wegelius, E.; Rissanen, K. *Angew. Chem., Int. Ed.* **2000**, *39*, 2504.
13. Real, J. A.; Andres, E.; Muñoz, M. C.; Julve, M.; Granier, T.; Bousseksou, A.; Varret, F. *Science* **1995**, *268*, 265.
14. Halder, G. J.; Kepert, C. J.; Moubaraki, B.; Murray, K. S.; Cashion, J. D. *Science* **2002**, *298*, 1762.
15. Madeja, K.; König, E. *J. Inorg. Nucl. Chem*. **1963**, *25*, 377.
16. Sieber, R.; Decurtins, S.; Stoeckli, H.; Evans, C.; Wilson, D.; Yufit, J. A. K.; Howard, S. C.; Capelli, A.; Hauser, A. *Chem. Eur. J*. **2000**, *6*, 361.

17. (a) Zerara, M.; Hauser, A. *Chem. Phys. Chem*. **2004**, *5*, 395. (b) Hauser A.; Amstutz, N.; Delahaye, S.; Schenker, S.; Sadki, A.; Sieber, R.; Zerara, M. *Struct. Bond*. **2004**, *106*, 81.
18. (a) Hogg, R.; Wilkins, R. G. *J. Chem. Soc*. **1962**, 341. (b) Judge, J. S.; Baker, W. A. *Inorg. Chim. Acta* **1967**, *1*, 68.
19. Figgis, B. N.; Kucharski, E. S.; White, A.H. *Aust. J. Chem*. **1983**, 36, 1537.
20. Scheidt, W. R.; Reed, C. A. *Chem*. *Rev*. **1981**, *81*, 543.
21. Bertani, I.; Gray, H. B.; Lippard, S. J.; Valentine, J. S. *Bioinorganic Chemistry*, University Science Books, Sausalito, CA, **1994**.
22. Lippard, S. J.; Berg, J. M. *Principles of Bioinorganic Chemistry*, University Science Books, Mill Balley, CA, **1995**.
23. Kaim, W.; Schwederski, B. *Bioinorganic Chemistry: Inorganic Elements in the Chemistry of Life*, Wiley, New York, **1995**.
24. Sligar, S. C. *Biochemistry* **1976**, *15*, 5399.
25. Mueller, E. J.; Lioda, P. J.; Sligar, S. C. in *Cytochrome P450: Structure, Mechanism and Biochemistry*, ed. Ortiz de Montellano, P.R. 2nd ed., Plenum Press, New York, **1995**, Chap. 3.
26. Rees, D. C.; Chan, M. K.; Kim, J. *Adv. Inorg. Chem*. **1993**, *40*, 89.
27. Burgess, B. K.; Lowe, D. J. *Chem. Rev*. **1996**, *96*, 2983.
28. Lopes, H.; Pettigrew, G. W.; Moura, I.; Moura, J. J. G. *J. Biol. Inorg. Chem*. **1998**, *3*, 632.
29. Hendry, P.; Ludi, A. *Adv. Inorg. Chem*. **1990**, *35*, 117.
30. Stynes, H.C.; Ibers, J.A. *Inorg. Chem*. **1971**, *10*, 2304.
31. Buhks, E.; Bixon, M.; Jortner, J.; Navon, G. *Inorg. Chem*. **1979**, *18*, 2014.
32. Geselowitz, D.A., Taube, H. *Adv. Inorg. Bioinorg. Mech*. **1982**, *1*, 391.
33. Larsson, S.; Ståhl, K.; Zerner, M.C. *Inorg. Chem*. **1986**, *25*, 3033.
34. Geselowitz, D.A. *Inorg. Chim. Acta* **1988**, *154*, 225.
35. Newton, M.D. *J. Phys. Chem.* **1991**, *95*, 30.
36. Shalders, R.D.; Swaddle, T.W. *Inorg. Chem*. **1995**, *34*, 4815.

37. Swaddle, T.W. *Can. J. Chem*. **1996**, *74*, 631.

38. Turner, J. W.; Schultz, F. A. *Inorg. Chem*. **1999**, *38*, 358.

39. Turner, J. W.; Schultz, F. A. *J. Phys. Chem. B* **2002**, *106*, 2009.

40. Lord, R. L.; Schultz, F. A., Baik, M.-H. *J. Am. Chem. Soc*. **2009**, *131*, 6189.

41. Nakamoto, K. in *Infrared and Raman Spectra of Inorganic and Coordination Compounds: Part B*, 6th ed., Wiley, New York, **2009**, pp. 96-104.

42. Harding, P.; Harding, D. J.; Phonsri, W.; Saithong, S.; Phetmung, H. *Inorg. Chim. Acta* **2009**, *362*, 78.

43. Cotton, F.A.; Wilkinson, G.; Murillo, C.A.; Bochmann, M. in *Advanced Inorganic Chemistry*, 6th ed.; John Wiley & Sons, New York, **1999**, pp. 817-822.

44. Bandoli, G.; Barreca, D.; Gasparotto, A.; Maccato, C.; Seraglia, R.; Tondello, E.; Devi, A.; Fischer, R. A.; Winter, M. *Inorg. Chem.* **2009**, *48*, 82.

45. Nagashima, N.; Kudoh, S.; Nakata, M. *Chem. Phys. Lett.* **2003**, *374*, 59.

46. Sankhla, D. S.; Mathur, R. C.; Misra, S. N. *J. Inorg. Nuc. Chem.* **1980**, *42*, 489.

47. Chassot, P.; Emmenegger, F. *Inorg. Chem.* **1996**, *35*, 5931.

48. Archer, R. D.; Cotsoradis, B. P. *Inorg. Chem.* **1965**, *4,* 1584.

49. York, R. J.; Bonds, W.D. Jr.; Cotsoradis, B. P.; Archer, R. A. *Inorg. Chem.* **1969**, *8*, 789.

50. Izumi, F.; Kurosawa, R.; Kawamoto, H.; Akaiwa, H. *Bull. Chem. Soc. Jpn.* **1975**, *48*, 3188.

51. Turner, J. W.; Schultz, F. A. *Coord. Chem. Rev.* **2001**, *219-221*, 81.

52. For examples of other Co complexes exhibiting RCSCO see (a) Buhks, E.; Dixon, M.; Jortner, J.; Navon, G. *Inorg. Chem.* **1979**, *18*, 2014. (b) Endicott, J. F.; Brubaker, G. R.; Ramasami, T.; Kumar, K.; Dwarakanath, K.; Cassel, J.; Johnson, D. *Inorg. Chem.* **1983**, *22*, 3754. (c) Hammershøi, A.; Geselowitz, D.; Taube, H. *Inorg. Chem.* **1984**, *32*, 979. (d) Bernhardt, P. V.; Jones, L. A.; Sharpe, P. C. *Inorg. Chem.* **1997**, *36*, 2420.

53. Johansson, F. B.; Bond, A. D.; Nielson, U. G.; Moubaraki, B.; Murray, K. S.; Berry, K. J.; Larrabee, J. A.; McKenzie, C. J. *Inorg. Chem*. **2008,** *47*, 5079.

54. De Alwis, D. C. L.; Schultz, F. A. *Inorg. Chem.* **2003**, *42*, 3616.

55. Wieghardt, K.; Schmidt, W.; Herrmann, W.; Kueppers, H. J. *Inorg. Chem*. **1983**, *22*, 2953.

56. Kueppers, H. J.; Neves, A.; Pomp, C.; Ventur, D.; Wieghardt, K.; Nuber, B.; Weiss, J. *Inorg. Chem*. **1986**, *25*, 2400.

57. Richards, T. C.; Geiger, W.E. *J. Am. Chem. Soc.* **1994**, *116*, 2028.

58. Gaussian 03, Revision D.01, Frisch, M. J.; Trucks, G. W.; Schlegel, H. B.; Scuseria, G. E.; Robb, M. A.; Cheeseman, J. R.; Montgomery, Jr., J. A.; Vreven, T.; Kudin, K. N.; Burant, J. C.; Millam, J. M.; Iyengar, S. S.; Tomasi, J.; Barone, V.; Mennucci, B.; Cossi, M.; Scalmani, G.; Rega, N.; Petersson, G. A.; Nakatsuji, H.; Hada, M.; Ehara, M.; Toyota, K.; Fukuda, R.; Hasegawa, J.; Ishida, M.; Nakajima, T.; Honda, Y.; Kitao, O.; Nakai, H.; Klene, M.; Li, X.; Knox, J. E.; Hratchian, H. P.; Cross, J. B.; Bakken, V.; Adamo, C.; Jaramillo, J.; Gomperts, R.; Stratmann, R. E.; Yazyev, O.; Austin, A. J.; Cammi, R.; Pomelli, C.; Ochterski, J. W.; Ayala, P. Y.; Morokuma, K.; Voth, G. A.; Salvador, P.; Dannenberg, J. J.; Zakrzewski, V. G.; Dapprich, S.; Daniels, A. D.; Strain, M. C.; Farkas, O.; Malick, D. K.; Rabuck, A. D.; Raghavachari, K.; Foresman, J. B.; Ortiz, J. V.; Cui, Q.; Baboul, A. G.; Clifford, S.; Cioslowski, J.; Stefanov, B. B.; Liu, G.; Liashenko, A.; Piskorz, P.; Komaromi, I.; Martin, R. L.; Fox, D. J.; Keith, T.; Al-Laham, M. A.; Peng, C. Y.; Nanayakkara, A.; Challacombe, M.; Gill, P. M. W.; Johnson, B.; Chen, W.; Wong, M. W.; Gonzalez, C.; and Pople, J. A.; Gaussian, Inc., Wallingford CT, 2004.

59. Meštrović, E; Kaitner, B. *J. Chem. Crystallogr*. **2006**, *36*, 599.

60. Barreca, D.; Massignan, C.; Daolio, S.; Fabrizio, M.; Piccirillo, C.; Armelao, L.; Tondello, E. *Chem. Mater.* **2001**, *13*, 588.

61. Barrios, L. A.; Ribas, J.; Aromí, G.; Ribas-Ariño, J.; Gamez, P.; Roubeau, O.; Teat, S. J. *Inorg. Chem.* **2007**, *46*, 7154.

62. Evans, D. F. *J. Chem. Soc.* **1959**, 2003–2005.

63. Shaw, M. J., Henson, R. L., Houk, S. E., Westhoff, J. W., Richter-Addo, G. B., Jones, M. W. *J. Electroanal. Chem.* **2002**, *534*, 47

64. Becke, A. D. *J. Chem. Phys*. **1993**, *98*, 1372.

65. Stephens, P. J.; Devlin, F. J.; Frisch, M. J.; Chabalowski, C. F. *J. Phys. Chem.* **1994**, *98*, 11623.

66. Dunning Jr., T. H.; Hay, P. J. in *Modern Theoretical Chemistry*, ed. H. F. Schaefer III, Vol. 3 Plenum, New York, **1976**, pp. 1-28.

67. Dolg, M.; Wedig, U.; Stoll, H.; Preuss, H. *J. Chem. Phys.* 86, **1987**, 866.

68. http://avogadro.openmolecules.net/ accessed 12/22/2009.

Appendix Five

Oral presentation at the Pure and Applied Chemistry International Conference (PACCON2011)

Electronic Communication Between Two Metal β-Diketonate Complexes Bridged by Diimine Linkers

Phimphaka Harding

Molecular Technology Research Unit,
School of Science,
Walailak University

PACCON 2011, 7th January 2011

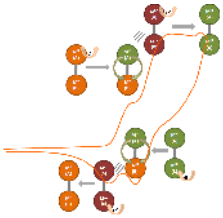

Molecular Technology Research Unit

This presentation focuses on communication between two metal centres in $[(\beta\text{-dkt})_2M(\mu\text{-L})M(\beta\text{-dkt})_2]$ complexes

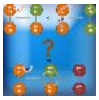

What is redox communication?

What system are we using?

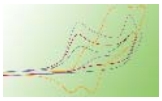

Results and Discussion

2

What is redox communication?

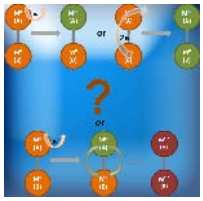

Electronic interaction between two or more redox centres.
The change in oxidation state of one redox centre will induce the electron transfer process across the linker hence the oxidation state of the next redox centre will be changed.

3

Common types of redox communication

Valence-trapped systems:
No electronic interaction between the two redox centres.

- ΔE^0 is small *ca.* 36 mV at 298 K

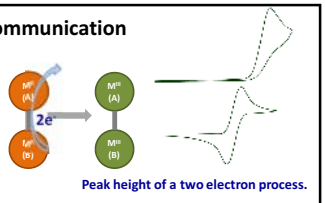

Peak height of a two electron process.

Valence-delocalized system:
Complete charge delocalization over the two redox centres.

- ΔE^0 is large *ca.* 600-700 mV at 298 K

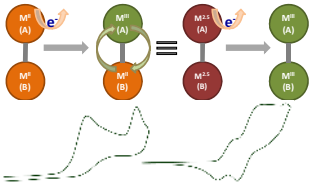

Two well-resolved peaks each corresponding to one electron.

4

Applications of redox communication

Redox switches

Molecular electronic devices (Nano wires)

Molecular magnets

Rewritable molecular memory devices and image processing

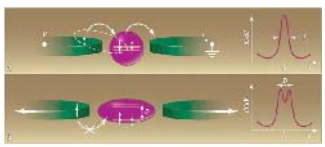

5

What system are we using?

Previous discovery monomeric MO_4N_2 show redox activity.

SCO complexes induced by redox process in Co cases.

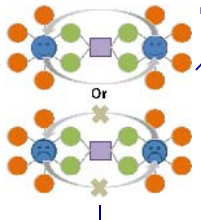

Length and electron density on the linker control the degree of communication.

6

How to design the system?

Co(II): d^7 or Ni(II): d^8

Monomers show redox activity

Spin state depends on the oxidation state and environment

β-diketonate

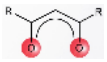

Oxygen donor:

Easy to change the substituent groups

Diimine linkers

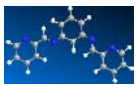

Two nitrogen donor sites:

Easy to modify the length and electron density

Redox process

Cheap and simple technique

Different oxidation states different redox potentials

7

Synthesis of $[(\beta\text{-dkt})_2M(\mu\text{-L})M(\beta\text{-dkt})_2]$ Complexes

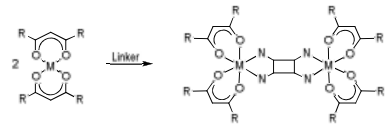

β-diketonate

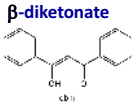

Bridging ligands

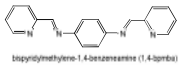

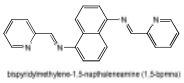

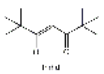

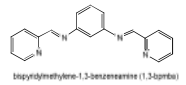

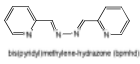

8

Results and Discussion

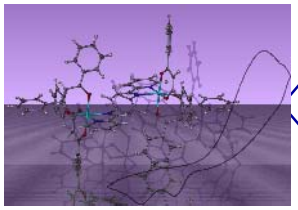

Characterization of $[(\beta\text{-dkt})_2M(\mu\text{-L})M(\beta\text{-dkt})_2]$

Cyclic voltammetry-a way to prove communication

9

Characterization of $[(\beta\text{-dkt})_2M(\mu\text{-L})M(\beta\text{-dkt})_2]$

IR spectroscopic data

The C=O stretches between 1592-1594 cm^{-1} for *dbm* complexes.

The C=O stretch for *tmhd complexes* is *ca.* 5-10 cm^{-1} lower than that of *dbm complexes*

The imine stretches of coordinated bridging ligands *ca.* 1600 and 1630 cm^{-1} are not observed as they masked by the strong C=O stretch of the β-diketonate ligand.

10

X-ray structure of of $[(\beta\text{-dkt})_2M(\mu\text{-L})M(\beta\text{-dkt})_2]$

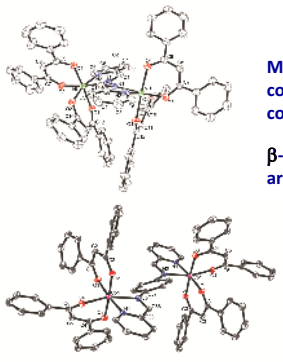

Metal centre is octahedrally coordinated with an O_4N_2 coordination environment

β-diketonate ligands adopt a *cis*-arrangement

11

Cyclic Voltammetric Studies of $[(\beta\text{-dbm})_2Ni(\mu\text{-L})Ni(\beta\text{-dbm})_2]$

L	Peak potential (V)			ΔE (mV) (Ep_2-Ep_1)
	Ep_1	Ep_2	Ep_3	
1,3-bpmba	1.26 (I)	1.54(I)	-	280
1,4-bpmba	1.24 (I)	1.61(I)	-	370
1,5-bpmna	1.32 (I)	1.68(I)	-	360
bpmhd	1.32(I)	1.40(I)	1.64(I)	320*

*Ep_3-Ep_1

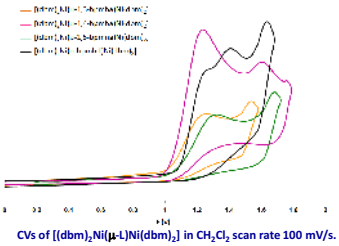

12

CVs of $[(dbm)_2Ni(\mu\text{-L})Ni(dbm)_2]$ in CH_2Cl_2 scan rate 100 mV/s.

Cyclic Voltammetric Studies of $[(\beta\text{-tmhd})_2Ni(\mu\text{-L})Ni(\beta\text{-tmhd})_2]$

L	Peak potential (V)			ΔE (mV) (Ep_2-Ep_1)
	Ep_1	Ep_2	Ep_3	
1,3-bpmba	0.96 (I)	1.54(I)	-	580
1,4-bpmba	1 03(I)	1.51 (I)	-	480
1,5-bpmna	0.94 (I)	1.54(I)	-	600
bpmhd	0.98*	1.23*	1.62(I)	640**

* $E_{1/2}$ for reversible process
**Ep_3-Ep_1

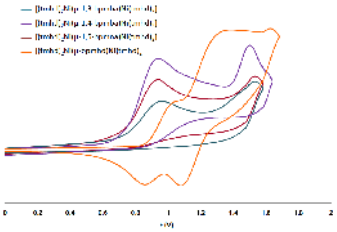

CVs of $[(tmhd)_2Ni(\mu\text{-L})Ni(tmhd)_2]$ in CH_2Cl_2 scan rate 100 mV/s.

13

What's CV telling us?

Mirrors the trend observed in the $[Ni(\beta\text{-dkt})_2(ppa^X)]$ series, the oxidation potential of *dbm* complexes is higher than that of *tmhd* complexes.

The separation between the first and second oxidation peaks is more than 36 mV and peaks height are one electron process. Therefore, there is communication between two Ni centres.

tmhd complexes show better communication between two metal centres.

bpmhd bridged complexes show 3 oxidation peaks and indicate rapid communication between the two metal centres.

14

What is going on in $[(\beta\text{-dkt})_2Ni(\mu\text{-bpmhd})Ni(\beta\text{-dkt})_2]$?

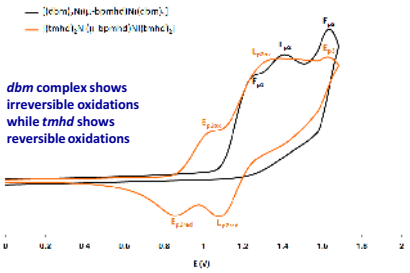

dbm complex shows irreversible oxidations while *tmhd* shows reversible oxidations

There is a third oxidation peak in both complexes. The extra oxidation peak is due to rapid communication between the metal centres over scan rate.

15

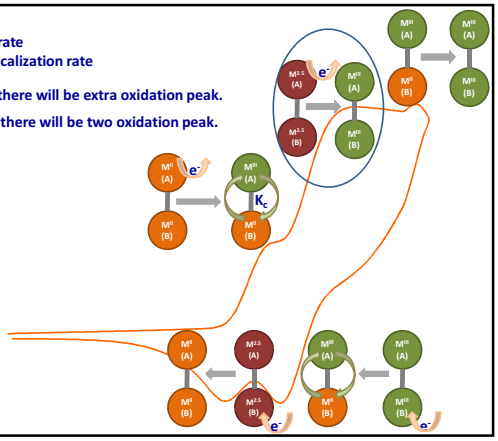

16

Vary scan rate: $[(\beta\text{-dbm})_2Ni(\mu\text{-bpmhd})Ni(\beta\text{-dbm})_2]$

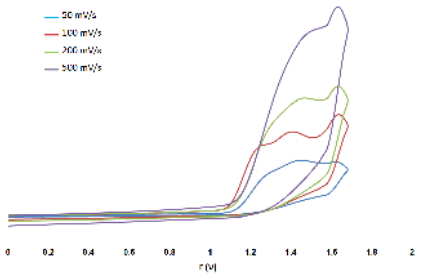

Faster scan rate less well resolved 1st and 2nd oxidation peaks.

17

Cyclic Voltammetric Studies of $[(\beta\text{-dkt})_2Co(\mu\text{-L})Co(\beta\text{-dkt})_2]$

Two oxidation peaks are observed as with the Ni analogous.

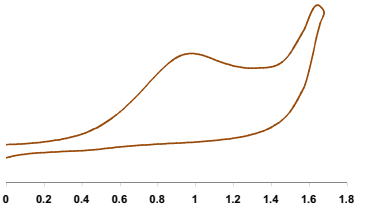

CV of $[(dbm)_2Co(\mu\text{-}1,4\text{-bpmba})Co(dbm)_2]$ in CH_2Cl_2 scan rate 100 mV/s.

However, we are looking for the unusual redox behaviour "*redox induced spin crossover*" in the system so we focus on the 1st oxidation.

18

Redox induced spin crossover in [Co(β-diketonate)$_2$(N-N)]

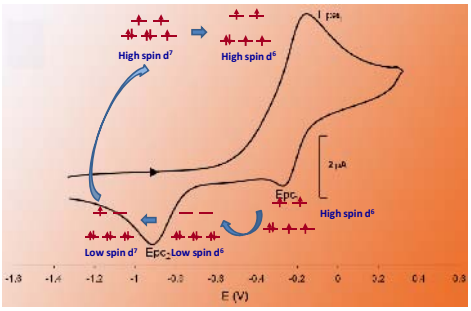

CV of [Co(tmhd)$_2$(phen)] in CH_2Cl_2 scan rate 100 mV/s

19

Cyclic Voltammetric Studies of [(β-dbm)$_2$Co(μ-L)Co(β-dbm)$_2$]

L	Peak potential (V)			ΔE (mV) (Ep$_1$-Ep$_3$)	
	Ep$_1$	Ep$_2$	Ep$_3$		
1,3-bpmba	0.92	-0.18	-	1100	
1,4-bpmba	1.02	-0.14	-	1160	
1,5-bpmna	0.88	0.04	-	920	
bpmhd	1.16	0.22	-0.12	1280*	*Ep$_1$-Ep$_3$

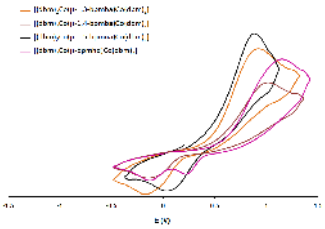

20

CVs of [(dbm)$_2$Co(μ-L)Co(dbm)$_2$] in CH_2Cl_2 scan rate 100 mV/s.

Cyclic Voltammetric Studies of [(β-tmhd)$_2$Co(μ-L)Co(β-tmhd)$_2$]

L	Peak potential (V)			ΔE (mV) (Ep$_1$-Ep$_3$)	
	Ep$_1$	Ep$_2$	Ep$_3$		
1,3-bpmba	1.16	-0.72	-0.96	2160	
1,4-bpmba	0.66	-0.28	-0.42	1080	
1,5-bpmna	0.70	-0.38	-	1080*	*Ep$_1$-Ep$_2$
bpmhd	1.28	0.14	-0.32	1600	

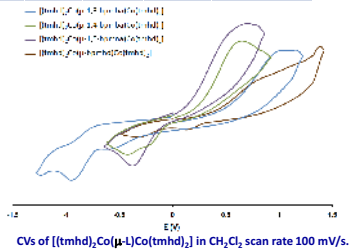

21

CVs of [(tmhd)$_2$Co(μ-L)Co(tmhd)$_2$] in CH_2Cl_2 scan rate 100 mV/s.

What's CV telling us?

The unusual redox behaviour appears to be the result of a spin change upon oxidation – an example of a '*redox induced spin crossover*' as found in the [Co(β-dkt)$_2$(N-N)] complexes.

Most of *tmhd* dimer complexes show two reduction peaks which indicate communication between the two metal centres.

Complication of '*redox induced spin crossover*' effect and metal communication therefore difficult to conclude only from CV studies.

22

In summary, we have synthesized and characterized redox active Ni(II) and Co(II) dimeric complexes which have potential to be the precursors for nanowires.

Further studies on electron communication rate by vary temperature CV, DPV *etc.*

⇩

Computer calculations.

⇩

Adjust the linker to fine tune communication.

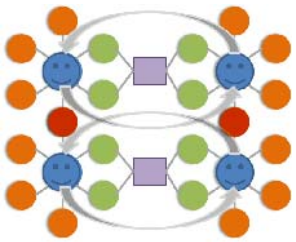

23

Molecular Technology Research Unit

Acknowledgements

Thailand Research Fund and Walialak University (Grant No. RSA5080007)

Molecular Technology Research Unit

Research Team for this work

Assoc. Prof. Dr. David Harding

24

Questions?

Appendix Six

Oral presentation at the Pure and Applied Chemistry International Conference (PACCON2010)

Redox Coupled-Spin Crossover in $[Co(\beta\text{-diketonate})_2(N\text{-}N)]^{0/+}$ Complexes

Phimphaka Harding

Molecular Technology Research Unit,
School of Science,
Walailak University

21st January 2010

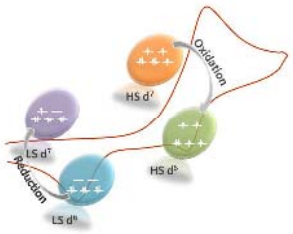

Molecular Technology Research Unit

This presentation focuses on redox coupled-spin crossover (RCSOC) in CoO_4N_2 complexes

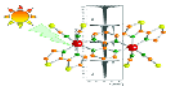

What is spin crossover (SCO)?

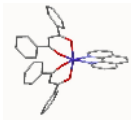

What is our system?

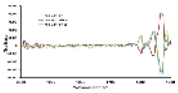

Results and Discussion

2

What is spin crossover (SCO)?

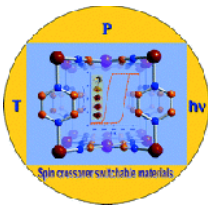

Spin-crossover is the process of changing the spin state of a molecule caused by external constraints (temperature, pressure, or electromagnetic radiation), which induce structural changes at molecular and lattice levels.

3

Common SCO examples

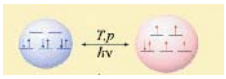

The most common SCO compounds are Fe(II) complexes.

Thermal is the most common external trigger.

Lately, increasing number of complexes have been controlled by light.

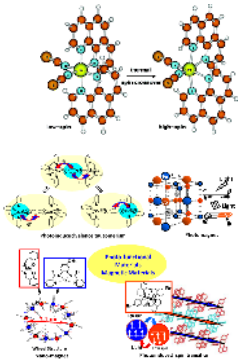

4

Applications of SCO Comlexes

Sensors

Molecular separators of gases

Photonic devices

Light modulators and filters

Rewritable molecular memory devices and image processing

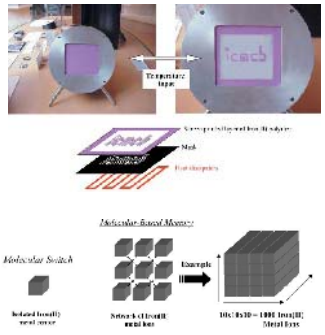

5

What is our system?

Rare SCO Co complexes: CoN_6 $[Co(terpy)_2]^{2+}$ and $[Co(bpy)_3]^{2+}$

Previous discovery NiO_4N_2 show redox activity.

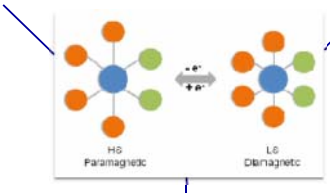

SCO complexes induce by redox process.

6

How to design the system?

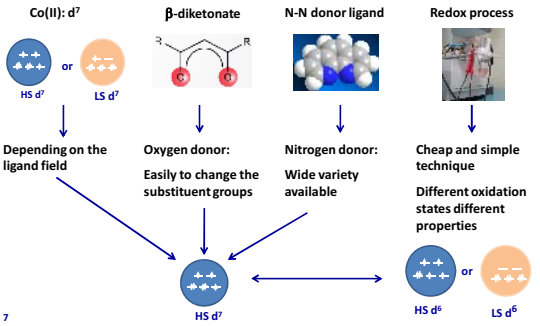

7

Synthesis of [Co(β-diketonate)$_2$(N-N)] Complexes

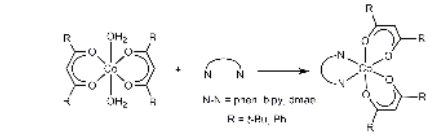

β-diketonate

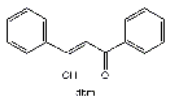

dbm

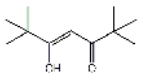

tmhd

N-N donor ligands

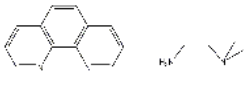

8

Results and Discussion

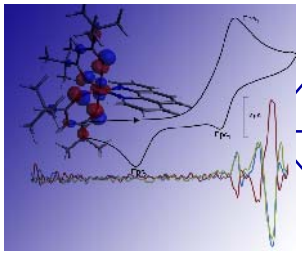

Characterization of [Co(β-diketonate)(N-N)]$^{0/+}$

Cyclic voltammetry-a new discovery!

Spectroelectrochemistry and DFT calculations

9

Characterization of [Co(β-diketonate)$_2$(N-N)]

IR spectroscopic data

C=O stretches between 1550-1600 cm^{-1} suggest symmetrically bound β-diketonate ligands

C-H stretches around 2955 cm^{-1} for tmhd ligands

UV-Vis spectroscopic data

Very strong bands at UV region consistent with ligand centred π-π* transitions

Low intensity d-d transitions were observed around 560 nm

10

X-ray structure of [Co(dbm)$_2$(phen)]

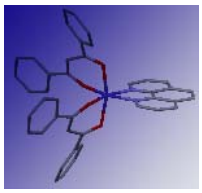

Cobalt metal centre is an octahedrally coordinated with an O_4N_2 coordination environment

β-diketonate ligands adopt a *cis*-arrangement

11

Cyclic Voltammetric Study of [Co(β-diketonate)$_2$(N-N)]

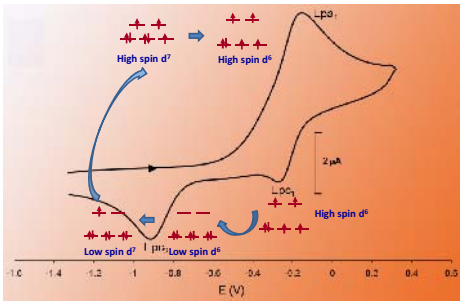

CV of [Co(tmhd)$_2$(phen)] in CH_2Cl_2 scan rate 100 mV/s

12

Fast Scan Cyclic Voltammetry

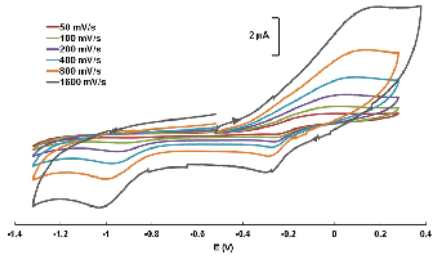

Small change in reversibility at fast scan rate indicate a rapid spin exchange equilibrium and slow electron transfer.

13

What's CV telling us?

The unusual redox behaviour appears to be the result of a spin change upon oxidation – an example of a *'redox induced spin crossover'.*

The oxidation potentials from the CVs indicate that it may be possible to oxidize the Co(II) complexes chemically.

14

Isolation of $[Co(\beta\text{-diketonate})_2(N\text{-}N)]^+$

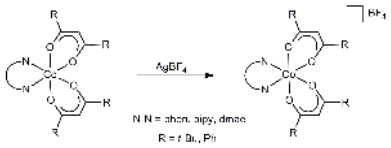

IR spectroscopy: $\nu_{C=O}$ (*ca.* 1550-1520 cm^{-1}) moves to lower wavenumbers compared with the neutral complexes.

The complexes are NMR active indicative of low spin d^6.

15

Cyclic Voltammetric Studies of $[Co(\beta\text{-diketonate})_2(N\text{-}N)]^+$

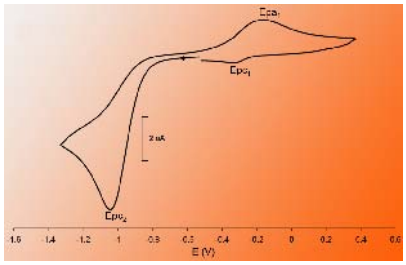

CV of $[Co(tmhd)_2(phen)][BF_4]$ in CH_2Cl_2 scan rate 100 mV/s

16

IR Spectroelectrochemical Studies (SCE)

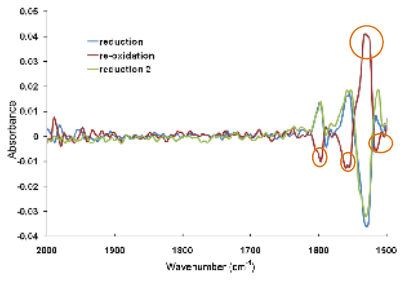

IR spectroelectrochemical difference spectra of $[Co(dbm)_2(phen)][BF_4]$

Loss of $\nu_{C=O}$ at *ca.* 1590, 1570, 1520, 1500 cm^{-1} due to Co(II) starting material.

Increasing of $\nu_{C=O}$ at *ca.* 1550 and 1520 cm^{-1} due to Co(III) product.

17

DFT of $[Co(\beta\text{-diketonate})_2(N\text{-}N)]^{0/+}$

B3LYP/SDD calculations confirm HS state is most stable for Co(II) and LS state for the Co(III) complexes.

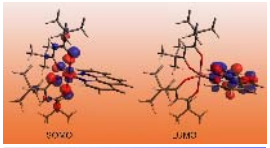

SOMO is composed of an antibonding interaction between β-diketonate oxygen *p*-orbitals and the Co d_{z^2} orbital for all *tmhd* complexes and $[Co(dbm)_2(dmae)]$.

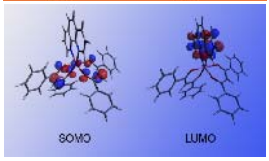

SOMO for other *dbm* complexes is composed of a weaker antibonding interaction between β-diketonate and the Co d_{xz} orbital

18

DFT Calculations & Electrochemical Studies

Complex	E(HS)-E(LS)/(kcal.mol^{-1})
[Co(tmhd)$_2$(phen)]	-15.63
[Co(tmhd)$_2$(2,2′-bpy)]	-14.55
[Co(tmhd)$_2$(dmae)]	-12.67
[Co(dbm)$_2$(phen)]	-13.84
[Co(dbm)$_2$(2,2′-bpy)]	-12.80
[Co(dbm)$_2$(dmae)]	-13.26
[Co(tmhd)$_2$(phen)]$^+$	16.12 (16.38)
[Co(tmhd)$_2$(2,2′-bpy)]$^+$	17.15 (17.19)
[Co(tmhd)$_2$(dmae)]$^+$	17.41 (17.60)
[Co(dbm)$_2$(phen)]$^+$	16.93 (17.31)
[Co(dbm)$_2$(2,2′-bpy)]$^+$	18.01 (18.16)
[Co(dbm)$_2$(dmae)]$^+$	17.93 (16.61)

ΔE(HS-LS) is small

Observed the HS d^6 intermediate in electrochemical studies

19

In summary, we have synthesized and characterized the redox coupled-spin crossover $Co^{2+/3+}$ complexes which have potential to be nano-switches.

Require low applied potential to induce SCO behaviour

⬇

Easy to fine tune by changing coordination environments

⬇

Extendable to multifunctionallized materials

20 Molecular Technology Research Unit

Acknowledgements

Thailand Research Fund and Walialak University (Grant No. RSA5080007)

Molecular Technology Research Unit

Research Team for this work

Assoc. Prof. Dr. David Harding

Asst. Prof. Dr. Yuthana Tantirungrotechai, National Nanotechnology Centre, Thailand

Theeraphol Thurakitsaree

Rattawat Daenggern

Prof. Dr. Mike Shaw and Brian Schutte, SIUE, USA

21

Questions?

22 Molecular Technology Research Unit

Appendix Seven

Oral presentation at The 8th Conference of the Inorganic Chemistry Division (IC08)

Electron Transfer of Co(II) and Ni(II) ß-Diketonate Complexes Incorporating Asymetric Diimine Ligands

Dr. Phimphaka Harding
Molecular Technology Research Unit
Walailak University

Introduction

- Aims
  - To study the electrochemical properties of metal β-diketonate complexes.
  - Fine tune the redox properties by varying the groups on the β-diketonate and diimine ligands.
- Background
  - Only a few β-diketonates studied.
  - Most diimines have been symmetric.
  - Virtually no electrochemical studies have been reported.

Ref:
1. P. Harding, D.J. Harding, W. Phonsri, S. Saithong and H. Phetmung, *Inorg. Chim. Acta*, 2009, 1, 78.
2. P. Chassot and F. Emmenegger, *Inorg. Chem.*, 1996, 35, 5931.

What is a Metal β-Diketonate?

- Metal β-diketonate complexes, $[M(\beta\text{-diketonate})_2]$ (M = Ni, Co, Fe, Cu *etc.*)
- Stable in air.
- Easy to make.
- Dissolve in organic solvents.
- Applications in catalysis, magnetic, electronic and optical devices.
- *Cis* and *trans* isomers are frequently encountered.

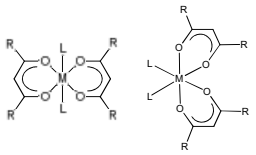

What do we use in this work?

- $[M(\beta\text{-diketonate})_2(H_2O)_2]$ when M = Ni and Co, β-diketonate ligands = dbm, tmhd and hfac.

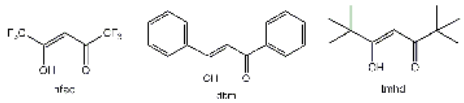

- (4-X-phenyl)-pyridin-2-ylmethylene-amine (ppa^X).

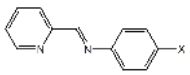

How to make Metal β-Diketonates?

- Reaction of β-diketonates with a metal acetate gives $[M(\beta\text{-diketonate})_2(H_2O)_2]$.

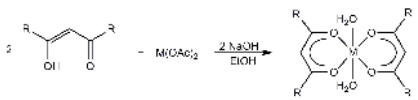

How to make the ppa^X ligands?

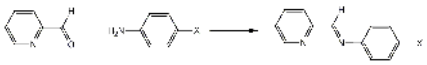

- X = H, Me, Et, OMe, F, Cl, Br and I.
- Molecular sieves are necessary to absorb water to allow isolation of the ppa^X ligands.

Ref:
1. S. Dehghanpour and A. Mahmoudi, *Main Group Chemistry*, 2007, 6, 121.
2. S. Dehghanpour, N. Bouslimani, R. Welter and F. Mojahed, *Polyhedron*, 2007, 26, 154.

Synthesis of [M(β-diketonate)$_2$ (ppa^x)] Complexes

- Simple addition of the ppa^X ligand to a solution of the metal β-diketonate yields the target compounds.

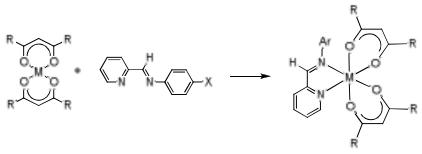

Characterization of Metal Complexes

Ni Complexes

- IR spectroscopy indicates chelating β-diketonate ligands ($\nu_{C=O}$ = 1588-1595 cm^{-1} for *dbm* and *tmhd* and 1647-1654 cm^{-1} for *hfac*).
- UV-Vis spectroscopy:

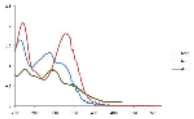

UV-Vis spectra of [Ni(β-diketonate)$_2$(ppa^{OMe})].

Co Complexes

- IR spectroscopy: $\nu_{C=O}$ = 1586-1596 cm^{-1} for *dbm* and *tmhd* complexes and 1646-1649 cm^{-1} for *hfac* complexes.
- UV-Vis spectroscopy:

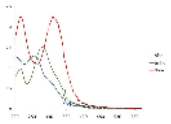

UV-Vis spectra of [Co(β-diketonate)$_2$(ppa^{OMe})].

X-ray Structures of Co and Ni Complexes

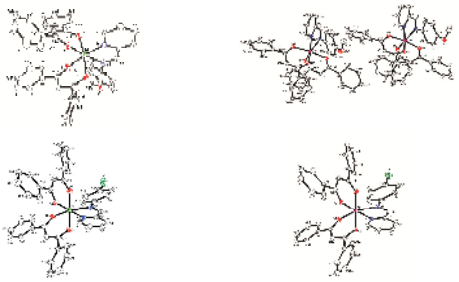

X-ray Structures of Co and Ni Complexes

- The *dbm* ligands exhibit both 'planar' and 'bent' coordination modes.

	Ni-ppa^{Cl}	Ni-ppa^{Me}	Ni-ppa^{OMe}	Co-ppa^{OMe}
M-N1	2.091(2)	2.090(4)	2.0812(14)	2.1408(14)
M-N2	2.189(2)	2.180(4)	2.1096(14)	2.1951(14)
M-O1	2.0091(16)	2.013(3)	2.0349(12)	2.0769(12)
M-O2	2.0205(17)	2.005(3)	2.0135(12)	2.0260(12)
M-O3	2.0165(16)	2.027(3)	2.0479(12)	2.0988(11)
M-O4	2.0128(16)	2.010(4)	2.0163(12)	2.0450(12)
β	2.98, 17.06	1.51, 16.57	31.94, 24.72	15.62, 21.94

Crystal Packing in [M(β-diketonate)$_2$ (ppa^x)] Complexes

[Ni(dbm)$_2$(ppa^{Cl})] **[Ni(dbm)$_2$(ppa^{OMe})]**

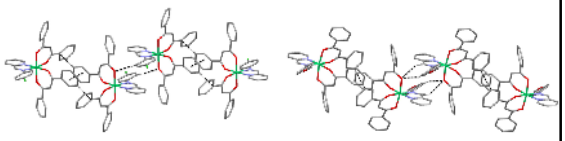

- The complexes are packed in chiral columns.
- CH…O interactions exist between the ppa^X and dbm ligands.
- For X = Cl, Me π…π and CH…π interactions are also observed.

Electron Transfer Studies of Ni Complexes

- Redox processes for the Ni complexes depend on the substituent groups of the β-diketonate ligands.
- The X group on the ppa^X ligands has only a small effect on the redox potential.
- When X is a halide an additional reduction wave is observed.

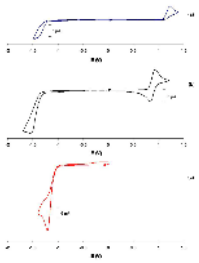

CVs of (a) [Ni(dbm)$_2$(ppa^F)], (b) [Ni(tmhd)$_2$(ppa^F)], (c) [Ni(hfac)$_2$(ppa^F)].

Electron Transfer Studies of Co Complexes

- In contrast to the Ni analogues the Co complexes show unexpected behaviour upon oxidation.
- In theory Co(III) is normally more stable than Ni(III).

Why do we observe an irreversible oxidation for the dbm and tmhd complexes?

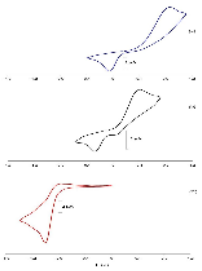

CVs of (a) [Co(dbm)$_2$(ppa^{Cl})], (b) [Co(tmhd)$_2$(ppa^{Cl})], (c) [Co(hfac)$_2$(ppa^{Cl})].

Electron Spin Change upon Oxidation

- The unusual redox behaviour appears to be the result of a spin change upon oxidation – an example of a '*redox induced spin crossover*'.

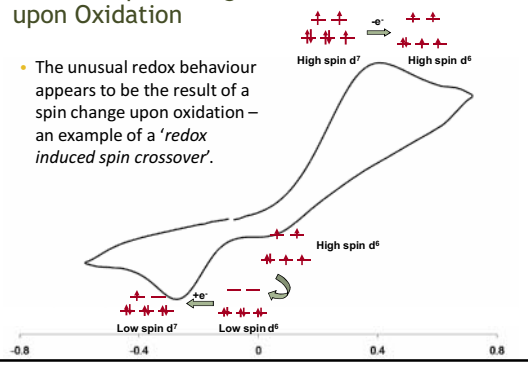

Electron Transfer Studies of Co Complexes

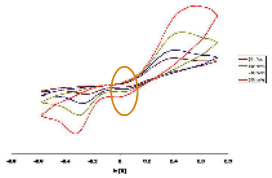

CVs of [Co(tmhd)$_2$(ppa^{Cl})] at different scan rates.

- At higher scan rates the reduction peak for the high spin Co(III) species becomes more visible.
- The stability of the high spin Co(III) species also depends on the nature of the substituent on the β-diketonate ligand.

Isolation of Co(III) Complexes

- The oxidation potentials from the CVs indicate that it may be possible to oxidize the Co(II) complexes chemically.

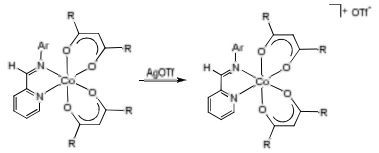

Characterization of Cationic Complexes

- IR spectroscopy: $\nu_{C=O}$ moves to lower wavenumbers compared with the neutral complexes.
- The complexes are NMR active indicative of low spin d^6.

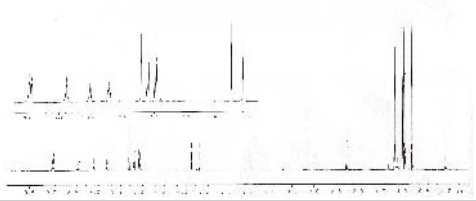

CVs of the Redox Pair

- The oxidation and reduction potentials of the neutral and cationic species are identical.

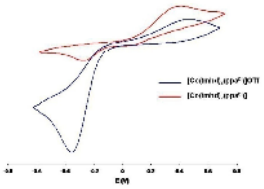

CV of [Co(tmhd)$_2$(ppa^{Cl})] (–) and [Co(tmhd)$_2$(ppa^{Cl})]$^+$ (–).

Acknowledgements

- Thailand Research Fund (TRF)
- Walailak University
- Molecular Technology Research Unit (MTRU)
- University of Sheffield for X-ray structures
- University of Bristol UK for CHN and MS
- Summer training students: Nitisasrt Soponrat, Kittaya Tinpun and Sirirat Samuadnuan
- Assoc. Prof. Dr. David J. Harding

Appendix Eight

Oral presentation at Metrohm Siam Ltd.

Simultaneous UV-Vis Spectroelectrochemistry

Assist. Prof. Dr. Phimphaka Harding
Molecular Design & Electrochemistry Laboratory
Walailak University

URL: http://sites.google.com/site/mdelwu

What is Simultaneous UV-Vis Spectroelectrochemistry

- The spectroelectrochemical technique that couples a UV-Vis spectrometer with an electrochemical apparatus.
- Uses a fiber-optic dip probe to achieve simultaneous results from the electrochemical cell.

1

What's new?

Normal UV-Vis SEC

Picture taken at Prof. Reynolds, University of Florida, USA

Fiber-Optic UV-Vis SEC

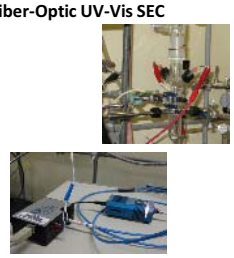

Picture taken at Prof. Mike Shaw, Southern Illinois University of Edwardsville (SIUE), USA

2

What do we need to set-up SEC (as at SIUE)?

- Potentiostat
- Light source
- Detector
- Fiber-optic probes
- Electrochemical cells
- Electrodes
- Labview program
- USB-6251-BNC: interface

3

Fiber-Optic Spectroelectrochemical Instrumentation Scheme

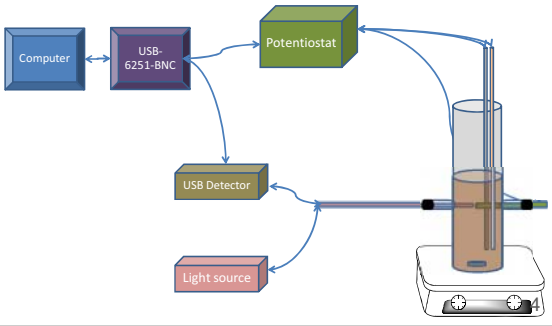

4

Step by Step Simultaneous UV-Vis Spectroelectrochemistry

Find the working electrode area (only one time for new electrode)

Find the diffusion coefficient of compound

Study Beer's Law Plot

Run Simultaneous UV-Vis Spectroelectrochemistry

5

Finding the working electrode area

- Prepare the mixed solution of $K_4[Fe(CN)_6]$ 1 mM and KCl 0.1 M in water.
- Using 3.0 mm Pt as working electrode, Pt wire as Aux. and Ag wire as Ref.
- Run Chronoamperometry at room temperature.

$$I = \frac{nFAD^{1/2}C_0}{\pi^{1/2}t^{1/2}}$$

Diffusion coefficient of $K_4[Fe(CN)_6]$ in 0.1 M KCl at 25 °C = 0.65 x 10^{-5} cm^2/s

Note: We need to do this only for first time!!

6

Instrumentation Scheme for Chronoamperometry (CA)

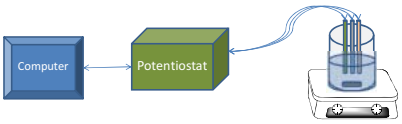

7

Program for Chronoamperometry Experiment

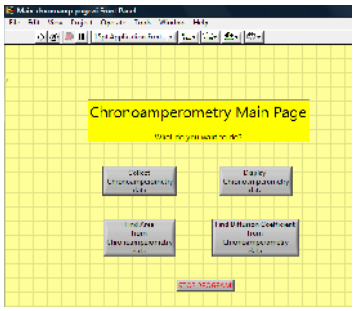

8

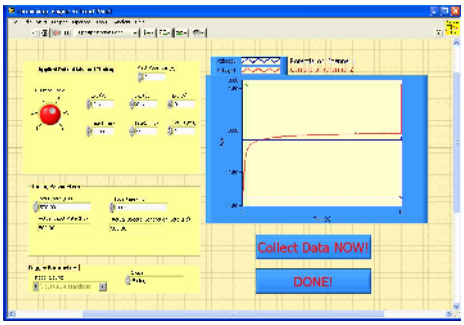

9

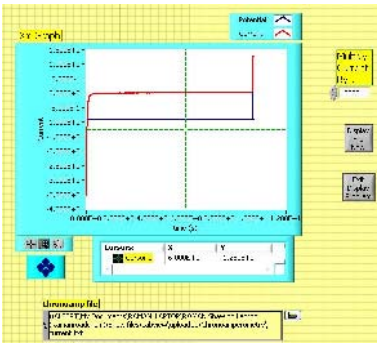

10

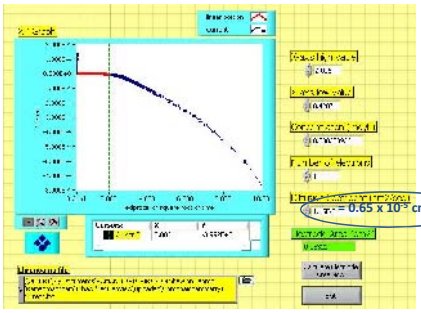

11

Finding the Diffusion Coefficient

- Prepare 1mM solution of the compound and $[NBu_4][PF_6]$ 0.1 M in 10 mL CH_2Cl_2
- Using 3.0 mm Pt as working electrode, Pt wire as an Aux. electrode and Ag wire as a Ref. electrode.
- Run Chronoamperometry at room temperature.
- Find the compound's Diffusion Coefficient.

12

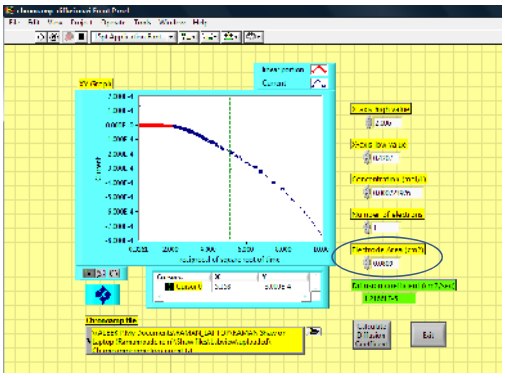

13

Beer's Law Plots Instrumentation Scheme

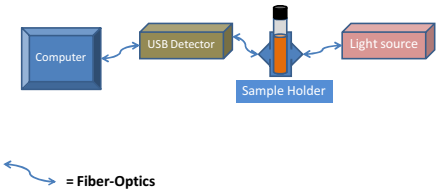

= Fiber-Optics

14

Beer's Law Plot

Experimental

- Prepare a stock solution of compound such as 0.5 mM.
- Make dilute solutions *e.g.* 0.1, 0.2, 0.3 and 0.4 mM.
- Measure the absorptions.
- Plot graph A vs. Conc.

15

Simultaneous UV-Vis SEC

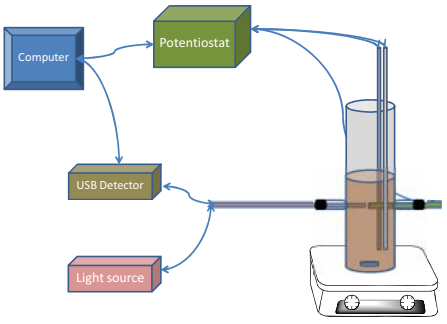

16

What do we do next?

- Firstly, apply a constant potential that will reduce or oxidize the compound.
- Then measure and collect the spectra of the species at the working electrode surface every 0.5 seconds, 20 times

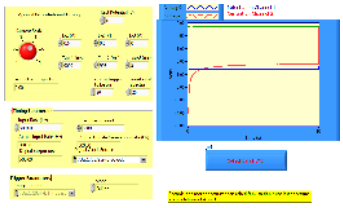

17

Principles of the experiment set-up

- The UV-Vis beam is focused from the spectrometer into a set of UV-Vis optical fibers.
- The beam exits the fibers through the probe assembly, travels through the reaction solution, bounces of the electrode and is collected by another set of fibers which lead to the detector.

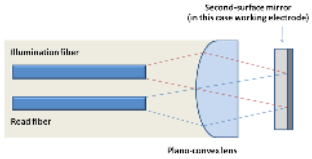

18

Principles of the experiment set-up

- The difference spectra between the bulk solution with no potential applied and spectra where potential has been applied for at least 15 sec. clearly indicate the presence and identity of the thus-formed electrode products.

19

What's going on in the cell

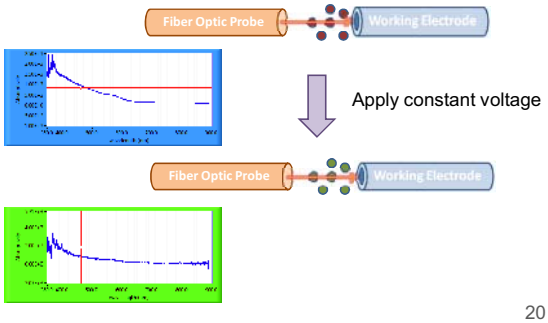

20

Data Manipulation

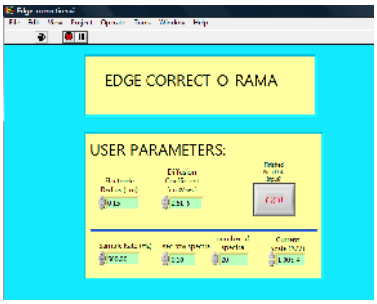

21

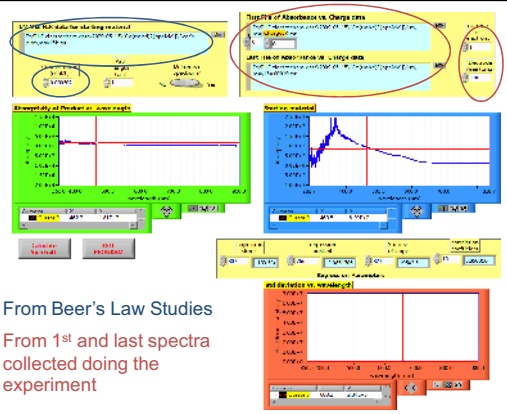

From Beer's Law Studies

From 1st and last spectra collected doing the experiment

22

Why do we need edge correction?

Ideal electrode:
No uneven electrode surface

Real electrode:
There is an edge on the electrode surface. → More reaction surface area than just the area of electrode as we use in the equation.

23

Edge Correction Data

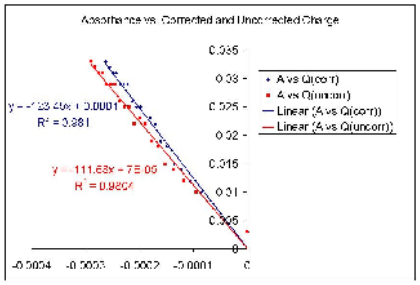

24

Ferrocene UV-Vis spectroelectrochemical spectra

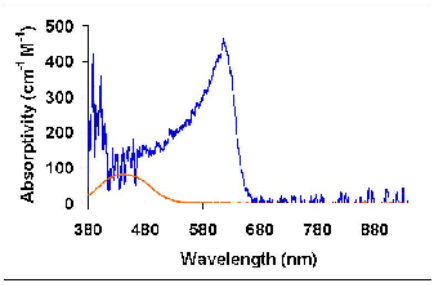

25

Acknowledgements

- UMAP and WU for travelling support to SIUE.
- TRF for research fund.
- Prof. Mike Shaw for access the SEC.
- Assoc. Prof. Dr. David Harding and Benjamin Harding for making life at SIUE more fun.
- Metrohm Siam Ltd. for today's seminar.
- Your attention!

26

Appendix Nine

Poster presentation the Annual Thailand Research Fund, Phetchaburi, Thailand, 2010

Redox Coupled-Spin Crossover Cobalt β-Diketonate Complexes: Synthesis, Electron Transfer Studies and DFT Calculations

Harding, P.[1*], Harding, D.J.[1], Tantirungrotechai, Y.[2] and Sayananon A.[3]

[1] *Molecular Technology Research Unit, School of Science, Walailak University, Nakhon Si Thammarat, 80161, Thailand*

[2] *National Nanotechnology Center, National Science and Development Agency, Pathumthani, 12120, Thailand*

[3] *Department of Chemistry, Faculty of Science, Thammasat University, Pathumthani, 12120, Thailand*

URL: http://sites.google.com/site/mdelwu E-mail: kphimpha@wu.ac.th

Objective

- To synthesize novel mononuclear metal complexes $[Co(\beta\text{-}dkt^R)_2(ppa^X)]$ and their cations.
- To investigate the effect of type of substituent groups on ligands on electron transfer of cobalt β-diketonate complexes.
- To study the electronic properties of $[Co(\beta\text{-}dkt^R)_2(ppa^X)]$ and their cations by using DFT calculations.
- To study inter- and intramolecular forces in the metal complexes.

Methodology

Ligand Synthesis

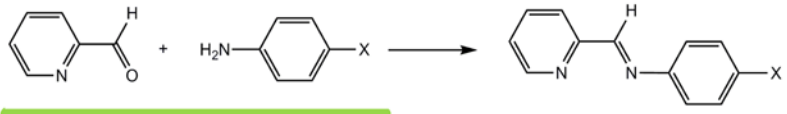

Co(II) Complexes Synthesis

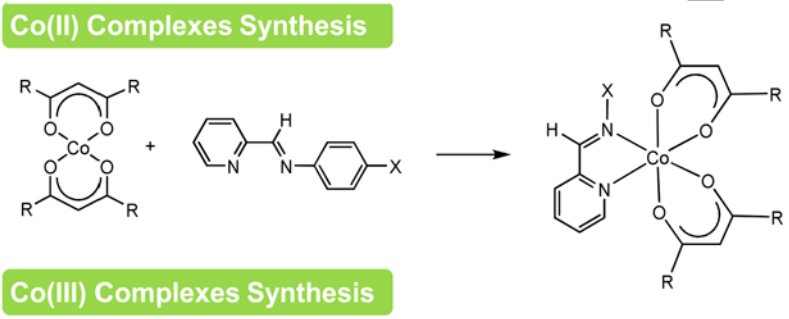

Co(III) Complexes Synthesis

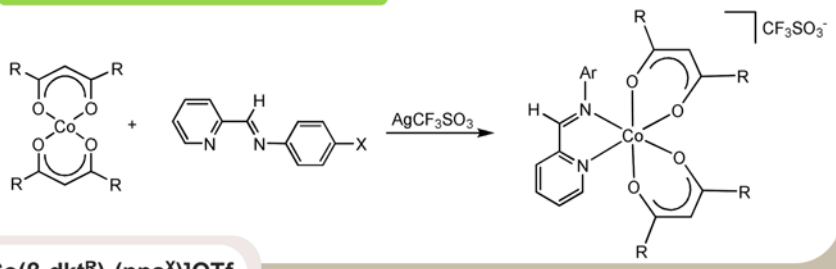

Results and Discussion

Electron Transfer Studies

The $[Co(\beta\text{-}dkt^R)_2(ppa^X)]$ complexes (β-dkt^R = dbm or tmhd) show an irreversible oxidation followed by a reduction of an unknown peak which indicative that upon oxidation there is a change in spin state from high spin to low spin. This behaviour is know as *"redox coupled spin-crossover"*.

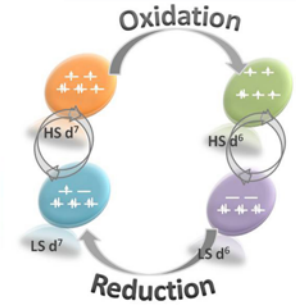

DFT Calculations

DFT calculations of $[Co(\beta\text{-diketonate})_2(ppa^X)]$ complexes have suggested that SOMO is constituted of Co (*ca.* 40%), β-diketonate (*ca.* 55%) and ppa^X (*ca.* 5%) hence the oxidation potential will depend mostly on the properties of substituents on the β-diketonate.

The CV of $[Co(\beta\text{-}dkt^R)_2(ppa^X)]OTf$ are almost identical to those found in the neutral analogues although there are slight deviations.

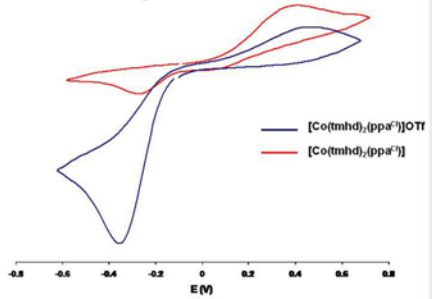

Figure 1 CVs of $[Co(tmhd)_2(ppa^{Cl})]$ and $[Co(tmhd)_2(ppa^{Cl})]OTf$

Acknowledgements and Output

Acknowledgements

We thank Walailak University and the Thailand Research Fund for supporting this research (RSA 5080007).

Output

1. P. Harding, D. J. Harding, K. Tinpun, S. Samuadnuan, N. Sophonrat and H. Adams, Synthesis and electrochemical studies of nickel β-diketonate complexes incorporating asymmetric diimine ligands, *Aust. J. Chem*, 2010, 63, 75.
2. P. Harding, D. J. Harding, N. Sophonrat and H. Adams, Bis(1,1,1,5,5,5-hexafluoropentane-2,4-dionato-κ^2-*O*,*O*')[(4-bromo-phenyl)pyridin-2-ylmethyleneamine-κ^2-*N*,*N*']cobalt(II), *Acta Cryst. Section E*, 2010, E66, m1138.

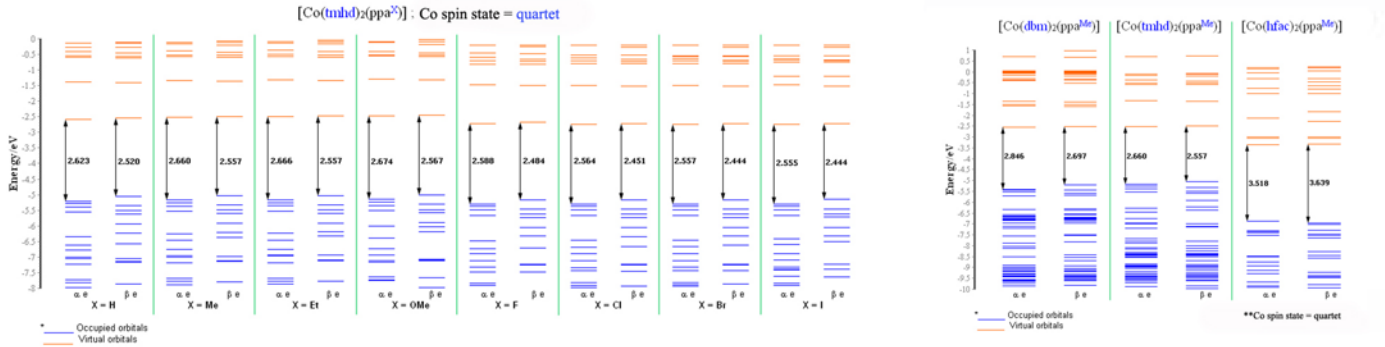

Figure 2 Plot of the SOMO-LUMO gap with the tmhd series showing the effect of the ppa^X ligand and the effect of the β-diektonate when the diimine is ppa^{Me}.

Appendix Ten

Poster presentation the Annual Thailand Research Fund, Phetchaburi, Thailand, 2009

Electronic Communication in Redox Coupled-Spin Crossover Cobalt Dimers

Phimphaka Harding* and David J. Harding

Molecular Technology Research Unit, School of Science, Walailak University, Thasala, Nakhon Si Thammarat, 80161, Thailand
E-mail: kphimpha@wu.ac.th URL: http://sites.google.com/site/mdelwu/

Introduction

The Co β-diketonate monomeric complexes *e.g.* [Co(β-diketonate)$_2$(ppa^X)] show redox coupled-spin crossover (RCSC) behaviour. In this work we explored the possibility of modified RCSC behaviour in a Co dimers.

Objectives

- To synthesize [(β-diketonate)$_2$Co(μ-L)Co(β-diketonate)$_2$] complexes.
- To investigate the redox coupled-spin crossover behaivour of the dimeric complexes using cyclic voltammetry.

Synthesis

The reaction of various diamines and pyridine-2-carboxaldehyde yields bispyridylmethylenediamine bridging ligands (Scheme 1).

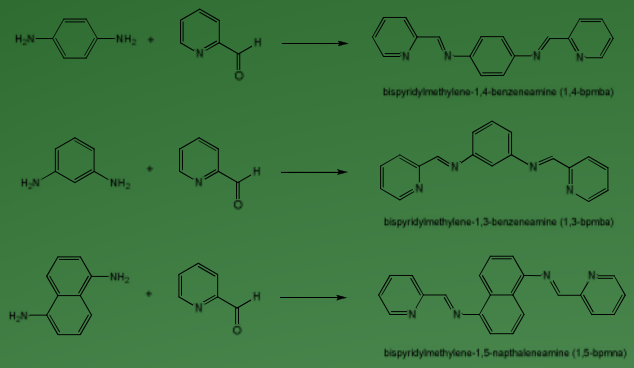

Scheme 1 Ligands synthesis.

The Co dimer complexes were prepared by the reaction of [Co(β-diketonate)$_2$] (β-diketonate = dbm and tmhd) with one equivalent of the bridging ligands (Scheme 2) resulting in formation of the novel Co dimer complexes, [(dbm)$_2$Co(μ-L)Co(dbm)$_2$] (L = 1,3-bpmba **1**, 1,4-bpmba **2** and 1,5-bpmna **3**) and [(tmhd)$_2$Co(μ-L)Co(tmhd)$_2$] (L = 1,3-bpmba **4**, 1,4-bpmba **5** and 1,5-bpmna **6**).

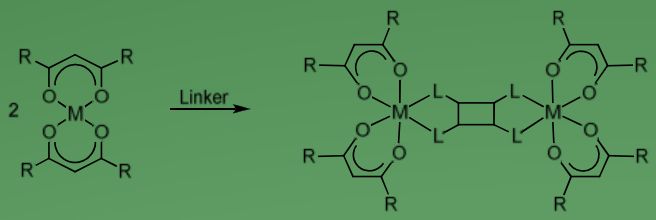

Scheme 2 Co dimers synthesis.

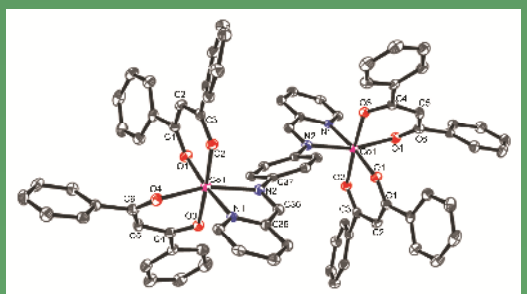

Figure 1 X-ray structure of [(dbm)$_2$Co(μ-1,4-bpmab)Co(dbm)$_2$] **2**.

Electrochemical Studies

The cyclic voltammograms of the Co dimers **1**-**6** show oxidation peaks followed by returned peaks which are separated from the oxidation peaks by *ca.* 800-2000 mV indicative of the RCSC behavior observed in the [Co(β-diketonate)$_2$(ppa^X)] and [Co(β-diketonate)$_2$(N-N)] complexes.

- In the *dbm* series the stabilization ability of the ligands is in the order of *1,4-bpmba > 1,3-bpmba > 1,5-bpmna*. While for the *tmhd* series no trend is observed.

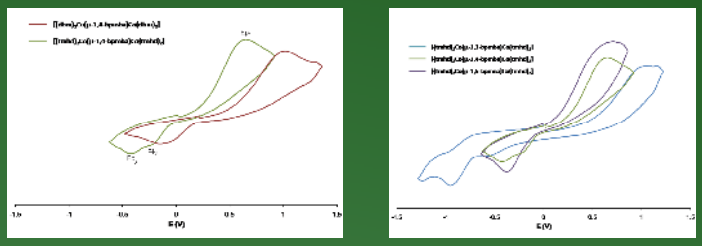

Figure 2 Cyclic voltammograms of Co dimers.

Comparison between the Co-tmhd complexes **4**-**6** found [(tmhd)$_2$Co(μ-1,3-bpmba)Co(tmhd)$_2$] **4** is more difficult to oxidize than the other two complexes by *ca.* 300 mV and also more difficult to oxidize than [(dbm)$_2$Co(μ-1,3-bpmba)Co(dbm)$_2$] **1** by *ca.* 100 mV. This unusual electron transfer behavior and might be due to strong communication between two metal centres through the bridging ligand. It is also possible that the structural reorganization required upon oxidation is more difficult to achieve as a result of increased steric interactions that would be expected in the 1,3-bpmba ligand complexes.

Table 1 Electrochemical data for Co dimers.

Complex	Peak potential (V)		
	Ep_1	Ep_2	Ep_3
[(dbm)$_2$Co(μ-1,3-bpmba)Co(dbm)$_2$] **1**	0.96	-	-0.16
[(dbm)$_2$Co(μ-1,4-bpmba)Co(dbm)$_2$] **2**	1.02	-	-0.14
[(dbm)$_2$Co(μ-1,5-bpmna)Co(dbm)$_2$] **3**	0.88	-	0.04
[(tmhd)$_2$Co(μ-1,3-bpmba)Co(tmhd)$_2$] **4**	1.04	-0.56	-0.96
[(tmhd)$_2$Co(μ-1,4-bpmba)Co(tmhd)$_2$] **5**	0.67	-0.22	-0.42
[(tmhd)$_2$Co(μ-1,5-bpmna)Co(tmhd)$_2$] **6**	0.70	-	-0.38

Acknowledgements

We acknowledge the Thailand Research Fund and Walailak University for research grant number RSA5080007.

Appendix Eleven

Poster presentation the Annual Thailand Research Fund, Phetchaburi, Thailand, 2008

Electron Transfer Studies of [Ni(β-diketonate)$_2$(ppa^X)] Complexes

P. Harding*[1], D.J. Harding[1], N. Sophonrat[2], K. Tinpun[2], S. Samuadnuan[2], H. Adams[3]

[1] Molecular Technology Research Unit, School of Science, Walailak University, Nakhon Si Thammarat, 80161, Thailand

[2] Department of Chemistry, Faculty of Science, Taksin University, Songkhla, 90000, Thailand

[3] Department of Chemistry, University of Sheffield, Brook Hill, Sheffield, S3 7HF, England

Corresponding author e-mail: kphimpha@wu.ac.th URL: http://resource.wu.ac.th/inorganic_synthesis

Introduction

Metal β-diketonate complexes have found many applications but the redox chemistry of these systems is under developed. In this work we synthesize a series of novel Ni(II) β-diketonate complexes incorporating asymmetric diimine ligands, [Ni(β-diketonate)$_2$(ppa^X)]. These complexes have been investigated by cyclic voltammetry to better understand their redox behaviour.

Synthetic Method

The reaction of [Ni(dbm)$_2$], [Ni(tmhd)$_2$] or [Ni(hfac)$_2$] with eight (4-X-phenyl)-pyridin-2-ylmethylene-amine ligands, ppa^X, when X = H **1**, Me **2**, Et **3**, OMe **4**, F **5**, Cl **6**, Br **7** and I **8** in CH_2Cl_2 , THF or acetone affords yellow, red or orange solids of the octahedral complexes, [Ni(dbm)$_2$(ppa^X)] (X = H **9**, Me **10**, Et **11**, OMe **12**, F **13**, Cl **14**, Br **15** and I **16**), [Ni(tmhd)$_2$(ppa^X)] (X = H **17**, Me **18**, Et **19**, OMe **20**, F **21**, Cl **22**, Br **23** and I **24**), [Ni(hfac)$_2$(ppa^X)] (X = H **25**, Me **26**, Et **27**, OMe **28**, F **29**, Cl **30**, Br **31** and I **32**). (Scheme 1)

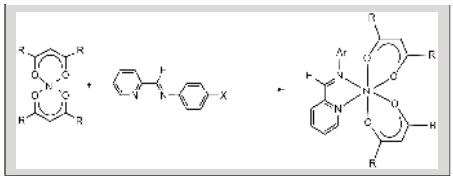

Scheme 1 *Synthesis of [Ni(β-diketonate)$_2$(ppa^X)] complexes.*

Results and Discussion

Molecular structure of complexes **10**, **12** and **14** were determined by X-ray crystallography. The structure of **10** is shown in Figure 1. Complexes **10**, **12** and **14** assume slightly distorted octahedral coordination geometries. The β-diketonate ligands exhibit a *cis* arrangement enforced by the chelating ppa^X ligand.

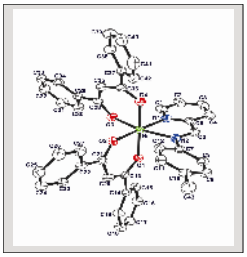

Figure 1 *Molecular structure of [Ni(dbm)$_2$(ppa^{Me})] **10**.*

The redox chemistry of complexes **9**-**32** were studied by cyclic voltammetry in CH_2Cl_2 at room temperature (Table 1).

Table 1 *Electrochemical data of [Ni(β-diketonate)$_2$(ppa^X)] complexes.*

Complex	E_{ox} (V)	E_p^{red} (V)	Complex	E_{ox} (V)	E_p^{red} (V)
9	1.19 (I)	-	**21**	0.87	-1.57 (I)
10	1.18 (I)	-	**22**	0.87	-1.49 (I)
11	1.18 (I)	-	**23**	0.88	-1.46 (I)
12	1.18 (I)	-	**24**	0.89	-1.48 (I)
13	1.20 (I)	-1.42 (I)	**25**	-	-1.24 (I)
14	1.24 (I)	-1.32 (I)	**26**	-	-1.27 (I)
15	1.20 (I)	-1.33 (I)	**27**	-	-1.17 (I)
16	1.22 (I)	-1.31 (I)	**28**	-	-1.22 (I)
17	0.85	-	**29**	-	-1.21 (I)
18	0.84	-	**30**	-	-1.05 (I)
19	0.83	-	**31**	-	-1.09 (I)
20	0.84, 1.49(I)	-	**32**	1.10 (I)	-1.09 (I)

[a] All measurements were performed at 298 K, in dried and degassed CH_2Cl_2 0.1 M [NBu$^n_4$][PF$_6$] solution; scan rate 100 mVs^{-1}; calibrated with [Fe(η-C$_5$H$_5$)$_2$], $E^{o'} = 0.52$ V. [b] E_{ox} represents $E^{o'}$ if the oxidation is reversible and the peak potential, E_p^{ox}, if the oxidation is irreversible. [c] Uncalibrated as the compound reacts with [Fe(η-C$_5$H$_5$)$_2$].

The results show that changing the substitutents on the β-diketonate ligands plays a more important role in the electron transfer behaviour than that of the ppa^X ligand. The increase in electron donating ability from hfac to tmhd and the corresponding change in redox-behaviour from no oxidation to irreversible oxidation to quasi-reversible oxidation, in the case of hfac, dbm and tmhd respectively (Figure 2). Moreover, when the substitutent on the ppa^X is a halide, the complexes undergo an irreversible reduction in all cases.

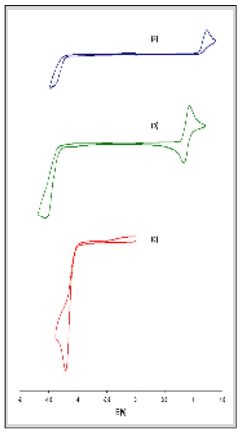

Figure 2 *Cyclic voltammograms of (a) [Ni(dbm)$_2$(ppa^F)], **13** (b) [Ni(tmhd)$_2$(ppa^F)], **21** (c) [Ni(hfac)$_2$(ppa^F)] **29**.*

Conclusion

The electron transfer behaviour of Ni(II) complexes, [Ni(β-diketonate)$_2$(ppa^X)], are irreversibly or reversibly oxidised to Ni(III) in the case of [Ni(dbm)$_2$(ppa^X)] and [Ni(tmhd)$_2$(ppa^X)], respectively. With the exception of [Ni(hfac)$_2$(ppa^I)] which show no oxidation processes. The β-diketonate ligand has a significant effect on the redox potential while the ppa^X ligands have only a very minor effect.

References

1. P. Harding, D. J. Harding, W. Phonsri, S. Saithong, H. Phetmung, *Inorg. Chim. Acta.*, **2008**, DOI:10.1016/j.ica.2008.03.014.
2. P. Chassot and F. Emmenegger, *Inorg. Chem.*, 1996, **35**, 5931-5934.
3. D. V. Soldatov, I. L. Moudrakovski, C. I. Ratcliffe, R. Dutrisac and J. A. Ripmeester, *Chem. Mater.*, 2003.

Acknowledgements

We would like to thank the Thailand Research Fund (TRF) and Walailak University for financial support (RSA-5080007).